

厚生労働科学研究費補助金
労災疾病臨床研究事業

悪性胸膜中皮腫のヒト化 CD26 抗体療法確立のための
予後・治療効果予測バイオマーカーの開発

令和2年度 総括・分担研究報告書

研究代表者 森本 幾夫

令和3(2021)年3月

目 次

I. 総括研究報告

悪性胸膜中皮腫のヒト化CD26抗体療法確立のための予後・治療効果予測バイオマーカーの開発
..... 1

研究代表者 森本 幾夫
順天堂大学大学院医学研究科 免疫病・がん先端治療学講座 特任教授

II. 分担研究報告

1. ヒト化CD26抗体の予後・治療効果予測バイオマーカーの探索：
国内第I/II相臨床試験の血清および末梢血リンパ球の解析
..... 13

研究代表者 森本 幾夫
順天堂大学大学院医学研究科 免疫病・がん先端治療学講座 特任教授

研究分担者 岸本 卓巳
独立行政法人労働者健康安全機構
アスベスト疾患研究・研修センター 所長

研究分担者 山田 健人
埼玉医科大学 病理学 教授

研究協力者 波多野 良
順天堂大学大学院医学研究科 免疫病・がん先端治療学講座 特任助教

研究協力者 金子 有太郎
ワイズ・エー・シー株式会社 代表取締役CEO
近畿大学 客員教授(元)

研究協力者 藤本 伸一
岡山労災病院 腫瘍内科部長

研究協力者 青江 啓介
山口宇部医療センター 腫瘍内科 内科系診療部長

2. 悪性胸膜中皮腫におけるCD26発現評価とヒト化CD26抗体療法における
予後・治療効果予測バイオマーカーの開発..... 25

研究分担者 山田 健人
埼玉医科大学 病理学 教授

研究分担者 岸本 卓巳
独立行政法人労働者健康安全機構
アスベスト疾患研究・研修センター 所長

研究協力者 藤本 伸一
岡山労災病院 腫瘍内科部長

研究協力者 青江 啓介
山口宇部医療センター 腫瘍内科 内科系診療部長

研究協力者 波多野 良
順天堂大学大学院医学研究科 免疫病・がん先端治療学講座 特任助教

3. ヒト化 CD26 抗体を用いた悪性中皮腫に対する新たな併用療法の開発

..... 31

研究代表者	森本 幾夫 順天堂大学大学院医学研究科 免疫病・がん先端治療学講座 特任教授
研究分担者	岸本 卓巳 独立行政法人労働者健康安全機構 アスベスト疾患研究・研修センター 所長
研究分担者	山田 健人 埼玉医科大学 病理学 教授
研究協力者	波多野 良 順天堂大学大学院医学研究科 免疫病・がん先端治療学講座 特任助教
研究協力者	大沼 圭 順天堂大学大学院医学研究科 免疫病・がん先端治療学講座 准教授
研究協力者	金子 有太郎 ワイズ・エー・シー株式会社 代表取締役 CEO 近畿大学 客員教授(元)

III. 研究成果の刊行に関する一覧表..... 39

IV. 研究成果の刊行物・別刷

I. 総括研究報告

労災疾病臨床研究事業費補助金
総括研究報告書
悪性胸膜中皮腫のヒト化 CD26 抗体療法確立のための
予後・治療効果予測バイオマーカーの開発

研究代表者 森本 幾夫 順天堂大学大学院医学研究科
免疫病・がん先端治療学講座 特任教授

研究要旨

悪性胸膜中皮腫はアスベストばく露によって起こる難治性悪性腫瘍であり、現時点で満足できる治療法はなく、新たな治療法の確立が望まれる。研究代表者は抗腫瘍効果の強いヒト化 CD26 抗体 YS110 の開発に成功し、フランスにて悪性中皮腫を中心とした CD26 陽性腫瘍に対する First-in-Human 第 I 相臨床試験を施行した。2017 年 7 月から国内でも悪性中皮腫に対する第 I/II 相臨床試験を施行し、2019 年に第 I 相、第 II 相臨床試験計 40 例の投与が終了した。今年度は抗腫瘍効果について最終的な中央判定結果を基に、これまでのデータを再解析（グループ分け）し、CD26 抗体の有効性予測バイオマーカー候補として SDF-1 α β , MIP-1d, MCP1 を見出した。また、Gro-b, CTACK, MCP2 も有効性の予測に役立つ可能性が考えられる。血清中の可溶性 CD26 濃度/DPP4 酵素活性の変動解析については、血清検体採取のタイミングを再度検討する必要があることが示された。末梢血リンパ球のフェノタイプ解析により、CD26 抗体有効例では特に CD8 T 細胞で細胞傷害性エフェクター T 細胞 (CD26 陰性・CD28 陰性・KLRG1 陽性サブセット) の割合が高く、免疫チェックポイント分子の中で PD1 と TIGIT の発現陽性率が高い可能性を見出した。CD26 抗体の臨床応用を目指すうえでこれらのバイオマーカー候補が有効性予測に役立つことを期待する。

昨年、R&D 社ポリクローナル抗体による免疫染色（フランスでの治験と同一、A 法）および新規開発されたコンパニオン診断キットによる免疫染色（B 法）の二つの染色方法により CD26 発現について検討し、B 法が CD26 発現をより正確に評価することを報告した。CD26 染色の感度が上がった B 法による検討と HE 染色標本により、中皮腫腫瘍部分へのリンパ球並びに CD26 陽性単核細胞（リンパ球と単球等）浸潤について治療効果との比較を試みた。その結果、long SD 5 症例中では腫瘍浸潤リンパ球 3+が 4 症例、+1 が 1 症例であり、治療効果が長い症例では CD26+単核細胞浸潤が多い傾向があった。一方、PD16 症例では、腫瘍浸潤リンパ球が 3+は 3 症例、+2 は 5 症例、+1 は 8 症例であり、CD26+単核細胞浸潤が少ない傾向が窺われた。これらの結果は、中皮腫においてリンパ球浸潤および CD26 陽性単核細胞の半定量評価が治療効果予測のバイオマーカーとなる可能性を示唆する。

治療抵抗性の悪性中皮腫患者に対して、CD26 抗体単剤でも高い割合で Stable Disease・Partial Response となり抗腫瘍効果は認められたが、より長期間抗腫瘍効果を発揮し、無増悪生存期間を与えられる本抗体を用いた新たな併用療法の開発も重要な課題である。そこで、ヒト免疫化マウスを用いたヒト悪性中皮腫細胞株担がんモデルを確立し、ヒト化 CD26 抗体と

PD-1 抗体との併用効果を検討した結果、それぞれの単剤よりも強い相乗効果が認められる予備実験データを得た。

研究分担者

岸本 卓巳：独立行政法人労働者健康安全機構 アスベスト疾患研究・研修センター 所長

山田 健人：埼玉医科大学 病理学 教授

研究協力者

藤本 伸一：岡山労災病院 腫瘍内科部長

青江 啓介：山口宇部医療センター 腫瘍内科 内科系診療部長

大沼 圭：順天堂大学大学院医学研究科 免疫病・がん先端治療学講座 准教授

波多野 良：順天堂大学大学院医学研究科 免疫病・がん先端治療学講座 特任助教

金子有太郎：ワイズ・エー・シー株式会社 CEO, 近畿大学 客員教授(元)

A. 研究目的

悪性中皮腫は効果的な治療法はなく、予後は極めて不良で労災疾病行政上も大きな問題となっている。抗ヒト PD-1 抗体ニボルマブが 2018 年 8 月に、悪性中皮腫に対する治療薬として日本でも認可され、約 2-3 割の患者には有効性が認められる一方で、食欲減退、下痢、発熱などの副作用が高い割合で見られ、自己免疫様疾患として甲状腺機能異常、大腸炎、下垂体異常および間質性肺疾患などの重篤な副作用も報告されている。このことから、悪性中皮腫に対する安全かつ有効な新規治療法の確立は依然として重要な課題である。研究代表者は CD26 単クローン抗体の開発、CD26 cDNA の単離を世界に先駆けて行い(J

Immunol. 1989, 1992)、抗腫瘍効果の強いヒト化 CD26 抗体の開発に成功した。悪性中皮腫における CD26 発現の解析、抗体の抗腫瘍作用機構の解明に取り組み、この抗体は抗体医薬特有の ADCC(抗体依存性細胞傷害)活性に加え、腫瘍細胞膜上の CD26 タンパクに CD26 抗体が結合することで細胞周期停止の誘導や、CD26 分子と CD26 抗体の複合体が細胞膜から核へ移行し、増殖抑制に働くこと、さらに、近年では腫瘍免疫の促進にも働きうることを明らかにしてきた(Clin Cancer Res. 2007, 2012, PLoS One. 2013, Br J Cancer. 2014, Nat Immunol. 2015)。また、抗体療法の確立に不可欠な病理組織の CD26 発現診断用抗体、可溶性 CD26/DPPIV 値測定系を開発し(Diagn Pathol. 2014, PLoS One. 2019, J Clin Lab Anal. 2015)、フランスにて治療抵抗性悪性中皮腫を中心とした First-in-Human 第 I 相臨床試験を施行した。免疫チェックポイント阻害薬のような特記すべき有害事象もなく安全性が確認されるとともに、有効性を示唆するデータも得られたが(Br J Cancer. 2017)、CD26 抗体療法が有効な患者を判別できるバイオマーカーの開発が課題とされた。

そこでフランスでの第 I 臨床試験患者血清を解析し、CD26 抗体投与前後の血清中可溶性 CD26/DPPIV 値の変動解析が Stable Disease(SD)・Progressive Disease(PD)の予測バイオマーカーとなる可能性が示唆された($p < 0.016$)。この予備結果を実証すること、また、CD26 抗体の治療効果を予測できる新たなバイオマーカーを確立することを

目指し、本邦で2017年7月から開始した悪性中皮腫の第I/II相臨床試験検体を用いて、(1)腫瘍病理組織でのCD26発現の定量・定性解析の確立と、腫瘍組織DNA・RNA profileと治療効果との相関解析(2)CD26抗体の治療効果・予後を予測する血清バイオマーカー、及び(3)末梢血リンパ球バイオマーカーの確立に取り組む。

初年度(2018年度)は、2018年3月に最終患者への投与が終了した国内第I相臨床試験検体(全9例)、及び2018年6月から開始した国内第II相臨床試験検体の一部を用いて、(1)腫瘍病理組織でのCD26発現解析と(3)末梢血リンパ球の解析を行った。また、国内第I相臨床試験検体(全9例)の(2)血清中可溶性CD26/DPPIV酵素活性値の測定を行った。2018年度終了時点ではまだ解析検体数が少なく、次年度以降の検体数の追加が必要とされた。

2年度目(2019年度)は、2019年内に国内第II相臨床試験全31例へのCD26抗体投与が終了した。昨年に引き続き、国内第II相臨床試験検体を用いて(1)腫瘍病理組織でのCD26発現解析と(3)末梢血リンパ球の解析を行った。また、国内第I相臨床試験検体(全9例)の(2)血清中サイトカイン・ケモカインの多項目解析、ならびに国内第II相臨床試験検体(全31例)の(2)血清中可溶性CD26/DPPIV酵素活性値の測定とサイトカイン・ケモカインの多項目解析を行い、CD26抗体の抗腫瘍効果と相関する新規バイオマーカー候補の絞り込みを行った。

最終年度(2020年度)は、国内第I/II相臨床試験検体の合計40例の中で、Partial Response(PR)またはSDが4サイクル(約6ヶ月)以上持続した検体を中心として、これ

までの解析で得られた(1)血清バイオマーカー、及び(2)末梢血リンパ球バイオマーカー解析(3)腫瘍周囲に浸潤する免疫細胞における発現を免疫組織染色によって解析する。国内臨床試験40例中免疫チェックポイント阻害薬PD-1抗体(Nivolumab)無効性が13例含まれておりうち評価可能性11例中Partial Response(PR)が1例、Stable Disease(SD)が7例、Progressive Disease(PD)が2例で72.7%(8/11)がPR、SDであり、CD26抗体が免疫チェックポイント抵抗性患者に有効である可能性が示唆された。そこでヒト化CD26抗体単剤でも有効性を示す結果は得られているが、さらに悪性中皮腫患者に、より長期間抗腫瘍効果を発揮できる現行の単剤療法を改善させるためヒト化CD26抗体とPD-1抗体との併用効果を探る目的でヒト免疫化マウスを用いて(4)悪性中皮腫株JMN担癌モデルを構築してヒト化CD26抗体とPD-1抗体との併用効果を検討した。これにより新規バイオマーカー候補によってCD26抗体療法が有効な患者を判別しうるか明らかにし、安全かつ革新的なCD26抗体療法の確立と抗体療法適用患者の適切な選択を可能とする。

B. 研究方法

各分担研究報告書に著述

(倫理面への配慮)

成人健常者ならびに岡山労災病院、山口宇部医療センターの悪性胸膜中皮腫患者・良性石綿胸水患者の末梢血を用いた研究については、森本が講座責任者である順天堂大学大学院医学研究科、岸本・藤本が勤務する岡山労災病院、青江が勤務する山口宇部医療センターそれぞれの施設で、本研究を行うための研

究計画書等を倫理審査委員会へ提出し、承認を得ている(順大医倫第 2018127 号、岡山労災病院 115 号、山口宇部医療センター29-21 号)。また、ヒト化 CD26 抗体の国内第 I/II 相臨床試験の被験者検体を用いたバイオマーカー探索研究については、キッセイ薬品工業株式会社内の臨床試験審査委員会、各治験実施施設内の治験審査委員会にて、試験の実施と合わせてバイオマーカー探索用採血・腫瘍組織検体の提供について協議され、実施承認を取得済みである。検体の提供を受ける際には、研究対象者に対する人的擁護上の配慮及び研究により研究対象者が受ける不利益、利益等の説明を行い、書面でのインフォームド・コンセントを得ている。

フランスでの第 I 相臨床試験におけるヒトおよびヒト由来の試料を対象とした研究は、世界医師会によって作成された人体実験に関する一連の倫理的原則に従って実施された。血清検体の提供を受ける際には、研究対象者に対する人的擁護上の配慮及び研究により研究対象者が受ける不利益、利益等の説明を行い、書面でのインフォームド・コンセントを得ている。

本研究に必要な動物実験の実施については、「動物の愛護及び管理に関する法律」、「実験動物の飼養及び保管並びに苦痛の軽減に関する基準」(平成 18 年環境省告示第 88 号)、「研究機関等における動物実験等の実施に関する基本指針」(平成 18 年文部科学省告示第 71 号)に基づいて制定された順天堂大学動物実験等管理規則を遵守して行う。実験はいわゆる 3R に基づいて計画し、順天堂大学医学部実験動物委員会に計画書を提出し審議の上、受理されている(承認番号:2020270)。

C. 研究結果

1-a) 国内第 I/II 相臨床試験患者の血清中サイトカイン・ケモカインの多項目解析

第 I/II 相臨床試験全 40 例のうち、血清中バイオマーカー解析の同意を得られたのは 29 例で、うち抗腫瘍効果評価可能例は 25 例であった。今回の第 I/II 相臨床試験では PR が 2 例、long SD が 5 例で、それぞれの症例数が十分ではないため、両者を併せて long SD・PR として解析を行った。Bio-Plex システムによりサイトカイン・ケモカイン 49 種類の多項目測定を行い、抗腫瘍効果評価可能 25 症例を PR・long SD, short SD, PD に分けて解析を行った。その結果、ケモカイン SDF-1 α , β /CXCL12 及び MIP-1d/CCL15 の血清中濃度は、健常者よりも悪性中皮腫患者の方が高く、特に PD 症例で高値を示した一方で、long SD・PR 症例では低値を示す傾向が見られた。また、MCP1/CCL2 は PD 症例及び short SD 症例では CD26 抗体投与により血清中濃度が大幅に上昇したのに対し、long SD・PR 症例では抗体投与後の上昇幅が小さかった。以上の結果から、SDF-1 α , β ・MIP-1d・MCP1 は CD26 抗体治療が特に有効だった PR または long SD となる患者を選択できるバイオマーカー候補である可能性が考えられる。また、ケモカイン Gro-b/CXCL2、CTACK/ CCL27、MCP2/CCL8 の血清中濃度は、健常者よりも悪性中皮腫患者の方が顕著に高く、特に PD 症例で高値を示したが、short SD 症例と long SD・PR 症例では比較的 low 値を示す傾向が見られた。しかしながら、long SD・PR 症例と short SD 症例との間では明白な差は見られなかった。このことから、これらの因子は CD26 抗体が有効ではない PD 症例と、CD26 抗体による抗腫瘍効果が少なくと

も一定期間認められる症例(short SDを含むSD症例及びPR症例)との判別には有用である可能性が期待される。

1-b) 国内第 I/II 相臨床試験患者の血清中可溶性 CD26 値/DPP4 酵素活性値の変動解析

フランスでの第 I 相臨床試験において、SD 症例では PD 症例と比較して可溶性 CD26/DPP4 酵素活性値が有意に低く維持されており ($p < 0.016$)、CD26 抗体投与による血清中可溶性 CD26 値および DPP4 酵素活性の変動解析が、CD26 抗体の治療効果予測バイオマーカーとなる可能性が示された。フランス第 I 相臨床試験では CD26 抗体初回投与直後 (day1post) に可溶性 CD26 値及び DPP4 酵素活性値が顕著に低下し、2 週に 1 度の頻度で CD26 抗体を 2 回目投与する前 (day15pre) の時点では値が部分的に回復した。国内第 I/II 相臨床試験では毎週 1 回投与を行ううゑに投与量もほとんどが 6mg/kg の高容量で、抗体 3 回目投与前 (day15pre) の時点で全ての症例が低値で維持されていた。このことから、抗体投与直後に下がった血清中可溶性 CD26 値/DPP4 酵素活性値の変動(回復)を解析するためには、抗体を毎週 1 回高容量投与するプロトコルでは day2 から day8pre にかけて今回の day15pre よりも早い段階での血清採取が必要であることが予想される。

2) 国内第 I/II 相臨床試験患者の末梢血リンパ球のフェノタイプ解析

次に、末梢血リンパ球に関して、国内第 I/II 相臨床試験患者の末梢血を用いて、フローサイトメトリーによるフェノタイプの比較を行った。末梢血リンパ球に関しては、第 I/II 相計 40 例のうち、バイオマーカー解析の同意を得られたのが 28 例で、うち 24 例は抗腫瘍効果の評価が可能であった。血清

は day1・day15・day29 の time point で解析を行うことができたが、末梢血リンパ球の解析は CD26 抗体初回投与前 1 点のみ解析を行った。まず、末梢血単核球中の CD4 T 細胞・CD4⁺CD25^{high} 制御性 T 細胞・CD8 T 細胞・NK 細胞・単球の細胞数及び割合と、long SD・PR 症例との間に、いずれも特徴的な相関は認められなかった。

次に、細胞傷害性エフェクター T 細胞の割合に着目した。CD26 は健常者の末梢血 CD4 T 細胞、CD8 T 細胞ともに、CD26 高発現 (CD26^{high})・CD26 低発現 (CD26^{low/int})・CD26 陰性 (CD26^{nega}) の三相性の特徴的な発現パターンを示し、それぞれが Naive・Central Memory・Effector Memory・Terminal Effector といった T 細胞の分化段階と密接に関連している (Immunology, 2013)。代表的な T 細胞共刺激分子である CD28 と組み合わせると CD8 T 細胞の CD26/CD28 の発現分布を解析した結果、意外なことに、ほとんどの悪性中皮腫患者の末梢血 CD8 T 細胞は、Terminal Effector を意味する CD26^{nega} CD28^{nega} の割合が非常に高く、健常者と比較して末梢血中の CD8 T 細胞が異常に活性化した状態にあることが示唆された (2018 年度報告書に記載)。血清の解析と同様に、PD、short SD、long SD・PR に分類して解析を行った結果、健常者と比較して悪性中皮腫患者の末梢血 CD8 T 細胞は、細胞傷害性エフェクター T 細胞のマーカーである CD26 陰性・CD28 陰性の割合が顕著に高いが、特に long SD・PR 症例ではその割合が高い傾向が見られた。また、抗原感作マーカーである KLRG1 の陽性率においても、特に long SD・PR 症例ではその割合が高い傾向が見られ、細胞傷害性エフェクター T 細胞マーカーである CD57 の陽性率においても同様の

傾向が見られた。

免疫系に抑制シグナルを伝達するチェックポイント分子には、既に治療薬として承認されている CTLA4, PD1 に加え、現在臨床試験が行われている LAG3、その他 TIM3, TIGIT, BTLA, CD160, 2B4 (CD244) などがある。健常者、悪性中皮腫患者ともに末梢血 CD4 T 細胞・CD8 T 細胞に CTLA4, LAG3, CD160 はほとんど発現しておらず(陽性率 0-3%)、TIM3 と BTLA の発現陽性率も 5%未満と非常に低かった。一方、PD1, TIGIT, 2B4, CD39, CD73 は明確な発現が認められた。

今回の CD26 抗体の国内第 I/II 相臨床試験には、抗ヒト PD1 抗体ニボルマブを投与して無効だったニボルマブ無効例の患者も含まれている。末梢血 CD4 T 細胞・CD8 T 細胞の PD1 陽性率を解析した結果、ニボルマブ投与経験のあるニボルマブ無効例では CD4 T 細胞・CD8 T 細胞ともに PD1 の陽性率が極端に低かった。このことは、今回のフローサイトメトリーの解析に用いた PD1 抗体(clone EH12.2H7)のエピトープがニボルマブのエピトープと重複しているために、PD1 に結合できなかつたか、もしくはニボルマブの投与によって PD1 陽性細胞が減少していたかによるものと考えられる。そこで、PD1 の解析はニボルマブ投与歴のない患者に絞って行った結果、long SD・PR 症例では末梢血 CD4 T 細胞・CD8 T 細胞ともに PD1 陽性率が高い傾向が見られた。TIGIT に関しては、CD4 T 細胞では健常者と悪性中皮腫患者との間で大きな違いは見られなかったが、CD8 T 細胞の TIGIT 陽性率は中皮腫患者の方が健常者よりも高く、特に long SD・PR 症例で高い傾向が見られた。

3) 腫瘍組織に浸潤する免疫細胞

国内臨床試験の病理組織について R&D 社ポリクローナル抗体による免疫染色 (A 法) および新規コンパニオン診断キット (B 法) による CD26 発現検討では B 法による評価が A 法より CD26 発現をより正確に評価できることが明らかになった。今回 CD26 染色標本と HE 染色標本により、中皮腫腫瘍部分へのリンパ球並びに CD26 陽性単核細胞 (リンパ球と単球等) 浸潤について治療効果との比較を行った。細胞浸潤の解析は、半定量的評価 (+1, +2, +3 の 3 段階評価) を行った。その結果、long SD 5 症例中では腫瘍浸潤リンパ球 3+ が 4 症例、+1 が 1 症例であり、治療効果が長い症例では CD26+単核細胞浸潤が多い傾向があった。一方、PD16 症例では、腫瘍浸潤リンパ球が 3+ は 3 症例、+2 は 5 症例、+1 は 8 症例であり、CD26+単核細胞浸潤が少ない傾向が窺われた。

4) ヒト免疫化マウスの作製

ヒト化 CD26 抗体と PD-1 抗体との併用効果を検討するためには、ヒト免疫細胞が生着したヒト免疫化マウスを作製する必要がある。そのためには、重度の免疫不全マウスである NOG マウスに低線量の放射線を照射し、ヒトの造血幹細胞を移植する必要があるが、臨床現場で造血幹細胞移植を行う際にも解凍から移植までの時間は非常に重要と考えられている。ヒト臍帯血 CD34 陽性造血幹細胞を購入している RIKEN BioResource Center が公開しているプロトコルと、NOG マウスを開発した実験動物中央研究所が公開しているプロトコルを比較検討して RIKEN BioResource Center が公開しているプロトコルではヒト T 細胞の発生が安定して確認され、洗浄 buffer や遠心時間を改変した我々が樹立したプロトコルでは検討した全

てのマウスでヒト T 細胞の発生が漏れなく確認された。ヒト造血幹細胞を移植して 10 週間経過するまではマウスの血中のヒト免疫細胞の約 90%が B 細胞(CD20 陽性)で、10 週以降はヒト CD4 T 細胞(CD3 陽性 CD4 陽性)・CD8 T 細胞(CD3 陽性 CD8 陽性)の割合が徐々に増えていき 14 週目ではヒトの血球細胞の約 20%が T 細胞、18 週目では約 30%が T 細胞であることが確認された。このモデルではヒト NK 細胞(CD56 陽性)は 1-2%程度、ヒト単球細胞(CD14 陽性)は約 1%程度であった。悪性中皮腫細胞株 JMN は、in vivo での増殖が非常に遅く、マウスの皮下に移入してから腫瘍を形成するまでに 5-6 週間かかるため、マウス体内でヒト T 細胞の細胞数が増えてくる造血幹細胞移植 13 週目に JMN 細胞株を皮下移入することとした。

5) ヒト化 CD26 抗体と PD-1 抗体との併用効果の検討

JMN 細胞株をヒト免疫化マウスの側腹部に皮下移入して 5 週間経過し、小さな腫瘍形成を確認した時点から、control human IgG1、ヒト化 CD26 抗体単独、mouse anti-human PD-1 mAb (以下、PD-1 抗体)単独、ヒト化 CD26 抗体と PD-1 抗体の併用をそれぞれ 200 μ g/dose で週 3 回投与を続けた。腫瘍サイズを週に 2 回採寸した結果、control 抗体投与群と比較して、CD26 抗体単独(YS alone)、PD-1 抗体単独(PD1 alone)それぞれで腫瘍増殖の抑制が見られたが、両抗体投与群(YS+PD1)ではさらに腫瘍サイズが小さいことが示された。JMN 移入 9 週間後にマウスを解剖し、皮下の腫瘍を回収して一部は病理学的解析を行い、残りは腫瘍内浸潤リンパ球の精製に用いてフェノタイプの解析を行っている。現時点でまだ各群の n 数が少ないが、

解剖する 9 週時点での腫瘍体積および回収した腫瘍重量の両方で、control 群と YS alone 群、または control 群と PD1 alone 群で有意差は認められない一方、control 群と YS+PD1 群で $p < 0.05$ の有意差が認められ(Fisher の多重比較検定)、両抗体の併用効果が期待される。

D. 考察

本年度の解析により、CD26 抗体の予後・治療効果を予測する新規バイオマーカー候補として、血清では SDF-1 α , β /CXCL12・MIP-1d/CCL15・MCP1/CCL2、また、PR・SD 症例と PD 症例とを判別するマーカー候補として、Gro-b/CXCL2・CTACK/CCL27・MCP2/CCL8 を見出した。ケモカインはケモカインレセプターとの関係性が 1 対 1 対応しておらず、1 種類のケモカインが複数のケモカインレセプターに結合することや、複数種類のケモカインが 1 つのケモカインレセプターに結合する関係にあり、細胞遊走活性だけでも非常に複雑で多様な作用が考えられる。今回の解析の結果、CD26 抗体が有効な症例では血清中のこれらのケモカイン濃度がいずれも低値を示しており、今後、これらのケモカインの機能の詳細を調べ、ヒト化 CD26 抗体の作用機序との関係性について考察する必要がある。

がん微小環境に浸潤した T 細胞は、がん細胞自身が産生する免疫抑制性因子や PD1/PDL1・PDL2、CTLA4/CD80・CD86 に代表される免疫チェックポイント分子シグナルによって、エフェクター機能が抑制されていることが様々ながん種で報告されている。悪性中皮腫患者では末梢血 CD8 T 細胞中の細胞傷害性エフェクター T 細胞(CD26 陰性 CD28 陰性

CD57 陽性 KLRG1 陽性)の割合が健常者と比較して明らかに高いことが示された。このような perforin と granzyme を発現する細胞傷害性エフェクター T 細胞は本来、ウイルスに感染した細胞やがん細胞を体内から除去するために働く細胞だが、悪性中皮腫患者の末梢血中にどうして細胞傷害活性を有する T 細胞がこれほど多く存在するのか、何の抗原に対して活性化された T 細胞なのか、アスベストばく露による慢性的な炎症が関係しているのかは興味深い疑問である。免疫チェックポイント分子の中で、悪性中皮腫患者の末梢血 CD8 T 細胞は TIGIT の発現陽性率が健常者よりも明白に高く、long SD・PR 症例では特に PD1 と TIGIT の陽性率が高い傾向が見られた。免疫チェックポイント分子の発現は T 細胞の活性化状態や血清中の TGF- β 濃度などに関係していることが予想される。このような末梢血中の T 細胞のフェノタイプと、悪性中皮腫周囲に浸潤した腫瘍浸潤リンパ球のフェノタイプとの関係性については是非検討したい課題である。

我々の研究結果から新規コンパニオン診断キットによる免疫染色法 (B 法) が中皮腫における CD26 発現をより正確に評価するのに適していると考えられた。

中皮腫腫瘍部分へのリンパ球並びに CD26 陽性単核細胞 (リンパ球と単球等) 浸潤について治療効果との比較では、リンパ球浸潤の程度が強い群で長期の治療効果が得られており、これらの浸潤リンパ球には、CD26 発現リンパ球が含まれており、その浸潤程度も治療効果と相関がある可能性がある。一方、PD16 症例では、腫瘍浸潤リンパ球が CD26+ 単核細胞浸潤が少なく、CD26 陽性単核細胞も少ない傾向が明らかであった。今回の解析

では浸潤リンパ球並びに CD26 陽性単核細胞の分画の詳細は明らかにできなかったが、中皮腫に浸潤しているリンパ球はこれまでの染色結果から、CD4+あるいは CD8+の T リンパ球が主体で、少数の CD68+単球が含まれることが明らかとなっている。また今回、long SD 5 症例中 4 症例では、腫瘍における CD26 発現がそれぞれ 2%, 5%, 5%, 100%であるにもかかわらず、抗体療法の長期間の効果が見られたことと併せると、これらの腫瘍浸潤 CD26+単核細胞へ抗体が作用した可能性がある。本抗体の新たな作用機序の可能性も考慮する必要があるかもしれない。

ヒト化 CD26 抗体の副作用が少ない利点を活かした新たな併用療法を開発するために、ヒト免疫化マウスを用いたヒト悪性中皮腫株担癌モデルにて、ヒト化 CD26 抗体と PD1 抗体との併用効果を検討し、相乗作用が得られた。

CD26 はヒト T 細胞に活性化シグナルを伝達する T 細胞共刺激分子でもあり、ヒト化 CD26 抗体は CD26 のリガンドである caveolin-1 と CD26 との結合、つまりは T 細胞への CD26 共刺激シグナルの伝達をブロックする。一方で、マウス T 細胞の CD26 は共刺激分子として機能しない。T 細胞以外の免疫細胞における CD26 の発現に関しても、ヒトでは T 細胞以外は NKT 細胞で CD26 発現が見られるが、B 細胞や NK 細胞では CD26 はほとんど発現していないのに対し、マウスでは B 細胞でも T 細胞と同等の弱陽性を示す。このように、T 細胞における機能や免疫細胞における発現パターンなどがヒトとマウスとは大きな違いがあるため、免疫系における CD26 の機能解析ではヒト免疫系での解析が不可欠である。ICI が抗腫瘍効果を発揮する

ためには、T細胞を中心とした免疫系の存在が不可欠であることから、ヒト化CD26抗体とICIとの併用効果を検討する実験にはヒト免疫化マウスを用いる必要がある。

CD26の機能の一つに dipeptidyl peptidase 4 (DPP4) 酵素活性があり、近年、マウス担癌モデルにおいて、DPP4 inhibitor (Sitagliptin) をエサと一緒にマウスに食べさせることで、腫瘍免疫が増強し、腫瘍サイズが縮小することが報告された (Nat Immunol. 2015, 2019)。そのメカニズムとして、がん微小環境から産生されるケモカインの中で DPP4 酵素の基質の一つである IP-10/CXCL10 と Eotaxin/CCL11 に着目し、本来は産生されたそれらのケモカインが DPP4 酵素による切断を受けると活性が低下するのに対し、DPP4 inhibitor 摂取により活性が維持されると、レセプターである CXCR3 陽性の CD4 T 細胞、CD8 T 細胞、NK 細胞や CCR3 陽性の好酸球ががん細胞周囲により集積し、腫瘍を攻撃しやすくなる。フランス及び国内のヒト化 CD26 抗体の臨床試験の結果から、CD26 抗体を投与すると血清中の可溶性 CD26 量が低下し、それに伴い DPP4 酵素活性も低下する (Br J Cancer. 2017, 論文投稿中)。このことから、CD26 抗体を投与した場合においても、がん細胞周囲に集積する免疫細胞数の増加が起こる可能性が考えられる。しかしながら、ヒト化 CD26 抗体はヒト CD26 に対する結合親和性が非常に高い一方で、マウス CD26 には結合しない。そのため、今回のヒト免疫化マウスを用いた担癌モデルにおいて、CD26 抗体はヒト T 細胞上の CD26 とヒト腫瘍細胞株上の CD26 には結合するが、マウスの血管内皮細胞や線維芽細胞などにも発現する CD26 には反応できず、そ

れらのマウス CD26 にもヒト CD26 と同様に DPP4 酵素活性があるため、本来のがん患者に CD26 抗体を投与した時のような DPP4 酵素活性低下作用は期待できないと予想される。この点に関しても今後さらなる実験モデルの改善が必要と考えられる。

E. 結論

1) 今年度は国内第 I/II 相臨床試験の最終集計結果を基に、これまでの血清及び末梢血リンパ球のデータの再解析を行い、ヒト化 CD26 抗体の予後・治療効果予測バイオマーカー候補として、SDF-1・MIP-1d・MCP1 を見出し、また補足マーカーとして Gro-b・CTACK・MCP2 を見出した。また、末梢血リンパ球のフェノタイプ解析により、CD26 抗体有効例では特に CD8 T 細胞で細胞傷害性エフェクター T 細胞 (CD26 陰性・CD28 陰性・KLRG1 陽性サブセット) の割合が高く、免疫チェックポイント分子の中で PD1 と TIGIT の発現陽性率が高い可能性を見出した。

2) 臨床試験における悪性中皮腫検体における CD26 発現評価を行い、半定量的解析法を終了し、CD26 抗体療法におけるコンパニオン診断キットの開発に成功した。また中皮腫における腫瘍浸潤リンパ球および腫瘍浸潤 CD26+ 単核細胞が本抗体療法の新たなバイオマーカーとなる可能性が示された。

3) ヒト免疫化マウスにヒト悪性中皮腫細胞株を皮下移入する担癌モデルにおいて、ヒト化 CD26 抗体と PD-1 抗体との併用効果を検討した結果、それぞれの単剤よりも強い腫瘍増殖抑制効果が見られることが示唆された。

F. 健康危険情報

現時点では特記すべき健康危険情報は無い。

G. 今後の展望

本研究課題の遂行により、国内第 I/II 相臨床試験は合計 40 症例で症例数の制約がある中、ヒト化 CD26 抗体の有効性を予測し得るいくつかの興味深いバイオマーカー候補を見出した。今後、CD26 抗体の臨床応用を目指すうえでこれらのバイオマーカー候補が有効性予測に役立つことを期待する。

H. 研究発表

1. 論文発表

- 1) Corridoni D, Antanaviciute A, Gupta T, Fawcner-Corbett D, Aulicino A, Jagielowicz M, Parikh K, Repapi E, Taylor S, Ishikawa D, Hatano R, Yamada T, Xin W, Slawinski H, Bowden R, Napolitani G, Brain O, Morimoto C, Koohy H, Simmons A. Single-cell atlas of colonic CD8⁺ T cells in ulcerative colitis. *Nat Med.* 2020;26(9):1480-1490
- 2) Kaneko Y, Hatano R, Hirota N, Isambert N, Trillet-Lenoir V, You B, Alexandre J, Zalcman G, Valleix F, Podoll T, Umezawa Y, Takao S, Iwata S, Hosono O, Taguchi T, Yamada T, Dang NH, Ohnuma K, Angevin E, Morimoto C. Serum soluble CD26/DPP4 titer variation is a potential prognostic biomarker in cancer therapy with a humanized anti-CD26 antibody. *Biomarker Research* (in press)
- 3) Sumiyoshi M, Kotani Y, Ikuta Y, Suzue K, Ozawa M, Katakai T, Yamada T, Abe T, Bando K, Koyasu S, Kanaho Y, Watanabe T, Matsuda S. Arf1 and Arf6 Synergistically Maintain Survival of T Cells during Activation. *J Immunol.* 2021;206(2):366-375
- 4) Nishikawa A, Suemori T, Aoki R, Suzuki S, Uebayashi K, Miura E, Shimoda M, Yamada T. Appendiceal adenocarcinoma critically diagnosed by fine-needle aspiration cytology: A letter to the editor. *Cytopathology.* 2020; 31: 362-363
- 5) Sasaki H, Saisho Y, Inaishi J, Watanabe Y, Tsuchiya T, Makio M, Sato M, Kitago M, Yamada T, Itoh H. Associations of birth weight and history of childhood obesity with beta cell mass in Japanese adults. *Diabetologia.* 2020; 63(6):1199-1210
- 6) Hotta K, Fujimoto N. Current evidence and future perspectives of immune-checkpoint inhibitors in unresectable malignant pleural mesothelioma. *J Immunother Cancer.* 2020; 8(1): e000461
- 7) Hotta K, Fujimoto N, Kozuki T, Aoe K, Kiura K. Nivolumab for the treatment of unresectable pleural mesothelioma. *Expert Opin Biol Ther.* 2020; 20(2):109-114
- 8) Kishimoto T, Fujimoto N, Mizuhashi K, Kozawa S, Miura M. Retrospective investigation on diagnostic process for benign asbestos pleural effusion (BAPE) using checklist. *J Occup Health.* 2020; 62(1): 12182
- 9) Baas P, Scherpereel A, Nowak AK, Fujimoto N, Peters S, Tsao AS, Mansfield AS, Popat S, Jahan T, Antonia S, Oulkhair Y, Bautista Y, Cornelissen R, Greillier L, Grossi F, Kowalski D, Rodríguez-Cid J, Aanur P, Oukessou A,

- Baudelet C, Zalcman G. First-line nivolumab plus ipilimumab in unresectable malignant pleural mesothelioma (CheckMate 743): a multicentre, randomised, open-label, phase 3 trial. *The Lancet*. 2021; 397(10272):375-386
- 10) Fujimoto N. An appropriate choice for immunotherapy in malignant pleural mesothelioma. *EBio Medicine*. 2020; 62: 103057
- 11) 山田健人 免疫染色の基礎:抗原賦活法、増感法、ラビット抗体. 病理と臨床免疫組織化学. 2020; 38 巻臨時増刊号: 38-42
- H.** 知的財産権の出願・登録状況（予定を含む）
1. 特許取得
発明者: 森本幾夫, 大沼圭, 波多野良, 伊藤匠, 金子有太郎. 発明の名称: 抗癌剤への抵抗性改善剤. 出願日: 2020年6月8日. 出願番号: 特願2020-099449. 出願人: ワイズ・エー・シー株式会社, 学校法人順天堂
 2. 実用新案登録
なし
 3. その他
なし

2. 著書

なし

3. 学会発表

- 1) Komiya E, Hatano R, Itoh T, Honda K, Kamata Y, Toyama S, Moniaga CS, Otsuka H, Takahashi N, Ohnuma K, Tominaga M, Morimoto C, Takamori K. Endomorphin preferentially induces mechanical allodynia under the control of DPP-IV enzyme. The 45th Annual Meeting of the Japanese Society for Investigative Dermatology, web開催, 2020年12月11日
- 2) 古宮栄利子, 富永光俊, 大沼圭, 森本幾夫, 高森健二. 末梢 μ -オピオイドによるアロネーシス制御機構の解明. 第29回国際痒みシンポジウム, web開催, 2021年3月6日

II. 分担研究報告

労災疾病臨床研究事業費補助金

分担研究報告書

ヒト化 CD26 抗体の予後・治療効果予測バイオマーカーの探索：

国内第 I/II 相臨床試験の血清および末梢血リンパ球の解析

研究代表者	森本 幾夫	順天堂大学大学院医学研究科 免疫病・がん先端治療学講座 特任教授
研究分担者	岸本 卓巳	独立行政法人労働者健康安全機構 アスベスト疾患研究・研修センター 所長
研究分担者	山田 健人	埼玉医科大学医学部 病理学 教授
研究協力者	波多野 良	順天堂大学大学院医学研究科 免疫病・がん先端治療学講座 特任助教
研究協力者	金子有太郎	ワイズ・エー・シー株式会社 代表取締役 CEO 近畿大学 客員教授(元)
研究協力者	藤本 伸一	岡山労災病院 腫瘍内科部長
研究協力者	青江 啓介	山口宇部医療センター 腫瘍内科 内科系診療部長

研究要旨

悪性胸膜中皮腫はアスベストばく露によって起こる難治性悪性腫瘍であり、現時点で満足できる治療法はなく、新たな治療法の確立が望まれる。われわれは、新規治療標的分子として悪性胸膜中皮腫に発現する CD26 に着目し、ヒト化 CD26 抗体を開発しフランスにて第 I 相臨床試験を行った。安全性が確認され治療薬としての有効性を示唆する結果も得られ、2017 年から国内で悪性中皮腫に対する第 I/II 相臨床試験を開始した。2019 年中に第 I 相 9 例・第 II 相 31 例(計 40 例)への投与が終了し、結果を集計が完了した。今年度は抗腫瘍効果について最終的な中央判定結果を基に、これまでのデータを再解析(グループ分け)し、CD26 抗体の有効性予測バイオマーカー候補として SDF-1 α , MIP-1d, MCP1 を見出した。また、Gro-b, CTACK, MCP2 も有効性の予測に役立つ可能性が考えられる。血清中の可溶性 CD26 濃度/DPP4 酵素活性の変動解析については、血清検体採取のタイミングを再度検討する必要があることが示された。末梢血リンパ球のフェノタイプ解析により、CD26 抗体有効例では特に CD8 T 細胞で細胞傷害性エフェクター T 細胞(CD26 陰性・CD28 陰性・KLRG1 陽性サブセット)の割合が高く、免疫チェックポイント分子の中で PD1 と TIGIT の発現陽性率が高い可能性を見出した。CD26 抗体の臨床応用を目指すうえでこれらのバイオマーカー候補が有効性予測に役立つことを期待する。

A. 研究目的

悪性胸膜中皮腫はアスベストばく露によ

って起こる胸膜中皮由来の難治性悪性腫瘍である。アスベストばく露から発症までの潜

伏期間は約 30 年とされ、日本を含め中国やインドなどアジア・中東では患者数が今後ますます増加すると考えられている。予後は極めて悪く、手術療法、化学療法、放射線療法などが行われるが、いずれも満足できる治療成績ではなく、新たな治療法の確立が望まれる。われわれは、新規治療標的分子として悪性中皮腫細胞に発現する CD26 に着目し、ヒト化 CD26 抗体を開発してフランスにて悪性中皮腫を中心に First-in-Human 第 I 相臨床試験を行った。Infusion reaction (急性輸注反応)を除いて特記すべき副作用もなく、安全性が確認されるとともに、抗がん剤抵抗性の悪性中皮腫患者 19 例中 10 例が modified RESIST 評価で Stable Disease (SD)となり、そのうち 5 例は 6 ヶ月以上、最長で 399 日 SD が持続し、有効性を示唆する結果も得られた(Br J Cancer. 2017)。

このフランスでの結果を受け、どの患者に CD26 抗体療法が有効なのか、治療効果や予後を予測できるバイオマーカーの探索が課題として挙げられた。このことは、本抗体療法がより安全かつ効果的に行われるうえで極めて重要であり、かつ、抗体療法適用患者を適切に選択できれば期待していた治療効果が得られない患者にまで高額な医療費負担を強いることがなくなり、労災補償行政にも貢献できる。

我々はこれまでにヒト化 CD26 抗体の抗腫瘍作用メカニズムとして、抗体医薬特有の抗体依存性細胞傷害(ADCC)活性に加え、がん細胞の細胞膜上の CD26 に抗体が結合することによる直接的な作用を明らかにしてきた。CD26 に抗体が結合すると、cyclin dependent kinase inhibitor である p21 や p27 の発現が上昇し cell cycle arrest を引き

起こすこと (Clin Cancer Res. 2001, Immunology. 2002, Clin Cancer Res. 2007)、CD26 抗体と CD26 の複合体が細胞膜から細胞質、さらに核内へと移行し、RNA polymerase II のサブユニットである POLR2A 遺伝子の転写領域下流に結合することで POLR2A の転写を抑制し増殖抑制に働くことを明らかにした(PLoS One. 2013)。

また、CD26 はヒト T 細胞に活性化シグナルを伝達する T 細胞共刺激分子でもあり、ヒト化 CD26 抗体は CD26 のリガンドである caveolin-1 と CD26 との結合、つまりは T 細胞への CD26 共刺激シグナルの伝達をブロックする。また、CD26 の機能の一つに dipeptidyl peptidase 4 (DPP4)酵素活性があり、N 末から 2 番目にプロリンまたはアラニンを含むペプチドの 2 アミノ酸を切断する。生体内で様々な生理活性物質がその基質となることが知られているが、いくつかのケモカインも DPP4 による切断を受けその細胞遊走活性が不活性化される。ヒト化 CD26 抗体は DPP4 酵素活性自体に直接は影響しないが、これまでの臨床試験の結果から CD26 抗体の投与により血中の可溶性 CD26 の量が顕著に低下し、それにともない DPP4 酵素活性も同様に低下する (Br J Cancer. 2017)。DPP4 酵素活性が低下すると IP-10(CXCL10)や Eotaxin (CCL11)などのケモカインの切断と不活性化が抑えられ、免疫細胞が腫瘍組織に遊走しやすくなる可能性が考えられる (Nat Immunol. 2015, Nat Immunol. 2019)。これらの知見から、CD26 抗体は免疫系にも影響する可能性が強く示唆される。

そこで、これまでに我々が解明してきた CD26 抗体の抗腫瘍作用メカニズムに基づ

き、本抗体の予後・治療効果予測バイオマーカーを同定するために、2017年7月から本邦で開始した治療抵抗性(標準治療で Progressive Disease (PD))の悪性胸膜中皮腫に対するヒト化 CD26 抗体の第 I/II 相臨床試験患者の(1)中皮腫病理組織、(2)血清、(3)末梢血リンパ球の解析を行う。

本パートでは、(2)血清に関しては、フランスでの第 I 相臨床試験において、CD26 抗体投与による血清中可溶性 CD26 値および DPP4 酵素活性の変動解析が、CD26 抗体の治療効果予測バイオマーカーとなる可能性が示唆され($p < 0.016$)、国内臨床試験でも同様の検証を行った。また、前述のように CD26 抗体は腫瘍免疫にも何かしらの影響があることが予想される。そこで、CD26/DPP4 と関連するサイトカイン・ケモカインの多項目解析を行い、CD26 抗体投与による血清中濃度の変動を解析し、CD26 抗体の有効性との相関関係を解析した。(3)末梢血リンパ球に関しては、末梢血中の CD4 T 細胞・CD8 T 細胞・CD25 強陽性の制御性 CD4 T 細胞の細胞数・割合、CD26 および CXCR3(ケモカイン CXCL10 の受容体)の発現、Perforin や Granzyme 等のがん細胞や感染細胞を除去するための細胞傷害活性を有するエフェクター T 細胞の細胞数・割合、近年着目されている代表的な免疫チェックポイント分子の発現を解析し、CD26 抗体の有効性との相関関係を解析した。

B. 研究方法

1) 国内第 I/II 相臨床試験プロトコル

第 I 相臨床試験はヒト化 CD26 抗体を 2mg/kg, 4mg/kg, 6mg/kg でそれぞれ 3 例ずつ、初回投与日を day1 として day1, day8,

day15, day22, day29 まで週 1 回の間隔で 5 回静脈内投与を行い、投与を開始してから 6 週間後(day42)の時点で医師による抗腫瘍効果の判定が行われ、Partial Response (PR) または SD と判定された患者は、上記の抗体 5 回投与、6 週間後に抗腫瘍効果判定を 1 サイクルとして PD になるまでサイクルを継続した。

第 II 相臨床試験は全 31 例に CD26 抗体を 6mg/kg で週 1 回の間隔で 5 回静脈内投与を行い、上記と同様に抗体 5 回投与、6 週間後に抗腫瘍効果判定を 1 サイクルとして PD になるまでサイクルを継続した。

2) Bio-Plex マルチプレックスアッセイ

成人健常者および国内第 I/II 相臨床試験患者の CD26 抗体初回投与前(day1pre)・投与後(day1post)・3 回目投与前(day15pre)・投与後(day15post)・5 回目投与前(day29pre)・投与後(day29post)の 6 time point で血清の提供を受け、血清中サイトカイン・ケモカイン濃度を Bio-Plex マルチプレックスシステムにより測定した。Bio-Plex Pro Human Chemokine 40-Plex panel および Bio-Plex Pro Human Th17 Cytokine 15-Plex panel (Bio-Rad)を用いて、付属のプロトコルに従い Bio-Plex system (Bio-Rad)で測定を行い、得られたデータを Bio-Plex Manager (Bio-Rad)で解析した。

3) 血清中可溶性 CD26 値と DPP4 酵素活性値の測定

研究代表者森本が開発した、ヒト化 CD26 抗体とはエピトープがそれぞれ異なる mouse anti-human CD26 mAb 2 クローン(clone 5F8 と 9C11)を用いて、sandwich

ELISAによる血清中可溶性 CD26 値の定量と、DPP4 酵素活性値の測定を行った。株式会社新日本科学にて測定した値を解析に用いた。

4) 抗体と試薬

Flow cytometryには下記のヒト抗原特異抗体を用いた。PE-labeled anti-CD26 mAb (clone M-A261)は BD Biosciences から購入した。PE/Cy7-labeled anti-KLRG1 mAb (clone 13F12F2), PE/Cy7-labeled anti-TIGIT mAb (clone MBSA43), APC-labeled anti-KLRG1 mAb (clone 13F12F2), APC-labeled anti-TIGIT mAb (clone MBSA43) 及び APC-labeled anti-LAG3 mAb (clone 3DS223H)は eBioscience から購入した。FITC-labeled anti-CD4 mAb (clone RPA-T4), FITC-labeled anti-CD8 mAb (clone HIT8a), PE/Cy7-labeled anti-CD25 mAb (clone clone M-A251), PE/Cy7-labeled anti-CD28 mAb (clone clone CD28.2), PE/Cy7-labeled anti-CD56 mAb (clone 5.1H11), PE/Cy7-labeled anti-PD1 mAb (clone EH12.2H7), APC-labeled anti-CD28 mAb (clone clone CD28.2), APC-labeled anti-CD57 mAb (clone clone HCD57), APC-labeled anti-CXCR3 mAb (clone G025H7), APC-labeled anti-TRAIL mAb (clone RIK-2), APC-labeled anti-BTLA mAb (clone MIH26), APC-labeled anti-PD1 mAb (clone EH12.2H7), APC-labeled anti-Tim3 mAb (clone F38-2E2)及び抗体の非特異的な結合をブロックするための Human TruStain FcX は BioLegend から購入した。

5) フローサイトメトリー

成人健常者および国内第 I/II 相臨床試験患者から提供を受けた末梢血を、BD Pharm Lyse Lysing Buffer (BD Biosciences)にて溶血処理を行い、洗浄した後、Human TruStain FcX を添加し、続いて蛍光色素で標識した各種抗体を添加して細胞膜上の目的タンパク質の染色を行った。FACS Calibur (BD Biosciences)で測定を行い、得られたデータを FlowJo (BD Biosciences)で解析した。

(倫理面への配慮)

成人健常者の末梢血を用いた研究については、森本が講座責任者である順天堂大学大学院医学研究科で本研究を行うための研究計画書等を倫理審査委員会へ提出し、承認を得ている(順大医倫第 2018127 号)。また、ヒト化 CD26 抗体の国内第 I/II 相臨床試験の患者検体を用いたバイオマーカー探索研究については、臨床試験審査委員会、各治験実施施設内の治験審査委員会にて、試験の実施と合わせてバイオマーカー探索用採血・腫瘍組織検体の提供について協議され、実施承認を取得済みである。末梢血の提供を受ける際には、研究対象者に対する人的擁護上の配慮及び研究により研究対象者が受ける不利益、利益等の説明を行い、書面でのインフォームド・コンセントを得ている。

C. 研究結果

1-a) 国内第 I/II 相臨床試験患者の血清中サイトカイン・ケモカインの多項目解析

本研究課題の目的は、ヒト化 CD26 抗体療法が有効な患者を選択できるバイオマーカーを探索することである。そのために、

CD26 抗体の投与によって PR もしくは SD が長期間持続した症例を区別して解析を行う必要があり、今回の解析では長期間持続のラインを 4 サイクル(24 週間)以上に設定した。つまりは、CD26 抗体投与を開始して 24 週間以上 PR または SD が持続した症例を long SD・PR、SD の持続期間が 6 週間以上 24 週間未満の症例を short SD、抗体投与を開始して 6 週間後の抗腫瘍効果判定で PD だった症例は PD 症例として解析を行った。

第 I 相臨床試験は、第 1~3 コホート各 3 例、全 9 例実施し、うち抗腫瘍効果評価可能例は 6 例で、内訳は PR 1 例、SD 4 例、PD 1 であった(Lung Cancer. 2019)。第 II 相臨床試験は全 31 例実施し、うち抗腫瘍効果評価可能例は 29 例で、内訳は PR 1 例、SD 14 例、PD 14 例であった(論文投稿中)。国内第 I/II 相臨床試験の結果をまとめると、評価可能 35 例中、PR 2 例、long SD 5 例、short SD 13 例、PD 15 例で、PR・SD 率は 57.1% (20/35)であった(表 1)。フランスでの第 I 相臨床試験と同様に、免疫チェックポイント阻害薬で報告されているような自己免疫疾患様の重篤な副作用が出ることなく安全性が確認され、抗腫瘍効果としても有効性を強く示唆する結果が得られた。興味深いことに、国内第 I/II 相臨床試験全 40 例中、13 例は抗 PD-1 抗体ニボルマブ無効例で、その症例に絞って解析した結果、抗腫瘍効果評価可能例は 11 例で、PR 1 例、SD 7 例、PD 3 例、PR・SD 率は 72.7% (8/11)であった。全 40 例と比較して、抗 PD-1 抗体無効例に対しての方が PR・long SD の割合も高く、CD26 抗体は抗 PD-1 抗体無効例に対しても非常に有効であることが示された(表 1)。

表1 国内第I/II相臨床試験(全例)の抗腫瘍効果まとめ

Phase I/II Total 40 cases

	PR	SD(longSD)	PD	NE	Total	PR・SD
Epithelioid	2	14(2)	12	4	32	57.1%(16/28)
Biphasic	0	3(2)	2	0	5	60.0%(3/5)
Sarcomatoid	0	1(1)	1	1	3	50.0%(1/2)
Total	2	18(5)	15	5	40	57.1%(20/35)

※中央判定

13 cases refractory to Nivolumab

not evaluable

	PR	SD(longSD)	PD	NE	Total	PR・SD
Epithelioid	1	6(2)	2	2	11	77.8%(7/9)
Biphasic	0	1(1)	1	0	2	50.0%(1/2)
Sarcomatoid	0	0	0	0	0	
Total	1	7(3)	3	2	13	72.7%(8/11)

※中央判定

第 I/II 相臨床試験全 40 例のうち、血清中バイオマーカー解析の同意を得られたのは 29 例で、うち抗腫瘍効果評価可能例は 25 例であった(表 2)。今回の第 I/II 相臨床試験では PR が 2 例、long SD が 5 例で、それぞれの症例数が十分ではないため、両者を併せて long SD・PR として解析を行った。

表2 国内第I/II相臨床試験 血清解析症例の抗腫瘍効果まとめ

Phase I/II 血清 Total 29 cases (PI 6/9, PII 23/31)

	PR	SD(longSD)	PD	NE	Total
Epithelioid	2	10(2)	8	3	23
Biphasic	0	2(2)	1	0	3
Sarcomatoid	0	1(1)	1	1	3
Total	2	13(5)	10	4	29

※中央判定

血清 10 cases refractory to Nivolumab

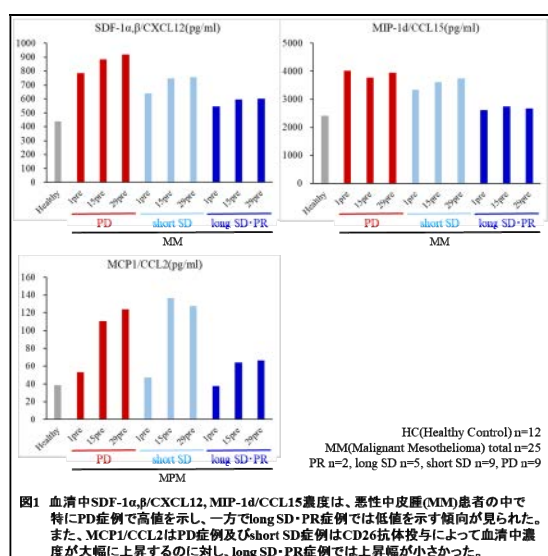
not evaluable

	PR	SD(longSD)	PD	NE	Total
Epithelioid	1	5(2)	1	1	8
Biphasic	0	1(1)	1	0	2
Sarcomatoid	0	0	0	0	0
Total	1	6(3)	2	1	10

※中央判定

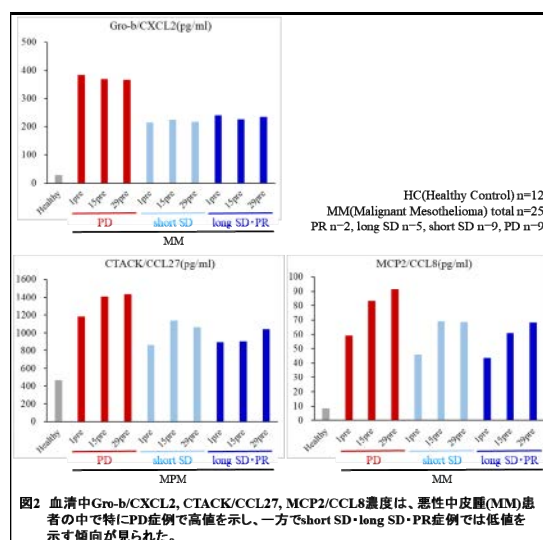
Bio-Plex システムによりサイトカイン・ケモカイン 49 種類の多項目測定を行い、抗腫瘍効果評価可能 25 症例を PR・long SD, short SD, PD に分けて解析を行った。その結果、ケモカイン SDF-1 α,β /CXCL12 及び MIP-1d/CCL15 の血清中濃度は、健常者よりも悪性中皮腫患者の方が高く、特に PD 症例で高値を示した一方で、long SD・PR 症

例では低値を示す傾向が見られた(図 1)。図中には各群の CD26 抗体初回投与前(day1pre)・3回目投与前(day15pre)・5回目投与前(day29pre)の 3 time point の各平均値を示した。また、MCP1/CCL2 は PD 症例及び short SD 症例では CD26 抗体投与により血清中濃度が大幅に上昇したのに対し、long SD・PR 症例では抗体投与後の上昇幅が小さかった。以上の結果から、SDF-1 α,β ・MIP-1d・MCP1 は CD26 抗体治療が特に有効だった PR または long SD となる患者を選択できるバイオマーカー候補である可能性が考えられる。



また、ケモカイン Gro-b/CXCL2、CTACK/CCL27、MCP2/CCL8 の血清中濃度は、健常者よりも悪性中皮腫患者の方が顕著に高く、特に PD 症例で高値を示したが、short SD 症例と long SD・PR 症例では比較的低値を示す傾向が見られた(図 2)。しかしながら、long SD・PR 症例と short SD 症例の間では明白な差は見られなかった。このことから、これらの因子は CD26 抗体が有効ではない PD 症例と、CD26 抗体による抗腫瘍効果が少なくとも一定期間認められる症例

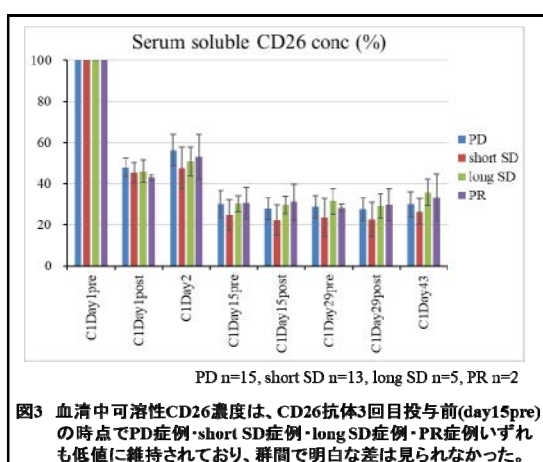
(short SD を含む SD 症例及び PR 症例)との判別には有用である可能性が期待される。



興味深いことに、図 1 中の MCP1 や図 2 中の MCP2 の他にも IL-6 や IL-8 など CD26 抗体初回投与前(day1pre)と比較して 3 回目投与前(day15pre)・5 回目投与前(day29pre)の方が血清中の濃度が明らかに増加しているサイトカイン・ケモカインがあり、反対に CD26 抗体の投与によって血清中の濃度が顕著に減少するサイトカイン・ケモカインも見られた(データ未掲載)。それらの因子は CD26 抗体の抗腫瘍効果を予測できるバイオマーカーとしては有用ではなかったが、CD26 抗体を投与した患者の 7-8 割に共通した変化であり、CD26 抗体が免疫系に与える影響として今後も着目する必要があると思われる。

1-b) 国内第 I/II 相臨床試験患者の血清中可溶性 CD26 値/DPP4 酵素活性値の変動解析
フランスでの第 I 相臨床試験において、SD 症例では PD 症例と比較して可溶性 CD26/DPP4 酵素活性値が有意に低く維持されており($p<0.016$)、CD26 抗体投与によ

る血清中可溶性 CD26 値および DPP4 酵素活性の変動解析が、CD26 抗体の治療効果予測バイオマーカーとなる可能性が示された。そこで、国内第 I/II 相臨床試験の血清検体でも同様の解析を試みたが、フランスでの第 I 相臨床試験とではヒト化 CD26 抗体の投与プロトコル(抗体投与量と投与頻度)が大きく変わっており、フランス第 I 相臨床試験では CD26 抗体初回投与直後(day1post)に可溶性 CD26 値及び DPP4 酵素活性値が顕著に低下し、2 週に 1 度の頻度で CD26 抗体を 2 回目投与する前(day15pre)の時点では値が部分的に回復した。国内第 I/II 相臨床試験では毎週 1 回投与を行ううえに投与量もほとんどが 6mg/kg の高容量で、抗体 3 回目投与前(day15pre)の時点で全ての症例が低値で維持されていた(図 3)。このことから、抗体投与直後に下がった血清中可溶性 CD26 値/DPP4 酵素活性値の変動(回復)を解析するためには、抗体を毎週 1 回高容量投与するプロトコルでは day2 から day8pre にかけて今回の day15pre よりも早い段階での血清採取が必要であることが予想される。



2) 国内第 I/II 相臨床試験患者の末梢血リンパ球のフェノタイプ解析

次に、末梢血リンパ球に関して、国内第 I/II 相臨床試験患者の末梢血を用いて、フローサイトメトリーによるフェノタイプの比較を行った。末梢血リンパ球に関しては、第 I/II 相計 40 例のうち、バイオマーカー解析の同意を得られたのが 28 例で、うち 24 例は抗腫瘍効果の評価が可能であった(表 3)。

表3 国内第I/II相臨床試験リンパ球解析症例の抗腫瘍効果まとめ

Phase I/II 全血(リンパ球) Total 28 cases (PI 5/9, PII 23/31)
not evaluable

	PR	SD(longSD)	PD	NE	Total
Epithelioid	1	10(2)	8	3	22
Biphasic	0	2(2)	1	0	3
Sarcomatoid	0	1(1)	1	1	3
Total	1	13(5)	10	4	28

※中央判定

全血(リンパ球) 10 cases refractory to Nivolumab
not evaluable

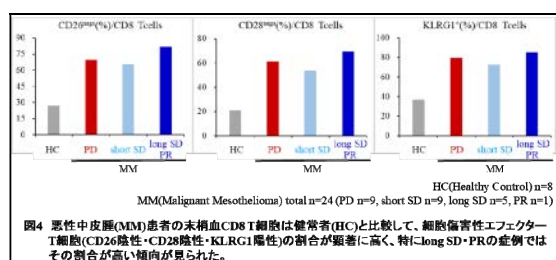
	PR	SD(longSD)	PD	NE	Total
Epithelioid	1	5(2)	1	1	8
Biphasic	0	1(1)	1	0	2
Sarcomatoid	0	0	0	0	0
Total	1	6(3)	2	1	10

※中央判定

血清は day1・day15・day29 の time point で解析を行うことができたが、末梢血リンパ球の解析は CD26 抗体初回投与前 1 点のみ解析を行った。まず、末梢血単核球中の CD4 T 細胞・CD4+CD25^{high} 制御性 T 細胞・CD8 T 細胞・NK 細胞・単球の細胞数及び割合と、long SD・PR 症例との間に、いずれも特徴的な相関は認められなかった(データ未掲載)。

次に、細胞傷害性エフェクター T 細胞の割合に着目した。CD26 は健常者の末梢血 CD4 T 細胞、CD8 T 細胞ともに、CD26 高発現(CD26^{high})・CD26 低発現(CD26^{low/int})・CD26 陰性(CD26^{nega})の三相性の特徴的な発現パターンを示し、それぞれが Naive・Central Memory・Effector Memory・Terminal Effector といった T 細胞の分化段階と密接

に関係している(Immunology. 2013)。代表的な T 細胞共刺激分子である CD28 と組み合わせると CD8 T 細胞の CD26/CD28 の発現分布を解析した結果、意外なことに、ほとんどの悪性中皮腫患者の末梢血 CD8 T 細胞は、Terminal Effector を意味する CD26^{neg}CD28^{neg} の割合が非常に高く、健常者と比較して末梢血中の CD8 T 細胞が異常に活性化された状態にあることが示唆された(2018 年度報告書に記載)。血清の解析と同様に、PD、short SD、long SD・PR に分類して解析を行った結果、健常者と比較して悪性中皮腫患者の末梢血 CD8 T 細胞は、細胞傷害性エフェクター T 細胞のマーカーである CD26 陰性・CD28 陰性の割合が顕著に高いが、特に long SD・PR 症例ではその割合が高い傾向が見られた(図 4)。また、抗原感作マーカーである KLRG1 の陽性率においても、特に long SD・PR 症例ではその割合が高い傾向が見られ(図 4)、細胞傷害性エフェクター T 細胞マーカーである CD57 の陽性率においても同様の傾向が見られた(データ未掲載)。



免疫系に抑制シグナルを伝達するチェックポイント分子には、既に治療薬として承認されている CTLA4, PD1 に加え、現在臨床試験が行われている LAG3、その他 TIM3, TIGIT, BTLA, CD160, 2B4(CD244)、また、ATP を分解してアデノシンを産生する酵素活性を有する CD39, CD73 などがある。健

常者、悪性中皮腫患者ともに末梢血 CD4 T 細胞・CD8 T 細胞に CTLA4, LAG3, CD160 はほとんど発現しておらず(陽性率 0-3%)、TIM3 と BTLA の発現陽性率も 5%未満と非常に低かった(データ未掲載)。一方、PD1, TIGIT, 2B4, CD39, CD73 は明確な発現が認められた(データ未掲載)。

今回の CD26 抗体の国内第 I/II 相臨床試験には、抗ヒト PD1 抗体ニボルマブを投与して無効だったニボルマブ無効例の患者も含まれている。末梢血 CD4 T 細胞・CD8 T 細胞の PD1 陽性率を解析した結果、ニボルマブ投与経験のあるニボルマブ無効例では CD4 T 細胞・CD8 T 細胞ともに PD1 の陽性率が極端に低かった(図 5)。このことは、今回のフローサイトメトリーの解析に用いた PD1 抗体(clone EH12.2H7)のエピトープがニボルマブのエピトープと重複しているために、PD1 に結合できなかつたか、もしくはニボルマブの投与によって PD1 陽性細胞が減少していたかによるものと考えられる。そこで、PD1 の解析はニボルマブ無効例を除いたニボルマブ投与歴のない患者に絞って行った結果、long SD・PR 症例では末梢血 CD4 T 細胞・CD8 T 細胞ともに PD1 陽性率が高い傾向が見られた(図 5)。TIGIT に関しては、CD4 T 細胞では健常者と悪性中皮腫患者との間で大きな違いは見られなかつたが、CD8 T 細胞の TIGIT 陽性率は中皮腫患者の方が健常者よりも高く、特に long SD・PR 症例で高い傾向が見られた(図 5)。今回の第 I/II 相臨床試験では CD26 抗体投与前 1 点での末梢血リンパ球のフェノタイプ解析しか行えなかつたが、今後、末梢血 CD8 T 細胞の細胞傷害性エフェクター T 細胞の割合、CD4 T 細胞の PD1 陽性率、CD8

T 細胞の PD1 と TIGIT の陽性率に着目し、CD26 抗体投与後の変動にも着目して解析を行いたい。

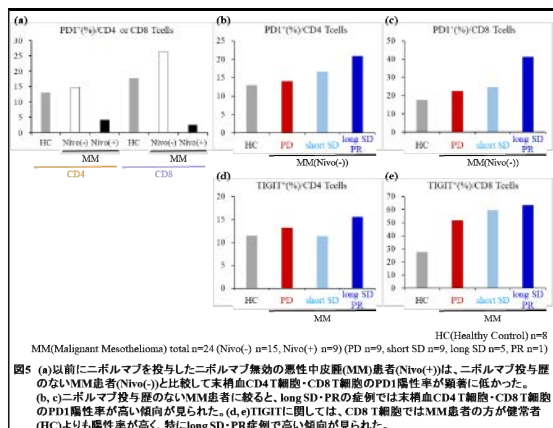


図5 (a)以前にニボルマブを投与したニボルマブ無効の悪性中皮腫(MM)患者(Nivo(+))は、ニボルマブ投与歴のないMM患者(Nivo(-))と比較して末梢血CD4 T細胞・CD8 T細胞のPD1陽性率が顕著に低かった。(b, c)ニボルマブ投与歴のないMM患者に較べ、long SD・PRの症例では末梢血CD4 T細胞・CD8 T細胞のPD1陽性率が高い傾向が見られた。(d, e)TIGITに関しては、CD8 T細胞ではMM患者の方が健康者(HC)よりも陽性率が高く、特にlong SD・PR症例で高い傾向が見られた。

D. 考察

ヒト化 CD26 抗体の予後・治療効果予測バイオマーカーを開発するために、抗腫瘍効果について最終的な中央判定結果を基に、これまでの血清及び末梢血リンパ球のデータの再解析(グループ分け)を行った。

ヒト化 CD26 抗体の予後・治療効果を予測可能なバイオマーカーを探索するために、CD26 抗体の投与によって PR もしくは SD が長期間持続した症例を区別して解析を行う必要があり、今回の解析では長期間持続のラインを 4 サイクル(24 週間)以上に設定した。このラインに絶対的な正当性はなく、無増悪生存期間(Progression-Free Survival: PFS)等の全ての臨床試験結果が公開された後には、有効性についての総合的な評価がより望ましいと考えられる。

本年度の解析により、CD26 抗体の予後・治療効果を予測する新規バイオマーカー候補として、血清では SDF-1 α , β /CXCL12・MIP-1d/CCL15・MCP1/CCL2、また、PR・SD 症例と PD 症例とを判別するマーカー候補として、Gro-b/CXCL2・CTACK/CCL27・

MCP2/CCL8 を見出した。ケモカインはケモカインレセプターとの関係性が 1 対 1 対応しておらず、1 種類のケモカインが複数のケモカインレセプターに結合することや、複数種類のケモカインが 1 つのケモカインレセプターに結合する関係にあり、細胞遊走活性だけでも非常に複雑で多様な作用が考えられる。また、細胞遊走以外の機能が報告されているものも存在する。SDF-1 α , β /CXCL12 は CXCR4 と CXCR7 のリガンドであり、リンパ球遊走の他に、白血球活性化や癌増殖、転移促進、血管新生等の機能が報告されている。MIP-1d/CCL15 は CCR1 と CCR3 のリガンドであり、好中球・単球・リンパ球遊走機能が報告されている。MCP1/CCL2 は CCR2 と CCR4 のリガンドであり、単球・T 細胞・樹状細胞を炎症部位に集積させ、その他に単球の活性化作用等も報告されている。今回の解析の結果、CD26 抗体が有効な症例では血清中のこれらのケモカイン濃度がいずれも低値を示しており、今後、これらのケモカインの機能の詳細を調べ、ヒト化 CD26 抗体の作用機序との関係性について考察する必要がある。

今回解析に用いた Bio-Plex システムは sandwich ELISA とフローサイトメトリーの技術を応用した実験手法であり、ELISA では最終的に酵素反応により生成した基質の発色を吸光度で測定するが、Bio-Plex は蛍光色素 PE を用いて検量線と各サンプルの蛍光強度から濃度を算出する。Bio-Plex は一度に多種類の抗体を mix したアッセイ方法であるため、sandwich ELISA で個別に測定を行い、結果の再現性を確認する必要があるが、酵素反応による比色定量と蛍光強度による濃度換算の違いから、Bio-Plex シ

ステムの方が ELISA よりも測定感度が高く、sandwich ELISA ではほとんどの血清サンプルが検出限界未満になってしまうものも多く、測定方法の更なる検討が必要である。

がん微小環境に浸潤した T 細胞は、がん細胞自身が産生する免疫抑制性因子や PD1/PDL1・PDL2、CTLA4/CD80・CD86 に代表される免疫チェックポイント分子シグナルによって、エフェクター機能が抑制されていることが様々ながん種で報告されている。悪性中皮腫患者では末梢血 CD8 T 細胞中の細胞傷害性エフェクター T 細胞(CD26 陰性 CD28 陰性 CD57 陽性 KLRG1 陽性)の割合が健常者と比較して明らかに高いことが示された(図 4)。このような perforin と granzyme を発現する細胞傷害性エフェクター T 細胞は本来、ウイルスに感染した細胞やがん細胞を体内から除去するために働く細胞だが、悪性中皮腫患者の末梢血中にどうして細胞傷害活性を有する T 細胞がこれほど多く存在するのか、何の抗原に対して活性化された T 細胞なのか、アスベストばく露による慢性的な炎症が関係しているのかは興味深い疑問である。免疫チェックポイント分子の中で、悪性中皮腫患者の末梢血 CD8 T 細胞は TIGIT の発現陽性率が健常者よりも明白に高く、long SD・PR 症例では特に PD1 と TIGIT の陽性率が高い傾向が見られた(図 5)。免疫チェックポイント分子の発現は T 細胞の活性化状態や血清中の TGF- β 濃度などと関係していることが予想される。このような末梢血中の T 細胞のフェノタイプと、悪性中皮腫周囲に浸潤した腫瘍浸潤リンパ球のフェノタイプとの関係性については是非検討したい課題だが、今回の臨床試験では提供された病理組織の標本数が非常に限

られており、今後の検討課題としたい。

E. 結論

今年度は国内第 I/II 相臨床試験の最終集計結果を基に、これまでの血清及び末梢血リンパ球のデータの再解析を行い、ヒト化 CD26 抗体の予後・治療効果予測バイオマーカー候補として、SDF-1・MIP-1d・MCP1 を見出し、また補足マーカーとして Gro- β ・CTACK・MCP2 を見出した。また、末梢血リンパ球のフェノタイプ解析により、CD26 抗体有効例では特に CD8 T 細胞で細胞傷害性エフェクター T 細胞(CD26 陰性・CD28 陰性・KLRG1 陽性サブセット)の割合が高く、免疫チェックポイント分子の中で PD1 と TIGIT の発現陽性率が高い可能性を見出した。

F. 今後の展望

本研究課題の遂行により、国内第 I/II 相臨床試験は合計 40 症例で症例数の制約がある中、ヒト化 CD26 抗体の有効性を予測し得るいくつかの興味深いバイオマーカー候補を見出した。今後、CD26 抗体の臨床応用を目指すうえでこれらのバイオマーカー候補が有効性予測に役立つことを期待する。

G. 研究発表

1. 論文発表

- 1) Corridoni D, Antanaviciute A, Gupta T, Fawcner-Corbett D, Aulicino A, Jagielowicz M, Parikh K, Repapi E, Taylor S, Ishikawa D, Hatano R, Yamada T, Xin W, Slawinski H, Bowden R, Napolitani G, Brain O, Morimoto C, Koohy H, Simmons A. Single-cell atlas of colonic CD8⁺ T cells

in ulcerative colitis. Nat Med.

2020;26(9):1480-1490

- 2) Kaneko Y, Hatano R, Hirota N, Isambert N, Trillet-Lenoir V, You B, Alexandre J, Zalcmán G, Valleix F, Podoll T, Umezawa Y, Takao S, Iwata S, Hosono O, Taguchi T, Yamada T, Dang NH, Ohnuma K, Angevin E, Morimoto C. Serum soluble CD26/DPP4 titer variation is a potential prognostic biomarker in cancer therapy with a humanized anti-CD26 antibody. Biomarker Research (in press)

発明者: 森本幾夫, 大沼圭, 波多野良, 伊藤匠, 金子有太郎. 発明の名称: 抗癌剤への抵抗性改善剤. 出願日: 2020年6月8日. 出願番号: 特願2020-099449. 出願人: ワイズ・エー・シー株式会社, 学校法人順天堂

2. 実用新案登録
なし
3. その他
なし

2. 著書

なし

3. 学会発表

- 1) Komiya E, Hatano R, Itoh T, Honda K, Kamata Y, Toyama S, Moniaga CS, Otsuka H, Takahashi N, Ohnuma K, Tominaga M, Morimoto C, Takamori K. Endomorphin preferentially induces mechanical allodynia under the control of DPP-IV enzyme. The 45th Annual Meeting of the Japanese Society for Investigative Dermatology, web開催, 2020年12月11日
- 2) 古宮栄利子, 富永光俊, 大沼圭, 森本幾夫, 高森健二. 末梢 μ -オピオイドによるアロネーシス制御機構の解明. 第29回国際痒みシンポジウム, web開催, 2021年3月6日

H. 知的財産権の出願・登録状況 (予定を含む)

1. 特許取得

厚生労働科学研究費補助金（労災疾病臨床研究事業）

分担研究報告書

悪性胸膜中皮腫におけるCD26発現評価とヒト化CD26抗体療法における予後・治療効果予測バイオマーカーの開発

研究分担者 山田 健人 埼玉医科大学 病理学・教授

研究分担者 岸本 卓巳 独立行政法人労働者健康安全機構
アスベスト疾患研究・研修センター 所長

研究協力者 藤本 伸一 岡山労災病院アスベスト疾患ブロックセンター・副センター長

研究協力者 青江 啓介 国立病院機構山口宇部医療センター・内科系診療部長

研究協力者 波多野 良 順天堂大学・医学研究科・免疫病・がん先端治療学講座
特任助教

研究要旨

悪性胸膜中皮腫に対する抗CD26抗体療法の国内第I/II相臨床試験において、中皮腫病理検体として、第I相は9例中6例、第II相では、31例全例の計37症例（組織型は、上皮型29例、二相型5例、肉腫型3例）が収集された。昨年、R&D社ポリクローナル抗体による免疫染色（フランスでの治験と同一、A法）および新規開発されたコンパニオン診断キットによる免疫染色（B法）の二つの染色方法によりCD26発現について検討し、A法よりもB法でCD26陽性率が上昇した症例が36例中23例あり、その中で陽性率が20%以上上昇した症例が11例認められたことを報告した。そこで、CD26染色の感度が上がったB法による検討とHE染色標本により、中皮腫腫瘍部分へのリンパ球並びにCD26陽性単核細胞（リンパ球と単球等）浸潤について治療効果との比較を試みた。その結果、long SD 5症例中では腫瘍浸潤リンパ球3+が4症例、+1が1症例であり、治療効果が長い症例ではCD26+単核細胞浸潤が多い傾向があった。一方、PD16症例では、腫瘍浸潤リンパ球が3+は3症例、+2は5症例、+1は8症例であり、CD26+単核細胞浸潤が少ない傾向が窺われた。これらの結果は、中皮腫においてリンパ球浸潤およびCD26陽性単核細胞の半定量評価が治療効果予測のバイオマーカーとなる可能性を示唆する。また本抗体療法が腫瘍浸潤しているCD26+単核細胞へも影響があるか否か検討が必要と考えられ

A. 研究目的

フランスで施行されたヒト化CD26抗体療法の第I相臨床試験では、特記すべき有害事象なく、26症例中13症例で「安定」(Stable Disease;SD)への導入が可能であり、安全性のみならず、その腫瘍効果も期

待される成果が得られた(Br J Cancer 116:1126-1134, 2017)。本邦でも2017年7月から第I相臨床試験がスタートし(第1~3コホート各3例)、2018年3月に終了、9例中8例が評価可能でPartial Response(PR)1例、SD5例と有効性も示

唆された。6月からスタートした第II相臨床試験は、2019年10月時点で31例が終了している。そこで本研究においては、まず悪性中皮腫症例におけるCD26発現を詳細に明らかにし、標的分子としてどのような発現パターンを示すのかを明らかにし、CD26抗体療法の治療効果との相関を明らかにするための基礎的検討を行った。またCD26発現は現在用いられているアリムタ、シスプラチンなど化学療法剤の治療効果予測バイオマーカーとしても有望な結果を得て報告(Clin Cancer Res 18:1447, 2012)してきたが、さらに今回、CD26発現を細胞局在、陽性率、陽性強度など様々な要素で解析し、各種の臨床パラメーターとの相関を明らかにすることで、バイオマーカーとなりうるかどうかを検討することを目的とした。またCD26染色標本とHE染色標本により、中皮腫腫瘍部分へのリンパ球並びにCD26陽性単核細胞(リンパ球と単球等)浸潤について治療効果との比較を行った。

B. 研究方法

CD26の発現解析には、ヒト組織としてホルマリン固定したパラフィン切片(CD26陽性である正常ヒト腎、肝、前立腺及び悪性中皮腫の組織および肺)および生検や手術材料を用いた。抗原賦活化として、オートクレーブ処置(120℃、20分、0.01M Citrate Buffer pH8.0)を行い、二次抗体は、Peroxidase付加抗ラビットIgG抗体(ImmPRESS社製)を用い、発色は、DAB液(Simple Stain DAB, Histofine)を用いた。国内第I/II相臨床試験(YS1101、キッセイ薬品工業株式会社)における悪性中皮腫37症例症例の腫瘍の病理組織(生検及び手術材料、10%ホルマリン固定、パラフィン切片)について、CD26の免疫染色を行った。抗原賦活化は、オートクレーブ処置

(120℃、20分、0.01M Citrate Buffer pH8.0)を行った。抗CD26抗体は、私の臨床試験で使用したR&D社製抗CD26ヤギ・ポリクロナール抗体(Lot.No. JOQ107061)を用いた。二次抗体は、Peroxidase付加抗ヤギIgG抗体(ImmPRESS社製)あるいはPeroxidase付加抗マウスIgG抗体(ImmPRESS社製)を用い、発色は、DAB液(Simple Stain DAB, Histofine)を用いた。いずれの染色においても、陽性対照には、正常ヒト腎、肝、前立腺及び悪性中皮腫を用い、陰性対照には、これらの正常組織切片内の各種組織(平滑筋、脂肪組織、結合組織など)とCD26陰性肺癌組織を用いた。

新規コンパニオン診断キットは、一次抗体は私の臨床試験で使用したR&D社製抗CD26ヤギ・ポリクロナール抗体で同一であるが、抗原賦活化試薬や条件をキット用に開発・至適化しており、二次抗体や発色試薬も改良を加えた(ニチレイバイオサイエンス株式会社との共同研究)。スクリーニングはFFPE切片(CD26陽性である正常ヒト腎、肝、前立腺及び悪性中皮腫の組織および肺)の免疫染色により行い、至適化されたプロトコルを用いて中皮腫検体の染色を行なった。CD26染色標本とHE染色標本での腫瘍部分へのリンパ球並びにCD26陽性単核細胞(リンパ球と単球等)浸潤について、半定量解析(+1, +2, +3の3段階評価)を行った。

(倫理面への配慮)

患者検体などについては研究対象者に対する人権擁護上の配慮及び研究により研究対象者が受ける不利益、利益等の説明を患者及び遺族に対して行い、書面でのインフォームド・コンセントを得ている。また病理組織について免疫染色してCD26発現を解析する研究については、埼玉医科大学の倫理審査委員会にて承認されている

(承認番号 794, 861)。

C. 研究結果

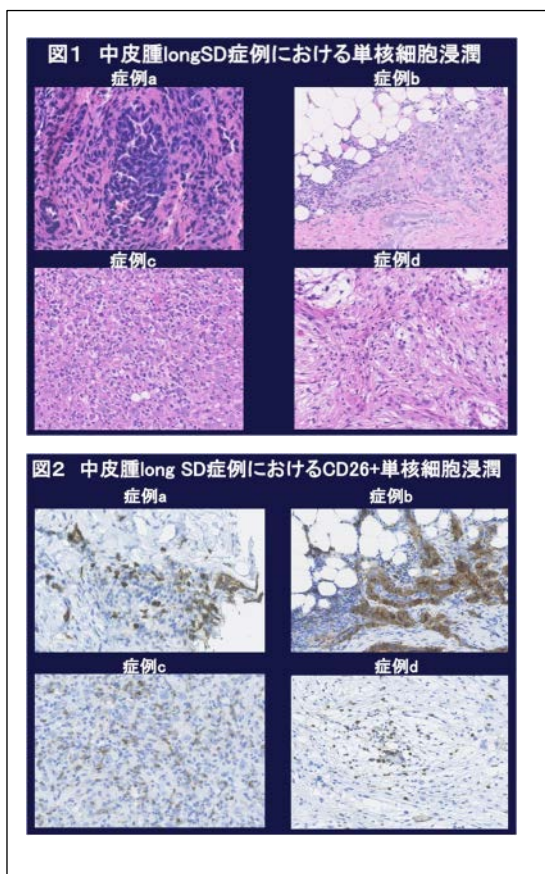
国内第 I/II 相臨床試験 (第 I 相は 9 例中 6 例、第 II 相では 31 例全例) における悪性中皮腫 37 症例について、病理組織像および R&D 社ポリクローナル抗体による免疫染色 (フランスでの治験と同一の方法、A 法) および新規コンパニオン診断キット

(B 法) による CD26 発現について検討した。37 症例の組織型は、上皮型 29 例、二相型 5 例、肉腫型 3 例であった。なお 37 例中 1 例は腫瘍細胞が数個のみであったため評価対象外とし、36 例の検体で CD26 発現の評価を行なった。A 法での結果では、CD26 発現は、上皮型で 5%以下 1 例、5%~50% 3 例、50%~70% 11 例、70%~100% 13 例であり、二相型では、2%、12%、20%、70%がそれぞれ 1 例、肉腫型では 2%、5%、50%がそれぞれ 1 例であった。これらの症例の中で CD26 発現と YS110 治療効果の関係をみると、Stable disease (SD) 以上の効果が見られた上皮型の症例は陽性率が 30%であったが、二相型と肉腫型では陽性率が 1%、2%の症例にも SD が認められた。症例数が少ないため、組織型および CD26 発現と YS110 効果との統計学的な有意な相関関係は明らかではないが、CD26 陽性率と治療効果には一定の傾向は明らかではなかった。これらの染色標本をデジタル画像とし、imageProPlus プログラムにて詳細に半定量的に発現解析を行った。その結果、CD26 は細胞膜および細胞質に 95%が、核内に 1-2%の発現が認められた。

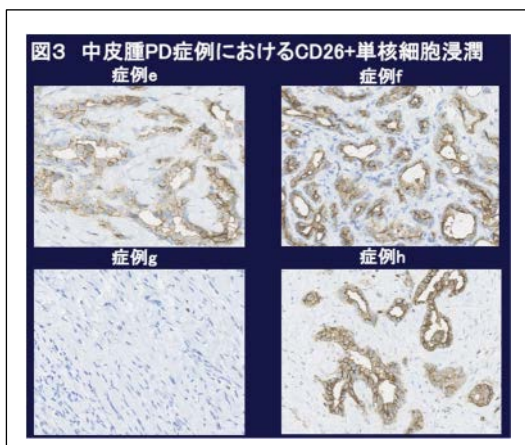
また FFPE 臨床検体における CD26 発現評価のために新規開発した B 法と上記 A 法との比較を行った。その結果、A 法での CD26 陽性率が 20%以上の症例は、37 例中 30 例、20%未満の症例が 6 例であったのに対して、B 法では 20%以上の症例は、37 例中 32 例、20%未満の症例が 4 例であっ

た。それぞれの組織型における CD26 陽性率 20%以上の症例は、上皮型 29 例中 A 法 B 法ともに 27 例、二相型 5 例中 A 法 2 例、B 法 3 例、肉腫型 3 例中 A 法 1 例、B 法 2 例であった。また A 法よりも B 法で CD26 陽性率が上昇した症例は 36 例中 23 例であり、その中で陽性率が 20%以上上昇した症例が 11 例認められた (図 2)。また正常ヒト組織、特に肝臓や腎臓において、B 法において A 法よりも鮮明な染色結果が得られる組織が確認された。

また CD26 染色標本と HE 染色標本により、中皮腫腫瘍部分へのリンパ球並びに CD26 陽性単核細胞 (リンパ球と単球等) 浸潤について治療効果との比較を行った。細胞浸潤の解析は、半定量的評価 (+1, +2, +3 の 3 段階評価) を行った。その結果、long SD 5 症例中では腫瘍浸潤リンパ球 3+ が 4 症例 (図 1)、+1 が 1 症例であり、治療効果が長い症例では CD26+単核細胞浸潤が多い傾向があった (図 2)。



一方、PD16 症例では、腫瘍浸潤リンパ球が 3+は 3 症例、+2 は 5 症例、+1 は 8 症例であり、CD26+単核細胞浸潤が少ない傾向が窺われた (図 3)。



D. 考察

これらの結果および正常ヒト組織での CD26 染色性の向上から、この新規コンパニオン診断キットによる免疫染色法 (B 法) が中皮腫における CD26 発現をより正確に評価するのに適していると考えられた。

中皮腫腫瘍部分へのリンパ球並びに CD26 陽性単核細胞 (リンパ球と単球等) 浸潤について治療効果との比較では、リンパ球浸潤の程度が強い群で長期の治療効果が得られており、これらの浸潤リンパ球には、CD26 発現リンパ球が含まれており、その浸潤程度も治療効果と相関がある可能性がある。一方、PD16 症例では、腫瘍浸潤リンパ球が CD26+単核細胞浸潤が少なく、CD26 陽性単核細胞も少ない傾向が明らかであった。今回の解析では、臨床試験へ提供されたスライド標本に限りがあり、浸潤リンパ球並びに CD26 陽性単核細胞の分画の詳細は明らかにできなかったが、中皮腫に浸潤しているリンパ球はこれまでの染色結果から、CD4+あるいは CD8+の T リンパ球が主体で、少数の CD68+単球が含まれ

ることが明らかとなっている。また今回、long SD 5 症例中 4 症例では、腫瘍における CD26 発現がそれぞれ 2%, 5%, 5%, 100%であるにもかかわらず、抗体療法の長期間の効果が見られたことと併せると、これらの腫瘍浸潤 CD26+単核細胞へ抗体が作用した可能性がある。本抗体の新たな作用機序の可能性も考慮する必要があるかもしれない。

今後は、これらの CD26 陽性率と YS110 療法の効果や既存の治療法や各種臨床パラメーターとの相関について解析し、組織型とともに発現パターン (細胞局在、陽性率、陽性強度などの各種パラメーター) を詳細に定量評価することにより、抗体療法の効果や予後などの関連性あるいは臨床パラメーターを検証する基礎を構築していくことが重要と考える。

E. 結論

臨床試験における悪性中皮腫検体における CD26 発現評価を行い、半定量的解析法を終了し、CD26 抗体療法におけるコンパニオン診断キットの開発に成功した。また中皮腫における腫瘍浸潤リンパ球および腫瘍浸潤 CD26+単核細胞が本抗体療法の新たなバイオマーカーとなる可能性が示された。

G. 研究発表

1. 論文発表

- 1) Sumiyoshi M, Kotani Y, Ikuta Y, Suzue K, Ozawa M, Katakai T, Yamada T, Abe T, Bando K, Koyasu S, Kanaho Y, Watanabe T, Matsuda S. Arf1 and Arf6 Synergistically Maintain Survival of T Cells during Activation. J Immunol. 206(2):366-375, 2021
- 2) Corridoni D, Antanaviciute A, Gupta T, Fawcner-Corbett D, Aulicino

A, Jagielowicz M, Parikh K, Repapi E, Taylor S, Ishikawa D, Hatano R, Yamada T, Xin W, Slawinski H, Bowden R, Napolitani G, Brain O, Morimoto C, Koohy H, Simmons A. Single-cell atlas of colonic CD8+ T cells in ulcerative colitis. Nat Med. 26(9):1480-1490, 2020

3) Nishikawa A, Suemori T, Aoki R, Suzuki S, Uebayashi K, Miura E, Shimoda M, Yamada T. Appendiceal adenocarcinoma critically diagnosed by fine-needle aspiration cytology: A letter to the editor. Cytopathology. 31: 362-363, 2020

4) Sasaki H, Saisho Y, Inaishi J, Watanabe Y, Tsuchiya T, Makio M, Sato M, Kitago M, Yamada T, Itoh H. Associations of birth weight and history of childhood obesity with beta cell mass in Japanese adults. Diabetologia. 63(6):1199-1210, 2020

5) 山田健人 免疫染色の基礎：抗原賦活法、増感法、ラビット抗体 病理と臨床 38 巻臨時増刊号 免疫組織化学 pp38-42 2020年4月1日 文光堂

3. その他
なし

2. 学会発表
なし

H. 知的財産権の出願・登録状況（予定を含む）

1. 特許
なし

2. 実用新案登録
なし

労災疾病臨床研究事業費補助金
分担研究報告書

ヒト化 CD26 抗体を用いた悪性中皮腫に対する新たな併用療法の開発

研究代表者	森本 幾夫	順天堂大学大学院医学研究科 免疫病・がん先端治療学講座 特任教授
研究分担者	岸本 卓巳	独立行政法人労働者健康安全機構 アスベスト疾患研究・研修センター 所長
研究分担者	山田 健人	埼玉医科大学医学部 病理学 教授
研究協力者	波多野 良	順天堂大学大学院医学研究科 免疫病・がん先端治療学講座 特任助教
研究協力者	大沼 圭	順天堂大学大学院医学研究科 免疫病・がん先端治療学講座 准教授
研究協力者	金子有太郎	ワイズ・エー・シー株式会社 代表取締役 CEO 近畿大学 客員教授(元)

研究要旨

悪性胸膜中皮腫はアスベストばく露によって起こる難治性悪性腫瘍であり、現時点で満足できる治療法はなく、新たな治療法の確立が望まれる。われわれは、新規治療標的分子として悪性胸膜中皮腫に発現する CD26 に着目し、ヒト化 CD26 抗体を開発した。フランスにて悪性中皮腫を中心とした第 I 相臨床試験を実施し、国内でも悪性中皮腫に対する第 I/II 相臨床試験を実施した。2019 年中に第 II 相臨床試験の最終患者への投与が終了し、今年度結果の集計が完了した。安全性が確認され、フランスでの第 I 相臨床試験と同等の有効性を示唆する結果も得られた。治療抵抗性の悪性中皮腫患者に対して、CD26 抗体単剤でも高い割合で **Stable Disease・Partial Response** となり抗腫瘍効果は認められたが、より長期間抗腫瘍効果を発揮し、無増悪生存期間を与えられる本抗体を用いた新たな併用療法の開発も重要な課題である。そこで、ヒト免疫化マウスを用いたヒト悪性中皮腫細胞株担がんモデルを確立し、ヒト化 CD26 抗体と PD-1 抗体との併用効果を検討した結果、それぞれの単剤よりも強い相乗効果が認められる予備実験データを得た。今後、抗腫瘍作用メカニズムをより詳細に解析し、併用療法に関しても臨床試験へ繋げることを目指す。

A. 研究目的

悪性胸膜中皮腫はアスベストばく露によって起こる胸膜中皮由来の難治性悪性腫瘍である。アスベストばく露から発症までの潜

伏期間は約 30 年とされ、日本を含め中国やインドなどアジア・中東では患者数が今後ますます増加すると考えられている。予後は極めて悪く、手術療法、化学療法、放射線療法

などが行われるが、いずれも満足できる治療成績ではなく、新たな治療法の確立が望まれる。われわれは、新規治療標的分子として悪性中皮腫細胞に発現する CD26 に着目し、ヒト化 CD26 抗体を開発してフランスにて悪性中皮腫を中心に First-in-Human 第 I 相臨床試験を行った。Infusion reaction (急性輸注反応)を除いて特記すべき副作用もなく、安全性が確認されるとともに、抗がん剤抵抗性の悪性中皮腫患者 19 例中 10 例が modified RESIST 評価で Stable Disease (SD)となり、そのうち 5 例は 6 ヶ月以上、最長で 399 日 SD が持続し、有効性を示唆する結果も得られた(Br J Cancer. 2017)。

本邦でも抗がん剤抵抗性の悪性中皮腫に対する第 I/II 相臨床試験を実施し、第 I 相は 1~3 コホート各 3 例ずつの計 9 例、第 II 相は 31 例に投与を行い、2019 年中に第 II 相の最終患者への投与が終了した。第 I/II 相で計 40 例に投与を行い、うち抗腫瘍効果を評価可能だったのが 35 例で、内訳は Partial Response (PR) 2 例・SD 18 例・Progressive Disease (PD) 15 例で、PR・SD 率は 57.1% (20/35)で抗がん剤抵抗性の悪性中皮腫患者に対して高い割合で抗腫瘍効果が認められるも、完全奏功(Complete Response: CR)はなく、また、比較的短い期間で SD から PD となった患者もいたことから、より長期間抗腫瘍効果を発揮し、無増悪生存期間を与えられる本抗体を用いた新たな併用療法の開発も重要な課題である。

我々はこれまでにヒト化 CD26 抗体の抗腫瘍作用メカニズムとして、抗体医薬特有の抗体依存性細胞傷害(ADCC)活性に加え、がん細胞の細胞膜上の CD26 に抗体が結合することによる直接的な増殖抑制作用を明ら

かにしてきた(Clin Cancer Res. 2001, Immunology. 2002, Clin Cancer Res. 2007, PLoS One. 2013)。また、近年の知見から CD26 抗体は免疫系にも影響する可能性が強く示唆され(Nat Immunol. 2015, Nat Immunol. 2019)、ヒト化 CD26 抗体は多様なメカニズムを介して抗腫瘍効果を発揮していると考えられる。特記すべきは、国内第 I/II 相臨床試験 40 例の中には PD-1 抗体 Nivolumab 無効例が 13 例含まれており、そのうち 11 例が抗腫瘍効果を評価可能で、PR 1 例・SD 7 例・PD 3 例で 72.7% (8/11)が PR・SD であり、このことから CD26 抗体は免疫チェックポイント阻害薬(ICI)抵抗性の患者にも有効であること、ICI とは異なるメカニズムで抗腫瘍効果を発揮することが強く示唆された。

そこで、副作用が非常に少ない CD26 抗体の利点を活かした他の分子標的薬、特に ICI との併用療法を開発すべく、ヒト化 CD26 抗体と PD-1 抗体との併用効果を検討した。ICI が抗腫瘍効果を発揮するためには T 細胞を中心とした免疫細胞が不可欠であり、マウスに同系のマウス腫瘍株を移入する担癌モデルがよく用いられる。一方で、CD26 抗体が抗腫瘍効果を発揮するためにはヒト CD26 分子上の結合部位も重要であり(Clin Cancer Res. 2007)、ヒトとマウスとでは免疫系における CD26 の機能も大きく異なることから(Immunol Rev. 1998)、ヒト化 CD26 抗体のデータ取得にはヒト腫瘍株並びにヒト免疫系での解析が必須である。以上の理由から、ヒト免疫化マウスを作製し、このマウスを用いた悪性中皮腫株担がんモデルにおいてヒト化 CD26 抗体と PD-1 抗体との併用効果を検討した。

B. 研究方法

1) 細胞

ヒト悪性中皮腫細胞株 JMN は、10% FBS を添加した RPMI1640 培地中で 37°C, 5% CO₂ 環境下で培養した。ヒト臍帯血 CD34 陽性造血幹細胞は RIKEN BioResource Center から購入した。

2) マウス

NOD/Shi-scid, IL-2R γ KO Jic (NOD.Cg-Prkdc^{scid} Il2rg^{tm1Sug/ShiJic})マウス(以下、NOG マウス)は In-Vivo Science Inc.から購入した。マウスは順天堂大学の specific pathogen free (SPF)施設で飼育した。

3) 抗体と試薬

Flow cytometry には下記のヒト抗原特異抗体を用いた。BUV395-labeled anti-CD56 mAb (clone NCAM16.2)及び PE-labeled anti-CD26 mAb (clone M-A261)は BD Biosciences から購入した。Brilliant Violet 421-labeled anti-CD4 mAb (clone RPA-T4), Brilliant Violet 510-labeled anti-CD14 mAb (clone M5E2), FITC-labeled anti-CD8 mAb (clone HIT8a), PerCP/Cy5.5-labeled anti-CD20 mAb (clone 2H7), APC-labeled anti-CD45 mAb (clone HI30), APC/Fire 750-labeled anti-CD3 mAb (clone SK7)及び Brilliant Violet 605-labeled anti-mouse CD45 mAb (clone 30-F11)及び抗体の非特異的な結合をブロックするための Human TruStain FcX, TruStain FcX (anti-mouse CD16/32)は BioLegend から購入した。また、Brilliant Violet 同士の非特異的な結合を抑えるため

の Brilliant Stain Buffer plus は BD Biosciences から購入した。

4) ヒト免疫化マウスを用いた担癌モデル

NOG マウスに低線量(100cGy)の放射線照射を行い、翌日ヒト臍帯血 CD34 陽性造血幹細胞 1x10⁵ cells を尾静脈内から移入した。経時的にマウス尾静脈から採血を行い、ヒト免疫細胞の生着を確認した。ヒト造血幹細胞を移植して 13 週後に、JMN 細胞の細胞懸濁液と Matrigel を 1:1 混合して 1 匹あたり 1x10⁶ cells ずつ側腹部に皮下移入した。JMN を皮下移入して 5 週間経過し、小さな腫瘍形成を確認した時点から、control human IgG1 (Bio X Cell), ヒト化 CD26 抗体 (Y's AC Co., Ltd) 単独, mouse anti-human PD-1 mAb (Bio X Cell; clone J116) 単独, ヒト化 CD26 抗体と PD-1 抗体の併用をそれぞれ 200 μ g/dose で週 3 回投与を続けた。腫瘍サイズは週に 2 回採寸し、JMN 移入後 9 週間後にマウスを解剖し、皮下の腫瘍を回収して重量を測定した。腫瘍の一部は病理解析のために 10%ホルマリンで固定し、残りは Liberase TL Research Grade (Roche) 0.25mg/ml で酵素処理を行い、DNase I (Roche)存在下で組織を破碎して腫瘍組織中の細胞を得た。腫瘍内浸潤リンパ球の解析では、MagniSort Human CD3 Positive Selection Kit (invitrogen) 及び EasySep Magnet (STEMCELL)を用いてリンパ球精製を行った。また、腫瘍内浸潤リンパ球との性質比較のために、脾臓のリンパ球解析も行った。

5) フローサイトメトリー

マウス体内のヒト免疫細胞の生着を確認

するために、マウスの尾静脈から採血して得た末梢血を、Human と Mouse に対する TruStain FcX を両方添加し、蛍光色素標識抗体で染色した後、BD FACS Lysing Solution (BD Biosciences)にて溶血と固定処理を行い、洗浄した後、BD LSRFortessa (BD Biosciences)で測定を行い、得られたデータを FlowJo (BD Biosciences)で解析した。

(倫理面への配慮)

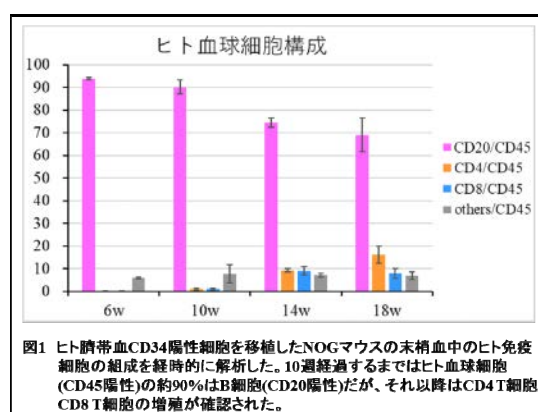
ヒト臍帯血 CD34 陽性造血幹細胞を用いた研究については、森本が講座責任者である順天堂大学大学院医学研究科で本研究を行うための研究計画書等を倫理審査委員会へ提出し、承認を得ている(順大医倫第2017167号)。動物実験の実施はいわゆる 3R に基づいて行い、順天堂大学医学部実験動物委員会に実験計画書を提出し審議の上、承認されている(承認番号: 2020270)。

C. 研究結果

1) ヒト免疫化マウスの作製

ヒト化 CD26 抗体と PD-1 抗体との併用効果を検討するためには、ヒト免疫細胞が生着したヒト免疫化マウスを作製する必要がある。そのためには、重度の免疫不全マウスである NOG マウスに低線量の放射線を照射し、ヒトの造血幹細胞を移植する必要があるが、臨床現場で造血幹細胞移植を行う際にも解凍から移植までの時間は非常に重要と考えられている。ヒト臍帯血 CD34 陽性造血幹細胞を購入している RIKEN BioResource Center が公開しているプロトコルと、NOG マウスを開発した実験動物中央研究所が公開しているプロトコルでは、洗浄 buffer や洗浄(遠心)回数、遠心時間などに

違いがあり、安定してヒト免疫細胞が生着するプロトコルの検討を行った。その結果、実験動物中央研究所が公開しているプロトコルでは、ヒト B 細胞は安定して生着するもののヒト T 細胞が移植後 20 週経過しても発生してこない問題があることが明らかになった(データ未掲載)。一方で、RIKEN BioResource Center が公開しているプロトコルではヒト T 細胞の発生が安定して確認され、洗浄 buffer や遠心時間を改変した我々が樹立したプロトコルでは検討した全てのマウスでヒト T 細胞の発生が漏れなく確認された。ヒト造血幹細胞を移植して 10 週間経過するまではマウスの血中のヒト免疫細胞の約 90%が B 細胞(CD20 陽性)で、10 週以降はヒト CD4 T 細胞(CD3 陽性 CD4 陽性)・CD8 T 細胞(CD3 陽性 CD8 陽性)の割合が徐々に増えていき 14 週目ではヒトの血球細胞の約 20%が T 細胞、18 週目では約 30%が T 細胞であることが確認された(図 1)。このモデルではヒト NK 細胞(CD56 陽性)は 1-2%程度、ヒト単球細胞(CD14 陽性)は約 1%程度であった(データ未掲載)。

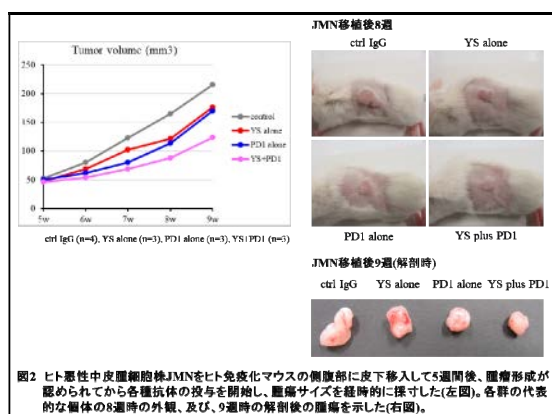


悪性中皮腫細胞株 JMN は、in vivo での増殖が非常に遅く、マウスの皮下に移入してから腫瘍を形成するまでに 5-6 週間かかるた

め、マウス体内でヒト T 細胞の細胞数が増えてくる造血幹細胞移植 13 週目に JMN 細胞株を皮下移入することとした。

2) ヒト化 CD26 抗体と PD-1 抗体との併用効果の検討

JMN 細胞株をヒト免疫化マウスの側腹部に皮下移入して 5 週間経過し、小さな腫瘍形成を確認した時点から、control human IgG1, ヒト化 CD26 抗体単独, mouse anti-human PD-1 mAb (以下、PD-1 抗体) 単独, ヒト化 CD26 抗体と PD-1 抗体の併用をそれぞれ 200 μ g/dose で週 3 回投与を続けた。腫瘍サイズを週に 2 回採寸した結果、control 抗体投与群と比較して、CD26 抗体単独(YS alone)、PD-1 抗体単独(PD1 alone)それぞれで腫瘍増殖の抑制が見られたが、両抗体投与群(YS+PD1)ではさらに腫瘍サイズが小さいことが示された(図 2)。



JMN 移入 9 週間後にマウスを解剖し、皮下の腫瘍を回収して一部は病理学的解析を行い、残りは腫瘍内浸潤リンパ球の精製に用いてフェノタイプの解析を行っている。現時点でまだ各群の n 数が少ないが、解剖する 9 週時点での腫瘍体積および回収した腫瘍重量の両方で、control 群と YS alone 群、ま

たは control 群と PD1 alone 群で有意差は認められない一方、control 群と YS+PD1 群で $p < 0.05$ の有意差が認められ(Fisher の多重比較検定)、両抗体の併用効果が期待される。

今後、各群の n 数をさらに増やすとともに、腫瘍内浸潤リンパ球のフェノタイプ解析、腫瘍の病理学的解析を行い、CD26 抗体と PD1 抗体との抗腫瘍作用メカニズムの違いについてより詳細に解析し、併用効果の有効性を実証する。

D. 考察

ヒト化 CD26 抗体の副作用が少ない利点を活かした新たな併用療法を開発するために、ヒト免疫化マウスを用いたヒト悪性中皮腫株担癌モデルにて、ヒト化 CD26 抗体と PD1 抗体との併用効果を検討した。

CD26 はヒト T 細胞に活性化シグナルを伝達する T 細胞共刺激分子でもあり、ヒト化 CD26 抗体は CD26 のリガンドである caveolin-1 と CD26 との結合、つまりは T 細胞への CD26 共刺激シグナルの伝達をブロックする。一方で、マウス T 細胞の CD26 は共刺激分子として機能しない。また、CD26 の発現に関しても、ヒト T 細胞では CD26 は強陽性・弱陽性・陰性の三相性パターンを示すのに対し、マウス T 細胞は一律に弱陽性である。T 細胞以外の免疫細胞における CD26 の発現に関しても、ヒトでは T 細胞以外は NKT 細胞で CD26 発現が見られるが、B 細胞や NK 細胞では CD26 はほとんど発現していないのに対し、マウスでは B 細胞でも T 細胞と同等の弱陽性を示す。このように、T 細胞における機能や免疫細胞における発現パターンなどがヒトとマウスとでは大きな違いがあるため、免疫系における

CD26 の機能解析ではヒト免疫系での解析が不可欠である。ICI が抗腫瘍効果を発揮するためには、T 細胞を中心とした免疫系の存在が不可欠であることから、ヒト化 CD26 抗体と ICI との併用効果を検討する実験にはヒト免疫化マウスを用いる必要がある。

しかしながら、ヒト免疫化マウスを用いた担癌モデルでは、問題点も存在する。一つは、マウスに同種同系(syngeneic)のマウス腫瘍細胞株を移入する担癌モデルでは、免疫系と腫瘍との MHC が合致しており、ヒトのがん患者と同様にがん抗原特異的な免疫応答を解析することができる。一方で、ヒト免疫化マウスを用いた研究では、免疫細胞がヒト臍帯血造血幹細胞由来の HLA を発現しているのに対し、ヒト腫瘍細胞株は通常その HLA とは異なる HLA を発現しているため、同種異系(allogeneic)の T 細胞応答を見ることになり、本来のがん抗原特異的な応答とは異なることが考えられる。また、ヒト免疫細胞の組成に関しても、今回のモデルではヒト T 細胞と B 細胞に関してはマウス体内で十分な生着が認められるが、一方でヒト NK 細胞や抗原提示細胞の生着率は非常に低い。この問題を解決するために、ヒト IL-15 など特定の遺伝子を強制発現させた NOG マウスなども開発・市販されているが、場合によってはそれらのマウスでの検討も必要になると考えられる。

また、CD26 の機能の一つに dipeptidyl peptidase 4 (DPP4)酵素活性があり、近年、マウス担癌モデルにおいて、DPP4 inhibitor (Sitagliptin)をエサと一緒にマウスに食べさせることで、腫瘍免疫が増強し、腫瘍サイズが縮小することが報告された(Nat Immunol. 2015, 2019)。そのメカニズムと

して、がん微小環境から産生されるケモカインの中で DPP4 酵素の基質の一つである IP-10/CXCL10 と Eotaxin/CCL11 に着目し、本来は産生されたそれらのケモカインが DPP4 酵素による切断を受けると活性が低下するのに対し、DPP4 inhibitor 摂取により活性が維持されると、レセプターである CXCR3 陽性の CD4 T 細胞、CD8 T 細胞、NK 細胞や CCR3 陽性の好酸球ががん細胞周囲により集積し、腫瘍を攻撃しやすくなる。フランス及び国内のヒト化 CD26 抗体の臨床試験の結果から、CD26 抗体を投与すると血清中の可溶性 CD26 量が低下し、それに伴い DPP4 酵素活性も低下する(Br J Cancer. 2017, 論文投稿中)。このことから、CD26 抗体を投与した場合においても、がん細胞周囲に集積する免疫細胞数の増加が起こる可能性が考えられる。しかしながら、ヒト化 CD26 抗体はヒト CD26 に対する結合親和性が非常に高い一方で、マウス CD26 には結合しない。そのため、今回のヒト免疫化マウスを用いた担癌モデルにおいて、CD26 抗体はヒト T 細胞上の CD26 とヒト腫瘍細胞株上の CD26 には結合するが、マウスの血管内皮細胞や線維芽細胞などにも発現する CD26 には反応できず、それらのマウス CD26 にもヒト CD26 と同様に DPP4 酵素活性があるため、本来のがん患者に CD26 抗体を投与した時のような DPP4 酵素活性低下作用は期待できないと予想される。この点に関しても今後さらなる実験モデルの改善が必要と考えられる。

E. 結論

ヒト免疫化マウスにヒト悪性中皮腫細胞株を皮下移入する担癌モデルにおいて、ヒト

化CD26抗体とPD-1抗体との併用効果を検討した結果、それぞれの単剤よりも強い腫瘍増殖抑制効果が見られることが示唆された。

F. 今後の展望

今後、各群の n 数をさらに増やすとともに、腫瘍内浸潤リンパ球のフェノタイプ解析、腫瘍の病理学的解析を行い、CD26 抗体とPD1 抗体との抗腫瘍作用メカニズムの違いについてより詳細に解析し、併用効果の有効性を実証する。また、腫瘍を皮下移入するモデルの他に、より悪性中皮腫のモデルに近い胸腔内移入モデルにおいても併用効果の有効性を検討する。

G. 研究発表

1. 論文発表

- 1) Corridoni D, Antanaviciute A, Gupta T, Fawcner-Corbett D, Aulicino A, Jagielowicz M, Parikh K, Repapi E, Taylor S, Ishikawa D, Hatano R, Yamada T, Xin W, Slawinski H, Bowden R, Napolitani G, Brain O, Morimoto C, Koohy H, Simmons A. Single-cell atlas of colonic CD8⁺ T cells in ulcerative colitis. *Nat Med*. 2020;26(9):1480-1490
- 2) Kaneko Y, Hatano R, Hirota N, Isambert N, Trillet-Lenoir V, You B, Alexandre J, Zalcman G, Valleix F, Podoll T, Umezawa Y, Takao S, Iwata S, Hosono O, Taguchi T, Yamada T, Dang NH, Ohnuma K, Angevin E, Morimoto C. Serum soluble CD26/DPP4 titer variation is a potential prognostic biomarker in cancer therapy with a humanized anti-CD26 antibody. *Biomarker Research* (in press)

2. 著書

なし

3. 学会発表

- 1) Komiya E, Hatano R, Itoh T, Honda K, Kamata Y, Toyama S, Moniaga CS, Otsuka H, Takahashi N, Ohnuma K, Tominaga M, Morimoto C, Takamori K. Endomorphin preferentially induces mechanical allodynia under the control of DPP-IV enzyme. The 45th Annual Meeting of the Japanese Society for Investigative Dermatology, web 開催, 2020 年 12 月 11 日
- 2) 古宮栄利子, 富永光俊, 大沼圭, 森本幾夫, 高森健二. 末梢 μ -オピオイドによるアロネーシス制御機構の解明. 第 29 回国際痒みシンポジウム, web 開催, 2021 年 3 月 6 日

H. 知的財産権の出願・登録状況（予定を含む）

1. 特許取得

発明者: 森本幾夫, 大沼圭, 波多野良, 伊藤匠, 金子有太郎. 発明の名称: 抗癌剤への抵抗性改善剤. 出願日: 2020 年 6 月 8 日. 出願番号: 特願 2020-099449. 出願人: ワイズ・エー・シー株式会社, 学校法人順天堂

2. 実用新案登録

なし

3. その他

なし

Ⅲ. 研究成果の刊行に関する一覧表

研究成果の刊行に関する一覧表

雑誌

発表者氏名	論文タイトル名	発表誌名	巻号	ページ	出版年
Corridoni D, Antanaviciute A, Gupta T, Fawcner-Corbett D, Aulicino A, Jagielowicz M, Parikh K, Repapi E, Taylor S, Ishikawa D, Hatanano R, Yamada T, Xin W, Slawinski H, Bowden R, Napolitani G, Brain O, Morimoto C, Kohy H, Simmons A	Single-cell atlas of clonal CD8 ⁺ T cells in ulcerative colitis.	Nat Med.	26(9)	1480-1490	2020
Kaneko Y, Hatanano R, Hirota N, Isambert N, Trillet-Lenoir V, You B, Alexandre J, Zalcman G, Valleix F, Podoll T, Umezawa Y, Takao S, Iwata S, Hosono O, Taguchi T, Yamada T, Dang NH, Ohnuma K, Angevin E, Morimoto C	Serum soluble CD26/DPP4 titer variation is a potential prognostic biomarker in cancer therapy with a humanized anti-CD26 antibody.	Biomarker Research			(in press)
Sumiyoshi M, Kotani Y, Ikuta Y, Suzue K, Ozawa M, Katakai T, Yamada T, Abe T, Bando K, Koyasu S, Kanaho Y, Watanabe T, Matsuda S	Arf1 and Arf6 Synergistically Maintain Survival of T Cells during Activation.	J Immunol.	206(2)	366-375	2020
Nishikawa A, Suehara T, Aoki R, Suzuki S, Uebayashi K, Miura E, Shimoda M, Yamada T	Appendiceal adenocarcinoma critically diagnosed by fine-needle aspiration cytology: A letter to the editor.	Cytopathology.	31	362-363	2020

発表者氏名	論文タイトル名	発表誌名	巻号	ページ	出版年
Sasaki H, Saisho Y, Inaishi J, Watanabe Y, Tsuchiya T, Makiyama M, Sato M, Kitago M, Yamada T, Itoh H	Associations of birth weight and history of childhood obesity with beta cell mass in Japanese adults.	Diabetologia	63(6)	1199-1210	2020
Hotta K, Fujimoto N	Current evidence and future perspectives of immune-checkpoint inhibitors in unresectable malignant pleural mesothelioma.	J Immunother Cancer.	8(1)	E000461	2020
Hotta K, Fujimoto N, Kozuki T, Aoe K, Kiura K.	Nivolumab for the treatment of unresectable pleural mesothelioma.	Expert Opin Biol Ther.	20(2)	109-114	2020
Kishimoto T, Fujimoto N, Mizuhashi K, Koza S, Miura M.	Retrospective investigation on diagnostic process for benign asbestos pleural effusion (BAPE) using checklist.	J Occup Health.	62(1):	12182	2020
Baas P, Scherpereel A, Nowak AK, Fujimoto N, Peters S, Tsao AS, Mansfield AS, Popat S, Jahan T, Antonia S, Oulkhair Y, Bautista Y, Cornelissen R, Greillier L, Grossi F, Kowalski D, Rodríguez-Cid J, Aanur P, Oukessou A, Baudelet C, Zalcman G.	First-line nivolumab plus ipilimumab in unresectable malignant pleural mesothelioma (CheckMate 743): a multicentre, randomised, open-label, phase 3 trial.	The Lancet.	S0140-6736(20)	32714-8	2021
Fujimoto N.	An appropriate choice for immunotherapy in malignant pleural mesothelioma.	EBio Medicin	62	103057	2020
山田 健人	免疫染色の基礎: 抗原賦活法、増感法、ラビット抗体	病理と臨床免疫組織化学	38巻臨時増刊号	38-42	2020

IV. 研究成果の別刷



Single-cell atlas of colonic CD8⁺ T cells in ulcerative colitis

Daniele Corridoni^{1,2,10}, Agne Antanaviciute^{1,3,10}, Tarun Gupta^{1,2,10}, David Fawkner-Corbett^{1,2}, Anna Aulicino^{1,2}, Marta Jagielowicz^{1,2}, Kaushal Parikh^{1,2}, Emmanouela Repapi⁴, Steve Taylor⁴, Dai Ishikawa⁵, Ryo Hatano⁶, Taketo Yamada⁷, Wei Xin⁸, Hubert Slawinski⁹, Rory Bowden⁹, Giorgio Napolitani¹, Oliver Brain², Chikao Morimoto⁶, Hashem Koohy^{1,3}✉ and Alison Simmons^{1,2}✉

Colonic antigen-experienced lymphocytes such as tissue-resident memory CD8⁺ T cells can respond rapidly to repeated antigen exposure. However, their cellular phenotypes and the mechanisms by which they drive immune regulation and inflammation remain unclear. Here we compiled an unbiased atlas of human colonic CD8⁺ T cells in health and ulcerative colitis (UC) using single-cell transcriptomics with T-cell receptor repertoire analysis and mass cytometry. We reveal extensive heterogeneity in CD8⁺ T-cell composition, including expanded effector and post-effector terminally differentiated CD8⁺ T cells. While UC-associated CD8⁺ effector T cells can trigger tissue destruction and produce tumor necrosis factor (TNF)- α , post-effector cells acquire innate signatures to adopt regulatory functions that may mitigate excessive inflammation. Thus, we identify colonic CD8⁺ T-cell phenotypes in health and UC, define their clonal relationships and characterize terminally differentiated dysfunctional UC CD8⁺ T cells expressing IL-26, which attenuate acute colitis in a humanized IL-26 transgenic mouse model.

The pathology of inflammatory bowel diseases (IBDs), such as UC, involves immune-mediated tissue destruction secondary to a combination of barrier dysfunction, genetic risk and dysbiosis. The colonic lamina propria houses a vast quantity of tissue-resident CD8⁺ T cells that may contribute to tissue damage in IBD^{1,2}. Despite evidence of CD8⁺ T-cell contribution to IBD pathology³, the extent of heterogeneity, transcriptional regulation and effector function of distinct populations has not been investigated in an unbiased manner. Furthermore, their connections, hierarchy and how they may dynamically remodel to influence inflammation in IBD remain unclear. Here we conduct multimodal single-cell profiling of CD8⁺ cells from the human colon in health and UC, defining T-cell changes in active disease; we link this with coupled T-cell receptor (TCR) analysis to define the functional interrelationship of identified cell states and their crosstalk with epithelial cell subtypes.

Results

Topology of human colonic CD8⁺ T-cell states. We initially profiled colonic single CD8⁺ T cells from three healthy volunteers and three patients with UC using droplet-based, single-cell RNA sequencing (scRNA-seq) (Fig. 1a and Supplementary Fig. 1a,b; patient characteristics shown in Supplementary Table 1a). Following quality control (Methods), we compiled gene expression data from 8,581 cells for clustering analyses (Supplementary Fig. 1c–f). This revealed 14 CD8⁺ cell populations that were visualized as uniform manifold approximation and projection (UMAP) embeddings (Fig. 1b). Population nomenclature was designated by specific gene expression, identifying naïve, memory, tissue-resident memory

(T_{RM}), effector and double-positive (DP) CD8⁺CD4⁺ cells, as well as populations with innate-like features including mucosal-associated invariant T cells (MAITs), intraepithelial lymphocytes (IELs) and IL26⁺-expressing CD8⁺ cells (Fig. 1c,d, Supplementary Table 2 and Extended Data Fig. 1).

We further investigated cluster-specific gene signatures by performing Gene Ontology (GO)⁴ enrichment analysis (Fig. 1e), followed by area-under-the-receiving operating characteristic analysis (Methods). We found localized activity of the IL-17 pathway in DP and IL26⁺ cells; similarly, IEL clusters and some IL26⁺ cells were highly enriched for natural killer (NK) pathways. (Fig. 1f). Thus, our analysis charts the extent of the heterogeneity within colonic CD8⁺ T cells, including IL26⁺ cells with hybrid innate and adaptive features and DP regulatory CD8⁺ T cells.

Dynamic restructuring of colonic CD8⁺ T cells in UC. We observed marked changes in CD8⁺ population structures in UC; for example, T_{RM}-like T cells constituted on average 45% of all cells recovered in health but only ~10% of CD8⁺ cells in UC. Other populations affected included activated effector T cells and IL26⁺ cells, with the latter comprising ~18% (up to 29%) of all CD8⁺ cells recovered in UC. We also observed an increase in the DP CD4⁺CD8⁺FOXP3⁺ cell population, reduced natural TYROBP⁺ and expanded induced TYROBP⁺ IELs⁵ (Fig. 2a).

Furthermore, within these subpopulations, we identified 997 differentially expressed genes (DEGs) (Fig. 2b and Extended Data Fig. 2a). GO enrichment analysis of upregulated genes highlighted strong signatures for both type I and type II interferon responses,

¹Medical Research Council (MRC) Human Immunology Unit, MRC Weatherall Institute of Molecular Medicine (WIMM), John Radcliffe Hospital, University of Oxford, Oxford, UK. ²Translational Gastroenterology Unit, John Radcliffe Hospital, University of Oxford, Oxford, UK. ³MRC WIMM Centre For Computational Biology, MRC WIMM, John Radcliffe Hospital, University of Oxford, Oxford, UK. ⁴Computational Biology Research Group, University of Oxford, John Radcliffe Hospital, Oxford, UK. ⁵Department of Gastroenterology, Juntendo University School of Medicine, Tokyo, Japan. ⁶Department of Therapy Development and Innovation for Immune Disorders and Cancers, Juntendo University, Tokyo, Japan. ⁷Department of Pathology, Saitama Medical University, Saitama, Japan. ⁸Department of Pathology, Case Western Reserve University, Cleveland, OH, USA. ⁹Wellcome Trust Centre for Human Genetics, University of Oxford, Oxford, UK. ¹⁰These authors contributed equally: Daniele Corridoni, Agne Antanaviciute, Tarun Gupta. ✉e-mail: hashem.koohy@rdm.ox.ac.uk; alison.simmons@imm.ox.ac.uk

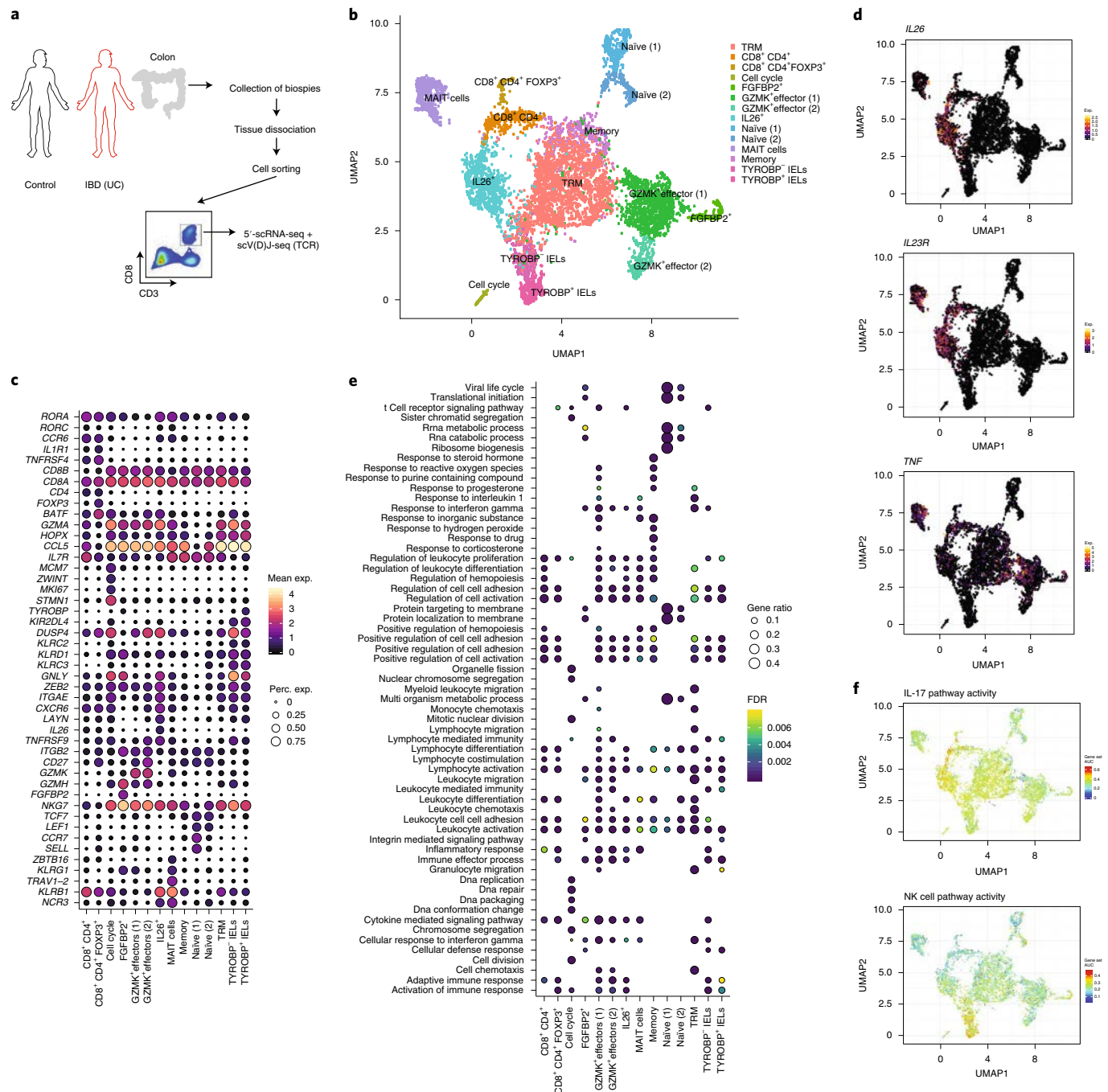


Fig. 1 | Colonic CD8⁺ T-cell transcriptional atlas. **a**, Schematic representation of scRNA-seq and variable-(diversity)-joining TCR gene segment sequencing (scV(D)J-seq) experimental design and sorting strategy. **b**, UMAP plot visualization of colonic CD8⁺ T-cell clusters detected in healthy controls (HC) ($n=3$) and UC ($n=3$). **c**, Dotplot heatmap showing expression and cellular detection rate of selected cluster marker genes. **d**, Expression (Exp.) profiles of selected subpopulation-specific marker genes (cells from $n=3$ UC, $n=3$ HC donors). **e**, Dotplot heatmap showing GO biological process terms enriched in cluster marker genes. Hypergeometric test for overrepresentation; Benjamini-Hochberg multiple test correction. **f**, Individual cell AUC score overlay for selected canonical pathway activities (cells from $n=3$ UC, $n=3$ HC donors).

T-cell activation, cytokine production, cell killing and upregulated innate immune response pathways (Extended Data Fig. 2b). The majority (615) of identified DEGs were significantly differentially expressed within a single cluster only, with only 34 genes significantly differentially expressed in more than four clusters. These cell type-independent response genes encompassed loss of expression of *SPINK2*, *FOS* and *CD160*, but upregulated *TNFRSF9* and *CTLA4* in T_{RM} , effector and IEL populations (Extended Data Fig. 2a). We

posit that this result reflects differential pathway activity in effector populations in IBD, where we observe higher levels of costimulation by CD28, TCR signaling, antigen processing, antigen presentation and PD1 and CTLA4 pathways (Fig. 2b and Extended Data Fig. 2c).

Because our single-cell analyses provided high-resolution expression data, we next sought to explore the transcriptomic landscape of IBD genetic susceptibility loci within the colon (Methods). We found that an overall higher enrichment of Genome-Wide

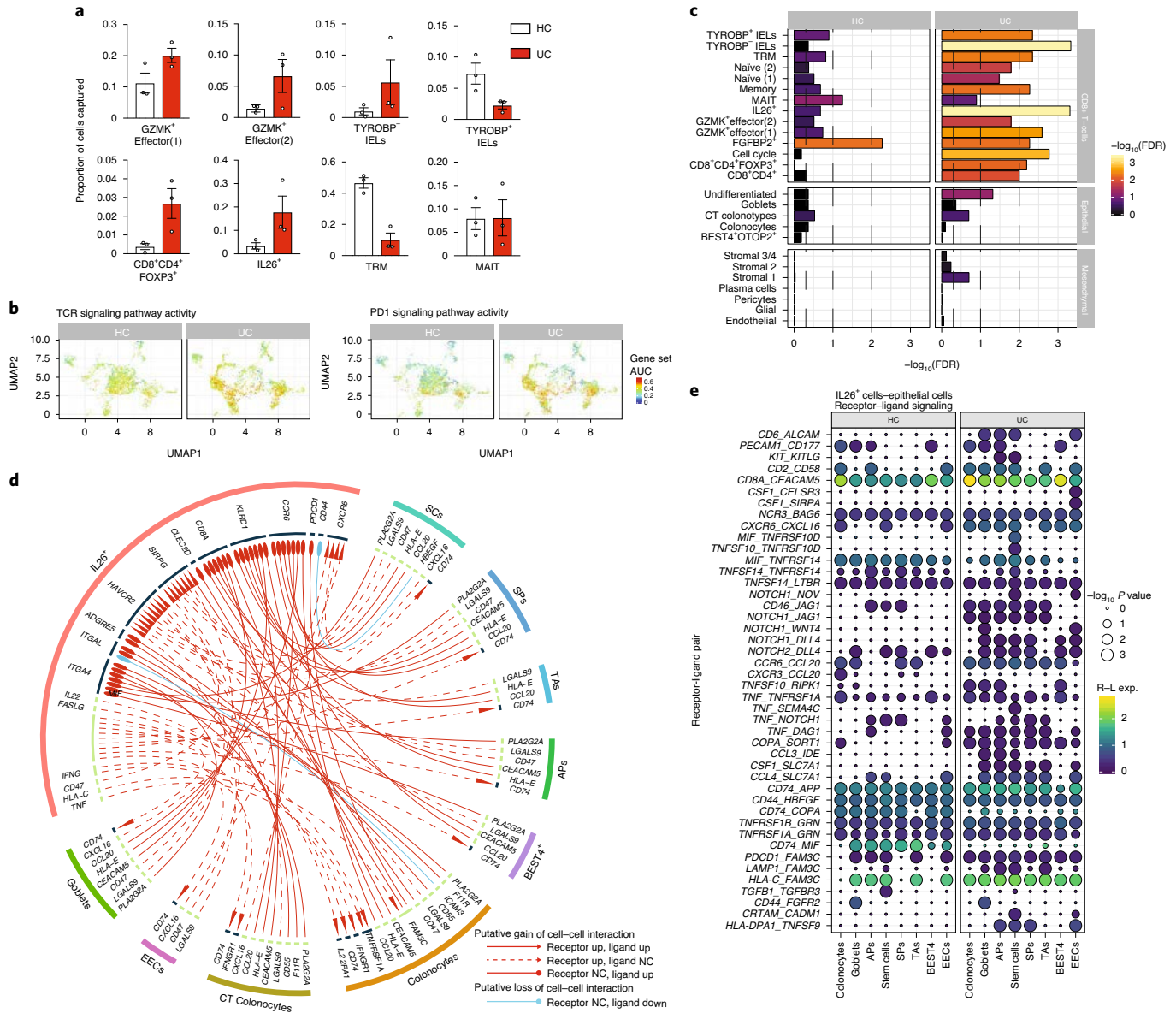


Fig. 2 | Colonic CD8⁺ T-cell remodeling in active UC. **a**, Changes in selected CD8⁺ subpopulation composition in health and IBD. *n* = 3 donors per group, mean and s.e.m. shown. **b**, Individual cell AUC score overlay for selected differential canonical pathway activities in health (cells from *n* = 3 donors) and IBD (cells from *n* = 3 donors). **c**, Barplot showing the significance ($-\log_{10}(\text{FDR})$) of IBD GWAS signal enrichment in single-cell clusters in CD8⁺ (*n* = 3 donors per group), epithelial (*n* = 3 donors per group) and mesenchymal (*n* = 3 donors per group) subpopulations in cells from healthy and UC donors. SNPsea empirical distribution *P* value; Benjamini–Hochberg multiple testing correction. **d**, Circos plots showing all putative gain or loss of cell–cell interaction events in active UC via receptor–ligand pair signaling between CD8⁺/IL26⁺ T cells and epithelial cell subtypes. SCs, stem cells; SPs, secretory progenitors; TAs, transit-amplifying cells; APs, absorptive progenitors; CT colonocytes, crypt-top colonocytes; EECs, enteroendocrine cells; NC, no significant change. **e**, Dotplot of selected significant paracrine receptor–ligand interactions between CD8⁺/IL26⁺ and epithelial cells discovered using CellphoneDB (empirical permutation *P* value). R–L exp., receptor–ligand expression.

Association Study (GWAS) genes from UC-associated loci showed expression specificity in active inflammation (Fig. 2c). The highest overall signal enrichment was found in IELs and IL26⁺ cells, driven by high and specific expression of genes including *KIR3DL2* (ref. ⁶) (*rs17771967*), *IL26* (*rs2870946*)⁷ and *IL23R*⁸ (multiple risk alleles) (Fig. 1c,d, Extended Data Fig. 2d and Supplementary Data).

UC alters crosstalk between epithelial and CD8⁺ subpopulations. Because CD8⁺ T cells may drive tissue damage in UC by direct interactions with colonic epithelial cells, we explored T-cell and epithelial cell receptor–ligand pairing in both health and UC. We discovered between 15 and 51 interactions between pairwise CD8⁺ and epithelial

subcluster comparisons in health, and 14–80 in UC. Examining differentially expressed receptor–ligand pairs, irrespective of cluster specificity we further identified 1,716 (104 unique receptor–ligand pairs across 22 cell types) total putative crosstalk alterations in UC; interaction gains constituted the majority (1,575) of these events. The nonclassical MHC molecule *HLA-E*³ was strongly induced in multiple epithelial subpopulations in UC while its corresponding ligands were induced in CD8⁺ T cells. Lineage-specific interactions included *IL18-IL18R1/IL18RAP* and *TNF-TNFRSF1A* signaling between absorptive, but not secretory, cells and multiple CD8⁺ subclusters (Fig. 2d,e, Extended Data Fig. 3a–c, Supplementary Fig. 2 and Supplementary Data).

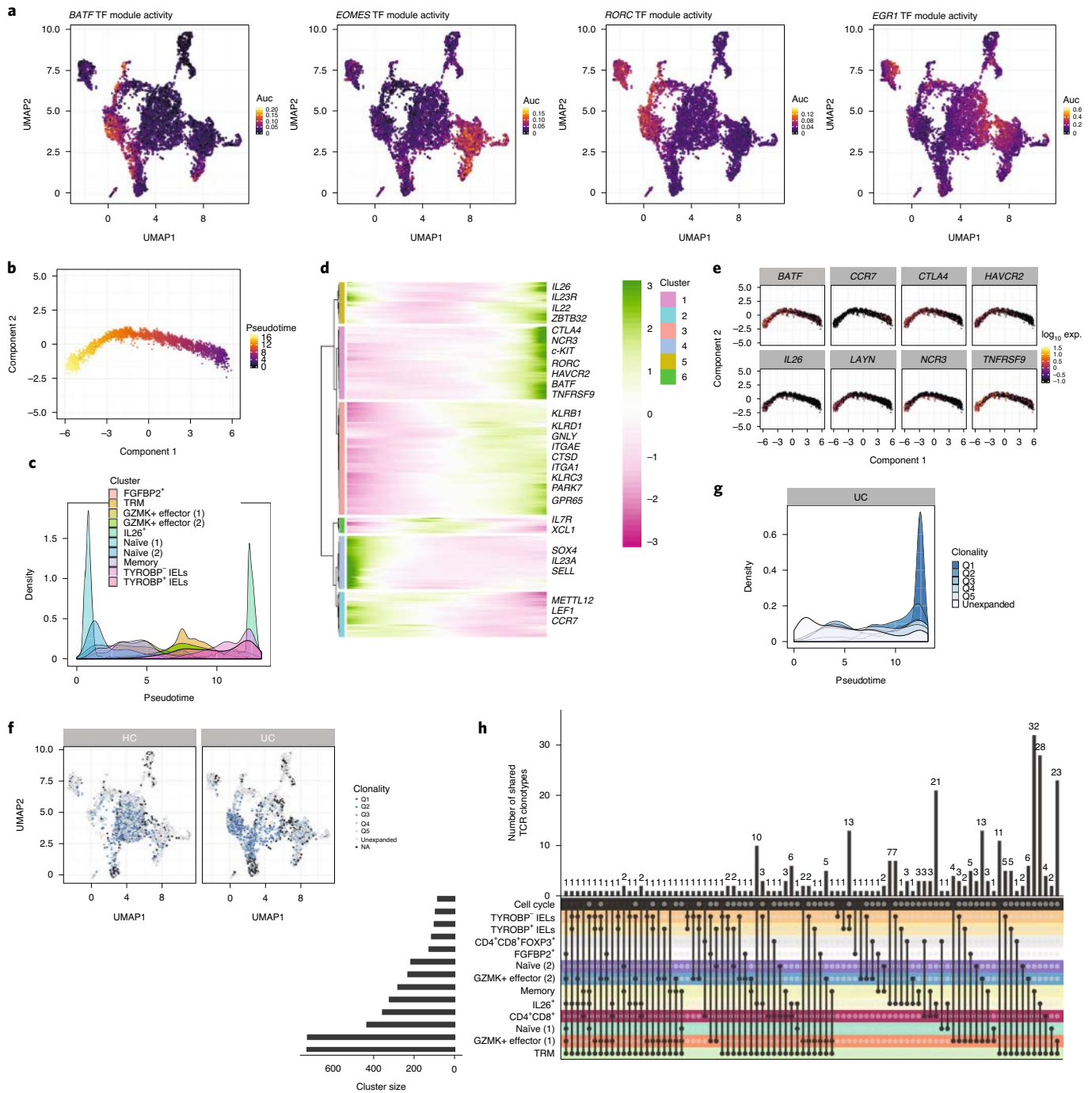


Fig. 3 | Transcriptional modules, pseudotime and clonality define UC CD8⁺ T-cell lineages. **a**, Selected transcription factor network activity AUC score cluster distributions (cells from $n=3$ donors UC, $n=3$ donors HC). **b**, Trajectory analysis of CD8⁺ T cells captures a linear pseudotime progression (cells from $n=3$ donors UC, $n=3$ donors HC). **c**, Cluster distribution density along pseudotime. **d**, Heatmap showing relative expression (exp.) of genes significantly (<1% FDR) varying with pseudotime. Selected genes are highlighted. Negative binomial likelihood ratio test, Benjamini-Hochberg multiple testing correction. Cells from $n=3$ donors UC, $n=3$ donors HC. **e**, Expression of selected genes along pseudotime (cells from $n=3$ donors UC, $n=3$ donors HC). **f**, TCR clonality on expression-driven UMAP overlay showing the distribution of clonal and unexpanded cell populations in cell clusters in health and UC. Cells with no reconstructed TCR clonotype are shown in black and are labeled as NA (cells from $n=3$ donors UC, $n=3$ donors HC). **g**, TCR clonality density distribution along pseudotime in UC. Unexpanded: clones captured in three or fewer cells; Q1: cells encompassing the top 20% of the most expanded clones per sample; Q5: cells encompassing the bottom 20% of the most expanded clones; Q2-4 represent the middle three quantiles. **h**, Upset plot showing TCR clones shared between different clusters, each shared clone visualized as an 'interaction' and indicated by a black circle joined by black lines. Each unique clone is counted once only, regardless of degree of expansion. The barplot at the top indicates the total number of shared TCR clones for those cluster intersections. Cluster intersections without shared TCRs are omitted for clarity.

Given the increase in the number of *IL26*⁺-producing CD8⁺ cells in UC, we examined expression of the IL-26 receptor, *IL10RB/IL20RA*¹⁰, in scRNA-seq data from colonic cells in both health and

UC. *IL10RB* localized to colonocytes in the epithelium and was ubiquitously expressed by mesenchymal cells, but not by CD45⁺ cells, in health and UC, while the detection rate of *IL20RA* was low

(Extended Data Fig. 4a–d). In contrast, *IL10RA* expression was limited to the CD45⁺ compartment (Supplementary Fig. 3a,b). In line with scRNA-seq findings, IL10RB/IL20RA was found to be coexpressed at the protein level in minor fractions of epithelial (1.9%), mesenchymal (1.73%) and immune compartments (3.7%) and did not increase in UC (Supplementary Fig. 4a,b); this was confirmed by quantitative PCR (qPCR) in an independent cohort ($n=17$ UC, $n=5$ health; Supplementary Table 1b and Supplementary Fig. 4c). Conversely, *IL26* expression in whole tissue was found to correlate with degree of inflammation (Supplementary Fig. 4d). This suggests that increased IL-26 signaling in UC is not due to induced expression of its receptor, although we cannot discount the possibility that some effects may be mediated through a hitherto undiscovered receptor¹¹.

Transcriptional networks directing colonic CD8⁺ plasticity in UC. To define the regulatory networks directing colonic CD8⁺ T-cell plasticity in IBD, we performed gene coexpression analysis and then scored each cell for activity of gene modules, which were both coexpressed with and enriched for transcription factor (TF) *cis*-regulatory motifs, identifying 273 active TF activity-associated circuits. Hierarchical clustering highlighted networks expressed exclusively in specific T-cell clusters, revealing both new and established transcriptional regulators (Fig. 3a, Extended Data Fig. 5a,b and Supplementary Table 2).

We observed a group of modules, including *EGR1* and *EGR2*, whose activity was localized to the cell transition gradient between T_{RM} cells and GZMK⁺ effectors (Fig. 3a). This result highlighted a distinct T-cell state missed by our initial clustering analysis. These transitional cells also showed high, localized coexpression of *IFNG* and *TNF*, as well as activity of *FOS*, *FOSB*, *FOSL1*, *JUN* and *JUNB* networks (Fig. 1d and Extended Data Figs. 1 and 5a,b). These TFs are well-characterized, immediate, early-response genes that are rapidly induced by various stimuli¹², suggesting that *EGR*-expressing T cells showed recent activation and harbored most pathogenic *TNF* expression within colonic CD8⁺ T cells.

Our TF activity analysis also highlighted gene modules that were not only cell state specific, but also showed differential activity levels in IBD (Methods), including *ETV7*, *PRDM1/BLIMP-1* and *STAT3* (Supplementary Fig. 5a–d).

Innate reprogramming adopted by adaptive IL26⁺ T cells in UC. Within the single-cell profiles, we identified clusters of innate CD8⁺ lymphocytes including MAIT cells and $\gamma\delta$ IELs. While overall there was little heterogeneity within MAIT cells (Extended Data Fig. 6a), in UC they expressed analogous programs of activation as observed for conventional CD8⁺ cells. This included coexpression of early-response genes *EGR1* and *EGR2* together with *TNF* and *IFNG*, and a gradual transitional state gradient characterized by expression of coinhibitory and costimulatory molecules (Extended Data Fig. 6b,c).

While we found a high proportion of V δ 1 $\gamma\delta$ cells within CD8⁺ IEL-like clusters (Extended Data Fig. 1), TCR- $\alpha\beta$ cells also predominantly expressed innate markers⁹ such as killer cell immunoglobulin-like receptors (KIRs) (for example, *KIR2DL4* and *KIR2DL2*), NK cell receptors (for example, *NCR1*) and *FCER1G* (Extended Data Fig. 6d,e). We found that *MKI67*⁺ cells expressed some of these genes, suggesting that the IEL compartment was undergoing active proliferation in UC (Extended Data Fig. 6d,e and Supplementary Data).

To better understand IEL populations at the single-cell level, we further interrogated T-cell populations captured in a colonic epithelium scRNA-seq dataset¹³. We reasoned that these immune cells, captured during an epithelial crypt-specific dissociation protocol, are likely to be enriched for IELs. Within these cells (total, 927) we found that the majority were CD8⁺ with only small populations of

CD4⁺ cells present (Supplementary Fig. 6a). While we could distinguish seven CD8⁺ subclusters with a combination of marker genes, including *CD6*, *LAYN* and *GZLN* (Supplementary Fig. 6a,b and Supplementary Data), these cells uniformly expressed many IEL-specific cluster markers that we had identified earlier, such as NK receptor *KLRC2* (Supplementary Fig. 6c). We grouped these clusters into natural and induced IELs based on *TYROBP* expression, observing a similar shift towards induced phenotype in active UC in line with earlier observations⁵ (Supplementary Fig. 6b,d–f).

While innate features of IELs are well described¹⁴, we found that the adaptive CD8⁺ IL26⁺ cells, which were increased in UC, also displayed innate-like features that differed from IEL transcriptional profiles. IL26⁺ cells lacked expression of *KLRC2* (Supplementary Fig. 6c) and IEL-specific KIRs (Extended Data Fig. 6e), but expressed *NCR1*, *NCR3* and *KIR2DL4* (Extended Data Fig. 6e), typical of type 2 ILC3s, lineage-negative innate lymphoid cells. Type 2 ILC3s are also characterized by expression of the TFs *AHR*, *KIT* and *RORC* (Extended Data Figs. 1 and 6e) and a Th17-like cytokine profile¹⁵, another feature shared with IL26⁺ cells. Based on these results, we conclude that CD8⁺ IL26⁺ cells, while lineage positive, express hybrid Tc17 and type 2 ILC3 features.

Chronic activation of IL26⁺ cells in UC. In UC we observed an accumulation of cell clusters, including GZMK⁺ effector and IL26⁺ cells, with features of ‘exhaustion’, a hallmark of tumor-infiltrating CD8⁺ T cells. This was marked by concerted expression of coinhibitory molecules including *HAVCR2*, *LAYN*, *ENTPDI*, *CTLA4* and *PDCDI*, as well as TFs *TOX* and *EOMES* (Figs. 1c and 3a, Extended Data Fig. 1 and Supplementary Data). Because the relationship between exhausted colonic CD8⁺ cells and those observed in cancer remains unclear¹⁶, we interrogated recently published scRNA-seq datasets from tumor-infiltrating T cells (TILs) in liver, breast and colorectal cancers (Methods). We observed clear conservation of chronic stimulation-associated signatures between subpopulations of colonic T cells in UC and all three TIL datasets (Extended Data Fig. 7a,b). However, expression of type 17 signature¹⁷ in exhausted T cells was UC exclusive, suggesting that either these are Tc17/ILC3-like cells¹⁸ subject to chronic overstimulation in UC or this phenotype is acquired in a ‘post-effector’ cell state (Extended Data Fig. 7b and Supplementary Data).

TCR profiling defines connectedness of diverse CD8⁺ phenotypes in UC. Because our data probably captured T cells asynchronously transitioning from one transcriptomic state to the next, we performed pseudotime analysis, capturing a linear trajectory progressing from naïve-like cells at the start to memory, T_{RM}, GZMK⁺ effectors and culminating with IL26⁺ cells (Fig. 3b,c). To understand the biological processes driving pseudotime components, we asked which genes covary in expression with pseudotime. We clustered all genes identified as significantly (false discovery rate (FDR) < 1%) covarying with pseudotime (Fig. 3d) and identified groups of genes expressed early, mid/mid-late and late. In keeping with cluster distribution, naïve and early central memory T-cell markers, such as *CCR7*, were expressed early while coinhibitory receptors (*HAVCR2*, *CTLA4*) were expressed late (Fig. 3d,e). We found a strong signal for T-cell activation markers, along with a gradual gain in coinhibitory molecules, as suggested by the pseudotime cluster distribution. We observed increasing expression of *BATF*, *CTLA4*, *HAVCR2*, *LAYN* and *TNFRSF9*, while molecules associated with effector function, such as *GZMK*, were steadily lost (Fig. 3c–e).

We next sought to elucidate lineage and clonal dynamics between subtypes via matched single-cell TCR- $\alpha\beta$ profiling (Methods and Supplementary Data). We found that naïve, MAIT and DP T-cell populations exhibited highly diverse clonal structures, with most cells expressing a unique TCR CDR3 sequence pair (Fig. 3f). In CD8⁺ cells derived from healthy colon, T_{RM}-like cells showed the

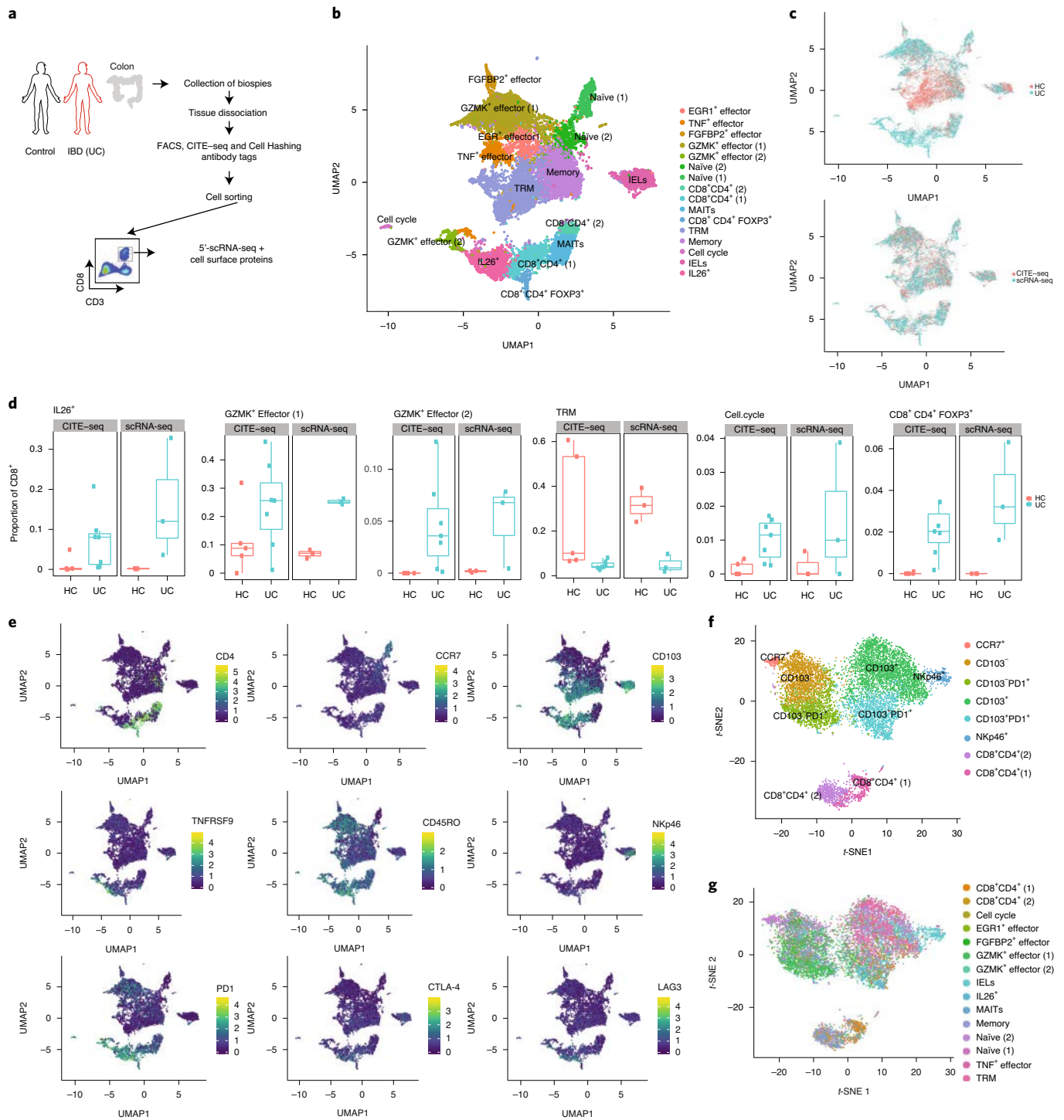


Fig. 4 | Combined transcriptomic and proteomic profiles of CD8⁺ T cells using CITE-seq and Cell Hashing. **a**, Schematic representation of experimental design and sorting strategy for single-cell 5' RNA-seq, CITE-seq and Cell Hashing. **b**, UMAP plot of colonic CD8⁺ T cells in health ($n=5$) and UC ($n=7$), clustered based on gene expression profiles. **c**, Differential distribution of CD8⁺ T-cell populations derived from health and UC (top), with broad overlap between gene expression data derived from hashed CD8⁺ T cells (CITE-seq, validation cohort, $n=5$ HC, $n=7$ UC donors) and nonmultiplexed CD8⁺ T cells (scRNA-seq, initial cohort, $n=3$ donors per group) (bottom). **d**, Relative abundance of CD8⁺ T cells from selected clusters in health and UC derived from either hashed (CITE-seq $n=5$ HC, $n=7$ UC donors) or nonmultiplexed (scRNA-seq, $n=3$ per group) samples. Boxplots show the median, first and third quartiles, fifth percentile as minima and 95th percentile as maxima. **e**, Cell surface protein expression data (derived from CITE-seq, $n=5$ HC, $n=7$ UC donors) overlaid on colonic CD8⁺ T cells clustered by gene expression profiling. **f**, UMAP of colonic CD8⁺ T cells clustered by cell surface protein expression determined using CITE-seq ($n=5$ HC, $n=7$ UC donors). **g**, Overlay of mRNA-derived clusters on UMAP of cells clustered by cell surface protein expression ($n=5$ HC, $n=7$ UC donors).

highest enrichment of frequently observed T-cell clones. In contrast, we found a marked enrichment of clonal T cells in UC-associated *IL26*⁺ cells, because the majority of the largest clones in each sample

comprised this population in UC. These observations aligned with our pseudotime analysis, because unexpanded cells in UC were enriched at the start of the trajectory and the most expanded clones

occupied its end (Fig. 3g). Overall, expanded clones were diverse (we did not detect any shared specificity groups¹⁹) and had largely private TCR repertoires, although we detected 93 TRB CDR3 sequences shared between at least two donors. These included known public TRB sequences²⁰ for common Epstein–Barr virus, cytomegalovirus and influenza-derived peptides, reflecting past exposure to common antigens, and none of these were expanded in UC.

In total, 320 out of 3,835 unique clonotypes occurred in more than one cluster. These constituted the clonally expanded populations, with a total of 2,438 cells sharing their clonotype with those in other clusters (Fig. 3h). We examined all unique TCR clonotypes shared by different clusters and their degree of overlap. As expected, we observed clonotypes present within the T_{RM} population in many other cell types/states²¹. When we observed a clone in more than two different clusters, it also appeared in the T_{RM} population (Fig. 3h). The greatest overlaps between pairs of clusters occurred between T_{RM} and $IL26^+$, $GZMK^+$ effector and memory cell populations, respectively, with 28, 32 and 23 unique TCRs reconstructed in cells from these cluster pairs. The largest ‘triplet’ included ten unique clonotypes detected in cells from the small, actively cycling cluster, $IL26^+$ cells and T_{RM} cells. These results are consistent with the high clonal expansion of $IL26^+$ cells and suggest that these cells may arise either directly from T_{RM} cells or as a post-effector phenotype.

Given the small overall size of the captured TCR- $\alpha\beta$ populations in IELs, $TYROBP^+$ and $TYROBP^-$ cells also shared a large number of clonotypes (13), supporting the idea of naturally induced IEL transition.

Although some clonotypes could be attributed to the wrong cluster due to the somewhat fluid boundaries between detected populations, we detected multiple instances of clonotypes shared between four or more clusters linking distant populations. Thus, TCR repertoire analysis revealed the phenotypic journey of single TCR clones demonstrating transit through diverse T-cell states in UC.

Multimodal analysis of colonic CD8⁺ T cells confirms heterogeneity and remodeling in UC. To validate single-cell signatures at the protein level, we next profiled an additional seven UC and five healthy samples using single-cell cellular indexing of transcriptomes and epitopes by sequencing (CITE-seq) coupled with cell hashing technology, integrating transcriptomic and proteomic profiles from an additional 9,062 cells (Fig. 4a,b, Supplementary Tables 1–3, Supplementary Fig. 7a–h and Methods).

Integrative data analysis revealed high reproducibility between our initial scRNA-seq and subsequent CITE-seq analysis (Fig. 4b–d and Extended Data Fig. 8a–c). We were able to partition effector cells into two additional clusters characterized by expression of TNF (TNF^+ effector) and $EGR1/EGR2$ ($EGR1^+$ effector), which we had previously noted as a likely transitional population between T_{RM} and $GZMK^+$ effector cells (Fig. 4b).

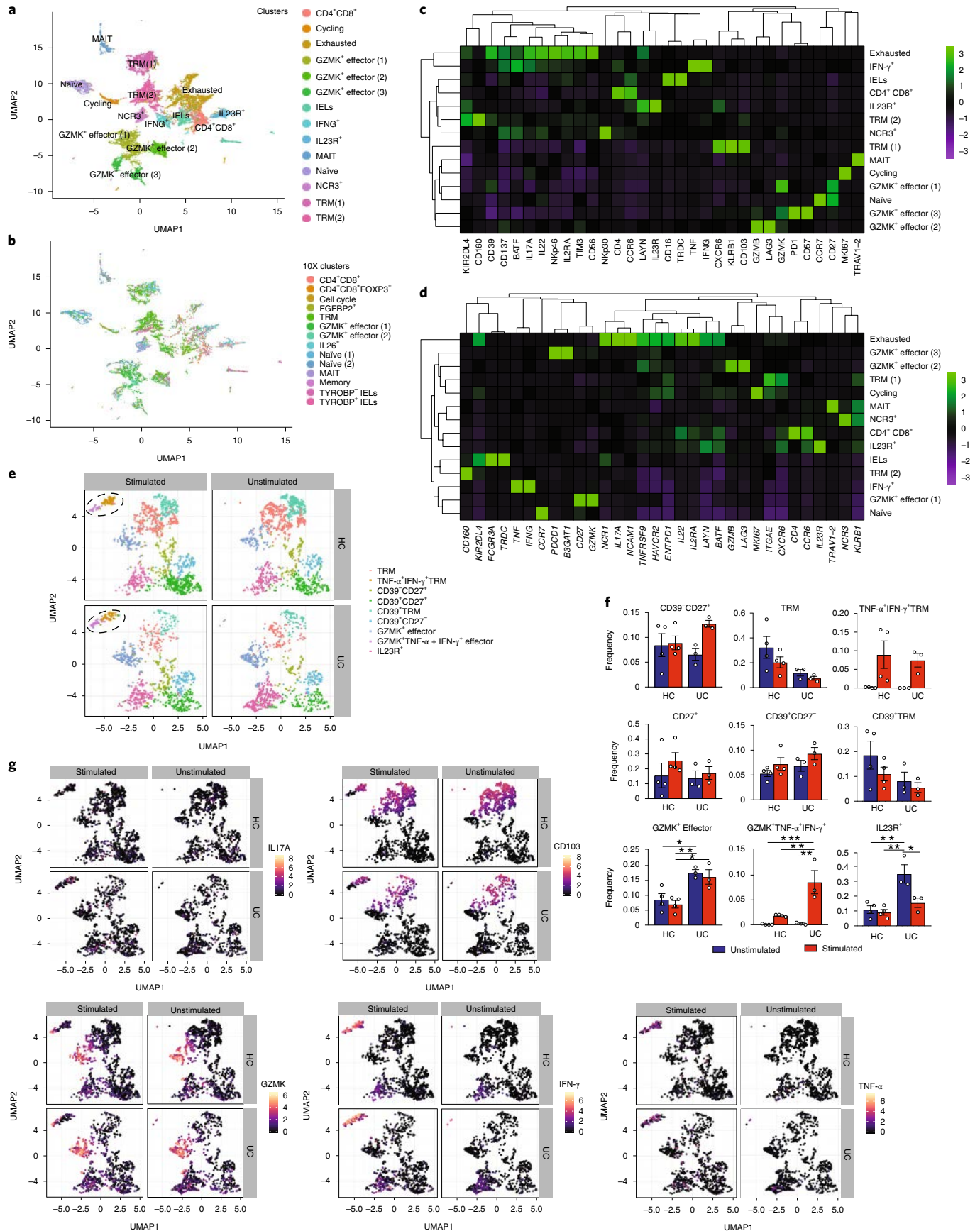
CITE-seq allowed us to map the expression of a panel of 14 proteins to all CD8⁺ cell subpopulations (Fig. 4e,f and Extended Data Fig. 8d). The combination of CD45RO, CD103, CD69 and CCR7 clearly delineated T_{RM} , intraepithelial, $IL26^+$ and CD4⁺/CD8⁺ DP

cell populations from naïve and effector CD8⁺ T cells, confirming our previous observations of differences in tissue residency and migration dynamics between these populations. Coinhibitory molecules PD1, TIM3 and LAG3 marked mostly CD103⁺ cells, including $GZMK^+$ effector (2) and $IL26^+$ cells, while fewer CD103⁻ cells showed features of chronic T-cell stimulation at the protein level (Fig. 4e,f and Extended Data Fig. 8d). Finally, because IL-26 is a secreted cytokine and we could not capture its protein level expression in our CITE-seq panel, we confirmed its increased production by colonic CD8⁺ T cells in UC using enzyme-linked immunosorbent assay (ELISA) (Extended Data Fig. 8e).

Multimodal data integration and functional analysis of UC remodeled CD8⁺ T cells. Clustering analysis using CITE-seq protein expression highlighted that the 14 selected proteins were sufficient to delineate key features of only tissue residency, exhaustion and memory, with the majority of $IL26^+$ cells falling within the CD103⁺ PD1⁺ population (Fig. 4f,g). Thus, we developed a mass cytometry time-of-flight (CyTOF) panel incorporating 39 markers expressed in specific scRNA-seq clusters (Extended Data Fig. 9a and Supplementary Table 3). Applying this panel to CD8⁺ cells isolated from additional healthy ($n=3$) or inflamed UC ($n=3$) colon samples (Supplementary Table 1a), we defined 19 protein expression-driven clusters, six of these showing significant alterations in frequency in health and UC (Extended Data Fig. 9b–d). Using CyTOF data as a reference, we next performed multimodal single-cell data integration²² (Methods) to infer the most probable counterpart cells between these two expression modalities (Fig. 5a,b and Supplementary Fig. 8a–c). Many key markers showed conserved coexpression in both protein and messenger RNA datasets (Fig. 5c,d). Largely one-to-one relationships between mRNA and CyTOF clusters were observed for some populations (for example, $CCR7^+$ /naïve cells), while one to many relationships highlighted a need to refine the CyTOF panel, guided by scRNA-seq data, to more accurately capture discrete phenotypic states. $IL26^+$ cells were found to be enriched in $IL23R^+$, $NKp30/NCR3^+$, T_{RM} and exhausted clusters (Fig. 5c,d and Supplementary Fig. 8c).

To assess the functional capacity of the UC-associated CD8⁺ subpopulations, we undertook ex vivo stimulation with phorbol myristate acetate (PMA) and ionomycin. Using our CyTOF panel, we profiled cells from additional healthy donors ($n=4$) and those with inflamed UC ($n=3$) following stimulation. Both donor groups exhibited the emergence of a subpopulation of CD103⁺ T_{RM} cells that expressed $TNF-\alpha$ and $IFN-\gamma$. In contrast, reactivated cells from UC donors were also enriched for $GZMK^+$ effector markers (Fig. 5e–g). Curiously, few $IL23R^+$ cells (mainly comprising $IL26^+$, some MAITs and DP cells) responded to stimulation. These results suggest that clonally expanded $IL23R^+/IL26^+$ cells observed in UC may have limited effector function, in line with their transcriptional ‘post-effector’ terminally differentiated signatures. While detected at baseline in UC $IL23R^+/IL26^+$ cells, IL-17 was also induced in stimulated UC CD8⁺ cells in $TNF-\alpha/IFN-\gamma$ clusters despite the

Fig. 5 | Functional CyTOF analysis of UC CD8⁺ T cells. **a**, Integrated cluster analysis of CyTOF ($n=3$ donors per group) and 10x scRNA-seq ($n=3$ donors per group) datasets visualized in UMAP. **b**, Distribution of original 10x scRNA-seq ($n=3$ donors per group) clusters in relation to integrative analysis. **c**, Relative mean cluster protein expression in cells from CyTOF dataset. **d**, Relative mean cluster RNA expression in cells from 10x scRNA-seq dataset. **e**, UMAP plot visualization of clusters obtained after ex vivo stimulation with PMA and ionomycin ($n=3$ UC, $n=4$ HC donors per group) and unstimulated CD8⁺ T cells from healthy ($n=4$) and UC ($n=3$) donors in CyTOF data. **f**, Changes in cell cluster proportions in CyTOF data clusters following stimulation in health ($n=4$ donors) and UC ($n=3$ donors). Mean and s.e.m. shown. $GZMK^+$ effector, $F=9.075$, $d.f=3$, $*P=0.0213$ (healthy unstimulated versus UC unstimulated), $**P=0.0077$ (healthy stimulated versus UC unstimulated); $*P=0.0187$ (healthy stimulated versus UC stimulated); $GZMK^+TNF-\alpha^+IFN-\gamma^+$, $F=15.22$, $d.f=3$, $***P=0.0005$ (healthy unstimulated versus UC stimulated), $**P=0.0032$ (healthy stimulated versus UC stimulated); $**P=0.0011$ (UC unstimulated versus UC stimulated); $IL23R^+$, $F=11.09$; $d.f=3$; $**P=0.0029$ (healthy unstimulated versus UC unstimulated), $**P=0.0017$ (healthy stimulated versus UC unstimulated), $*P=0.0177$ (UC unstimulated versus UC stimulated); one-way ANOVA (Tukey’s multiple comparison test). **g**, Selected protein expression UMAP overlay in stimulated and unstimulated cells in health ($n=4$ donors) and UC ($n=3$ donors).



absence of IL23R (Fig. 5g), suggesting that mucosal CD8⁺ T cells in UC are transcriptionally more permissive towards adopting a Tc17-like phenotype.

IL-26 attenuates the severity of acute colitis. The role of IL-26 in colitis remains unclear²³. Even though the *IL26* gene is absent in rodents, its heterodimeric receptor comprising IL-20RA and

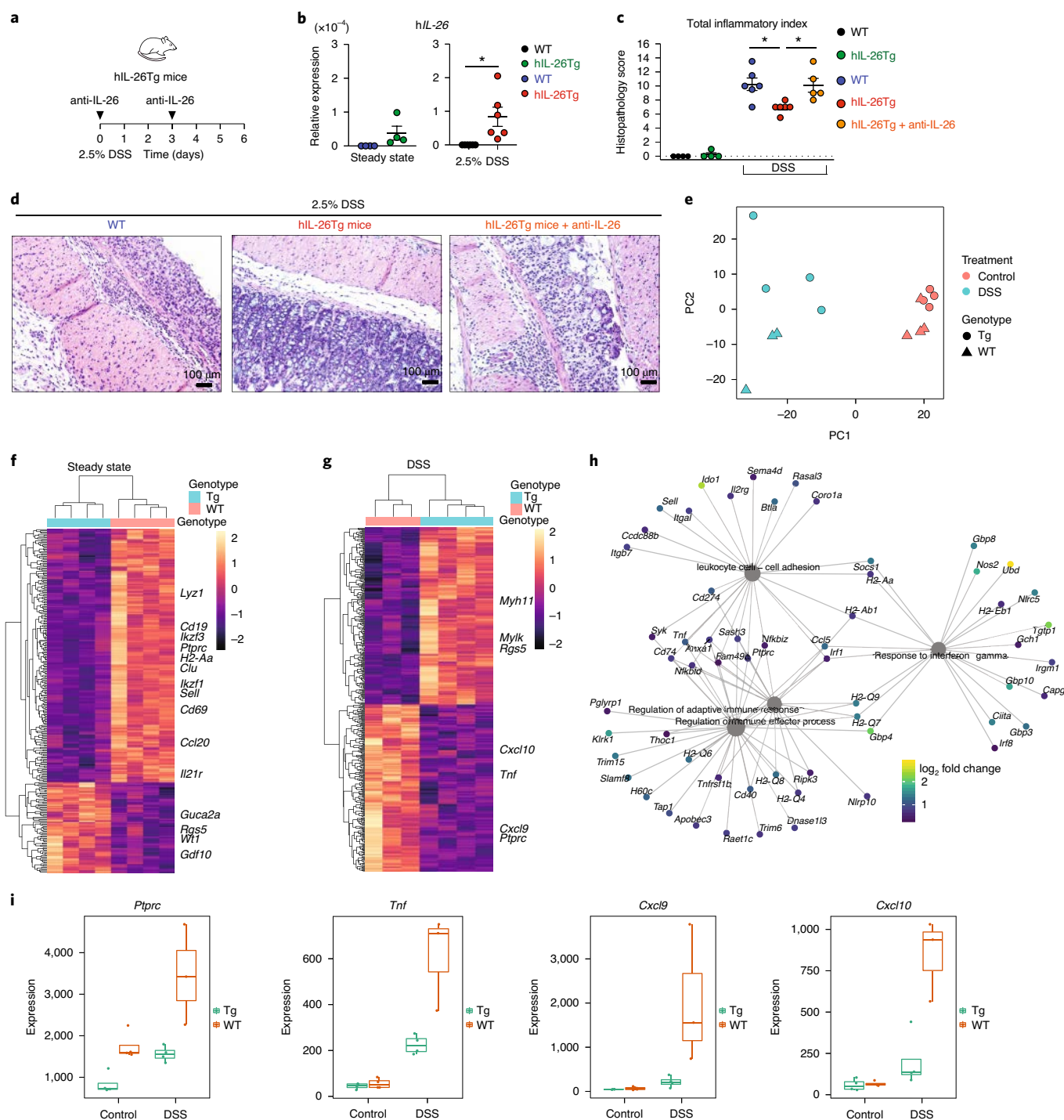


Fig. 6 | IL-26 attenuates acute colitis severity. **a**, Strategy for induction of 2.5% DSS and intraperitoneal injection of anti-IL-26 antibody or mlgG1, κ isotype control antibody. **b**, hIL-26 expression in colon from WT ($n=4$ mice) and hIL-26Tg ($n=6$) mice at baseline/steady state or after 6 days of challenge with 2.5% DSS. $*P=0.0152$, two-tailed, unpaired t -test ($t=2.923$, $d.f=10$). **c**, Colonic total inflammatory scores (Methods) ($n=4$ control mice, $n=6$ DSS-treated mice, $n=5$ DSS treatment + anti-IL-26 mice); $F=6.338$, $d.f=2.0$, $*P=0.0168$ (WT DSS versus hIL-26Tg DSS); $*P=0.0290$ (hIL-26Tg DSS versus hIL-26Tg with anti-IL-26 DSS); mean and s.e.m. shown, one-way ANOVA (Tukey's multiple comparison test). **d**, Representative photomicrographs ($n=6$ DSS-treated mice, $n=5$ DSS treatment + anti-IL-26 mice) of hematoxylin and eosin-stained colonic tissues following DSS challenge (original magnification $\times 20$). **e**, PCA of mRNA derived from bulk RNA-seq of WT ($n=4$ DSS-treated mice, $n=3$ control mice) and hIL-26 ($n=4$ mice per group) mouse colonic tissue under different experimental conditions. **f**, Heatmap of differentially expressed genes at steady state from WT and hIL-26Tg mice. Wald test, Benjamini-Hochberg multiple testing correction. **g**, Heatmap of differentially expressed genes under DSS challenge from WT and hIL-26Tg mice. Wald test, Benjamini-Hochberg multiple testing correction. **h**, Cnetplot showing the top most enriched GO terms in significantly downregulated genes in DSS- ($n=4$ hIL-26Tg mice, $n=3$ WT mice) challenged hIL-26 mice. Hypergeometric overrepresentation test, Benjamini-Hochberg multiple testing correction. **i**, Comparative expression of selected genes under DSS challenge between WT ($n=3$) and hIL-26Tg ($n=4$) mice, demonstrating lower inflammatory signatures in hIL-26-expressing Tg mice. Boxplots show the median, first and third quartiles, fifth percentile as minima and 95th percentile as maxima.

IL10RB is expressed in mice and can signal in response to human IL-26 (refs. ^{10,24}). We used a humanized IL-26 transgenic (hIL-26Tg) mouse model²⁵ to assess whether IL-26 can affect acute colitis severity. The colon from hIL-26Tg mice showed no differences at steady state compared to littermate controls or sibling wild-type (WT) C57BL/6J (B6) mice (Extended Data Fig. 10a). We exposed hIL-26Tg and control B6 mice to 2.5% dextran sulfate sodium (DSS) in drinking water and treated hIL-26Tg mice with either anti-IL-26 monoclonal antibody (mAb) or control mAb administered intraperitoneally on days 0 and 3 (Fig. 6a,b).

DSS-challenged WT mice had a significantly higher total inflammatory score than DSS-challenged hIL-26Tg mice given control antibody. The inflammatory effect of DSS was restored in these hIL-26Tg mice after administration of concomitant anti-IL-26 mAb (Fig. 6c,d and Extended Data Fig. 10b), suggesting a potential protective role for IL-26 in the acute phase of inflammation.

To characterize the effect of *IL26* expression, we next performed RNA-seq on colonic tissue at baseline and with DSS. Principal component analysis (PCA) highlighted clear differences between RNA-seq profiles of baseline and DSS (Fig. 6e), with DSS samples showing increased variability within the group as could be expected given the drastic tissue perturbation; samples from WT and Tg animals showed separation in the second principal component. In line with PCA, at baseline we identified 295 significantly (<5% FDR) differentially expressed genes between WT and hIL-26Tg mice (Fig. 6f and Supplementary Data). GO enrichment analysis highlighted strong T- and B-cell activation and leukocyte proliferation signature in WT animals, which was strongly reduced in Tg animals (Fig. 6f and Supplementary Data) suggesting that, even under non-inflammatory conditions, expression of *IL26* may either diminish immune infiltration of the mucosa or downregulate activation and proliferation signals. This was supported by differential expression of genes such as the B-cell marker *Cd19* and lymphocyte differentiation transcription factors *Ikzf1* and *Ikzf3* (Extended Data Fig. 10c). We further observed an increase in lysozyme expression in WT (Fig. 6f and Extended Data Fig. 10c), a molecule expressed by Paneth cells (but typically not present in the colon) and macrophages, suggesting that *IL26* overexpression may also reduce the presence of myeloid cells in the mucosa. Conversely, RNA expression profiles from Tg animals showed a relative increase in gene signature associated with nonimmune compartments, including muscularis and circulatory system processes and increase in expression of genes such as canonical pericyte marker *Rgs5* (Fig. 6f, Extended Data Fig. 10c and Supplementary Data).

Next, we compared the RNA profiles of WT and Tg mice under DSS conditions, identifying 473 differentially expressed genes (Fig. 6g). In line with expression profiles at baseline, in hIL-26 mice we again observed a clear decrease in expression of immune response-associated transcripts (Fig. 6g-i and Extended Data Fig. 10c) and an increase in stromal compartment signatures (Fig. 6g and Extended Data Fig. 10c). While the expression of many immune compartment-associated markers was already decreased in hIL-26 mice at baseline (for example, *Ptprc/CD45*; Fig. 6i), we found that induction of both proinflammatory cytokines (for example, *Tnf*) and chemokines (for example, *Cxcl9* and *Cxcl10*) was reduced in hIL-26 mice under DSS (Fig. 6i). We further confirmed these observations by qPCR (Extended Data Fig. 10d). Based on these results, we propose a link between the role of IL-26 and the reported effect of cytokines (for example, Il33 and *Tnf*) in promoting context-dependant intestinal barrier integrity or mucosal damage in acute experimental colitis^{26,27}. Furthermore, our results provide initial evidence for an immunoregulatory role for IL-26 in acute colitis.

Discussion

Here we reveal the life course of colonic T cells in UC and their evolution to *GZMK*- and *TNF*-expressing effector states and to

clonally expanded *IL26* and coinhibitory receptor-expressing cells with type 17 and immunoregulatory features. An imbalance between *GZMK*⁺*TNF*⁺ effectors and immunoregulatory *IL26*⁺ cells may facilitate tissue destruction that manifests as UC.

IL26⁺ CD8⁺ cells exhibited features of chronic stimulation, including expression of *HAVCR2*, and displayed a colitis-specific *ETV7* transcriptional network that limits inflammation through inhibition of *ETS1*-controlled genes (such as *T-bet* that drives Th1 responses)^{28,29}. This cluster also adopted key innate properties, such as induction of *NCR3*, an NK cell receptor that participates in anti-tumor responses. Previously, TCR and NCR costimulation has been shown to have a synergistic effect in circulating NKp30⁺/*NCR3*⁺ CD8⁺ T cells³⁰. In UC, this suggests a possible mechanism for a sustained T-cell response under chronic stimulation conditions where innate programs may help these cells retain response functions in the absence of antigen-specific cues.

Induction of *IL26* protected against epithelial damage in a mouse model of acute colitis. While mouse models that incorporate chemicals to induce colitis (for example, DSS) can be useful in studying the acute phase of tissue injury and repair mechanisms, the resulting inflammation is generally not fully representative of the immune dysregulation present in the inflamed colon of patients with IBD³¹. Although the *IL26* phenotype may be protective in acute inflammation, we suspect that its role in chronic inflammation may be different because Th17 responses can indicate a more severe disease in UC³². Alternatively, the protective effects of IL-26 may be inadequate in chronic UC. In contrast to the protective effects in acute inflammation, the *IL26*⁺ cluster also strongly induced a *STAT3* network required for Th17 responses. *IL26* is expressed by infiltrating proinflammatory IL-17-producing T cells in chronically inflamed IBD tissue³³, signaling through the *IL-10R2/IL-20R1* heterodimeric receptor to induce expression of *IL-10* and *TNF*; furthermore, IL-26 may have direct antimicrobial effects^{10,11}. However, characterization of the role of *IL26* during chronic inflammation will be important because it could have, like other cytokines, a dichotomous role depending on the temporal phase of the inflammatory process²⁷. Transcriptional regulation of *IL26* expression in T cells is not well defined, although it may require IL23R signaling. Future studies will delineate the mechanism for IL-26 expression by IBD-associated *IL23R* and *IL26* polymorphisms, and whether the divergence of observed phenotypes among single clones reflects their geographical location and specific local exposures or derives from a continuum of differentiation.

Online content

Any methods, additional references, Nature Research reporting summaries, source data, extended data, supplementary information, acknowledgements, peer review information; details of author contributions and competing interests; and statements of data and code availability are available at <https://doi.org/10.1038/s41591-020-1003-4>.

Received: 31 July 2019; Accepted: 4 June 2020;

Published online: 03 August 2020

References

- Mueller, S. N. & Mackay, L. K. Tissue-resident memory T cells: local specialists in immune defence. *Nat. Rev. Immunol.* **16**, 79–89 (2016).
- Stockenhuber, K. et al. Foxp3⁺ T reg cells control psoriasisiform inflammation by restraining an IFN- γ -driven CD8⁺ T cell response. *J. Exp. Med.* **215**, 1987–1998 (2018).
- Lee, J. C. et al. Gene expression profiling of CD8⁺ T cells predicts prognosis in patients with Crohn disease and ulcerative colitis. *J. Clin. Invest.* **121**, 4170–4179 (2011).
- The Gene Ontology Consortium. The Gene Ontology resource: 20 years and still GOing strong. *Nucleic Acids Res.* **47**, D330–D338 (2019).
- Cheroutre, H., Lambolez, F. & Mucida, D. The light and dark sides of intestinal intraepithelial lymphocytes. *Nat. Rev. Immunol.* **11**, 445–456 (2011).

6. Liu, J. Z. et al. Association analyses identify 38 susceptibility loci for inflammatory bowel disease and highlight shared genetic risk across populations. *Nat. Genet.* **47**, 979–986 (2015).
7. Silverberg, M. S. et al. Ulcerative colitis-risk loci on chromosomes 1p36 and 12q15 found by genome-wide association study. *Nat. Genet.* **41**, 216–220 (2009).
8. McGovern, D. P. B. et al. Genome-wide association identifies multiple ulcerative colitis susceptibility loci. *Nat. Genet.* **42**, 332–337 (2010).
9. Saunders, P. M. et al. A bird's eye view of NK cell receptor interactions with their MHC class I ligands. *Immunol. Rev.* **267**, 148–166 (2015).
10. Hör, S. et al. The T-cell lymphokine interleukin-26 targets epithelial cells through the interleukin-20 receptor 1 and interleukin-10 receptor 2 chains. *J. Biol. Chem.* **279**, 33343–33351 (2004).
11. Meller, S. et al. TH17 cells promote microbial killing and innate immune sensing of DNA via interleukin 26. *Nat. Immunol.* **16**, 970–979 (2015).
12. Bahrami, S. & Drablos, F. Gene regulation in the immediate-early response process. *Adv. Biol. Regul.* **62**, 37–49 (2016).
13. Parikh, K. et al. Colonic epithelial cell diversity in health and inflammatory bowel disease. *Nature* **567**, 49–55 (2019).
14. Mazzurana, L., Rao, A., Van Acker, A. & Mjösberg, J. The roles for innate lymphoid cells in the human immune system. *Semin. Immunopathol.* **40**, 407–419 (2018).
15. Zeng, B. et al. ILC3 function as a double-edged sword in inflammatory bowel diseases. *Cell Death Dis.* **10**, 315 (2019).
16. McKinney, E. F., Lee, J. C., Jayne, D. R. W., Lyons, P. A. & Smith, K. G. C. T-cell exhaustion, co-stimulation and clinical outcome in autoimmunity and infection. *Nature* **523**, 612–616 (2015).
17. Maggi, L. et al. CD161 is a marker of all human IL-17-producing T-cell subsets and is induced by RORC. *Eur. J. Immunol.* **40**, 2174–2181 (2010).
18. Constantinides, M. G., McDonald, B. D., Verhoef, P. A. & Bendelac, A. A committed precursor to innate lymphoid cells. *Nature* **508**, 397–401 (2014).
19. Glanville, J. et al. Identifying specificity groups in the T cell receptor repertoire. *Nature* **547**, 94–98 (2017).
20. Shugay, M. et al. VDJdb: a curated database of T-cell receptor sequences with known antigen specificity. *Nucleic Acids Res.* **46**, D419–D427 (2018).
21. Bartolomé-Casado, R. et al. Resident memory CD8 T cells persist for years in human small intestine. *J. Exp. Med.* **216**, 2412–2416 (2019).
22. Welch, J. D. et al. Single-cell multi-omic integration compares and contrasts features of brain cell identity. *Cell* **177**, 1873–1887 (2019).
23. Fujii, M. et al. Expression of Interleukin-26 is upregulated in inflammatory bowel disease. *World J. Gastroenterol.* **23**, 5519–5529 (2017).
24. Schoenborn, J. R. et al. Comprehensive epigenetic profiling identifies multiple distal regulatory elements directing Ifng transcription. *Nat. Immunol.* **8**, 732–742 (2007).
25. Collins, P. L., Henderson, M. A. & Aune, T. M. Lineage-specific adjacent IFNG and IL26 genes share a common distal enhancer element. *Genes Immun.* **13**, 481–488 (2012).
26. Lopetuso, L. R. et al. IL-33 promotes recovery from acute colitis by inducing miR-320 to stimulate epithelial restitution and repair. *Proc. Natl Acad. Sci. USA* **115**, E9362–E9370 (2018).
27. Bamias, G., Corridoni, D., Pizarro, T. T. & Cominelli, F. New insights into the dichotomous role of innate cytokines in gut homeostasis and inflammation. *Cytokine* **59**, 451–459 (2012).
28. Grenningloh, R., Kang, B. Y. & Ho, I.-C. Ets-1, a functional cofactor of T-bet, is essential for Th1 inflammatory responses. *J. Exp. Med.* **201**, 615–626 (2005).
29. Vivekanand, P. & Rebay, I. The SAM domain of human TEL2 can abrogate transcriptional output from TEL1 (ETV-6) and ETS1/ETS2. *PLoS ONE* **7**, e37151 (2012).
30. Correia, M. P. et al. Distinct human circulating NKp30⁺ FcεRIγ⁺ CD8⁺ T cell population exhibiting high natural killer-like antitumor potential. *Proc. Natl Acad. Sci. USA* **115**, E5980–E5989 (2018).
31. Bamias, G., Arseneau, K. O. & Cominelli, F. Mouse models of inflammatory bowel disease for investigating mucosal immunity in the intestine. *Curr. Opin. Gastroenterol.* **33**, 411–416 (2017).
32. Ueno, A. et al. Th17 plasticity and its relevance to inflammatory bowel disease. *J. Autoimmun.* **87**, 38–49 (2018).
33. Abraham, C. & Cho, J. Interleukin-23/Th17 pathways and inflammatory bowel disease. *Inflamm. Bowel Dis.* **15**, 1090–1100 (2009).

Publisher's note Springer Nature remains neutral with regard to jurisdictional claims in published maps and institutional affiliations.

© The Author(s), under exclusive licence to Springer Nature America, Inc. 2020

Methods

Human specimens. Colonic biopsies were collected from patients attending endoscopy at Oxford University Hospitals NHS Foundation Trust. NHS National Research Ethics Service research ethics committee references for the study include nos. 18/WM/0237, GI 16/YH/0247 and IBD 09/H1204/30. Biopsies were collected following informed written consent from healthy individuals undergoing colonoscopic screening, or from patients with IBD administered ongoing clinical care. For patients with IBD, we used samples derived from those with ulcerative colitis and proven mucosal inflammation, as indicated by the Ulcerative Colitis Endoscopic Index of Severity²⁴.

Single-cell isolation. Tissues were collected from clinically inflamed distal colon and placed in in RPMI supplemented with 100 U ml⁻¹ penicillin, 100 µg ml⁻¹ streptomycin and 10 mM HEPES on ice. Samples were either processed immediately after collection or stored by freezing in 1 ml of Cryostor DS10 (Sigma-Aldrich) for experiments requiring multiple samples, to reduce batch effects. Viability and colonic CD8⁺ T-cell purity were similar to those of freshly isolated samples. After washing in PBS, biopsies were incubated in media with 3 mg ml⁻¹ Collagenase type II (Worthington Biochem), containing 50 µg ml⁻¹ DNase, for 60 min at 37 °C with agitation (250 r.p.m.), followed by 5–10× mechanical dissociation of the suspension through a 16-gauge needle (Stemcell Technologies). The cell suspension was washed in PBS and passed through a 70-µm filter. Cell counts and viability were confirmed with a Countess II automated cell counter (Thermo Fisher).

Flow cytometry. For single-cell RNA-seq experiments, single-cell suspensions were stained with anti-CD3 (clone SP34-2) BV711 and anti-CD8 (clone SK1) APC-R700 (BD Horizon), with DAPI added before sample acquisition, to assess cell viability. Flow sorting was performed on a FACSAria IIIu to collect live CD3⁺CD8⁺ T cells. Cells were collected in media and kept on ice before loading onto the 10× Chromium Single Cell Platform.

For IL-26 receptor quantification (heterodimer of IL-20Rα and IL-10Rβ), biopsies were dissociated into single-cell suspensions as described above in 'Single-cell isolation', followed by staining for anti-IL-10RB (clone 90220), anti-IL-20RA (clone 173714), anti-EPCAM (clone 9C4) and anti-CD45 (clone 5B1) for 30 min at 4 °C, with DAPI used for live–dead staining, followed by acquisition on a BD LSRII machine.

Droplet-based single-cell RNA-seq. CD3⁺CD8⁺ cells were washed in PBS with 0.04% bovine serum albumin (BSA) and resuspended at a concentration of ~500 cells µl⁻¹. Approximately 8,000 cells were loaded onto the Chromium 10x Genomics platform (10x Genomics) to capture single cells, as described in the manufacturer's protocol. The 10x Genomics 5' mRNA single-cell method was used in one run, including cells isolated from biopsies of healthy inflamed UC.

Library generation for 10x Genomics v2 chemistry was performed using the Chromium Single Cell 5' and Chromium Single Cell V(D)J Reagent Kits (user guide, no. CG000086).

Quantification of complementary DNA was performed using the Qubit dsDNA HS Assay Kit (Life Technologies, no. Q32851) and Agilent High Sensitivity D5000 ScreenTape (Agilent, no. 5067-5592). Library quantification was performed using the Qubit dsDNA HS Assay Kit (Life Technologies, no. Q32851) and D1000 ScreenTape (Agilent, no. 5067-5582). Libraries were sequenced on an Illumina HiSeq4000 platform to achieve an average of 50,000 reads per cell.

CITE-seq. For combined transcriptomic and protein data, we used CITE-seq antibodies combined with Cell Hashing (as per established protocols²⁵). Briefly, cell suspensions were derived from biopsies as described above in 'Single-cell isolation', washed in cold PBS (supplemented with 2% BSA and 0.01% Tween) followed by 10-min incubation with blocking antibody (TruStain FcX, Biolegend). Antibody mixes were prepared consisting of CITE-seq antibody (Biolegend Totalseq-C products, 0.5 µg antibody per 2 million cells; full list given in Supplementary Table 3), optimized concentrations of FACS antibody (anti-CD3 and anti-CD8a, 1.66 µl per 2 million cells) and hashing antibody (Biolegend, 0.5 µg per 2 million cells). Cells were incubated for 30 min at 4 °C followed by three washes to remove excess antibody, then CD3⁺CD8⁺ cells were isolated using FACS as described above in 'Flow cytometry'. CD8 cells from different donors bearing different hashes were pooled immediately before loading, where we superloaded 11,000–20,000 cells for each run.

Library generation for CITE-seq and hashed samples was performed using 10x Chromium Single Cell 5' V(D)J Reagent Kits with feature barcoding technology (user guide, no. CG000186).

Libraries were sequenced on an Illumina Novaseq 6000 S4 platform to achieve an average of 50,000 reads per cell for the gene expression libraries and 5,000 reads per cell for the cell surface protein and hashing protein libraries.

Real-time PCR. For quantitative real-time (qPCR) experiments, tissue samples were subjected to physical homogenization (with 100 mg of 1.4-mm ceramic beads, 4,000 r.p.m.), and total RNA was isolated using an RNeasy Miniprep kit (QIAGEN). cDNA was then synthesized using the high-capacity RNA-to-cDNA kit (Thermo Fisher) followed by rtPCR performed using TaqMan gene expression

assays on the QuantStudio 7-Flex system (Thermo Fisher). A list of primers used is given in Supplementary Table 4.

Bulk RNA-seq. RNA from mouse tissue was extracted as described for rtPCR. High-quality samples, as assessed by RNA integrity number quality, were then converted to strand-specific cDNA libraries using the NEBNext Ultra Directional RNA Library Prep Kit for Illumina (no. 7420), with an insert size of 250–300 base pairs. Samples were sequenced to a depth of 20 million reads per sample on a Novaseq 6000 S4 platform.

ELISA. Biopsies were dissociated into single-cell suspensions, as described above in 'Single-cell isolation', and CD8⁺ T cells purified by negative immunomagnetic bead selection (Miltenyi Biotec). Cells were plated in the presence of coated anti-CD3 (10 µg ml⁻¹) and soluble anti-CD28 (10 µg ml⁻¹) (BD Bioscience) for 72 h. Cell-free supernatants were collected before analysis of IL-26 secretion by ELISA (Cusabio).

Conjugation of metal isotopes to antibodies, staining and CyTOF acquisition. Purified antibodies were conjugated with metal isotopes using Maxpar Conjugation kits (Fluidigm). Briefly, the procedure involved initial preloading of polymer with lanthanide and partial antibody reduction, followed by antibody conjugation with the lanthanide-loaded polymer. Lanthanide metal-labeled antibodies were obtained from Fluidigm.

Cryopreserved colon biopsies from healthy individuals, or from patients with inflamed IBD and active inflammation, were thawed, washed twice in PBS and digested using Collagenase type II (Worthington Biochem) to obtain a single-cell suspension. In some experiments, single-cell suspensions were washed twice in PBS, resuspended in media and stimulated for 4 h at 37 °C in the presence of 40 ng ml⁻¹ PMA, 2 µg ml⁻¹ ionomycin (Sigma) and protein transport inhibitor containing Monensin (BD GolgiStop). Cells were washed twice in Maxpar Cell Staining Buffer (Fluidigm), then stained with metal-tagged surface antibody cocktail for 30 min at room temperature. Cisplatin was added for 5 min, cells were washed and then incubated for 30 min with Nuclear Antigen Staining Buffer followed by washing twice with Nuclear Antigen Staining Perm. Cells were incubated with intracellular metal-tagged antibody cocktail for 30–45 min, washed, then fixed in 1.6% paraformaldehyde. After washing of fixed cells, cellular DNA was labeled at room temperature with 72.5 nM iridium intercalator, obtained by the addition of Cell ID Intercalator-Ir to Maxpar Fix and Perm Buffer (Fluidigm).

Cells were washed twice with Maxpar Cell Staining Buffer and left pelleted until acquisition. Before acquisition of each sample, cells were washed twice with water, EQ Four Element Calibration Beads (Fluidigm) were added (10% of final volume) and the sample was filtered through a 0.35-µm cell strainer into a 5-ml polystyrene tube. Cells were acquired and analyzed on a CyTOF2 Helios mass cytometer (Fluidigm). Samples reported were stained and acquired on the same day, to minimize batch effects.

Mice. All mice were housed under standard conditions in the animal facility at the School of Medicine, Juntendo University, Tokyo, Japan. Animal experiments were conducted following protocols approved by the Animal Care and Use Committees at Juntendo University. C57BL/6 (B6) mice were obtained from CLEA Japan. B6 mice carrying a 190-kb bacterial artificial chromosome (BAC) transgene with the human genes *IFNG* and *IL26* (hIL-26Tg) were developed in T. Aune's laboratory²⁵. The expression of human *IL26* was tested in different organs and was demonstrated to be expressed at high levels in the colon and small intestine²⁵ of these mice. Mice were housed in a specific pathogen-free facility in microisolator cages with ad libitum access to autoclaved water and sterile standard food, and were maintained at 24 ± 2 °C under a 12/12-h light/dark cycle (lights on from 08:00 to 20:00). Both male and female B6 and hIL-26Tg mice at 10–14 weeks of age were selected for the DSS-induced colitis model. Mice at 20–24 weeks of age were used for analysis of spontaneous ileitis and colitis.

Induction of DSS colitis. Dextran sulfate sodium colitis was induced as previously reported, with minor adaptations²⁶. Briefly, sterilized 2.5% (w/v) DSS (TdB Consultancy) was added to the drinking water for 6 d. Adult control littermate B6 and hIL-26Tg mice were allowed ad libitum access to water. Daily monitoring was performed for body weight, fecal bleeding and the presence of loose stools. Mice were injected intraperitoneally with either anti-IL-26-neutralizing mAb (clone 69-10, 200 µg)^{37,38} or control mouse IgG_{1,k} isotype-matched mAb (clone MG1-45, 200 µg) at days 0 and 3.

Histology and assessment of inflammation. Ileal and colons from control littermate B6 and hIL-26Tg mice were removed, flushed of fecal contents using PBS, opened longitudinally and placed in formaldehyde solution for fixation. Tissues were kept in 70% ethanol solution until embedding in paraffin, and stained with hematoxylin and eosin. Inflammation was evaluated by a pathologist in a blinded fashion, using a previously described scoring system³⁹. Colon total inflammatory score represents the sum of the following subindices: active and chronic inflammation, percentage re-epithelialization, transmural index and percentage ulceration.

Bulk RNA-seq analysis. Raw sequence reads were quality checked using FastQC software⁴⁰. Cutadapt⁴¹ software was used to trim poor-quality bases (<20) and Illumina universal adapter sequences from raw reads before alignment.

The mouse mm10 reference genome analysis set was obtained from the University of California Santa Cruz (UCSC) ftp site⁴². The hIL-26 BAC sequence was added as an additional reference contig and indexed together with mm10 as a reference genome using STAR aligner⁴³. Reads were then aligned to this custom reference.

Picard tools⁴⁴ was used to mark duplicate sequences as an additional quality control step, and Samtools⁴⁵ was used to estimate total BAC read recovery. Raw gene expression counts were summarized with featureCounts⁴⁶ using a custom mm10 and hIL-26 BAC GTF file containing joint mouse and BAC transcriptome annotations. The MultiQC tool was used to aggregate quality metrics. Sample quality metrics and raw read counts were imported into R for further processing. The DESeq2 (ref. 47) R package was used to estimate library size factors, normalize counts and perform differential expression analyses. Benjamini–Hochberg multiple testing correction was used to compute FDR, and genes were considered significantly differentially expressed at <5% FDR. Principal component analysis was performed in R using the top 1,000 most variable genes, with normalized DESeq2 variance-stabilized transformation expression as input.

scRNA-seq analysis. Raw sequence read quality was assessed using FastQC software⁴⁰. The human hg38 reference genome analysis set was downloaded from the UCSC ftp site⁴². Cell Ranger software (v2.1.1) was downloaded from 10x Genomics (<https://support.10xgenomics.com/single-cell-gene-expression/software/downloads/latest>) and used to process raw data, align reads to the hg38 human reference genome and summarize unique molecular identifier (UMI) counts against the corresponding Ensembl gene annotations obtained in GTF format using the UCSC Table Browser Tool⁴⁸.

Empty wells were distinguished from barcoded cells using UMI count distributions. First, UMIs that were probably misassigned to an incorrect barcode due to sequencing index swapping were first removed using DropletUtils⁴⁹. The emptyDrops⁵⁰ function from DropletUtils was then used to distinguish cells from empty droplets containing only ambient RNA, with barcodes <5% FDR retained. In addition, droplet barcodes with low total UMI counts and droplets for which a high percentage of total UMIs originated from mitochondrial RNAs (>15%) were filtered out. For the remaining cells in each sample, doublet detection and filtering was performed using DoubletFinder⁵¹.

Cell cycle stage scoring and annotation was performed using the cyclone function implemented in the R package scran⁵². The Seurat R package was used to normalize expression values for total UMI counts per cell.

For clustering analysis, cells from multiple donors were merged. Cell cycle scores, together with total UMI counts per cell, percentage of mitochondrial features and individual donor effects, were considered as a source of unwanted variation and were regressed out using the Seurat package⁵³. Highly variable genes were identified by fitting the mean variance relationship for each sample, to avoid selecting for genes with highly variable between-sample effects and to prioritize those with high within-sample variation. Initially, dimensionality reduction was performed using PCA (R package irlba). Scree plots and Jackstraw permutation tests were used to determine significant principal components (with *P* cut-off <0.01) in the data. A *k*-nearest neighbor (*k*NN) graph was constructed from cells in the reduced dimension space in Seurat, using significant principal components as input and other parameters at default. Cells were then clustered using the Louvain algorithm for modularity optimization with the *k*NN graph as input and the resolution parameter set to 0.7. Cell clusters were visualized with the UMAP algorithm⁵⁴ using the R package uwot, with significant principal components as input and nearest neighbors 30, spread 1 and minimum distance 0.01.

For clustering analysis of single-cell data according to ref. 55, data were obtained from the Broad Data Use Oversight System (no. DUOS-000110) following institutional approval and processed as described above in this section. CD45⁺ cells were subset from lamina propria samples, and clusters were annotated according to the nomenclature and gene markers used by the original authors.

CITE-seq sample demultiplexing. CITE-seq samples were hashed together across multiple pools, which were demultiplexed as follows. Raw UMI counts for each hashing antibody oligonucleotide tag were calculated using Cellranger software, v3.1.0. Raw count matrices were first filtered to retain only droplet barcodes from cells passing quality control based on mRNA expression profiles, as described above in 'scRNA-seq analysis'. Barcodes with high antibody library yield but poor mRNA were discarded, as these were likely to arise from poor-quality/dying cells still with intact cell membranes and thus stable protein expression.

A filtered hashed feature counts matrix was then used to demultiplex samples, as described in ref. 55, using the HTODemux function in the R package Seurat. Briefly, counts were normalized using centered log ratio transformation and, for each pool, an initial clustering solution was obtained using Clara *k*-medoids clustering with *k* = 1 + number of samples in the pool. For each cluster/hash ID, we then fit a negative binomial distribution and defined a positive threshold at the 99th percentile of the recovered normalized UMI counts for the hashtag, with cells below this threshold considered negative for the tag. Cell identity was then

assigned based on individual hashtag thresholds and multiplets defined as cells positive for multiple tags. Multiplets were then filtered out. Cells negative for all hash tags based on these thresholds formed a minor fraction and were also filtered out, following inspection of their mRNA cluster distribution. Untagged cells correlated with cells with low total mRNA content and did not segregate with any particular cluster, and thus probably contained unstained/dying cells or free nuclei that had lost their cytoplasm during sample processing.

Demultiplexed cells were visualized as *t*-distributed stochastic neighbor-embedding (*t*-SNE) plots from Euclidian distance matrices.

CITE-seq data analysis. Messenger RNA data from the CITE-seq cohort were processed as described above in 'scRNA-seq analysis'. For clustering analysis of the CITE-seq protein panel, protein expression was first normalized using centered log ratio transformation. Euclidean distances between cells were then computed from normalized protein expression of all features (14 antibody readouts) using the *dist* function in R, with default parameters. A cell *k*NN graph was then contracted using the distance matrix as input and *k* = 20 nearest neighbors. The *k*NN graph was used as input for Louvain clustering as before, with final clustering resolution of 0.2 and other parameters as default. Varying cluster resolutions were examined and, given the relatively low dimensionality of CITE-seq data, a higher clustering resolution parameter (more clusters) overclustered the data where clusters were no longer driven by meaningful biological partitions.

scRNA-seq differential expression analysis and cluster marker detection. The R package MAST⁵⁶ was used to perform all single-cell differential gene expression analyses between conditions. In each case, confounding sources of variation stemming from cellular gene detection rate, cell cycle score and donor/batch effects were included in the model formula as covariates. Likelihood ratio tests between the full and reduced model formulas were used to identify differentially expressed genes between conditions. Benjamini–Hochberg multiple testing correction was used to estimate FDR, as implemented in the R package stats function, *p.adjust*. Genes with FDR < 5% were considered significantly differentially expressed.

To detect cluster marker genes, cells from each cluster were compared against all other cells in the experiment. As noted in the paragraph above, the MAST algorithm was used for statistical testing via the Seurat wrapper function FindMarkers, with default parameters for filtering out genes below a minimum log-fold change threshold of 0.25 and infrequently (10% of cells) expressed genes.

GO and pathway enrichment analyses. Gene Ontology⁴ and pathway enrichment analyses were performed using the clusterProfiler R package⁵⁷. The annotation Dbi R package org.Hs.eg.db was used to map gene identifiers. Cluster marker sets and differentially expressed genes were tested individually for overrepresentation, with all expressed/detected genes in each case used as a background control. In each case, GO gene sets were tested for overrepresentation in cluster markers or differentially expressed genes by computation of enrichment *P* values (the enricher R function, default parameters) from the hypergeometric distribution of total genes in the background gene set, the number of genes within background annotated with the gene set, the size of the gene set and the number of genes within the cluster marker/differentially expressed genes list annotated with the gene set. Hypergeometric *P* values were adjusted in each case for multiple testing using Benjamini–Hochberg correction as before. The results were visualized as dot plots and map plots using the R packages clusterProfiler⁵⁷, enrichPlot and ggplot2 (ref. 58).

To score individual cells for pathway activities, we used the R package AUCCell. First, for each cell we used an expression matrix to compute gene expression rankings in each cell with the AUCCell_buildRankings function, with default parameters. The canonical pathway database was downloaded from the Broad Institute website, and canonical pathway gene sets were then used to score each cell where, for each gene set and cell, area-under-the-curve (AUC) values were computed (AUCCell_calcAUC function) based on gene expression rankings, where AUC values represent the fraction of genes within the top-ranking genes for each cell that are defined as part of the pathway gene set.

Receptor–ligand pair analysis. Receptor–ligand analysis between T-cell and epithelial cell subpopulations was performed using CellphoneDB statistical analysis, v2.0 (ref. 59). We previously used epithelial single-cell data on both health and UC generated in our laboratory¹³. The total number of pairwise paracrine interactions between T cells and epithelium obtained using the CellphoneDB scoring method were visualized as heatmaps in the R package pheatmap. Top significant interactions from the aspect of selected relevant clusters were visualized as dot plots using the ggplot2 package in R. To identify putative altered cell–cell interactions between T-cell and epithelial cell subpopulations, irrespective of cell type specificity, we additionally employed a differential expression-based approach. First, we reformatted the CellphoneDB receptor–ligand database to break down and simplify interactions involving protein complexes into one-to-one interactions. Additionally, we also downloaded a larger database of known receptor–ligand pairs⁶⁰ following the same format for a parallel, independent analysis. Taking each cluster from both CD8⁺ cells and epithelial cell datasets, we first subset the receptor–ligand databases to retain only those receptors and ligands that were at

least minimally expressed in either dataset, by setting a threshold of detection in at least 10% of all cells within a given cluster in UC samples and/or samples from healthy donors. Then, we intersected the results from our differential expression analyses with the filtered receptor–ligand database. For differential expression analyses of colonic epithelium cells in UC, we used results previously reported¹³. Then, for each pairwise CD8⁺ and epithelial cell cluster comparison, we classified each receptor–ligand interaction categorically into ‘putative loss of interactions’, ‘putative gains of interactions’ or ‘no change’ based on up-/downregulation/no change in expression of these molecules in health versus UC samples. As described in ref. ⁶⁰, putative gain in cell–cell communication between a pair of clusters was defined as one of the following:

- (1) Significant upregulation of receptor expression in one cluster and significant upregulation of ligand expression in the other cluster between UC and healthy donor cells
- (2) Significant upregulation of receptor expression in one cluster but no statistically significant change in ligand expression in the other cluster, given that the ligand is detected in at least 10% of cells within the cluster
- (3) Significant upregulation of ligand receptor in one cluster but no statistically significant change in receptor expression in the other cluster, given that the receptor expression is detected in at least 10% of cells within the cluster

Likewise, putative loss of cell–cell interaction events was defined as:

- (1) Significant downregulation of receptor expression in one cluster and significant downregulation of ligand expression in the other cluster between UC and healthy donor cells
- (2) Significant downregulation of receptor expression in one cluster but no statistically significant change in ligand expression in the other cluster between UC and healthy donor cells
- (3) Significant downregulation of ligand expression in one cluster but no statistically significant change in receptor expression in the other cluster between UC and healthy donor cells
- (4) Significant downregulation of receptor in one cluster, while the other cluster shows statistically significant upregulation of corresponding ligand
- (5) Significant downregulation of ligand in one cluster, while the other cluster shows statistically significant upregulation of corresponding receptor.

All epithelial and CD8⁺ T-cell clusters were examined as pairwise combinations, and all putative loss and gain of cell–cell communication events were defined for all receptor–ligand pairs. The data were then examined from the aspect of individual CD8⁺ subpopulations, filtering putative altered interactions not directly involving the CD8⁺ cluster under consideration and visualized as Circos plots. Gains and losses of interactions were plotted separately. This analysis was repeated on two receptor–ligand databases independently, with the full results included in Supplementary Data.

Pseudotime trajectory analysis. Single-cell pseudotime trajectories were reconstructed using the Rpackage *monocle*⁶¹. Dimensionality reduction was first performed with the DRRTree algorithm, using the expression of all highly variable genes detected as described above in ‘scRNA-seq analysis’. As in scRNA-seq clustering analyses, to subtract confounding variation, cellular gene detection rate, percentage of mitochondrial gene expression, cell cycle scores and donor/batch effects were included as covariates in the residual model formula to subtract these effects from the data. Cell trajectory was then captured using the *orderCells* function, with the starting pseudotime state denoted as the end of the trajectory that was found to be enriched for naïve T-cell clusters. As before for differential gene expression analyses, the Rpackage *MAST* was used to detect genes significantly covarying with pseudotime, based on a log-likelihood ratio test between the model formula including cell pseudotime and a reduced model formula. Additional model covariates were included in the residual model formula as described in ‘scRNA-seq analysis’. Benjamini–Hochberg multiple testing correction was used to calculate FDR, and genes <5% FDR were considered to vary significantly with pseudotime.

Transcription factor module analysis. The Rpackage *SCENIC* workflow was used to detect active transcription factor modules in CD8⁺ cells. The normalized single-cell gene expression matrix was first filtered to exclude all genes detected in fewer than 20 cells. The *RcisTarget* database, containing transcription factor motif scores for gene promoters and around transcription start sites for the hg38 human reference genome, was downloaded from https://resources.aertslab.org/cistarget/databases/homo_sapiens/hg38/refseq_r80/mc9nr/gene_based/, and the expression matrix was further filtered to include only genes available in the *RcisTarget* database. The remaining genes were used to compute a gene–gene correlation matrix for coexpression module detection using the random forest-based *GENIE3* algorithm⁶², and the Rpackage *SCENIC*⁶³ was used to perform transcription factor network analysis to detect coexpression modules enriched for target genes of each candidate TF from the *RcisTarget* database. The *AUCCell*⁶³ package was used to compute a score for each TF module in each individual cell, as described above in ‘GO and pathway enrichment analyses’.

To prioritize/identify TF modules showing differential activity in UC versus healthy donor cells, AUC score distributions from UC-derived and healthy donor-derived cells were compared using the two-sample Kolmogorov–Smirnov test.

TCR analysis. Single-cell TCR clonotypes were assembled using *Cellranger* VDJ software. Single-cell barcodes were then used to link corresponding VDJ (variable-diversity-joining TCR gene segments) and gene expression data. *VDJTools*⁶⁴ was used to compute TCR repertoire statistics and gene segment usage for individual samples, as well as cluster-level statistics. Assembled TCR-β-CDR3 amino acid sequences were used to query *VDJdb*⁶⁰ for overlap with known and/or public TCR sequences, because the vast majority of the TCR sequence data curated in *VDJdb* are unpaired TRB sequences.

Clonality was defined for each sample individually, as follows: TCR clonotypes detected in fewer than three cells were considered unexpanded; while typically observation of two clones in a small pool of cells sequenced here would be indicative of clonal expansion, we cannot discount the possibility of undetected doublets occurring in the data. Furthermore, it has been shown that 10x may sometimes generate ‘barcode multiplets’, where one cell is indexed by two different barcodes⁶⁵ and could lead to attributing a TCR singlet to more than one cell. Thus, we consider clonotypes as ‘expanded’ based solely on this more stringent threshold. The expanded clonotypes were sorted based on their frequency and divided into five quantiles per sample, with Q1 representing the top 20% most expanded clonotypes and Q5 representing the bottom 20%.

TCR cluster ‘lineage’ tracing was performed by considering all clonotypes shared by cells from more than one cluster. Raw numbers of cluster clonotype intersections were analyzed and visualized as upset plots⁶⁶.

GWAS cell type specificity analysis. The *SNPsea* algorithm⁶⁷ was used to test for significant enrichment of tissue-specific expression in UC-associated GWAS loci genes in CD8⁺ T-cell clusters. In addition, as nonimmune outgroups, we used 10x single-cell data from colonic mesenchymal and colonic epithelial single cell clusters, as reported in refs. ^{13,68}. IBD-associated locus information was downloaded from the GWAS catalog⁶⁹ from refs. ^{6,70}, which report the largest number of UC-associated genomic loci to date. Data from the 1000 Genomes Project⁷¹ were used to sample matched control single-nucleotide polymorphisms (SNPs) and to link SNPs to genes. With single-cell RNA-seq data, for each CD8⁺ T cell, epithelial and mesenchymal cell cluster, a ‘pseudobulk’ dataset was created in health and UC separately by summing all UMI counts for each gene in each cluster. Cluster pseudobulk counts were normalized by computing size factors (Rpackage *DESeq2* (ref. ⁴⁷)) to account for differences in cell cluster sizes, and normalized data were used as input for *SNPsea*. *SNPsea* was then run with the following parameter settings: `–slop 10e3`, `–threads 8`, `–null-snpsets 1000`, `–min-observations 100`, `–max-iterations 1e7`, `–score single`. FDR rate was calculated using Benjamini–Hochberg multiple testing correction.

Comparison with single-cell scRNA-seq from TILs. Liver, colorectal and breast cancer TIL scRNA-seq datasets were downloaded from Gene Expression Omnibus (GEO) (accession nos. *GSE98638*, *GSE114724* and *GSE108989*)^{72–74}. Single-cell analysis, data normalization and clustering analysis for each dataset were performed as described above in ‘scRNA-seq analysis’, to standardize analysis workflows and parameters between colonic CD8⁺ data presented here and cancer TIL datasets. Clusters obtained from reanalysis of the cancer TIL datasets were labeled in accordance with original publications, and cluster markers were identified using Seurat negative binomial model likelihood ratio tests, modeling sources of confounding variation as covariates, as described in ‘scRNA-seq analysis’ and ‘scRNA-seq differential expression analysis and marker detection’. The closest cluster counterparts between different datasets were identified using the binary cluster marker overlap approach, as described in ref. ⁷⁵. Distances between clusters in different datasets were visualized using hierarchical clustering. The Rpackage *dendextend*⁷⁶ was used to produce visualizations.

CyTOF data analysis. Following acquisition, data were normalized as previously described⁷⁷ and exported as a flow cytometry file (FCS). Each sample was manually gated in *FlowJo*, and FCS files relative to viable CD45⁺CD3⁺CD8⁺ cells were exported for downstream analysis. The Rpackage *Cytofkit*⁷⁸ was used for downstream analysis. Data were arcsinh transformed with a cofactor of 5, and clustering was performed using the algorithm *Phenograph*⁷⁹. Cell clusters were visualized as either *t*-SNE or UMAP plots.

Multimodal CyTOF and 10x scRNA-seq data integration was performed by alignment of shared factors identified for each dataset by integrative non-negative matrix factorization, as implemented in the Rpackage *liger*⁷². The CyTOF dataset was used as a reference. First, mRNA expression matrices were filtered out to retain only those genes for which protein expression was available in our CyTOF panel. Data in each dataset were normalized individually, as before. The optimum number of factors, *k* (18), was first determined by computing the median Kullback–Leibler divergence from uniform for cell factor loadings (‘suggest’ function, default parameters) followed by optimization of the penalty parameter *lambda* (function *suggestLambda*, default parameters). Shared factors between datasets were then computed and quantile aligned (functions *optimiseALS* and *quantileAlignSNF*). Integrated clusters were visualized using the UMAP algorithm. Protein and mRNA gene cluster relative expression was visualized as heatmaps using the Rpackage *pheatmap*. CyTOF and mRNA cluster relationships in shared

data were visualized as a ribbon plot. To aid clarity, edges denoting <10 cells or <5% of total cells for the cluster are not shown.

Quantification and statistical analysis. Unless otherwise stated, all statistical comparisons between groups were carried out using two-sided *t*-tests in Prism. For experiments with more than two comparison groups, one-way analysis of variance (ANOVA) with Tukey's correction was used. All tests with $P < 0.05$ were considered statistically significant.

Reporting Summary. Further information on research design is available in the Nature Research Reporting Summary linked to this article.

Data availability

All raw and processed next-generation sequencing data have been deposited with GEO under accession nos. [GSE148837](https://www.ncbi.nlm.nih.gov/geo/query/acc.cgi?acc=GSE148837) and [GSE148505](https://www.ncbi.nlm.nih.gov/geo/query/acc.cgi?acc=GSE148505). Processed data are available as Supplementary Data. Source data are provided with this paper.

Code availability

Code used for data analysis is available at <https://github.com/antanaviciute-agne/singlecellcd8ibd>.

References

- Travis, S. P. L. et al. Developing an instrument to assess the endoscopic severity of ulcerative colitis: the Ulcerative Colitis Endoscopic Index of Severity (UCEIS). *Gut* **61**, 535–542 (2012).
- Stoeckius, M. et al. Cell Hashing with barcoded antibodies enables multiplexing and doublet detection for single cell genomics. *Genome Biol.* **19**, 224 (2018).
- Corridoni, D. et al. Genetic deletion of the bacterial sensor NOD2 improves murine Crohn's disease-like ileitis independent of functional dysbiosis. *Mucosal Immunol.* **10**, 971–982 (2017).
- Itoh, T. et al. Biological effects of IL-26 on T cell-mediated skin inflammation, including psoriasis. *J. Invest. Dermatol.* **139**, 878–889 (2019).
- Hatano, R. et al. Characterization of novel anti-IL-26 neutralizing monoclonal antibodies for the treatment of inflammatory diseases including psoriasis. *MAbs* **11**, 1428–1442 (2019).
- Corridoni, D. et al. Dysregulated NOD2 predisposes SAMP1/YitFc mice to chronic intestinal inflammation. *Proc. Natl Acad. Sci. USA* **110**, 16999–17004 (2013).
- Andrews, S. FastQC: a quality control tool for high throughput sequence data. *Babraham Bioinformatics* <http://www.bioinformatics.babraham.ac.uk/projects/fastqc/> (2010).
- Martin, M. Cutadapt removes adapter sequences from high-throughput sequencing reads. *EMBnet J.* **17**, 10 (2011).
- Kuhn, R. M., Haussler, D. & Kent, W. J. The UCSC genome browser and associated tools. *Brief. Bioinformatics* **14**, 144–161 (2013).
- Dobin, A. et al. STAR: ultrafast universal RNA-seq aligner. *Bioinformatics* **29**, 15–21 (2013).
- Wysoker, A., Tibbetts, K. & Fennell, T. Picard tools v.1.90 <http://broadinstitute.github.io/picard/> (Broad Institute, 2013).
- Li, H. et al. The sequence alignment/Map format and SAMtools. *Bioinformatics* **25**, 2078–2079 (2009).
- Liao, Y., Smyth, G. K. & Shi, W. The Subread aligner: fast, accurate and scalable read mapping by seed-and-vote. *Nucleic Acids Res.* **41**, e108 (2013).
- Love, M. I., Huber, W. & Anders, S. Moderated estimation of fold change and dispersion for RNA-seq data with DESeq2. *Genome Biol.* **15**, 550 (2014).
- Karolchik, D. et al. The UCSC table browser data retrieval tool. *Nucleic Acids Res.* **32**, 493D–496D (2004).
- Griffiths, J. A., Richard, A. C., Bach, K., Lun, A. T. L. & Marioni, J. C. Detection and removal of barcode swapping in single-cell RNA-seq data. *Nat. Commun.* **9**, 2667 (2018).
- Lun, A. T. L. et al. EmptyDrops: distinguishing cells from empty droplets in droplet-based single-cell RNA sequencing data. *Genome Biol.* **20**, 63 (2019).
- McGinnis, C. S., Murrow, L. M. & Gartner, Z. J. DoubletFinder: doublet detection in single-cell RNA sequencing data using artificial nearest neighbors. *Cell Syst.* **8**, 329–337 (2019).
- Scialdone, A. et al. Computational assignment of cell-cycle stage from single-cell transcriptome data. *Methods* **85**, 54–61 (2015).
- Satija, R., Farrell, J. A., Gennert, D., Schier, A. F. & Regev, A. Spatial reconstruction of single-cell gene expression. *Nat. Biotechnol.* **33**, 495–502 (2015).
- McInnes, L., Healy, J. & Melville, J. UMAP: uniform manifold approximation and projection for dimension reduction. Preprint at <https://arxiv.org/abs/1802.03426> (2018).
- Smillie, C. S. et al. Intra- and inter-cellular rewiring of the human colon during ulcerative colitis. *Cell* **178**, 714–730 (2019).
- Finak, G. et al. MAST: a flexible statistical framework for assessing transcriptional changes and characterizing heterogeneity in single-cell RNA sequencing data. *Genome Biol.* **16**, 278 (2015).
- Yu, G., Wang, L.-G., Han, Y. & He, Q.-Y. clusterProfiler: an R package for comparing biological themes among gene clusters. *OMICS* **16**, 284–287 (2012).
- Wickham, H. *ggplot2* <https://doi.org/10.1007/978-3-319-24277-4> (Springer, 2016).
- Efremova, M., Vento-Tormo, M., Teichmann, S. A. & Vento-Tormo, R. CellPhoneDB: inferring cell–cell communication from combined expression of multi-subunit ligand–receptor complexes. *Nat. Protoc.* **15**, 1484–1506 (2020).
- Wang, Y. et al. iTALK: an R package to characterize and illustrate intercellular communication. Preprint at <https://www.biorxiv.org/content/10.1101/507871v1> (2019).
- Qiu, X. et al. Reversed graph embedding resolves complex single-cell trajectories. *Nat. Methods* **14**, 979–982 (2017).
- Huynh-Thu, V. A., Irrthum, A., Wehenkel, L. & Geurts, P. Inferring regulatory networks from expression data using tree-based methods. *PLoS ONE* **5**, e12776 (2010).
- Aibar, S. et al. SCENIC: single-cell regulatory network inference and clustering. *Nat. Methods* **14**, 1083–1086 (2017).
- Shugay, M. et al. VDJtools: unifying post-analysis of T cell receptor repertoires. *PLoS Comput. Biol.* **11**, e1004503 (2015).
- Lareau, C. A., Ma, S., Duarte, F. M. & Buenrostro, J. D. Inference and effects of barcode multiplets in droplet-based single-cell assays. *Nat. Commun.* **11**, 866 (2020).
- Lex, A., Gehlenborg, N., Strobel, H., Vuilleumot, R. & Pfister, H. UpSet: visualization of intersecting sets. *IEEE Trans. Vis. Comput. Graph.* **20**, 1983–1992 (2014).
- Slowikowski, K., Hu, X. & Raychaudhuri, S. SNPsea: an algorithm to identify cell types, tissues and pathways affected by risk loci. *Bioinformatics* **30**, 2496–2497 (2014).
- Kinchen, J. et al. Structural remodeling of the human colonic mesenchyme in inflammatory bowel disease. *Cell* **175**, 372–386 (2018).
- Buniello, A. et al. The NHGRI-EBI GWAS Catalog of published genome-wide association studies, targeted arrays and summary statistics 2019. *Nucleic Acids Res.* **47**, D1005–D1012 (2019).
- de Lange, K. M. et al. Genome-wide association study implicates immune activation of multiple integrin genes in inflammatory bowel disease. *Nat. Genet.* **49**, 256–261 (2017).
- Consortium, T. 1000 G. P. A global reference for human genetic variation. *Nature* **526**, 68–74 (2015).
- Zhang, L. et al. Lineage tracking reveals dynamic relationships of T cells in colorectal cancer. *Nature* **564**, 268–272 (2018).
- Azizi, E. et al. Single-cell map of diverse immune phenotypes in the breast tumor microenvironment. *Cell* **174**, 1293–1308 (2018).
- Zheng, C. et al. Landscape of infiltrating T cells in liver cancer revealed by single-cell sequencing. *Cell* **169**, 1342–1356 (2017).
- Gao, X., Hu, D., Gogol, M. & Li, H. ClusterMap: compare multiple single cell RNA-Seq datasets across different experimental conditions. *Bioinformatics* **35**, 3038–3045 (2019).
- Galili, T. dendextend: an R package for visualizing, adjusting and comparing trees of hierarchical clustering. *Bioinformatics* **31**, 3718–3720 (2015).
- Finck, R. et al. Normalization of mass cytometry data with bead standards. *Cytometry A* **83A**, 483–494 (2013).
- Chen, H. et al. Cytofkit: a bioconductor package for an integrated mass cytometry data analysis pipeline. *PLoS Comput. Biol.* **12**, e1005112 (2016).
- Levine, J. H. et al. Data-driven phenotypic dissection of AML reveals progenitor-like cells that correlate with prognosis. *Cell* **162**, 184–197 (2015).

Acknowledgements

We thank all the patients who contributed to this study, the generous support of our endoscopy teams and the clinical research nurses led by S. Fourie, who made this work possible. We acknowledge support of the MRC WIMM Flow Cytometry, Single Cell and Mass Cytometry facilities, Oxford NIHR Biomedical Research Centre, Oxford Translational Gastroenterology Unit (TGU) Investigators, Targeting Immune Pathways in IBD study investigators, NIHR CRN Thames Valley and the Oxford Single Cell Consortium. We thank O. Acuto (Dunn School, University of Oxford, UK) and T. M. Aune (Vanderbilt University, Nashville, USA) for helpful discussions and technical assistance. This work was supported by a National Institutes of Health Research (NIHR) Senior Investigator Award (to A.S.), a Wellcome Investigator Award (to A.S.), the UK Medical Research Council (to H.K. and A.S.), Crohn's and Colitis UK (to D.C.), BMS (to A. Alicino and A. Antanaviciute), the Oxford NIHR Biomedical Research Centre (to K.P.), The Lee Placito Medical Fund (to T.G.) and a Wellcome Trust Clinical Research Fellowship (to D.F.-C.). Data from ref. ⁵⁵ were obtained from the Broad Data Use Oversight System (DUOS-000110) following institutional approval. We thank and acknowledge the original authors and funders who contributed to this study. The views expressed in this article are those of the authors and not necessarily those of the NIHR or the Department of Health and Social Care.

Author contributions

D.C., A. Antanaviciute and A.S. designed the project. D.C. and T.G. performed and analyzed experiments. D.F.-C., A. Alicino, M.J., K.P., H.S. and R.B. performed wet

laboratory experiments. D.C., D.I., R.H. and C.M. assisted with mouse models and in vivo experimental design. T.Y. and W.X. assisted with pathology and histology scoring. G.N. assisted with mass cytometry experiments. A. Antanaviciute and H.K. performed computational analysis. E.R. and S.T. assisted with computational analysis. D.C. and A. Antanaviciute performed mass cytometry computational analysis. Writing and editing were carried out by D.C., A. Antanaviciute, T.G., H.K. and A.S. H.K. and A.S. cosupervised. T.G. was also cosupervised by O.B. A.S. obtained funding.

Competing interests

The authors declare no competing interests.

Additional information

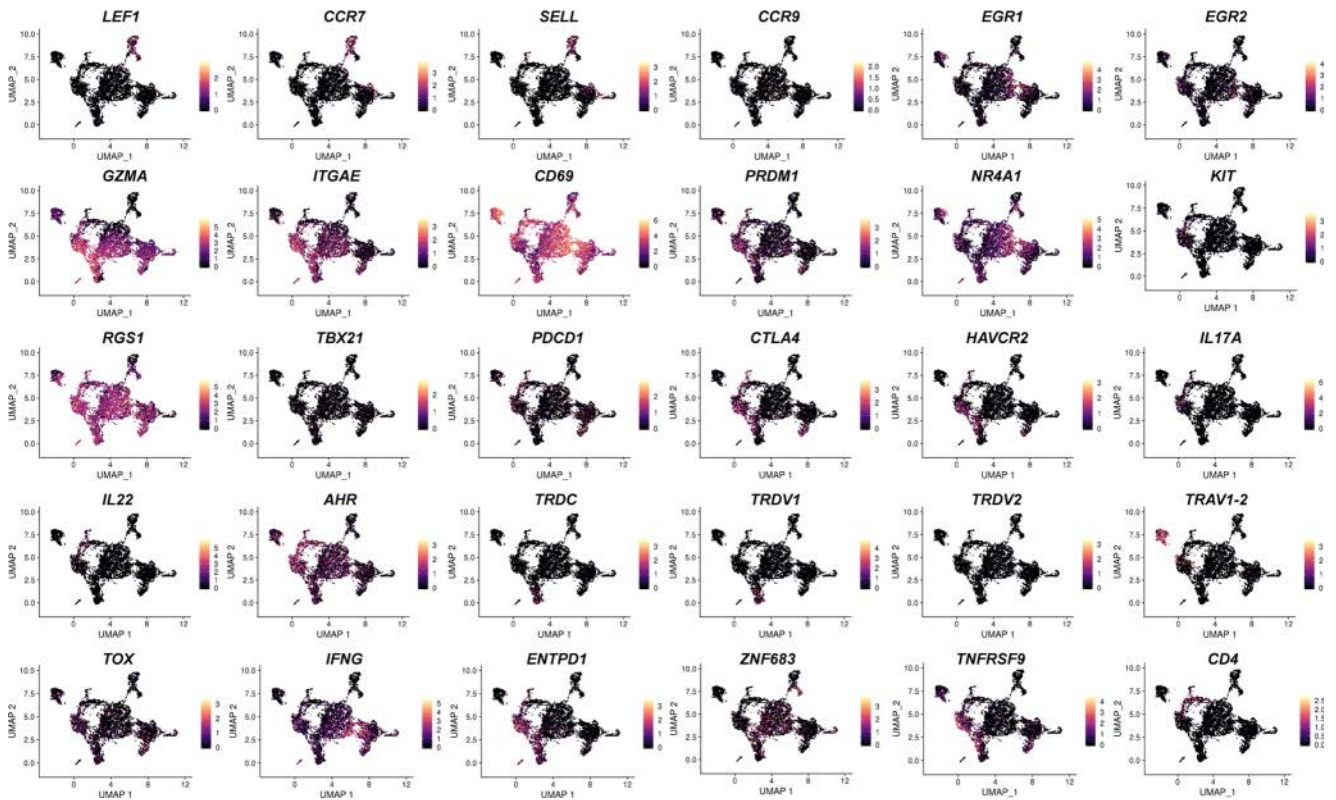
Extended data is available for this paper at <https://doi.org/10.1038/s41591-020-1003-4>.

Supplementary information is available for this paper at <https://doi.org/10.1038/s41591-020-1003-4>.

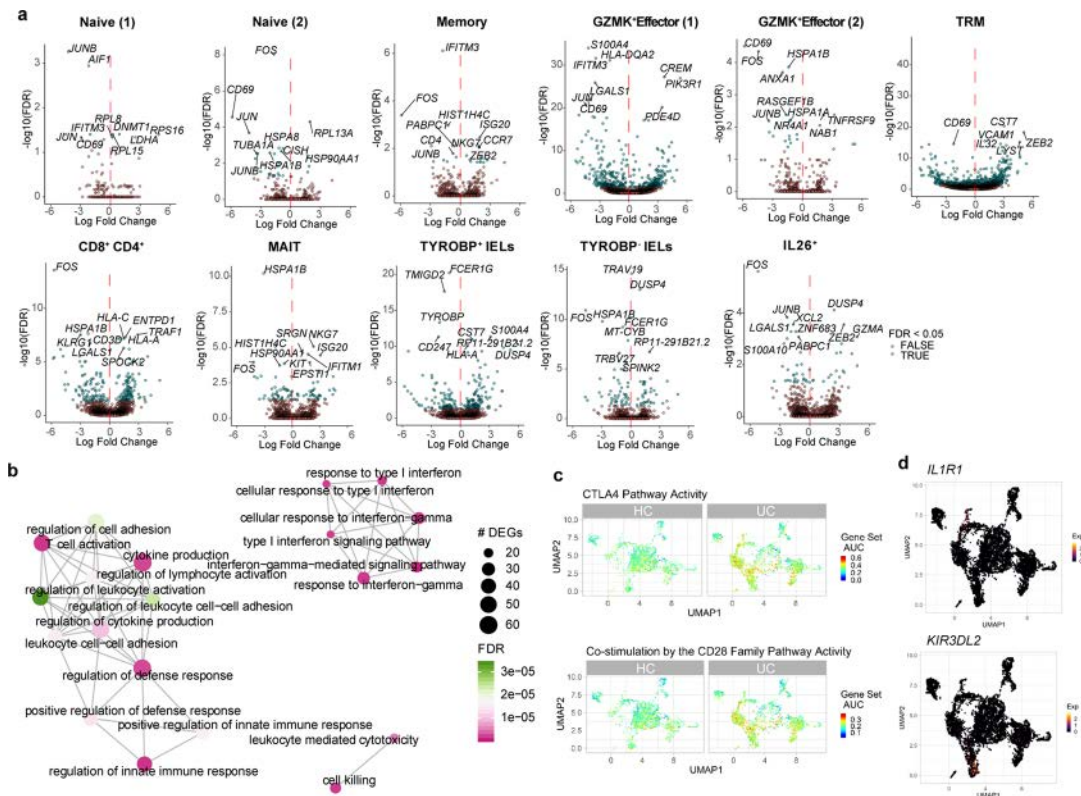
Correspondence and requests for materials should be addressed to H.K. or A.S.

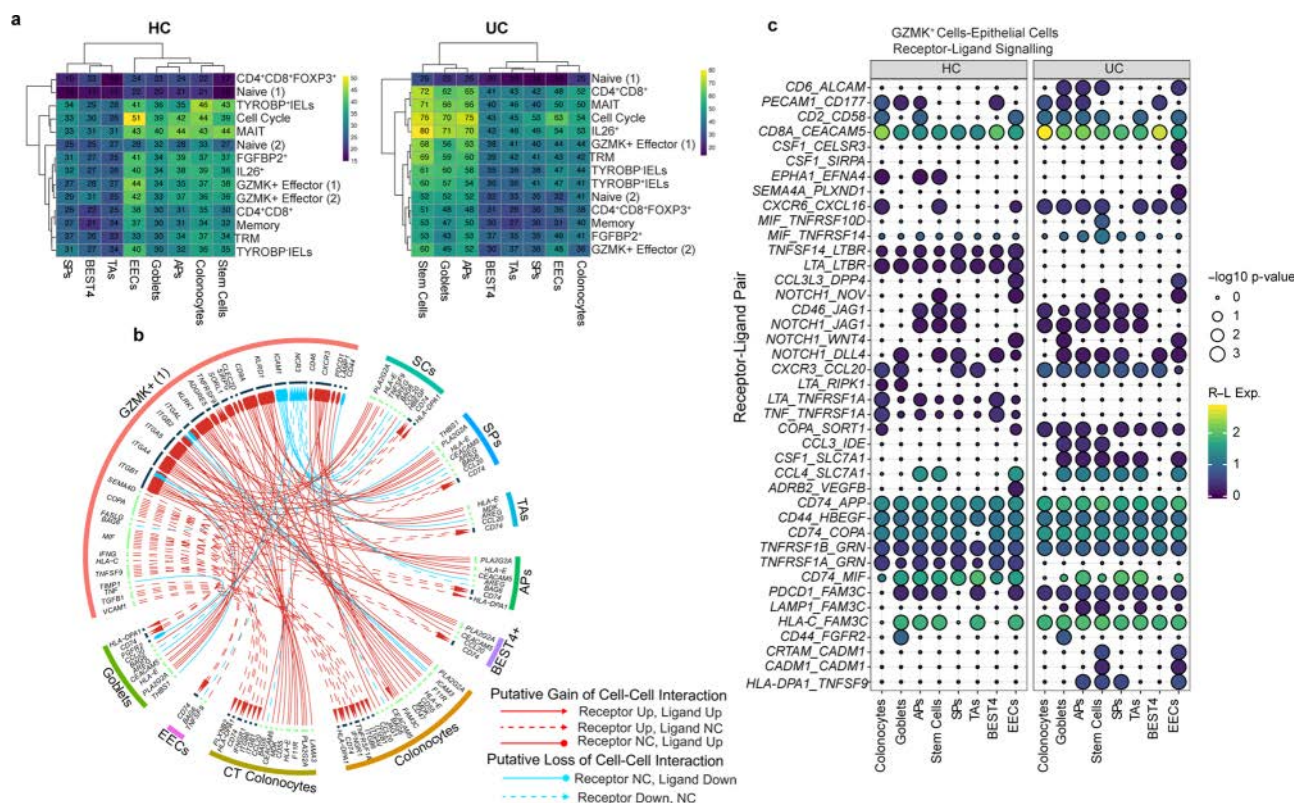
Peer review information Saheli Sadanand was the primary editor on this article and managed its editorial process and peer review in collaboration with the rest of the editorial team.

Reprints and permissions information is available at www.nature.com/reprints.

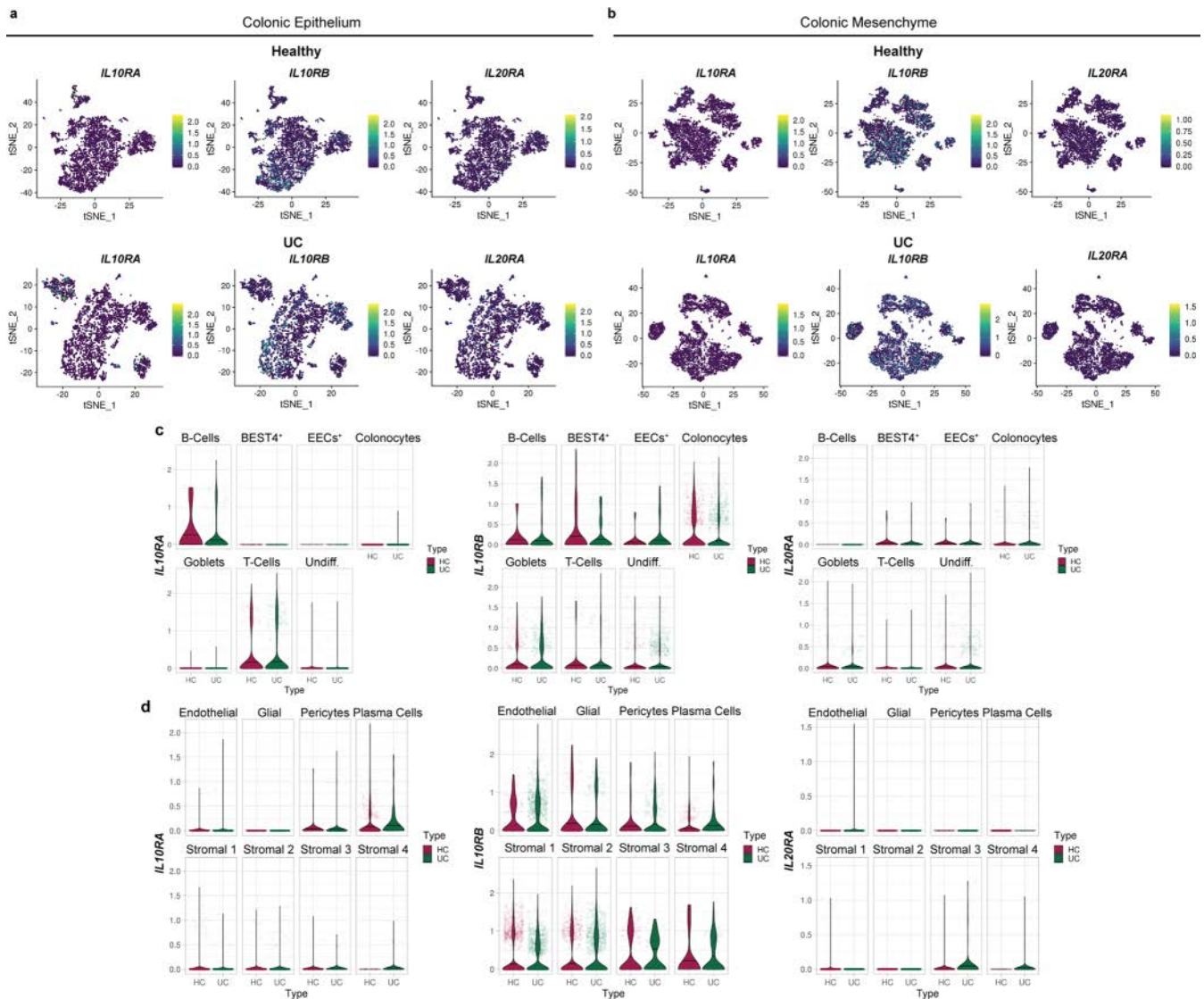


Extended Data Fig. 1 | Cluster-specific single cell gene expression. UMAP plot overlays showing selected gene expression distribution across clusters. Cells from $n = 3$ donors per group.

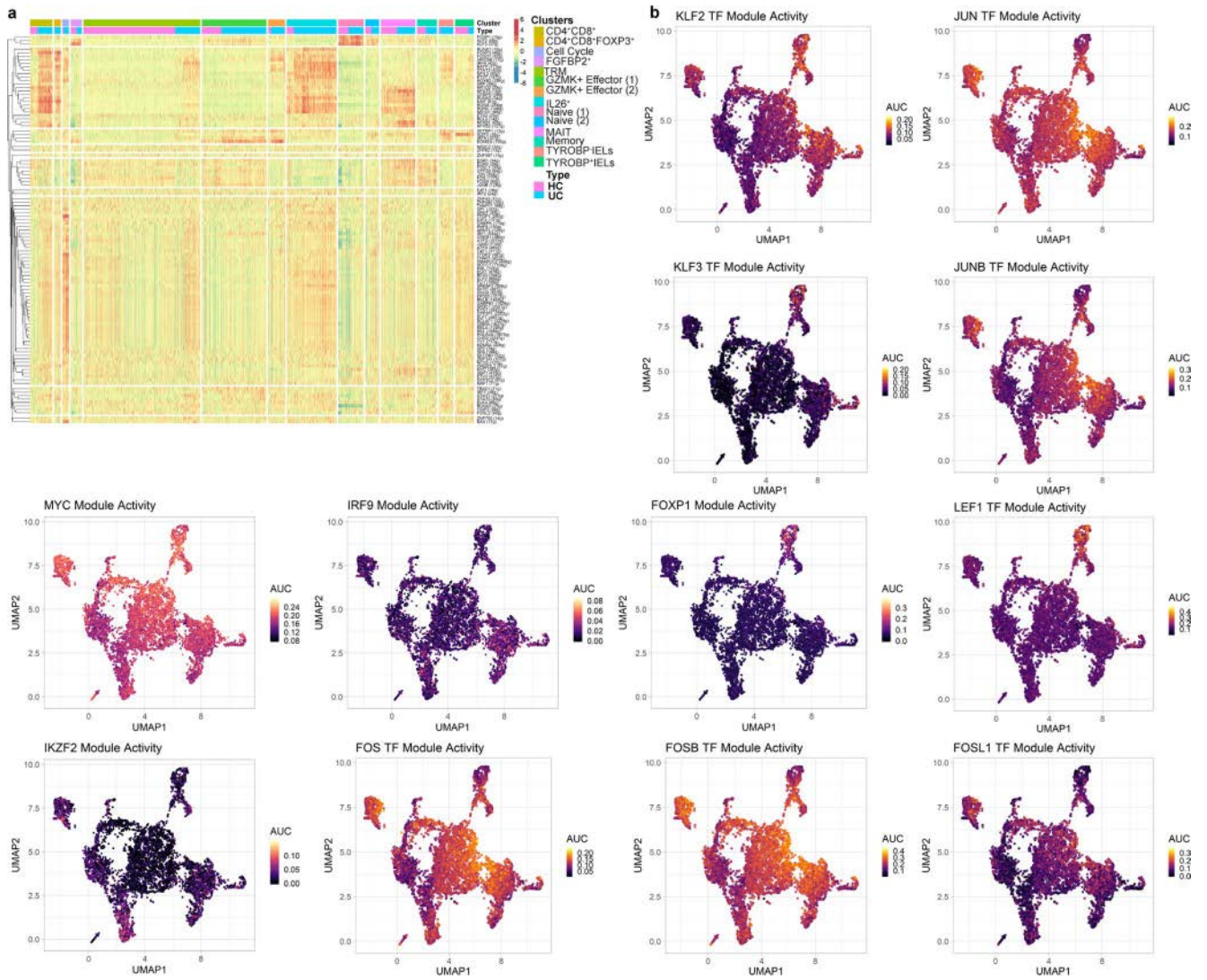




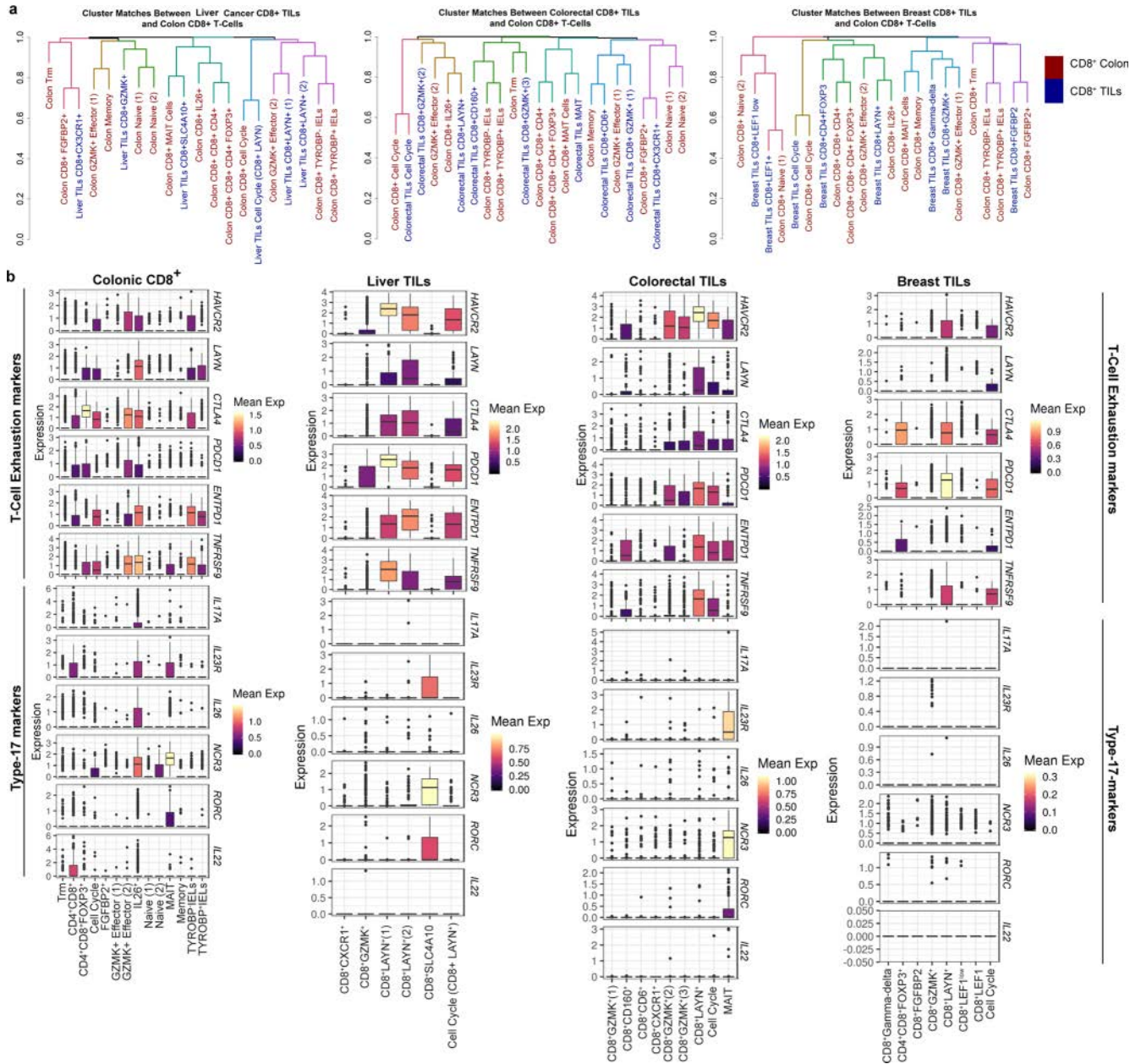
Extended Data Fig. 3 | Receptor-ligand interactions between CD8⁺ T-Cells and Epithelial Sub-population. **a**, Heatmap displaying the total number of paracrine CD8⁺ and epithelial cell sub-cluster receptor-ligand interactions discovered using CellphoneDB in clusters in health (left) and UC (right). **b**, Circos plot showing all putative alterations of cell-cell interaction events in active UC via receptor-ligand pair signalling between T-cell GZMK⁺ effector cells and epithelial cell sub-types. Putative gain of interaction events and loss of interaction events are shown separately for each CD8⁺ cluster viewpoint. Abbreviations: SCs: Stem Cells. SPs: Secretory Progenitors. TAs: transit-amplifying cells. APs: absorptive progenitors. CT Colonocytes: Crypt-top colonocytes. EECs: enteroendocrine cells. NC: No change. **c**, Dotplot of selected significant paracrine receptor-ligand interactions between GZMK⁺ Effector CD8⁺ cells (cells from n = 3 donors per group) and epithelial cells (cells from n = 3 donors per group) discovered using CellphoneDB. CellphoneDB empirical permutation p-value.



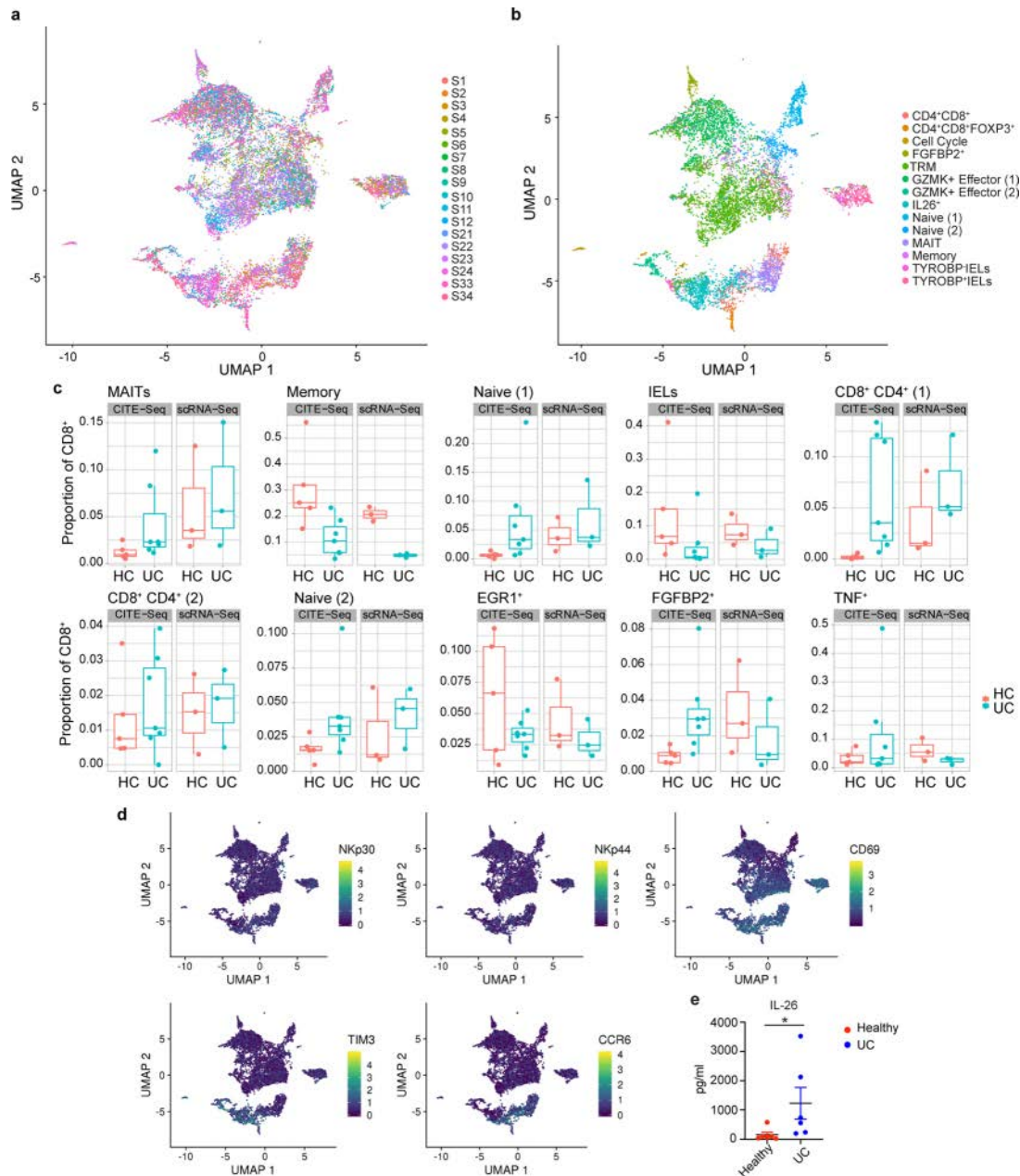
Extended Data Fig. 4 | Distribution of IL26 receptor expression in epithelial and mesenchymal compartments. **a**, tSNE plots showing expression distribution of *IL10RA* and IL-26 receptor genes, *IL10RB* and *IL20RA*, in single cell colonic epithelium dataset in health ($n=3$ donors) and UC ($n=3$ donors) from **(a)** Parikh *et al.*, 2019; **(b)** colonic mesenchymal dataset in health ($n=2$ donors) and UC ($n=2$ donors) from Kinchen *et al.*, 2018. **c**, Violin plots (median shown) comparing expression of IL-26 receptor genes in health (cells from $n=3$ donors) and UC (cells from $n=3$ donors) in colonic epithelium. **d**, Violin plots (median shown) comparing expression of *IL10RA* and IL-26 receptor genes in health (cells from $n=2$ donors) and UC (cells from $n=2$ donors) in colonic mesenchyme. Undifferentiated cells, encompassing stem cells, transit amplifying cells and secretory and absorptive progenitor cells are denoted as 'Undiff'.



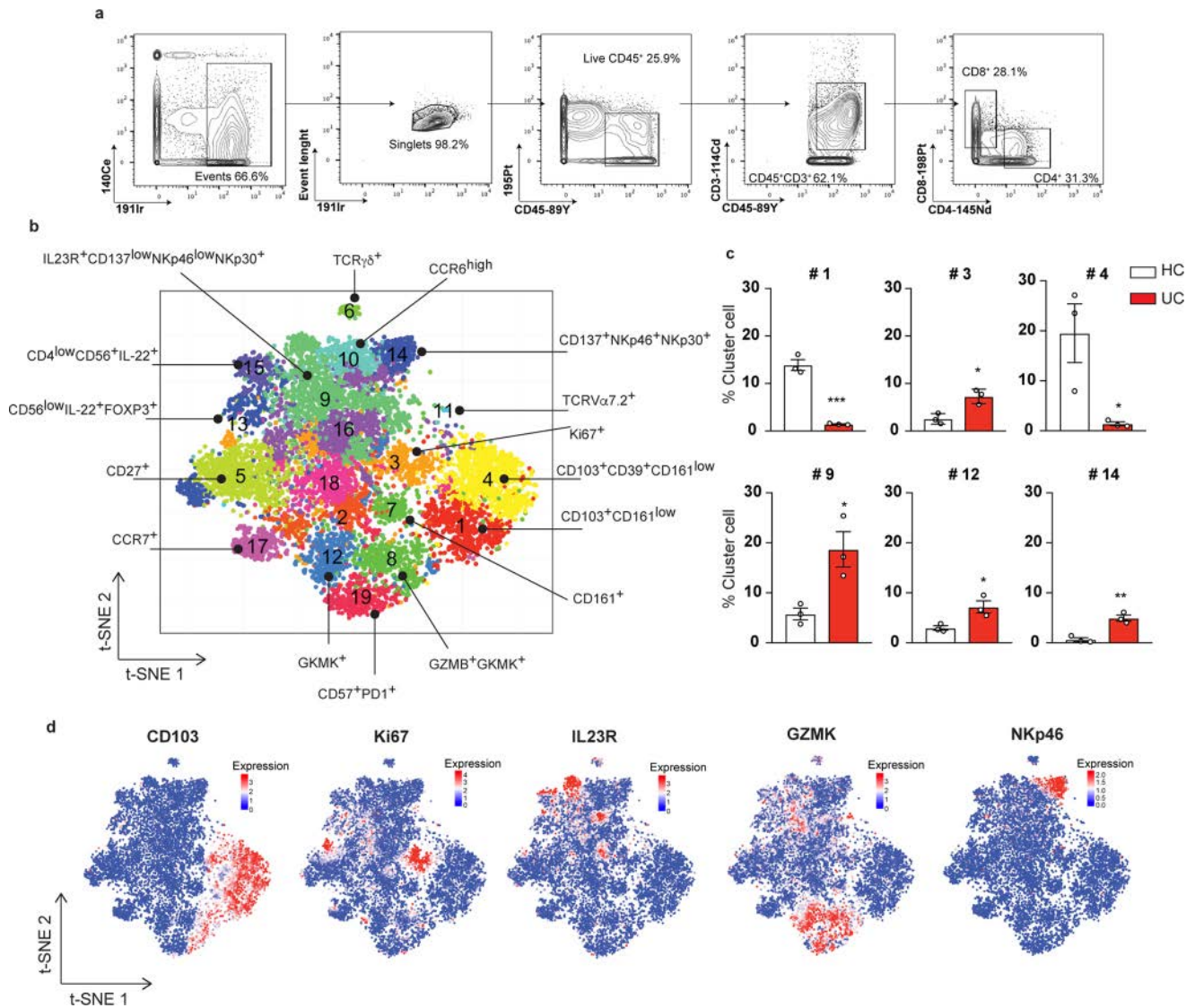
Extended Data Fig. 5 | Cluster-specific transcription factor module activities. **a**, Heatmap visualising relative transcription factor module activity (as AUC scores) for all detected transcription factor modules in cells from healthy (n=3) and UC (n=3) donors. **b**, UMAP overlay showing selected transcription factor network activity distribution at single cell level in cells from healthy (n=3) and UC (n=3) donors.



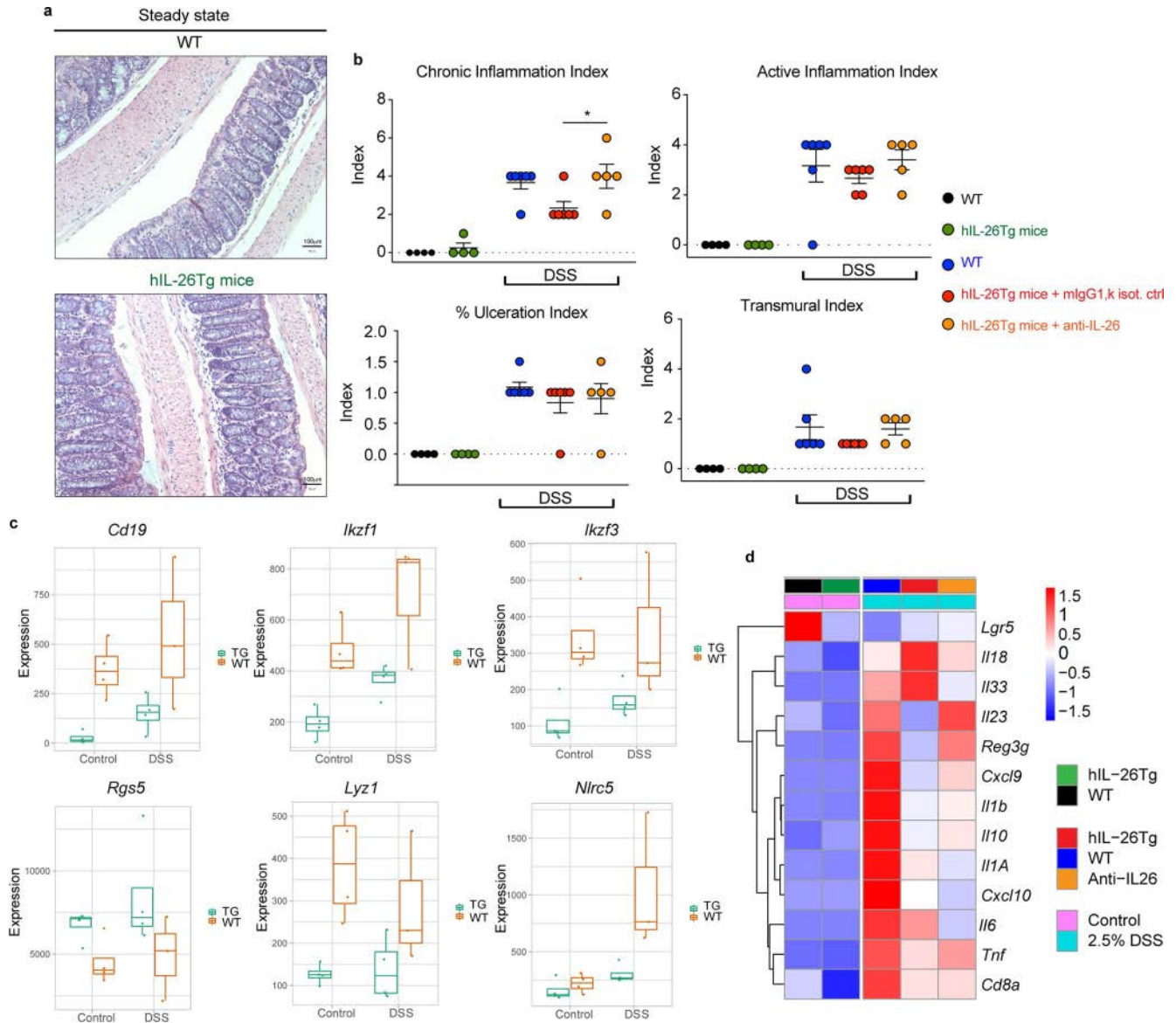
Extended Data Fig. 7 | CD8⁺ TILs share features of exhaustion, but not Type 17 signature with colonic IL26⁺ cells. a, Hierarchical clustering of CD8⁺ sub-populations detected in UC (cells from n=3 donors) together with CD8⁺ sub-populations detected in liver cancer tumor-infiltrating lymphocytes (TILs) (left) (cells from n=6 donors), colorectal cancer TILs (middle) (cells from n=11 donors) and breast cancer TILs (right) (cells from n=1 donor). **b**, Boxplot showing expression of selected exhaustion (top panels) and Type-17/ILC3 (bottom panels) signature genes in colonic CD8⁺ populations and tumour CD8⁺ TILs. Boxplots show the median, first and third quartiles, 5th percentile as minima and 95th percentile as maxima.



Extended Data Fig. 8 | Distribution of transcriptomic and proteomic CITE-Seq profiles in health and UC. a, UMAP overlay of donor cell-of-origin distribution for mRNA clusters obtained from integrated scRNA-Seq (cells from $n=3$ donors per group) and CITE-Seq cohorts (cells from $n=7$ UC donors and $n=5$ HC donors). **b**, Overlay of original clusters obtained from scRNA-Seq clusters onto the integrated scRNA-Seq (cells from $n=3$ donors per group) and CITE-Seq (cells from $n=7$ UC donors and $n=5$ HC donors) cohorts, **c**, Boxplots showing the proportion of all CD8⁺ cells for each joint cluster, split by original scRNA-Seq (cells from $n=3$ donors per group) and CITE-Seq cohorts (cells from $n=7$ UC donors and $n=5$ HC donors). Boxplots show the median, first and third quartiles, 5th percentile as minima and 95th percentile as maxima. **d**, Overlay of protein expression for selected proteins onto UMAP driven by mRNA expression (cells from $n=7$ UC donors and $n=5$ HC donors). **e**, Quantification of IL-26 protein levels from colonic CD8⁺ T cells of healthy ($n=6$) and UC-inflamed donors ($n=6$) following polyclonal activation with anti-CD3/anti-CD28. Mean and SEM are shown; $*P=0.0152$, two-tailed Mann-Whitney test.



Extended Data Fig. 9 | Heterogeneity of colonic CD8⁺ T-cells in health and UC by CyTOF. **a**, Representative gating strategy to identify CD45⁺ CD3⁺ CD8⁺ cell population in Mass Cytometry experiments used for further analysis; representative of six samples (n=6 donors) where same sorting strategy was applied. **b**, tSNE plot to visualise proportion of Phenograph clusters within CD45⁺CD3⁺CD8⁺ cells from healthy (n=3) and UC (n=3) donors. Selected clusters are annotated based on their phenotype. **c**, Bar graph showing significant sub-population changes in UC (n=3 donors) compared to healthy (n=3 donors). Cluster 1, t=10.78, DF=4, ***P=0.0004; Cluster 3, t=4.354, DF=4, *P=0.0121; Cluster 4, t=3.072, DF=4, *P=0.0372; Cluster 9, t=3.476, DF=4, *P=0.0254; Cluster 12, t=3.287, DF=4, *P=0.0303; Cluster 14, t=5.911, DF=4, **P=0.0041. Mean and SEM are shown; two-tailed unpaired t-test. **d**, tSNE overlay of selected protein expression markers in cells from healthy (n=3) and UC (n=3) donors.



Extended Data Fig. 10 | IL26 attenuates severity of acute DSS colitis and induces transcriptional changes at baseline in a humanised mouse model. a, Representative photomicrographs of H&E-stained colonic tissues of wild-type (WT, $n = 4$) and humanized IL-26 transgenic (hIL-26Tg, $n = 4$) mice (original magnification: 20 \times) at steady state. **b**, Colonic inflammatory scores for chronic inflammation, active inflammation, transmural index and percentage of ulceration ($n = 4$ control mice, $n = 6$ DSS treatment mice, $n = 5$ DSS treatment + anti-IL26 mice) in hIL-26Tg and WT mice at steady state and post-DSS challenge. $F = 4.230$, $DF = 2$, $*P = 0.0438$ (hIL26Tg DSS vs. hIL26Tg with anti-IL26 DSS); mean and SEM shown, one-way ANOVA (Tukey's multiple comparison test). **c**, Comparative expression of selected genes under DSS challenge between WT ($n = 3$ DSS, $n = 4$ control mice) and hIL-26Tg mice ($n = 4$ mice per group), demonstrating lower inflammatory signatures in hIL-26 expressing Tg mice. Boxplots show the median, first and third quartiles, 5th percentile as minima and 95th percentile as maxima. **d**, Cytokine, chemokine and epithelial cell markers mRNA expression measured by qPCR in whole-colon tissue from experimental mice ($n = 4$ control, $n = 6$ DSS treatment, $n = 5$ DSS treatment + anti-IL26 mice). Expression was averaged for mice within each group and converted to z scores.

Reporting Summary

Nature Research wishes to improve the reproducibility of the work that we publish. This form provides structure for consistency and transparency in reporting. For further information on Nature Research policies, see [Authors & Referees](#) and the [Editorial Policy Checklist](#).

Statistics

For all statistical analyses, confirm that the following items are present in the figure legend, table legend, main text, or Methods section.

- | | |
|-------------------------------------|--|
| n/a | Confirmed |
| <input type="checkbox"/> | <input checked="" type="checkbox"/> The exact sample size (n) for each experimental group/condition, given as a discrete number and unit of measurement |
| <input type="checkbox"/> | <input checked="" type="checkbox"/> A statement on whether measurements were taken from distinct samples or whether the same sample was measured repeatedly |
| <input type="checkbox"/> | <input checked="" type="checkbox"/> The statistical test(s) used AND whether they are one- or two-sided
<i>Only common tests should be described solely by name; describe more complex techniques in the Methods section.</i> |
| <input type="checkbox"/> | <input checked="" type="checkbox"/> A description of all covariates tested |
| <input type="checkbox"/> | <input checked="" type="checkbox"/> A description of any assumptions or corrections, such as tests of normality and adjustment for multiple comparisons |
| <input type="checkbox"/> | <input checked="" type="checkbox"/> A full description of the statistical parameters including central tendency (e.g. means) or other basic estimates (e.g. regression coefficient) AND variation (e.g. standard deviation) or associated estimates of uncertainty (e.g. confidence intervals) |
| <input type="checkbox"/> | <input checked="" type="checkbox"/> For null hypothesis testing, the test statistic (e.g. F , t , r) with confidence intervals, effect sizes, degrees of freedom and P value noted
<i>Give P values as exact values whenever suitable.</i> |
| <input checked="" type="checkbox"/> | <input type="checkbox"/> For Bayesian analysis, information on the choice of priors and Markov chain Monte Carlo settings |
| <input checked="" type="checkbox"/> | <input type="checkbox"/> For hierarchical and complex designs, identification of the appropriate level for tests and full reporting of outcomes |
| <input type="checkbox"/> | <input checked="" type="checkbox"/> Estimates of effect sizes (e.g. Cohen's d , Pearson's r), indicating how they were calculated |

Our web collection on [statistics for biologists](#) contains articles on many of the points above.

Software and code

Policy information about [availability of computer code](#)

Data collection

See below (Data Analysis) for full description of collection software as used for Data analysis.
 Software for Collection included:
 Flow cytometry (FACS) - BD FACS Diva Software (BD FACS Aria III machine & BD FACS LSR II machine)
 Cytometry Time of Flight (CyTOF) Data acquisition - Fluidigm CyTOF Software v6.7 (Helios 2 CyTOF machine)
 Imaging - Aperio ImageScope - Pathology Slide Viewing Software v12.3.3 (Aperio ScanScope AT Turbo, Leica microscope)
 RT-PCR - ThermoFisher QuantStudio 7-Flex system v1.3
 Base Calling (Novaseq) - Novaseq analyse viewer v2.4.7
 BCL2FastQ conversion - Termius v5.11.0

Data analysis

Histological scoring of biopsy specimens was performed using picard-tools/2.3.0 in a blinded fashion, with scores entered analysed and presented using GraphPad PRISM v8.1.0 (<https://www.graphpad.com/scientific-software/prism/>).
 Quantitative RT-PCR: Initial quantification of results using Quantstudio Software (ThermoFisher) with raw data then presented using Prism (Graphpad) .
 Mouse biopsy slide Images viewed using QuPath v0.1.2 (<https://github.com/qupath/qupath/releases/tag/v0.1.2>).

 The following packages were used to Analyse the CyTOF data:
 FlowJo v10.5.3 (<https://www.flowjo.com/solutions/flowjo/downloads>) - Gating individual populations
 Cytokit v1.10.0 (<https://bioconductor.org/packages/3.6/bioc/html/cytokit.html>) and RPhenograph (<https://github.com/JinmiaoChenLab/Rphenograph>) - Clustering and comparisons between clusters.

 The following packages were used to analyze the sequencing data:
 FastQC Version 0.11.8 Software (<https://www.bioinformatics.babraham.ac.uk/projects/fastqc/>) - Raw sequence data quality control software.
 Samtools Version 1.9.0 - Aligned sequence data processing
 MultiQC Version 0.9 - Sequence data quality control

Cell Ranger Software (<https://support.10xgenomics.com/single-cell-gene-expression/software/downloads/latest>) - Aligning, Processing and Summarizing UMIs against the Human Reference Genome.
 SNPsea software, Version 1.0.3 - Over-representation testing of tissue-specific expression of GWAS loci genes.
 STAR Version 2.4.2 - Transcriptome alignment.
 Cutadapt Version 1.16 - Sequence data trimming

R Version 3.5.3 - Language for statistical analysis. The following packages were used in addition to base installation:

Seurat Bioconductor R Package, Version 2.3.2 - single cell data QC, normalisation, clustering and differential gene expression analysis.
 Monocle Bioconductor R Package, Version 2.8.0 - single cell data trajectory analysis.
 Cyclone, scran Bioconductor R Package, Version 1.6.9 - cell cycle score annotation.
 M3Drop, R Package, Version 1.6.0 - Highly variable gene selection for single cell dimensionality reduction.
 irlba, R Package, Version 2.3.2 - Principal component analysis.
 clusterProfiler, Bioconductor R Package, Version 3.6.0 - Gene Ontology enrichment analysis.
 ggplot2, R Package, Version 2.2.1 - Plotting package.
 DESeq2, Bioconductor R Package, Version 1.20.0 - Differential expression analysis of bulk /pseudobulk RNA sequencing data.
 liger, Version 0.4.1 - multi-modal data integration
 DoubletFinder, Version 2.0.1 - Multiplet identification
 SCENIC, Version 1.1.2-2 - Transcription Factor Analysis
 RcisTarget, Version 1.2.1 - Transcription Factor Analysis
 AUCell, Version 1.4.1 - Gene set cell scoring and transcription factor analysis
 umap, Version 0.2.2.0 - UMAP visualisations
 MAST, Version 1.8.2 - Single Cell differential gene expression
 randomForest, Version 4.6-14 - RF classifiers
 caret, Version 6.0-84 - RF classifier feature selection
 DropletUtils, Version 1.2.2 - data cleaning and cell identification

Additional general software:

VDJTools - <https://github.com/mikesh/vdjtools>
 VDJB (30th January 2019 Update Version)- <https://vdjb.cdr3.net/>
 CellPhoneDB v2.0 (<https://github.com/Teichlab/cellphonedb>) on Python v3.6.8 - Receptor-Ligand analysis

For manuscripts utilizing custom algorithms or software that are central to the research but not yet described in published literature, software must be made available to editors/reviewers. We strongly encourage code deposition in a community repository (e.g. GitHub). See the Nature Research [guidelines for submitting code & software](#) for further information.

Data

Policy information about [availability of data](#)

All manuscripts must include a [data availability statement](#). This statement should provide the following information, where applicable:

- Accession codes, unique identifiers, or web links for publicly available datasets
- A list of figures that have associated raw data
- A description of any restrictions on data availability

All raw sequencing data (scRNA, CITE-seq and Mouse tissue bulk RNA) has been made publicly available through the following GEO accessions: GSE148837 and GSE148505.

Code used for data analysis is available at <https://github.com/antanaviciute-agne/singlecellcd8ibd>

Publicly available datasets used in the analysis:

TIL datasets: GEO: GSE98638, GEO: GSE108989, GEO: GSE114724

Epithelial datasets: GEO: GSE116222

Colonic CD45+ dataset: DUOS-000110, available through Broad Data Use Oversight System

Colonic mesenchymal dataset: GSE95446

Field-specific reporting

Please select the one below that is the best fit for your research. If you are not sure, read the appropriate sections before making your selection.

Life sciences Behavioural & social sciences Ecological, evolutionary & environmental sciences

For a reference copy of the document with all sections, see [nature.com/documents/nr-reporting-summary-flat.pdf](https://www.nature.com/documents/nr-reporting-summary-flat.pdf)

Life sciences study design

All studies must disclose on these points even when the disclosure is negative.

Sample size

No formal sample size calculation was performed for samples. For mouse experiments, sample sizes (3-4 mice) were rationalized by balancing sufficient replication to detect moderate effect sizes with reduction of total animals used. For human single cell experiments, 3 samples from healthy and inflamed UC were chosen for single cell sequencing to allow for patient variability with the aim of capturing a minimum of 1000 single cells per donor, which would allow for detection of CD8+ cell sub-populations at ~1-2% rarity. The validation CITE-Seq cohort used additional 7 UC patients and 5 healthy controls. For CyTOF analysis, an initial cohort of 3 healthy and 3 UC samples were used. For PMA-ionomycin stimulation experiment, additional 4 healthy and 3 UC samples were used. Key findings were validated by qPCR in an independent

cohort of 5 healthy and 15 UC donors (across 17 independent samples). These sample sizes were deemed sufficient as gene expression patterns and cell populations detected were highly reproducible between initial and validation cohorts.

Data exclusions	For CITE-Seq, a single non-UC colitis control sample and a single UC from a non-inflamed region of the colon were excluded from the analysis. These samples were included in the sample pools to increase the overall number of samples in the hashed UC or healthy control samples and thereby increase the quality of the pools by introduction of additional tags to aid multiplet detection, as no additional inflamed UC or healthy control samples were available at the time. For single cells, cell barcodes were excluded as detailed in the methods based on the following criteria: cell barcodes above 5% FDR, as determined by emptyDrops, cells with total mitochondrial content >15%, cells determined as putative doublets by DropletUtils. For CITE-Seq, in addition to the criteria above, cells positive for multiple hashing antibody tags or negative for all hashing antibody tags were filtered out (99th percentile, as detailed in methods).
Replication	All single cell experiments, Cytometry Time-of-Flight (CyTOF) and mouse experiments were performed in triplicate or more in order to ensure reliability and reproducibility of results. All major findings were replicated in a validation cohort using CITE-Seq. Exact quantification for each replicate is described in methods and figure legends.
Randomization	For CITE-Seq, UC inflamed and control samples were randomised across sample pools in order to minimise batch effects. Histological sections were randomised prior to blinded scoring. Other samples were not randomised as appropriate biological controls were included in all other experiments.
Blinding	Histological sections from mice were scored for inflammation by an experienced pathologist in a blinded fashion. The results were then communicated back to the principal investigators who matched them back to the experimental conditions. NGS library preparation and sequencing was performed by lab personnel unaware of individual sample types. In other areas, blinding was not necessary as experimental read-outs were automated (ELISA, FACS, qPCR).

Reporting for specific materials, systems and methods

We require information from authors about some types of materials, experimental systems and methods used in many studies. Here, indicate whether each material, system or method listed is relevant to your study. If you are not sure if a list item applies to your research, read the appropriate section before selecting a response.

Materials & experimental systems

n/a	Involved in the study
<input type="checkbox"/>	<input checked="" type="checkbox"/> Antibodies
<input checked="" type="checkbox"/>	<input type="checkbox"/> Eukaryotic cell lines
<input checked="" type="checkbox"/>	<input type="checkbox"/> Palaeontology
<input type="checkbox"/>	<input checked="" type="checkbox"/> Animals and other organisms
<input type="checkbox"/>	<input checked="" type="checkbox"/> Human research participants
<input checked="" type="checkbox"/>	<input type="checkbox"/> Clinical data

Methods

n/a	Involved in the study
<input checked="" type="checkbox"/>	<input type="checkbox"/> ChIP-seq
<input type="checkbox"/>	<input checked="" type="checkbox"/> Flow cytometry
<input checked="" type="checkbox"/>	<input type="checkbox"/> MRI-based neuroimaging

Antibodies

Antibodies used

CytoF Antibodies:
 CD45 HI30 89Y Fluidigm 3089003B (lot 0381908) (100X)
 CD3 Qdot 605 UCHT1 111-116 Cd CyTOF Invitrogen Q10054 (lot 2040166) (250X)
 CD57 HCD57 115 In Biolegend 322325 (lot B196969)* (100X)
 CD196 (CCR6) G034E3 141 Pr Biolegend 353427 (lot 0751707) (100X)
 Granzyme B GB11 144 Nd Abcam Ab103159 (lot GR280921-3) * (200X)
 CD4 RPA-T4 145 Nd Biolegend 300516 (lot B213445)* (100X)
 LAG3 11C3C65 146 Nd Biolegend 369302 (lot B228374)* (100X)
 TIM-3 7D3 147 Sm BD 565768 (lot 6242612)* (100X)
 TNF-alpha Mab11 148 Nd Biolegend 502922 (lot B220533)* (100X)
 CD56 (NCAM) NCAM16.2 149 Sm BD 559043 (lot 7041682)* (200X)
 IL-22 22URTI 150 Nd DVS Sciences 3150007B (lot 2371412) (200X)
 CD103 Ber-ACT8 151 Eu Fluidigm 3151011B (lot 2381606) (100X)
 TCRgd 11F2 152 Sm Fluidigm 3152008B (lot 0441915) (50X)
 TCR Va7.2 3C10 153 Eu Fluidigm 3153024B (lot 0331601) (100X)
 IL-23R (PE) 218213 PE R&D FAB14001P (lot YAX1014071) (100X)
 anti-phycoerythrin (PE) PE001 154 Sm Biolegend 408102 (lot B201392)* (100X)
 CD279 (PD-1) EH12.2H7 155 Gd Fluidigm 3155009B (lot 2411725) (100X)
 CXCR6 K041E5 156 Gd Biolegend 356002 (lot B202393)* (100X)
 CD27 L128 158 Gd DVS Sciences 3158010B (lot 0421404) (100X)
 FOXP3 259D/C7 159 Tb BD 560044 (lot 8046558)* (100X)
 MIP1b D21-1351 160 Gd Fluidigm 3160013B (lot 0981518) (100X)
 LAYN 3F7D7E2 161 Dy Sino Biological 10208 MM02 (lot HB12OC3003)* (100X)
 CD337 (NK-p30) P30-15 162 Dy Biolegend 325202 (lot B226329)* (100X)
 IL-17 BL168 163 Dy Biolegend 512331 (lot B218932)* (50X)
 KI67 Ki-67 164 Dy Biolegend 350523 (lot B196966)* (100X)
 CD185 (CXCR5) RF8B2 166 Er BD 552032 (lot 70226764)* (100X)
 CD197 (CCR7) G043H7 MAB197 167 Er R&D Systems (lot FNP1014051)* (100X)

CD161 HP-3G10 168 Er Biolegend 339919 (lot B216481)* (100X)
 KIR2DL4/CD158 181703 169 Tm R&D MAB2238 (lot KMC0318081)* (100X)
 CD335 (NK-P46) 9 E2 170 Er Biolegend 331902 (lot B248469) (100X)
 CD160 BV55 171 Yb Biolegend 341202 (lot B198739)* (100X)
 CD25 (IL-2R) M-A251 172 Yb Biolegend 356102 (lot B186008)* (200X)
 CD39 A1 173 Yb Biolegend 328221 (lot B204310)* (100X)
 BATF 9B5A13 174 Yb Biolegend 654802 (lot B166356)* (50X)
 CD137 4B4-1 175 Lu Biolegend 309802 (lot B227357)* (100X)
 IFNg B27 176 Yb Biolegend 506502 (lot B141419)* (100X)
 CD8 RPA-T8 198 Pt Biolegend 301018 (lot B201679)* (33.3X)
 CD16 3G8 209Bi Fluidigm 3209002B (lot 3241802) (100X)

FACS Antibodies:

CD3 UCHT1 BV711 BD 563724 (lot 7193553) (60X)
 CD8 SK1 APC-R700 FACS BD 565192 (lot 7205806) (60X)
 CD45 5B1 FITC Miltenyi 130-113-679 (lot 5190814392) (250X)
 EPCAM 9C4 BV785 Biolegend 324237 (lot B262589) (50X)
 IL20Ra 173714 PE RnD FAB11762P (lot LUN0219041) (3.3X)
 IL10Rb 90220 AF647 RnD FAB874R-100UG (lot 1555514) (10X)

In vivo experiments (Mice):

IL-26 69-10 Unconjugated, Juntendo University
 IgG1,k isotype control MG1-45 Unconjugated. Invitrogen 14-4714-85

CITE-Seq Antibodies (All Diluted 100X - 0.5ug per 2 million cells):

CD4 SK3 Biolegend 344651 (lot B286667)
 CD45RO UCHL1 Biolegend 304259 (lot B282646)
 PD1 EH12.2H7 Biolegend 329963 (lot B284413)
 NKp46 9E2 Biolegend 331941 (lot B273791)
 CCR6 G034E3 Biolegend 353440 (lot B283733)
 CD103 BERTACT8 Biolegend 350233 (lot B286671)
 CD69 FN50 Biolegend 310951 (lot B292296)
 CCR7 G043H7 Biolegend 353251 (lot B282156)
 CTLA-4 BN13 Biolegend 369621 (lot B286666)
 LAG3 11C3C65 Biolegend 369335 (lot B289278)
 TIM3 E38-2E2 Biolegend 345049 (lot B286676)
 NKp44 P44-8 Biolegend 325119 (lot B288070)
 TNFRSF9 4B4-1 Biolegend 309839 (lot B284403)
 NKp30 P30-15 Biolegend 325219 (lot B282265)
 Anti-Human Hashtag 1 LNH-94 & 2M2 Biolegend 394661 (lot B282243)
 Anti-Human Hashtag 2 LNH-94 & 2M2 Biolegend 394663 (lot B293608)
 Anti-Human Hashtag 3 LNH-94 & 2M2 Biolegend 394665 (lot B282244)
 Anti-Human Hashtag 4 LNH-94 & 2M2 Biolegend 394667 (lot B282246)
 Anti-Human Hashtag 5 LNH-94 & 2M2 Biolegend 394669 (lot B282245)

Validation

Flow cytometry, CITE-Seq, Hashtag and Mass cytometry antibodies validated internally by suppliers on the respective product websites, all validated against human antigens. Multiple clone citations, exemplars below:

CD45 (HI30) - Lavin Y et al. 2017. Cell. 169(4):750-765
 CD3 (UCHT1) - Mayassi T, et al. 2019. Cell. 176:967
 CD57 (HCD57) - Naluyima P, et al. 2019. J Immunol. 203:2210
 CCR6 (G034E3) - Qu K et al. 2017. Cancer cell. 32(1):27-41
 Granzyme K (GM26E7) - de Andrade LF, et al. 2019. JCI Insight. 4:e133103
 Granzyme B (GB11) - Zhang J, et al. 2018. Nature. 553:91
 CD4 (RPA-T4) - Park MJ, et al. 2019. J Immunol. 203:127
 LAG3 (11C3C65) - Yeo L, et al. 2018. J Clin Invest. 128:3460
 TIM3 (7D3) - Wang F, et al. 2009. Immunobiology. 214(5):342-349
 TNFalpha (Mab11) - Sun Z, et al. 2019. J Cell Mol Med. 23:887.
 CD56 (NCAM16.2) - Gerosa F, et al. 2002. J Exp Med. 195:327-333
 IL-22 (22URT1) - Chen X, et al. 2018. Oncol Lett. 16(1):253-261
 CD103 (BerACT8) - Tew G, et al. 2016. Gastroenterology. 150:477-487
 TCRgd (11F2) - Blink SE et al. 2009. Curr Mol Med. 9(1):15-22
 TCR Va7.2 (3C10) - Keller A, et al. 2017. Nat Immunol. 18:402-411
 IL23R (218213) - Dendrou et al. 2016. Sci Transl Med 2;8(363) 363ra149
 Anti-PE (PE001) - Del Alcazar D, et al. 2019. Cell Rep. 28:3047
 PD-1 (EH12.2H7) - RY H, et al. 2016. Oncoimmunology. 6:e1249561
 CXCR6 (K041E5) - Swadling L, et al. 2020. Cell Rep. 30:687.
 CD27 (L128) - Elrefaei M, et al. 2003. Immunology. 110:513-518.
 FOXP3 (259D/C7) - Giovanna R et al. 2005 Eur J Immunol. 35
 MIP1b (D21-1351) - Marquardt N et al. 2019. Nat Comm. 10(1) 3841
 LAYN (3F7D7E2) - Zheng C et al. 2017. Cell. 169(7) 1342-1356.e16
 NKp30 (P30-15) - Sadallah S, et al. 2016. J Immunol. 197: 1663 - 1671
 IL17 (BL168) - Nobs SP, et al. 2017. J Exp Med. 214:3015.
 Ki67 (Ki-67) - Eccles JD, et al. 2020. Cell Rep. 30:351.
 CXCR5 (RF8B2) - Gunn MD et al. 1998. Nature. 391(6669):799-803.
 CCR7 (G043H7) - Del Alcazar D, et al. 2019. Cell Rep. 28:3047

CD161 (HP-3G10) - Cardoso V et al. 2017. Nature. 549:277.
 KIR2DL4 (181703) - Takei Y et al. 2017. Oncotarget. 8(23) 36964-36972
 NKp46 (9 E2) - Mandelboim O et al, 2001. Int J Biochem Cell Biol. 33(12):1147-1150
 CD160 (BY55) - Jensen S, et al. 2015. PLoS One. 10: e0139573.
 CD25 (M-A251) - Lavin Y et al. 2017. Cell. 169(4):750-765
 CD39 (A1) - Olin A et al. 2018. Cell. 174(5):1277-1292
 BATF (9B5A13) - Ma Y et al. 2017. Cell host & microbe. 21(5):580-591
 CD137 (4B4-1) - Lavin Y et al. 2017. Cell. 169(4):750-765
 IFNg (B27) - Lavin Y et al. 2017. Cell. 169(4):750-765
 CD8a (RPA-T8) - Hebbandi NR, et al. 2017. Cell. 171:655
 CD16 (3G8) - Dutertre CA et al. 2019. Immunity. 51(3):573-589
 CD3 (SP34-2) - Carter DL et al. 1999. Cytometry. 37(1):41-50.
 CD8 (SK1) - Shehata L, et al. 2019. Nat Commun. 10:1126.
 CD45 (5B1) - Kurian, L. et al. 2013. Nat. Methods 10(1): 77-83
 EPCAM (9C4) - Gee MH, et al. 2018. Cell. 172:549
 IL20RA (173714) - Maarof G et al. 2010. Blood. 115(9): 1718-26
 IL10RB (90220) - Charbit-He F et al. 2018. PLoS ONE. 13(10) e0205826
 CD4 (SK3) - Lima J, et al. 2016. Reprod Sci. 10.1177/1933719116653680
 CD45RO (UCHL1) - Shan L, et al. 2017. Immunity. 47:766
 NKp46 (9E2) - Sanz-Ortega L, et al. 2019. Front Immunol. 1.85625
 CCR6 (G034E3) - Ivan Jelcic et al. 2018. Cell. 175(1):85-100
 CD69 (FN50) - Lee YG, et al. 2019. Nat Commun. 10:2681
 CCR7 (G043H7) - Bradley T et al. 2018. Cell reports. 25(1):107-117
 CTLA4 (BN13) - Franchini DM et al. 2019. Cell reports. 26(1):94-107
 TIM3 (F38-2E2) - Iwahori K, et al. 2019. Sci Rep. 2.205555556
 NKp44 (P44-8) - Vaccari M, et al. 2018. Nat Med. 24:847
 TNFRSF9 - CD137 (4B41) - Cirelli KM et al. 2019. Cell. 177(5):1153-1171
 CD298 (LNH-94) - Kurelac I, et al. 2019. Nat Commun. 10:903
 Anti-Human B2 Microglobulin (2M2) - Chung H et al. 2018. Cell. 172(4):811-824

Starred (*) Antibodies were obtained unconjugated, then conjugated for use internally using the Maxpar conjugation kit (Fluidigm) as described in the Methods.

The antibodies used in in vivo experiments were developed as described by Itoh et al, J Invest Dermatol 2019 Apr;139(4): 878-889 (Ref 86 in Manuscript)

Animals and other organisms

Policy information about [studies involving animals](#); [ARRIVE guidelines](#) recommended for reporting animal research

Laboratory animals	Mice - C57BL/6 (B6) mice and hIL-26Tg mice - These were B6 mice carrying a 190-kb BAC transgene with human IFNG and IL26 gene, developed in Thomas Aune's laboratory (see reference 73 for details of mice including confirmed tissue expression of hIL26 in the colon). Mice were housed in a specific pathogen-free facility in micro-isolator cages with ad libitum access to autoclaved water and sterile standard food. Male and Female B6 and hIL-26Tg mice at 10-14 weeks of age were used for the DSS-induced colitis model. Male and Female mice at 20-24 weeks of age were used for the analysis of spontaneous ileitis and colitis
Wild animals	The study did not involve wild animals.
Field-collected samples	The study did not involve the use of field-collected samples.
Ethics oversight	Performed under the Ethical approval for animal research obtained by the School of Medicine, Juntendo University (Tokyo, Japan)

Note that full information on the approval of the study protocol must also be provided in the manuscript.

Human research participants

Policy information about [studies involving human research participants](#)

Population characteristics	For Single cell RNA sequencing, CITE-Seq and CyTOF analysis, biopsies were collected from volunteers attending endoscopy for routine colonoscopic screening (healthy) or as part of ongoing clinical care (UC patients) (Full patient demographic details are presented in Supplementary Table 1). For UC, we utilized tissue derived from patients with a proven clinical and histological diagnosis. Tissue was sampled from clinically inflamed distal colon regions by the endoscopist performing the procedure. Donors ranged from 17 to 88 years of age, with a mix of male (n=26) and female (n=31) donors across all patient experiments.
Recruitment	Patients presenting to the Oxford University Hospitals NHS Foundation Trust for assessment of their gastrointestinal health using endoscopy were approached at random. Clinical, Endoscopic and Histological findings were used to categorise the patients as having healthy mucosa or having ulcerative colitis, with severity scores recorded by the clinician performing the procedure contemporaneously. The patient and scoring clinician were blinded as to the subsequent use of their samples. The patients were selected at random from the available cohort and collected across the UK; therefore it is unlikely that any demographic biases occur, other than those that reflect the general population of the UK.

Ethics oversight

The collection and use of Biobank samples was performed by Clinical Research Nurses under three parallel Biobank cohorts approved by the following NHS Research Ethics Committee(s) : West Midlands (18/WM/0237 and IBD 09/H1204/30) and Yorkshire and Humber (GI 16/YH/0247)

Note that full information on the approval of the study protocol must also be provided in the manuscript.

Flow Cytometry

Plots

Confirm that:

- The axis labels state the marker and fluorochrome used (e.g. CD4-FITC).
- The axis scales are clearly visible. Include numbers along axes only for bottom left plot of group (a 'group' is an analysis of identical markers).
- All plots are contour plots with outliers or pseudocolor plots.
- A numerical value for number of cells or percentage (with statistics) is provided.

Methodology

Sample preparation

For flow cytometry sorting samples were processed identically to those described in methods section. Following this they were then washed with FACS buffer (50ml PBS with 2% Fetal Calf Serum and 0.25mM EDTA) and were then stained with appropriate antibodies (Flow cytometry/CITE-seq) at pre-optimized concentrations for 30 minutes. Samples were then washed and sorted directly as described without fixation. Prior to running samples compensations were calculated with an unstained cellular control and compensation beads (BD).

Instrument

BD FACS Aria IIIu, BD FACS LSR II

Software

BD FACS Diva Software, with Quantification performed using FlowJo v10.5.3

Cell population abundance

Describe the abundance of the relevant cell populations within post-sort fractions, providing details on the purity of the samples and how it was determined.

Gating strategy

Sorting CD8 T cells for Single-Cell RNA Sequencing: Cells were gated based on size using Forward and Side scatter, followed by identification of singlets using FSC-H and FSC-A. After gating on Live cells, we gated on CD3 positive cells. From these, the CD8 positive fraction was sorted for single cell sequencing.
 FACS Analysis for IL26 Receptor: Cells were gated based as above to identify Live cells. From here, we identified CD45+, EPCAM+ and double negative (Stromal) populations. Within each of these sub-categories, we identified cells double positive for IL20RA and IL10RB (using FMO controls and pre-optimized antibody concentrations).

- Tick this box to confirm that a figure exemplifying the gating strategy is provided in the Supplementary Information.



**SIMPLE, POWERFUL, ACCESSIBLE.
FULL SPECTRUM FLOW CYTOMETRY**

9+ color assays, together with high throughput or extended warranty, for just \$69.9K

ACT NOW



Arf1 and Arf6 Synergistically Maintain Survival of T Cells during Activation

This information is current as of December 24, 2020.

Mami Sumiyoshi, Yui Kotani, Yuki Ikuta, Kazutomo Suzue, Madoka Ozawa, Tomoya Katakai, Taketo Yamada, Takaya Abe, Kana Bando, Shigeo Koyasu, Yasunori Kanaho, Toshio Watanabe and Satoshi Matsuda

J Immunol published online 11 December 2020
<http://www.jimmunol.org/content/early/2020/12/10/jimmunol.2000971>

Supplementary Material <http://www.jimmunol.org/content/suppl/2020/12/10/jimmunol.2000971.DCSupplemental>

Why *The JI*? Submit online.

- **Rapid Reviews! 30 days*** from submission to initial decision
- **No Triage!** Every submission reviewed by practicing scientists
- **Fast Publication!** 4 weeks from acceptance to publication

**average*

Subscription Information about subscribing to *The Journal of Immunology* is online at: <http://jimmunol.org/subscription>

Permissions Submit copyright permission requests at: <http://www.aai.org/About/Publications/JI/copyright.html>

Email Alerts Receive free email-alerts when new articles cite this article. Sign up at: <http://jimmunol.org/alerts>

The Journal of Immunology is published twice each month by The American Association of Immunologists, Inc., 1451 Rockville Pike, Suite 650, Rockville, MD 20852
Copyright © 2020 by The American Association of Immunologists, Inc. All rights reserved.
Print ISSN: 0022-1767 Online ISSN: 1550-6606.



Arf1 and Arf6 Synergistically Maintain Survival of T Cells during Activation

Mami Sumiyoshi,* Yui Kotani,*[†] Yuki Ikuta,[†] Kazutomo Suzue,[‡] Madoka Ozawa,[§] Tomoya Katakai,[§] Taketo Yamada,[¶] Takaya Abe,^{||} Kana Bando,^{||} Shigeo Koyasu,[#] Yasunori Kanaho,** Toshio Watanabe,[†] and Satoshi Matsuda*

ADP-ribosylation factor (Arf) family consisting of six family members, Arf1–Arf6, belongs to Ras superfamily and orchestrates vesicle trafficking under the control of guanine nucleotide exchange factors (GEFs) and GTPase-activating proteins. It is well established that brefeldin A, a potent inhibitor of ArfGEFs, blocks cytokine secretion from activated T cells, suggesting that the Arf pathway plays important roles in T cell functions. In this study, because Arf1 and Arf6 are the best-characterized members among Arf family, we established T lineage-specific Arf1-deficient, Arf6-deficient, and Arf1/6 double-deficient mice to understand physiological roles of the Arf pathway in the immune system. Contrary to our expectation, Arf deficiency had little or no impact on cytokine secretion from the activated T cells. In contrast, the lack of both Arf1 and Arf6, but neither Arf1 nor Arf6 deficiency alone, rendered naive T cells susceptible to apoptosis upon TCR stimulation because of imbalanced expression of Bcl-2 family members. We further demonstrate that Arf1/6 deficiency in T cells alleviates autoimmune diseases like colitis and experimental autoimmune encephalomyelitis, whereas Ab response under Th2-polarizing conditions is seemingly normal. Our findings reveal an unexpected role for the Arf pathway in the survival of T cells during TCR-induced activation and its potential as a therapeutic target in the autoimmune diseases. *The Journal of Immunology*, 2021, 206: 000–000.

The ADP-ribosylation factor (Arf) proteins are small GTPases belonging to the Ras superfamily and orchestrate intracellular protein trafficking under the control of their activators, guanine nucleotide exchange factors (GEFs), and inhibitors, GTPase-activating proteins (GAPs) (1, 2). Mice have six Arf isoforms (Arf1–Arf6), whereas Arf2 has been lost in humans (2). Among Arf family proteins, Arf1 and Arf6 are best characterized (3). Initial studies demonstrate that Arf1 regulates formation of coated vesicles mainly at the Golgi apparatus, as do Arf2–5, whereas Arf6, the most divergent isoform from Arf1, functions at the plasma membrane (4–7). Several reports have demonstrated, however, that both Arf1 and Arf6 facilitate migration of cancer cells by regulating integrin localization (8–10), indicating that Arf1 and Arf6 play overlapping roles at least in some circumstances. It has also been shown that Arf1 as well as Arf6 is involved in the activation of mTOR via PLD-mediated phosphatidic acid generation (11–13). Moreover, by

using tissue-specific gene knockout strategy, Arf1 and Arf6 are revealed to play a critical role in the nervous system through Schwann cell myelination (14, 15). It is of interest to note that Arf6-GAP SMAP1 and Arf1-GAP SMAP2 synergistically regulate early embryonic development (16), also suggesting the genetic linkage between Arf1 and Arf6 during initial steps in ontogeny. In contrast, physiological roles of Arf family proteins in the immune system remain obscure.

Given that the intracellular protein trafficking system controls a diverse array of cellular responses, including proliferation, differentiation, and cell migration, one can assume that this is also the case with the immune responses. In fact, Rab family of small GTPases modulates TCR signal transduction through TCR recycling as well as trafficking various components to the immunological synapse (17, 18). In addition, Rab27a regulates the secretion of the lytic granules from cytotoxic T lymphocytes (19), and mutations in *RAB27A* gene are known to be associated with

*Department of Cell Signaling, Institute of Biomedical Science, Kansai Medical University, Hirakata, Osaka 573-1010, Japan; [†]Department of Biological Science, Graduate School of Humanities and Sciences, Nara Women's University, Nara 630-8506, Japan; [‡]Department of Parasitology, Gunma University Graduate School of Medicine, Maebashi, Gunma 371-8511, Japan; [§]Department of Immunology, Niigata University Graduate School of Medical and Dental Sciences, Niigata 951-8510, Japan; [¶]Department of Pathology, Saitama Medical University, Iruma-gun, Saitama 350-0495, Japan; ^{||}Laboratory for Animal Resources and Genetic Engineering, RIKEN Center for Biosystems Dynamics Research, Kobe, Hyogo 650-0047, Japan; [#]Laboratory for Immune Cell Systems, RIKEN Center for Integrative Medical Sciences, Yokohama, Kanagawa 230-0045, Japan; and **Department of Physiological Chemistry, Graduate School of Comprehensive Human Sciences, Faculty of Medicine, University of Tsukuba, Tsukuba, Ibaraki 305-8575, Japan

ORCID: 0000-0002-8959-5746 (K.S.); 0000-0001-5026-2306 (M.O.); 0000-0002-4290-7028 (T.K.); 0000-0001-5885-4875 (T.A.); 0000-0001-9585-3038 (S.K.).

Received for publication August 24, 2020. Accepted for publication November 12, 2020.

This work was supported in part by Japan Society for the Promotion of Science grants-in-aid for scientific research (19K16701 to M.S. and 20K07555 and 20H03776 to S.M.), a Kansai Medical University grant-in-aid for research (to M.S.), the branding program as a world-leading research university on intractable

immune and allergic diseases supported by the Ministry of Education, Culture, Sports, Science and Technology of Japan, and the Kansai Medical University Molecular Imaging Center of Diseases.

Address correspondence and reprint requests to Dr. Satoshi Matsuda, Department of Cell Signaling, Institute of Biomedical Science, Kansai Medical University, 2-5-1 Shinmachi, Hirakata, Osaka 573-1010, Japan. E-mail address: matsuda@hirakata.kmu.ac.jp

The online version of this article contains supplemental material.

Abbreviations used in this article: 7-AAD, 7-aminoactinomycin D; Arf, ADP-ribosylation factor; Arf1-KO, T lineage-specific Arf1-deficient; Arf1/6-KO, T lineage-specific Arf1/Arf6 doubly deficient; Arf6-KO, T lineage-specific Arf6-deficient; γ c, common γ -chain; DP, double-positive; EAE, experimental autoimmune encephalomyelitis; eF450, Cell Proliferation Dye eFluor 450; GAP, GTPase-activating protein; GC, germinal center; GEF, guanine nucleotide exchange factor; IBD, inflammatory bowel disease; LP, lamina propria; MLN, mesenteric lymph node; MOG, myelin oligodendrocyte glycoprotein; MS, multiple sclerosis; NAC, *N*-acetyl-L-cysteine; PP, Peyer patch; ROS, reactive oxygen species; SAS, Sigma Adjuvant System; SP, single-positive; Treg, regulatory T cell.

Copyright © 2020 by The American Association of Immunologists, Inc. 0022-1767/20/\$37.50

Griscelli syndrome type II in human (20). It has also been shown that CRACR2A, another member of Rab family, is involved in T cell activation by regulating vesicle trafficking to the immunological synapse (21). As is the case with Rab family, it seems likely that the Arf pathway contributes to T cell function as well. Accordingly, brefeldin A, a potent inhibitor of ArfGEFs, blocks the cytokine secretion from activated T cells, raising the possibility that Arf family proteins play important roles during T cell activation (22, 23).

To unmask the functional role of the Arf pathway in T cell, we established T lineage-specific Arf-deficient mice and found that the lack of both Arf1 and Arf6 renders T cells susceptible to apoptosis during activation. In contrast, contrary to our expectation, Arf deficiency had no impact on cytokine secretion. We also show that the Arf-deficient mice are resistant to Th17-mediated diseases while Ab responses are intact.

Materials and Methods

Mice

All mouse strains used in this study were backcrossed to C57BL/6 for at least seven generations. The floxed *Arf1* (*Arf1^{fl/fl}*) mouse line (accession no. CDB1027K; <http://www2.clst.riken.jp/arg/micelist.html>) was established (detailed characterization was described in Supplemental Fig. 1) and crossed with *Lck-Cre* (24) along with *Arf6^{fl/fl}* mice (14). Age-matched *Arf1^{+/+}*; *Arf6^{+/+}* and *Lck-Cre* mice or cohoused *Arf1^{fl/+}*; *Arf6^{fl/+}*; *Lck-Cre* and *Arf1^{fl/fl}*; *Arf6^{fl/fl}* littermates were used as a control. *Rag2^{-/-}* mice (stock number RAGN12) were obtained from Taconic. Mice systemically expressing tdRFP (referred to in this article as RFP mice) were derived from *Rosa26-tdRFP* reporter mice (kindly provided by H. J. Fehling, University of Ulm, Ulm, Germany) (25). We used male and female mice aged between 7 and 12 wk in all experiments unless otherwise stated. All mice were maintained in a specific pathogen-free facility and used according to our institutional guidelines.

Cell preparation

Naive (CD44^{lo}CD62L^{hi}CD25⁻) or effector (CD44^{hi}CD62L^{lo}CD25⁻) CD4⁺ T cells were obtained from splenocytes by using a MojoSort Mouse CD4 T Cell Isolation Kit (BioLegend), followed by cell sorting on a FACSAria III (BD Biosciences). RPMI 1640 (Fujifilm) supplemented with 10% FCS (HyClone), 55 μ M 2-ME, 100 U/ml penicillin, 100 μ g/ml streptomycin, nonessential amino acids, 1 mM sodium pyruvate, and 10 mM HEPES was used as a culture medium. Cytokines used in this study were purchased from BioLegend. Naive CD4⁺ T cells were stimulated either with immobilized anti-CD3 ϵ mAb (5 μ g/ml) and 1 μ g/ml soluble anti-CD28 mAb or 10 ng/ml IL-7 in 24-well plates. In some experiments, T cells were activated in the presence of 20 ng/ml IL-2, 20 ng/ml IL-4, 20 ng/ml IL-7, 50 ng/ml IL-21, or 50 μ M Z-VAD-FMK (MBL). In vitro Th differentiation was induced with 10 ng/ml IL-12 (Th1), 10 ng/ml IL-4 (Th2), 10 ng/ml IL-2 and 20 ng/ml TGF- β (regulatory T cell [Treg]), 30 ng/ml IL-6 and 3 ng/ml TGF- β (nonpathogenic Th17), or 30 ng/ml IL-6, 50 ng/ml IL-23, 30 ng/ml IL-1 β , and 1 μ g/ml anti-IL-2 Ab (pathogenic Th17), followed by stimulation with Dynabeads Mouse T-Activator CD3/CD28 (Thermo Fisher Scientific). To isolate lamina propria (LP) lymphocytes, the colon was digested with HBSS containing 1.3 mM CaCl₂, 0.5 mM MgCl₂, Liberase TM (200 μ g/ml; Roche Diagnostics), and DNase I (10 μ g/ml; Roche Diagnostics) after removing intraepithelial lymphocytes with HBSS containing 5 mM EDTA and 1 mM DTT. LP lymphocytes were obtained from the 40/80% Percoll (GE Healthcare) interface after centrifugation of the digested colon at 920 \times g for 20 min at 25°C.

Quantitative PCR

Total RNA was extracted using RNeasy Micro Kit (QIAGEN), followed by PrimeScript RT Master Mix (Takara) reaction. THUNDERBIRD SYBR qPCR Mix (Toyobo) was used to evaluate gene expression on a Rotor-Gene Q (QIAGEN). Primers used were as follows: *Arf1*, 5'-ACAGAGAGC-GTGTGAACGAG-3' and 5'-TGGCCTGAATGTACCAGTTC-3'; *Arf6*, 5'-TCCTAATGAGCGTCTCCAC-3' and 5'-TCCTAGGAATGGGTTT-TGGA-3'; and *Cyclophilin A*, 5'-ATGGCACTGGCGGCAGGTCC-3' and 5'-TTGCCATTCTGGACCCAAA-3'.

ELISA

Concentrations of IL-2, IFN- γ , IL-4, and IL-17A in culture supernatants (1×10^5 cells/ml) were detected with ELISA Max Deluxe (BioLegend).

To evaluate OVA-specific Ab response, mice were primed i.p. with 100 μ g of OVA (Sigma-Aldrich) along with Imject Alum adjuvant (Thermo Fisher Scientific) and boosted 14 d later. Alternatively, mice were immunized i.p. with 25 μ g of OVA along with Sigma Adjuvant System (SAS; Sigma-Aldrich). On day 28, sera were subjected to ELISA in 96-well plate coated with 10 μ g/ml OVA along with HRP-linked anti-mouse IgG F(ab')₂ Ab (GE Healthcare). Fecal extract was obtained with 20% w/v PBS containing 2 mM PMSF and 0.2 mg/ml benzamide, and IgA was quantified by ELISA using SBA Clonotyping System-C57BL/6-HRP (SouthernBiotech).

Abs

Abs used in this study were as follows: Mcl-1 (no. 600-401-394) from Rockland Immunochemicals; Erk2 (D2) from Santa Cruz Biotechnology; CD4 (GK1.5), CD8 (53-6.7), and CD62L (MEL-14) from Tonbo Biosciences; CD44 (IM7), CD25 (PC61), IL-17A (TC11-18H10.1), CD98 (RL388), CD71 (RI7217), CD45.1 (A20), CCR7 (4B12), and annexin V (no. 640912) from BioLegend; Foxp3 (MF23) and CXCR5 (2G8) from BD Biosciences; PD-1 (RMPI-30) from eBioscience; HSP90 (no. 4874), phospho-S6 ribosomal protein (Ser^{235/236}) (D57.2.2E), Bim (no. 2819), Bcl-2 (D17C4), and Bcl-x_L (54H6) from Cell Signaling Technology.

Flow cytometry

Isolated cells were stained with the appropriate Abs along with 7-aminoactinomycin D (7-AAD; Sigma-Aldrich). To evaluate cell proliferation, cells (2.5×10^6 cells/ml in PBS) were labeled with 3 μ M Cell Proliferation Dye eFluor 450 (eF450; eBioscience) at 37°C for 5 min, followed by washing with the culture medium. For intracellular staining of cytokines and transcription factor, cells were stimulated with PMA and ionomycin in the presence of brefeldin A (eBioscience) for 4 h, followed by treatment with Fixation and Permeabilization Buffer (eBioscience) or Cytofix/Cytoperm (BD Biosciences). Glucose uptake was assessed by using 2-NBDG (Thermo Fisher Scientific) (26). Reactive oxygen species (ROS) were measured by incubation for 30 min at 37°C with 5 μ M CellROX Deep Red (Thermo Fisher Scientific) after staining of surface markers. To assess the impact of ROS on cell survival, CD4⁺ T cells were stimulated with or without 10 mM *N*-acetyl-L-cysteine (NAC) for 3 d, followed by evaluation with annexin V and 7-AAD staining according to the manufacturer's instructions (BioLegend). For the analysis of the sub-G1 population, cells were fixed and permeabilized with 75% ethanol and stained with 10 μ g/ml 7-AAD. Data were acquired on an FACSCanto II (BD Biosciences) and analyzed with FlowJo Software (Tree Star).

Immunofluorescence

The spleen, mesenteric lymph node (MLN), and Peyer patches (PPs) were fixed with 1% paraformaldehyde. After fixation, tissues were equilibrated gradually with 10, 20, and 30% sucrose in PBS at 4°C, embedded in O.C.T. compound (Sakura Finetek), and frozen at -80°C. Frozen sections (10 μ m) were made using a cryostat (Leica Biosystems) and postfixed with cold acetone for 3 min. Sections were stained with PE-conjugated anti-CD3 ϵ (145-2C11), Alexa Fluor 488-conjugated anti-B220 (RA3-6B2) (eBioscience), and anti-desmin (Abcam), followed by Alexa Fluor 633-conjugated anti-rabbit IgG (Molecular Probes). The specimens were examined using an FV1200 confocal microscope (Olympus). Digital images were prepared using FV10-ASW (Olympus) and Adobe Photoshop CS6 (Adobe Systems).

Experimental autoimmune encephalomyelitis

Age- and sex-matched mice (7–9 wk old) were immunized s.c. in the flanks with an emulsion containing the myelin oligodendrocyte glycoprotein (MOG) peptide MOG_{35–55} (200 μ g/mouse) and *Mycobacterium tuberculosis* H37Ra extract (5 mg/ml in CFA, 200 μ l/mouse). Pertussis toxin (200 ng/mouse) was administered i.p. on days 0 and 2. Mice were assigned scores daily on a scale of 0–5 in a double-blinded manner as described (27).

Statistical analysis

Unless otherwise indicated, statistical analysis was performed using unpaired Student *t* test. A *p* value <0.05 was considered statistically significant.

Results

Arf deficiency in T cells has no impact on cytokine secretion

According to cDNA microarray analysis data presented on RefDIC (<http://refdic.rcai.riken.jp/profile.cgi>; RMPSTC027003 and RMPSTC028001), Arf1 and Arf6 are the top two Arf family

members predominantly expressed in splenic CD4⁺ and CD8⁺ T cells. We thus focused on Arf1 as well as Arf6 to investigate the role of the Arf pathway in T cells. Given that loss of Arf1 or Arf6 results in embryonic lethality (28, 29), we established T lineage-specific Arf1-deficient (Arf1-KO), T lineage-specific Arf6-deficient (Arf6-KO), and T lineage-specific Arf1/Arf6 doubly deficient (Arf1/6-KO) mice by crossing conditional knockout mice (Supplemental Fig. 1A) with *Lck-Cre* transgenic mice. Both Arf1-KO mice and Arf6-KO mice had normal numbers of thymocytes and peripheral T cells (Supplemental Fig. 1B, 1C), whereas PCR analysis of genomic DNA obtained from purified T cells revealed that *Arf* genes were completely deleted by *Lck-Cre* (data not shown). By using quantitative PCR analysis, we also confirmed that expression levels of Arf mRNAs were virtually absent (Fig. 1A). Essentially, the same result was obtained with Arf1/6-KO mice, but the detailed analysis revealed that Arf1/6-KO mice alone exhibited decreased numbers of CD4⁺ and CD8⁺ T cells in the spleen (Fig. 1B), whereas numbers of CD4 single-positive (SP) and CD8SP thymocytes were increased (Supplemental Fig. 1D, 1E). These

observations suggest that Arf1 and Arf6 play redundant roles in the T cells.

Increased numbers of CD4SP and CD8SP cells in the thymus can be explained by either enhanced efficiency in positive selection or suppression of T cell egress from the thymus. To examine these two possibilities, we first focused on the double-positive (DP) stage when positive selection takes place. We found that proportions of TCRβ^{hi}CD69^{hi} DP cells, which correspond to postselected DP cells, were comparable between control and Arf1/6-KO mice (Supplemental Fig. 1F). We further examined the expression profiles of chemokine receptor CCR7 in combination with CD69 to track developing thymocytes but found little or no difference between control and Arf1/6-KO mice (Supplemental Fig. 1G). Taking these results into account, it seems unlikely that positive selection is affected by the lack of Arf1 and Arf6. We next examined expression profiles of CD62L and CD69 because CD4SP as well as CD8SP cells can be subdivided into immature (CD62L^{lo}CD69^{hi}) and mature (CD62L^{hi}CD69^{lo}) SP cells, the latter of which are known as egress-competent cells (30). Arf1/6-KO

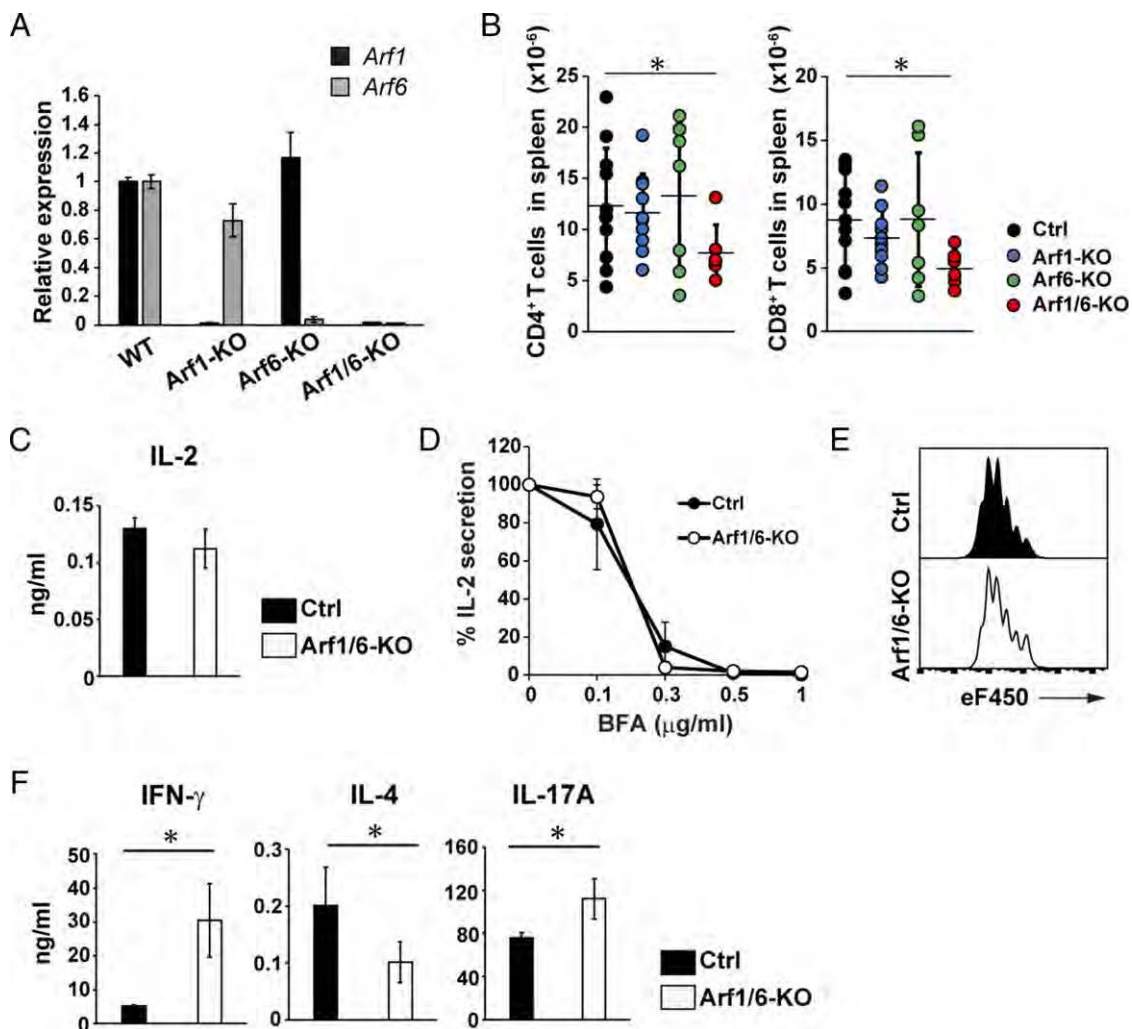


FIGURE 1. Characterization of peripheral T cells from Arf-deficient mice. **(A)** Quantitative PCR (qPCR) analysis of *Arf1* or *Arf6* relative to *Cyclophilin A* in splenic CD4⁺ T cells derived from the indicated mice ($n = 3$, each). Shown are relative expression levels normalized to wild type (WT) (mean \pm SD). **(B)** Number of CD4⁺ T cells (left) or CD8⁺ T cells (right) in the spleen from 5- to 7-wk-old control ($n = 10$, black), Arf1-KO ($n = 10$, blue), Arf6-KO ($n = 7$, green), and Arf1/6-KO mice ($n = 7$, red). Mean \pm SD. **(C)** IL-2 produced in naive CD4⁺ T cells from control (Ctrl; $n = 4$) and Arf1/6-KO ($n = 4$) mice was quantified by ELISA. Mean \pm SD. **(D)** CD4⁺ T cells from the indicated mice ($n = 4$, each) were stimulated with anti-CD3 ϵ /anti-CD28 mAbs along with the indicated concentration of brefeldin A (BFA) for 24 h. IL-2 were quantified by ELISA and indicated as the percentage of IL-2 secretion in the absence of BFA. **(E)** eF450-labeled Ctrl and Arf1/6-KO splenocytes were activated with anti-CD3 ϵ /anti-CD28 mAbs for 66 h. eF450 dilution plots gated in CD4⁺ T cells are shown as representative of three independent experiments. **(F)** Cytokines produced in Th1 (IFN- γ), Th2 (IL-4), and Th17 cells (IL-17A) were quantified by ELISA ($n = 3$). Mean \pm SD. * $p < 0.05$.

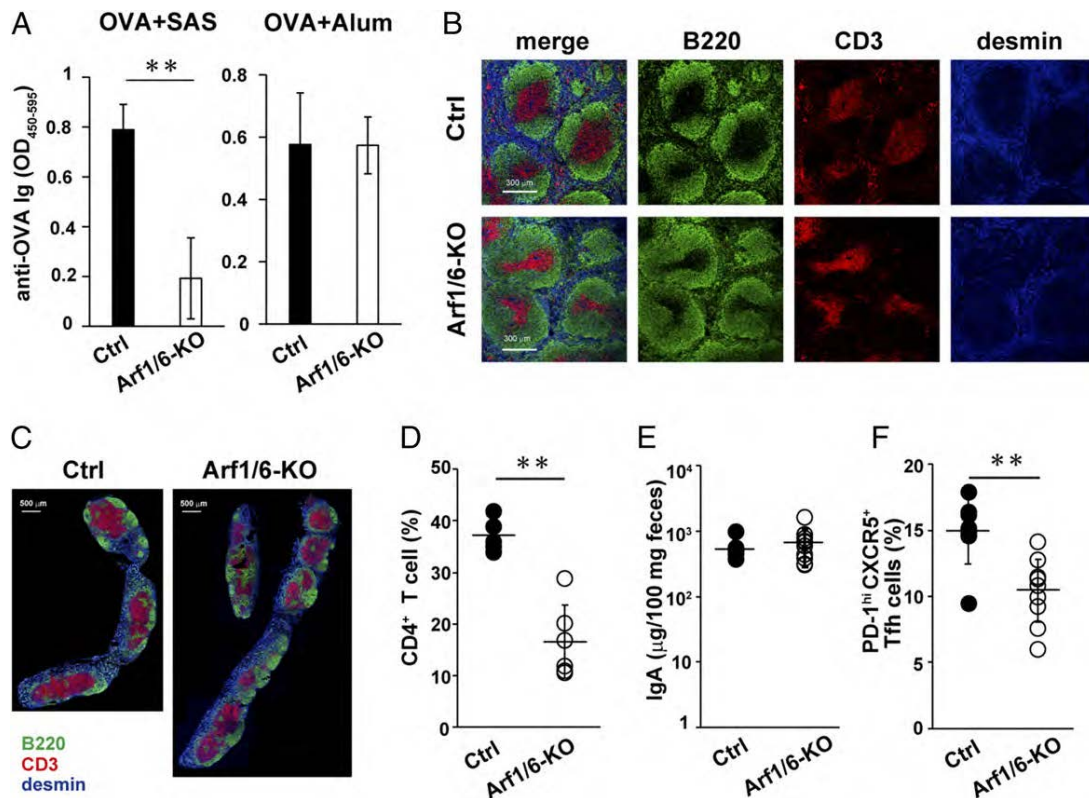


FIGURE 2. Ab responses in Arf1/6-deficient mice. **(A)** Either control (Ctrl; $n = 5$) or Arf1/6-TKO mice ($n = 5$) were immunized with OVA + SAS, and Ab titers were evaluated by ELISA. When immunized with OVA + Alum, Ctrl ($n = 3$) and Arf1/6-TKO ($n = 4$) were used. Mean \pm SD. **(B and C)** Immunohistochemical analysis of the spleen and MLN from Ctrl and Arf1/6-KO mice. Scale bars, 300 μ m (B) and 500 μ m (C). Shown are representative of three. **(D)** Proportions of CD4⁺ T cells in the MLN from 7- to 8-wk-old Ctrl ($n = 5$) and Arf1/6-KO ($n = 6$) mice. Mean \pm SD. **(E)** Fecal IgA levels of 9–11-wk-old Ctrl ($n = 9$) or Arf1/6-TKO ($n = 10$) mice were quantified by ELISA. Mean \pm SD. **(F)** Proportions of Tfh cells in the PPs from 9- to 11-wk-old Ctrl ($n = 8$) and Arf1/6-KO ($n = 10$) mice. Mean \pm SD. $**p < 0.01$.

mice contained a higher proportion of mature SP cells compared with control mice (Supplemental Fig. 1H), suggesting that CD4SP and CD8SP cells have a defect in thymic egress in Arf1/6-KO mice. Consistently, mixed bone marrow chimera between control (CD45.1⁺) and Arf1/6-KO (CD45.1⁻) mice demonstrated that the proportions of splenic CD4⁺ cells relative to thymic CD4SP cells (referred to in this study as the egress index, Supplemental Fig. 1I) were substantially decreased in Arf1/6-KO mice-derived CD45.1⁻ cells. Decreased numbers of splenic CD4⁺ and CD8⁺ T cells in Arf1/6-KO mice can also be explained by this partial defect in thymic egress.

Considering that brefeldin A, a well-known inhibitor for Arf-GEFs, which functions upstream of Arf1, is widely used to block cytokine secretion from activated T cells, it seems reasonable to speculate that Arf deficiency abrogates cytokine production. Contrary to our expectation, however, naive CD4⁺ T cells obtained from Arf1/6-KO mice produced IL-2 during activation to a level comparable to those from control mice (Fig. 1C). We also found that brefeldin A successfully blocked IL-2 secretion in both control and Arf1/6-deficient CD4⁺ T cells (Fig. 1D), excluding the possibility that Arf deficiency is compensated by a brefeldin A-independent secretory machinery. Consistent with this observation, Arf1/6-deficient T cells normally proliferated upon TCR stimulation (Fig. 1E). We further found that Arf1/6-deficient CD4⁺ T cells retained the potential to produce other cytokines, including IFN- γ , IL-4, and IL-17A as well (Fig. 1F). Although IL-4 production was decreased, Arf1/6-deficient CD4⁺ T cells secreted more IL-17A and IFN- γ than control cells. Collectively, we conclude that Arf1 and

Arf6 are dispensable for cytokine secretion, including IL-2, IFN γ , and IL-17A in activated T cells.

Arf1/6-deficient T cells facilitate Ab production in vivo

One of the most important functions of CD4⁺ T cells in immune system is to provide help for B cells to produce Ab against “nonself” in germinal centers (GCs). To examine whether Arf deficiency affects Ab response in vivo, we evaluated Ab production against OVA along with Th1-polarizing adjuvant SAS or Th2-polarizing adjuvant Alum (31, 32). Contrary to the in vitro observations (Fig. 1F), Arf1/6-KO mice produced normal level of OVA-specific Ab under Th2-polarizing conditions, although Th1-driven response was attenuated (Fig. 2A). Histological analysis revealed that Arf1/6-deficient mice contain seemingly normal lymphoid tissues, including spleen and MLN (Fig. 2B, 2C). Although the proportion of CD4⁺ T cells in the MLN were decreased in Arf1/6-KO mice, this may reflect the reduced numbers of CD4⁺ T cells in the spleen (Fig. 2D). We also found that there was no difference in the amount of fecal IgA, which is induced against intestinal commensal bacteria in the GALTs, including the PPs between control and Arf1/6-KO mice (Fig. 2E), albeit with slightly reduced proportions of Tfh cells (CD4⁺CXCR5⁺PD-1^{hi}) in the PPs (Fig. 2F) in Arf1/6-KO mice. These data indicate that T cell-dependent Ab response remains intact in the gut of Arf1/6-KO mice.

Arf1 and Arf6 are dispensable for mTORC1-regulated T cell function

Given that Arf1 contributes to the amino acid-induced mTORC1 activity in *Drosophila* S2 cells (33) and that Arf6 regulates tumor

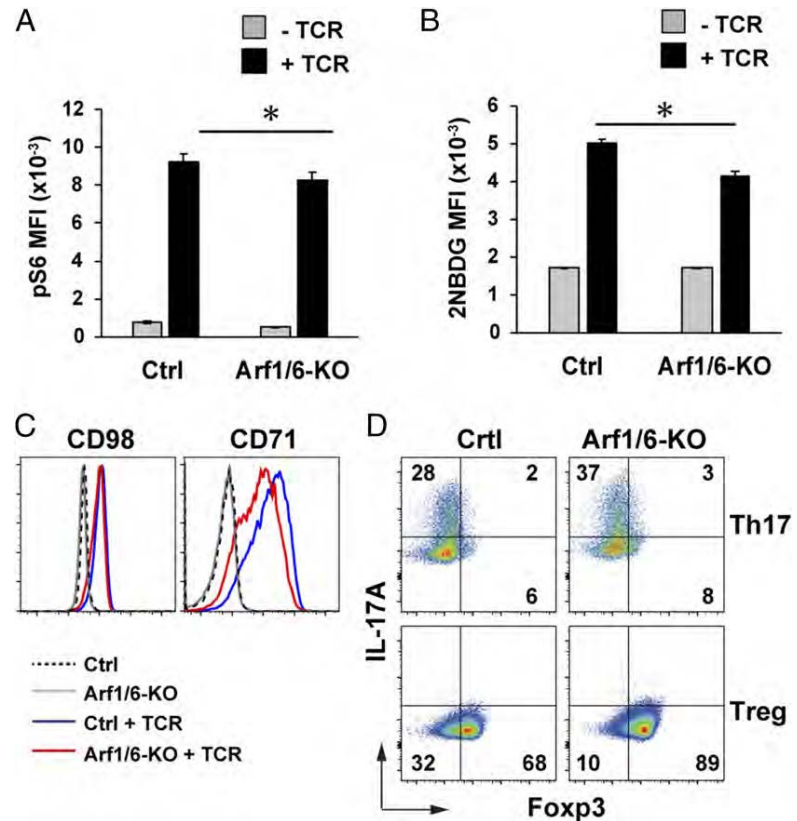


FIGURE 3. mTORC1 signal in Arf1/6-deficient T cells. (A–C) Evaluation of mTORC1 signal. Either control or Arf1/6-deficient CD4⁺ T cells were stimulated with or without anti-CD3 ϵ /anti-CD28 mAbs (+TCR) for 24 h and were assayed for pS6 signal (A), 2-NBDG uptake (B) and expression levels of CD98 and CD71 (C) by FACS. Mean \pm SD. Shown are representative of three. (D) Intracellular staining for IL-17A and Foxp3 in CD4⁺ T cells cultured under Th17- or Treg-inducing conditions for 4 d. Shown are representative of three. * $p < 0.05$.

cell proliferation via the PLD–mTORC1 pathway (11), we examined whether Arf deficiency affects mTORC1 signal in T cells. Arf1/6-deficient CD4⁺ T cells exhibited slightly lower levels of phosphorylated ribosomal protein S6 (pS6), a measure of active mTORC1 signal, when compared with control CD4⁺ T cells (Fig. 3A). Consistent with the previous reports demonstrating that mTORC1 regulates glycolytic metabolism in activated T cells, glucose uptake upon TCR stimulation was moderately impaired in Arf1/6-deficient CD4⁺ T cells (Fig. 3B). In contrast, we found little or no difference between control and Arf1/6-deficient CD4⁺ T cells in surface expression levels of the amino acid transporter CD98, a well-known downstream target of the mTORC1 pathway (Fig. 3C). We also evaluated expression levels of another target of the mTORC1 pathway, transferrin receptor CD71, and found that CD71 induction was slightly attenuated at 24 h after TCR stimulation in Arf1/6-deficient CD4⁺ T cells (Fig. 3C). It should be noted, however, that there was no significant difference in CD71 levels between control and Arf-deficient CD4⁺ T cells at 72 h after stimulation (data not shown). These results suggest that mTORC1 signal in Arf1/6-deficient CD4⁺ T cells, albeit slightly reduced, sufficiently supports metabolic reprogramming during T cell activation.

To further clarify the relationship between the Arf pathway and mTORC1 signal, we next focused on T cell differentiation program. The mTORC1 pathway is known to control the balance of Th17 versus Treg, and the blockade of mTORC1 signal results in skewing of naive CD4⁺ T cells toward Treg differentiation while attenuating Th17 differentiation (34, 35). We therefore examined whether Arf deficiency affects differentiation program of naive CD4⁺ T cells in vitro and found that Arf1/6-deficient CD4⁺ T cells normally differentiated to Th17 or Treg under appropriate conditions (Fig. 3D). We thus conclude

that the Arf pathway is dispensable for mTORC1-regulated T cell function.

Arf1/6-KO mice have fewer CD4⁺ T cells in the colon LP

Homeostatic proliferation generates two distinct populations: slow-dividing cells are induced in the presence of environmental cytokines like IL-7, whereas fast-dividing cells are thought to respond to gut microbiota (36). Interestingly, when compared with control CD4⁺ T cells, fast-dividing Arf1/6-deficient CD4⁺ T cells were markedly diminished, whereas slow-dividing ones appeared to be intact during homeostatic proliferation in lymphopenic *Rag2*^{-/-} mice (Fig. 4A), raising the possibility that Arf deficiency causes a defect in immune reaction in the gut. Actually, CD4⁺ T cells in the colonic LP were significantly decreased in Arf1/6-KO mice (data not shown). One can argue, however, that decreased proportion of Arf1/6-KO CD4⁺ T cells in the LP just reflects decreased number of splenic T cells (Fig. 1B). We thus analyzed mixed bone marrow chimeric mice as in Supplemental Fig. 11 and found that Arf1/6-deficient CD4⁺ T cells were defeated by control CD4⁺ T cells in the colonic LP, but not in the MLNs (Supplemental Fig. 2A), confirming that Arf deficiency leads to the reduction of CD4⁺ T cell number specifically in the gut. We therefore speculated the following two possibilities: Arf1/6-deficient CD4⁺ T cells have a defect in either migration into or survival in the colon.

Given that the CCR9 and the integrin $\alpha 4\beta 7$ play important roles in T cell homing to the gut under homeostatic conditions (37, 38), we first examined the surface expression levels of CCR9 in colonic CD4⁺ T cells. However, we failed to detect CCR9 even in the CD4⁺ T cells obtained from the colonic LP of control mice, presumably because of its internalization upon ligand binding, as is the case with other chemokine receptors, including CCR7 (39). Instead, we found that CD4⁺ T cells derived from Arf1/6-KO mice expressed CCR9 on the surface of thymocytes to a similar level to

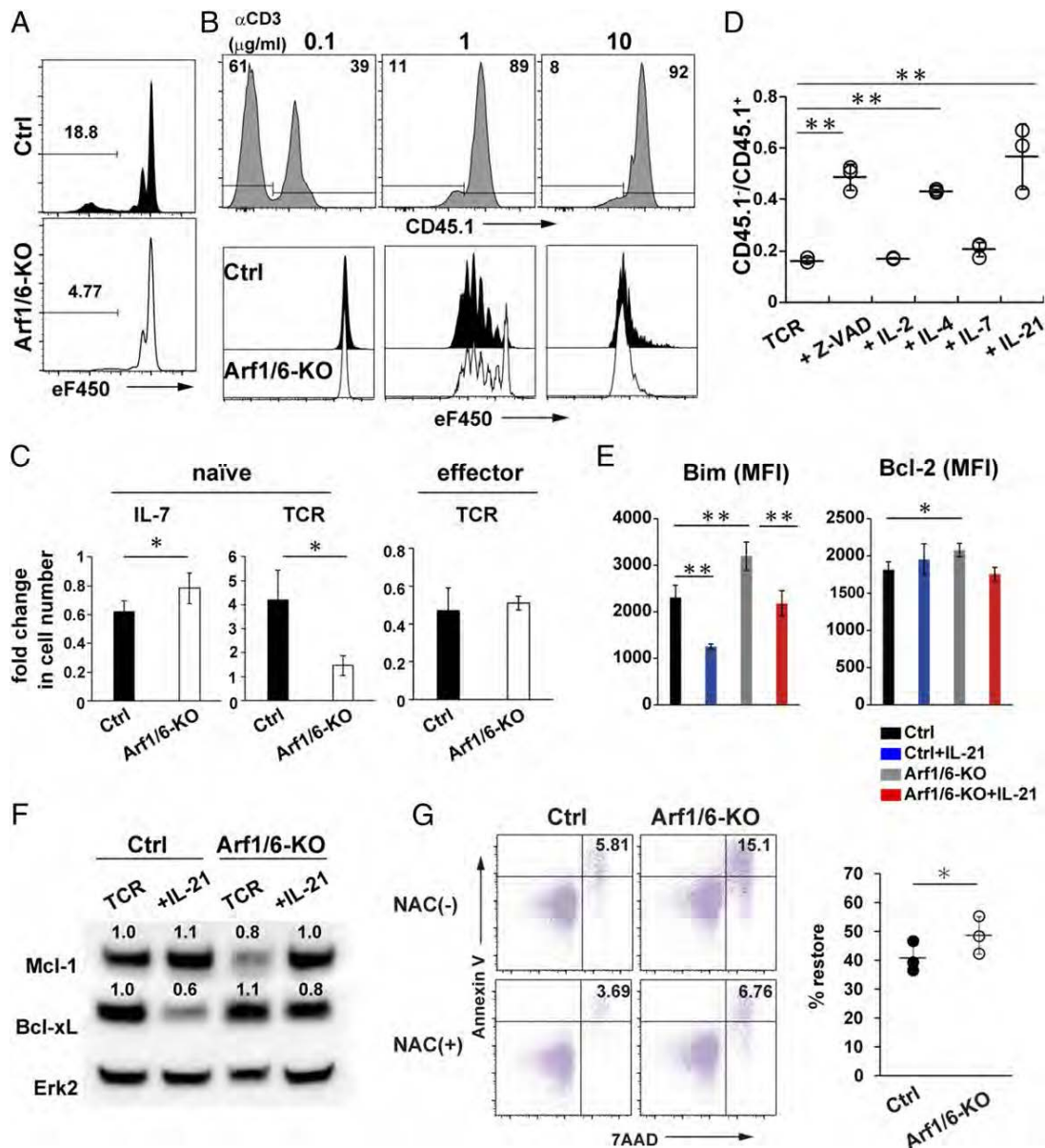


FIGURE 4. Activated Arf1/6-deficient T cells are susceptible to apoptosis. **(A)** Mixture of eF450-labeled CD4⁺ T cells from control (Ctrl; CD45.1⁺) and Arf1/6-KO (CD45.1⁻) mice was transferred into *Rag2*^{-/-} mice ($n = 3$), and eF450 dilution plot was obtained on day 4. Shown are representative of three. **(B)** CD4⁺ T cells from Ctrl (CD45.1⁺) and Arf1/6-KO mice (CD45.1⁻) were mixed at an equal ratio and activated with 0.1–10 μ g/ml plate-bound anti-CD3 ϵ mAb along with 1 μ g/ml soluble anti-CD28 mAb for 4 d, followed by FACS analysis (upper, CD45.1 plot; lower, eF450 dilution plots of CD45.1⁺ [Ctrl] and CD45.1⁻ cells [Arf1/6-KO]). Shown are representative of three. **(C)** Naive or effector CD4⁺ T cells from the indicated mice were treated with IL-7 or a combination of anti-CD3 ϵ /anti-CD28 mAbs (TCR) for 72 h. Fold changes in cell number compared with day 0 are estimated. Mean \pm SD. Shown are representative of three. **(D)** Naive CD4⁺ T cells from Ctrl (CD45.1⁺) and Arf1/6-KO (CD45.1⁻) mice were mixed at an equal ratio and stimulated with anti-CD3 ϵ /anti-CD28 mAbs (TCR) with or without the indicated reagent for 4 d, and the ratios were evaluated by FACS. Mean \pm SD. **(E and F)** Naive CD4⁺ T cells from the indicated mice ($n = 3$, each) were stimulated with anti-CD3 ϵ /anti-CD28 mAbs (TCR) along with or without IL-21 and analyzed at 48 h by FACS (E) or at 96 h by immunoblot against Bcl-2 family members (F). The values indicate relative density of the band normalized to Erk2. Shown are representative three. **(G)** CD4⁺ T cells from Ctrl ($n = 3$) and Arf1/6-KO ($n = 3$) mice were stimulated with anti-CD3 ϵ /anti-CD28 mAbs along with or without 10 mM NAC and analyzed at 72 h by FACS. Representative FACS profiles (left). Indicated are proportions of annexin V⁺7-AAD⁺ cells. Decrease in proportion of annexin V⁺7-AAD⁺ cells with NAC relative to that without NAC is quantified and indicated as percentage of restore (right). Mean \pm SD. * $p < 0.05$, ** $p < 0.01$.

those from control mice, suggesting that the Arf pathway is dispensable for CCR9 expression (data not shown). We also found that lack of both Arf1 and Arf6 rather augmented $\alpha 4\beta 7$ expression levels in CD4⁺ T cells, albeit only slightly (Supplemental Fig. 2B). It should be noted, however, that the affinity of integrin for its ligands is tightly regulated by intracellular signaling, so-called inside-out signal, which plays a pivotal role in cell adhesion,

spreading, and migration (40, 41). To further investigate whether integrin normally functions in Arf1/6-deficient CD4⁺ T cells, we estimated the size of adhesion area formed by interaction between LFA-1 integrin and its ligand ICAM-1 upon CCL21 stimulation, a measure of inside-out signal, and found that CCL21-stimulated, Arf1/6-deficient CD4⁺ T cells efficiently spread on the ICAM-1-coated plate (data not shown). Actually, by transferring a

mixture of control (CD45.1⁺) and Arf1/6-deficient CD4⁺ T cells (CD45.1⁻) into *Rag2*^{-/-} mice, we confirmed that control and Arf1/6-deficient CD4⁺ T cells equally migrated into the colon (Supplemental Fig. 2C), excluding the possibility that decreased CD4⁺ T cell number in the colon is caused by impaired cell migration.

We next focused on the hypothesis that Arf deficiency in T cells leads to a defect in survival in the colon. Given that LP CD4⁺ T cells are in a state of activation because of continuous exposure to microbial Ags, we examined whether TCR-induced activation affects viability of CD4⁺ T cells lacking Arf1 and Arf6. Stimulation with anti-CD3 ϵ and anti-CD28 mAbs resulted in marked decrease of Arf1/6-deficient CD4⁺ T cells in a signal intensity-dependent manner, although there was little or no difference in cell proliferation between control and Arf1/6-deficient CD4⁺ T cells, suggesting that Arf1/6-deficient CD4⁺ T cells are susceptible to cell death during activation (Fig. 4B). In contrast, CD4⁺ T cells lacking either Arf1 or Arf6 alone had no such defect in survival during TCR stimulation (Supplemental Fig. 3A, 3B), suggesting that Arf1 and Arf6 play a redundant role in cell survival. Essentially the same results were obtained with Arf1/6-deficient CD8⁺ T cells (Supplemental Fig. 3C, 3D). We further found that upon TCR stimulation, Arf1/6-deficient CD4⁺ T cells contained a higher proportion of sub-G1 cells (Supplemental Fig. 3E), which reflects apoptosis-related DNA fragmentation. Accordingly, treatment with Z-VAD-FMK, a pan-caspase inhibitor, partially blocked loss of Arf1/6-deficient CD4⁺ T cells induced by TCR stimulation (Supplemental Fig. 3F). It seems thus likely that the Arf pathway protects activated T cells from a caspase-mediated apoptotic program. Interestingly, the lack of Arf1 and Arf6 rendered only naive, but not effector, CD4⁺ T cells susceptible to apoptosis upon TCR stimulation (Fig. 4C). In contrast, we found no significant defect in IL-7-mediated survival between control and Arf1/6-deficient naive CD4⁺ T cells (Fig. 4C), consistent with the observation that Arf deficiency had no effect on slow-dividing population during homeostatic proliferation (Fig. 4A). These results taken together clearly demonstrated that Arf1 and Arf6 play a protective role exclusively in naive T cells during TCR-induced activation.

Because common γ -chain (γ c) cytokines like IL-2 promote the survival of activated T cells (42), we examined the survival effect of γ c cytokines on naive T cells upon TCR stimulation. Unexpectedly, IL-2 or IL-7 had no impact on the survival of TCR-stimulated, Arf1/6-deficient CD4⁺ T cells (Fig. 4D). In marked contrast, IL-4 as well as IL-21 successfully restored the viability of Arf1/6-deficient CD4⁺ T cells to a level similar to Z-VAD-FMK treatment, suggesting that IL-4 and IL-21 attenuate apoptosis caused by loss of Arf1 and Arf6. Apoptosis in T cells is triggered by two different pathways: the intrinsic pathway, which is controlled by the balance between pro- and antiapoptotic Bcl-2 family members (43–46), and the extrinsic pathway, which is initiated by signals delivered from death receptors such as Fas (47). Because Fas expression was intact in Arf1/6-deficient CD4⁺ T cells (data not shown), we focused on Bcl-2 family members and found that expression level of proapoptotic Bim was substantially increased in Arf1/6-deficient CD4⁺ T cells upon TCR stimulation, which was nearly completely attenuated in the presence of IL-21 (Fig. 4E, Supplemental Fig. 3G). In contrast, neither Arf deficiency nor IL-21 treatment had marked impact on expression levels of Bcl-2 (Fig. 4E, Supplemental Fig. 3G). Among three major isoforms of Bim, BimEL and BimL play a fundamental role in T cells (48). By using Western blotting analysis, we further found that BimL was the most abundantly upregulated in TCR-stimulated Arf1/6-deficient T cells (Supplemental Fig. 3H). Interestingly enough, treatment of Arf1/6-deficient T cells with

IL-21 markedly decreased exaggerated expression of BimL. We also found that Arf deficiency perturbed expression levels of other antiapoptotic Bcl-2 family members: Mcl-1 was downregulated, whereas Bcl-xL was rather upregulated, albeit to a slight extent (Fig. 4F). It should be noted, however, that IL-21 treatment attenuated Bcl-xL expression in both control and Arf1/6-deficient T cells, whereas Mcl-1 level was rescued to a level comparable to control cells. Considering the protective effect of IL-21 against apoptosis, it seems reasonable to assume that enhanced apoptosis in Arf1/6-deficient CD4⁺ T cells is attributed to upregulation of Bim along with downregulation of Mcl-1. The physiological relevance of Bcl-xL upregulation in Arf1/6-deficient T cells remained to be resolved. Because ROS enhance apoptosis of T cells during activation (49), we also assessed the impact of NAC, a widely used antioxidant, on the viability of Arf1/6-deficient CD4⁺ T cells. By treatment with NAC, the proportion of dead cells in Arf1/6-deficient CD4⁺ T cells was significantly reduced (Fig. 4G). We also found, however, that Arf-deficient CD4⁺ T cells exhibited a lower level of ROS (Supplemental Fig. 3I), raising the possibility that Arf1/6-deficient CD4⁺ T cells are more sensitive to ROS-induced apoptosis.

Arf deficiency in T cells suppresses the onset of autoimmune diseases

To directly evaluate the fate of Arf1/6-deficient naive CD4⁺ T cells upon activation in the colon, we used a naive CD4⁺ T cell-induced colitis model, one of widely used mouse models of inflammatory bowel disease (IBD), in which naive CD4⁺ T cells transferred into *Rag2*^{-/-} mice are activated with microbial Ags and differentiate to pathogenic Th17 cells in the colon. Actually, we found that *Rag2*^{-/-} mice transferred with control CD4⁺ T cells exhibited marked weight loss, which reflects colitis development, around 3 wk after the transfer (Fig. 5A). In contrast, the transfer of Arf1/6-deficient naive CD4⁺ T cells had no impact on body weights. Both thickening of the colon wall and severe infiltration of mononuclear cells in the colon confirmed the onset of colitis in control CD4⁺ T cell-transferred *Rag2*^{-/-} mice, whereas such histological changes were not detected in the mice transferred with Arf1/6-deficient CD4⁺ T cells (Fig. 5B), suggesting that naive CD4⁺ T cells lacking Arf1 and Arf6 failed to induce colitis. Considering that Th17 cells play a pivotal role in the pathogenesis of naive CD4⁺ T cell-induced colitis, one can argue that suppression of colitis could reflect the impaired ability of Arf1/6-deficient naive CD4⁺ T cells to differentiate to pathogenic Th17 cells. However, Arf1/6-deficient CD4⁺ T cells normally differentiated to pathogenic Th17 cells in vitro (Fig. 5C). In addition, pathogenic Th17 cells generated from Arf1/6-deficient CD4⁺ T cells were maintained in vivo to a level comparable to those from control (Supplemental Fig. 4A). We also found that CD4⁺ T cell number was systemically decreased in the mice transferred with Arf1/6-deficient CD4⁺ T cells when compared with those transferred with control T cells, whereas the frequency of IL-17A-producing CD4⁺ T cells were rather augmented (Supplemental Fig. 4B, 4C). We further found that Arf1/6-deficient CD4⁺ T cells were activated to a level comparable to control CD4⁺ T cells in the colon, which is indicated by upregulation of an activation marker CD44 (Fig. 5D). Furthermore, when transferred with control T cells into *Rag2*^{-/-} mice, Arf1/6-deficient T cells were virtually outcompeted (Fig. 5E). These results taken together suggest that the reason why transfer of Arf1/6-deficient naive CD4⁺ T cells did not develop colitis is likely due to the failure in expansion of activated T cells, but not due to the impaired differentiation or survival of pathogenic Th17 cells. Similar results

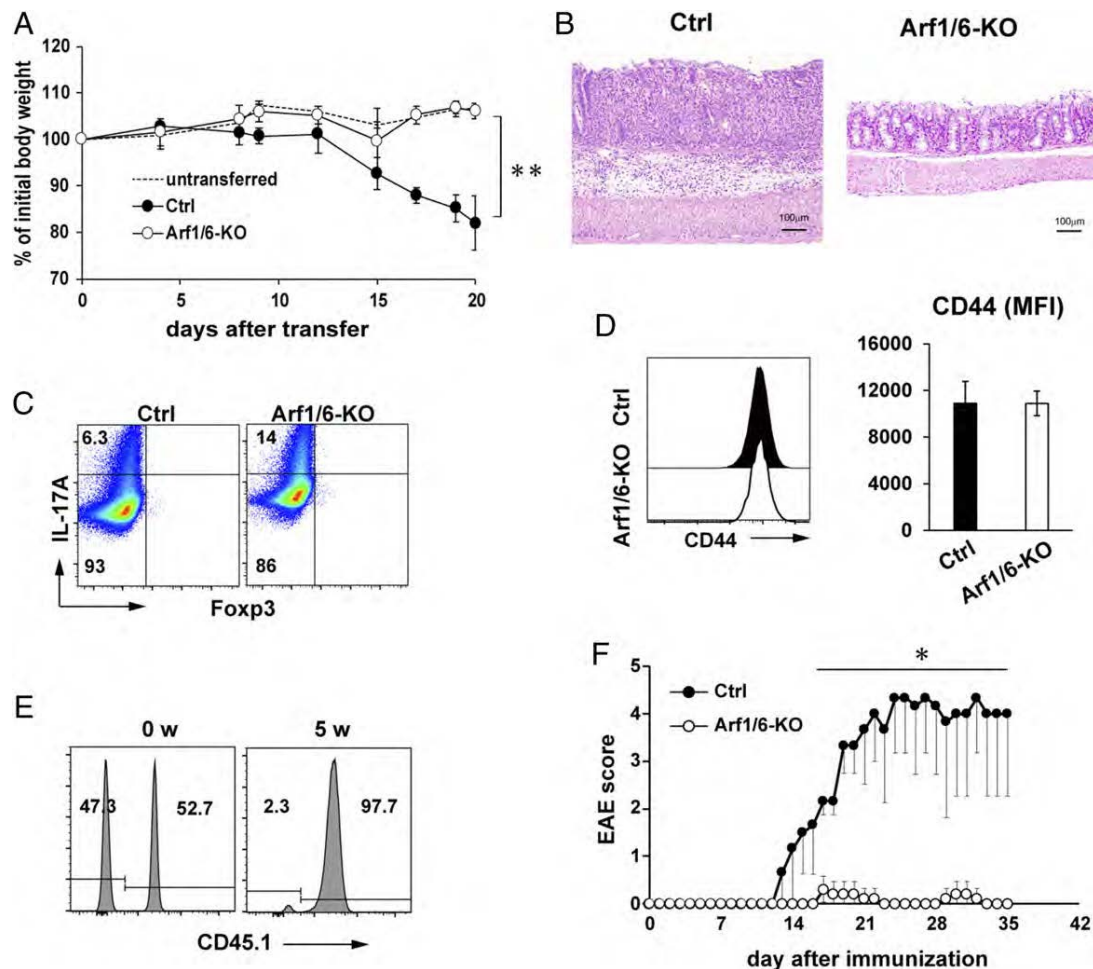


FIGURE 5. Autoimmune diseases are markedly attenuated in Arf1/6-deficient mice. **(A and B)** Colitis was induced in *Rag2*^{-/-} mice by transferring 4×10^5 naive CD4⁺ T cells from control (Ctrl; $n = 4$) or Arf1/6-KO ($n = 4$) mice. Body weights of mice with (Ctrl and Arf1/6-KO) or without (untransferred) cell transfer were monitored and indicated as the percentage of initial body weight (mean \pm SD) (A). Representative colonic histology. Scale bar, 100 μ m (B). **(C)** Intracellular staining for IL-17A and Foxp3 in CD4⁺ T cells cultured under pathogenic Th17-inducing conditions for 4 d. Shown are representative of three. **(D)** Expression levels of CD44 in colonic LP CD4⁺ T cells of recipient *Rag2*^{-/-} mice described in (A) were evaluated by FACS. Representative FACS profiles (left) and mean fluorescence intensity (MFI) (right). **(E)** Ctrl (CD45.1⁺) and Arf1/6-KO (CD45.1⁻) naive CD4⁺ T cells were mixed at an equal ratio (0 wk), and transferred into *Rag2*^{-/-} recipient mice. After 5 wk, the ratios of Ctrl to Arf1/6-KO cells in the colonic LP of recipient mice were evaluated by FACS. Data are representative of three independent experiments. **(F)** Clinical scores for EAE in Ctrl ($n = 3$) and Arf1/6-KO ($n = 3$) mice. Mean \pm SD. * $p < 0.05$, ** $p < 0.01$.

were observed in another type of Th17-mediated inflammatory disease of the CNS, experimental autoimmune encephalomyelitis (EAE): Arf1/6-deficient mice were completely resistant to induction of EAE after immunization with MOG₃₅₋₅₅ peptide, whereas control mice developed severe EAE (Fig. 5F). Collectively, these results suggest that the Arf pathway is required for the onset of Th17-mediated autoimmune diseases, which could be explained by the protective role of the Arf pathway against apoptosis during TCR stimulation.

Discussion

Intracellular cytokine staining combined with flow cytometry is a powerful method to assess T cell responses, in which the fungal metabolite brefeldin A plays a key role to retain cytokines within the activated T cells. Although brefeldin A is thought to inhibit Arf1 activation through its GEFs, physiological role of Arf family proteins in T cells has been unclear. In this study, we demonstrated that Arf1 along with Arf6 plays a pivotal role in developing autoimmune disease like colitis and EAE, presumably through suppressing apoptosis in activated T cells. In contrast, to our

surprise, cytokine secretion was seemingly normal in CD4⁺ T cells lacking both Arf1 and Arf6. It has been revealed that among Arf1-GEFs targeted by brefeldin A, GBF1, BIG1, and BIG2 are involved in the activation of Arf3 and/or Arf5 as well (50). Therefore, these other Arf isoforms might compensate for the absence of Arf1 as well as Arf6 in the activated CD4⁺ T cells. Actually, previous studies have demonstrated that Arf isoforms share some redundant functions: small interfering RNA-mediated single knockdown of Arf1, Arf3, Arf4, or Arf5 fails to cause any observable phenotype, whereas double knockdowns of any type of combination of them using pairwise small interfering RNA impair the particular steps in the vesicle trafficking pathway (51).

Upon TCR stimulation, Arf-deficient CD4⁺ T cells exhibited higher level of Bim, a predominant BH3-only protein functioning in the activated T cells, whereas expression of an antiapoptotic Bcl-2 family protein Mcl-1 was slightly impaired. Although we found that expression level of Bcl-xL, another Bcl-2 family member exerting antiapoptotic function, was substantially increased in Arf-deficient T cells as well, recent studies have revealed that Bcl-xL is dispensable for survival of peripheral

T cells as well as development of effector T cells (52, 53), suggesting that enhanced apoptosis in Arf-deficient T cells during activation is presumably due to the perturbed expression of Bim and/or Mcl-1. It is well established that Bim expression is negatively regulated by the PI3K/Akt and the Ras/Erk pathways. The former suppresses Bim expression at a transcriptional level through inhibition of Foxo transcription factor (54), whereas the latter induces proteasomal degradation of especially BimEL via Erk-mediated phosphorylation at Ser⁶⁵ (48). However, considering that the PI3K/Akt pathway plays an essential role in Th17 differentiation, the fact that Arf deficiency had no impact on Th17 differentiation strongly suggests that the PI3K/Akt pathway is intact in CD4⁺ T cells lacking Arf1 and Arf6. Consistently, phosphorylation status of S6 protein mediated by mTORC1 signal, which is a well-known target of the PI3K/Akt pathway, seemed normal in Arf-deficient T cells. We also found that the lack of Arfs unaffected surface expression levels of CD62L and CD69 (data not shown), which are controlled downstream of the Ras/Erk pathway, excluding the possibility that Arf deficiency impairs activation of the Ras/Erk pathway either. So, what is the molecular mechanism linking Arf deficiency and enhanced apoptosis in the activated T cells? Our data suggest that ROS are involved, at least partly, in the apoptosis of Arf1/6-KO CD4⁺ T cells. Actually, it has been reported that the accumulation of ROS enhances the expression of Bim in T cells (55). Considering that ROS levels were decreased in Arf-deficient CD4⁺ T cells, however, we rather speculate that the lack of Arf1 and Arf6 renders T cells more sensitive to apoptosis-triggering cues including ROS. One intriguing possibility is autophagy. Several studies have demonstrated that both Arf1 and Arf6 play a critical role in autophagy through the formation of autophagosomes (56, 57). Because autophagy negatively regulates Bim expression as well (58), it stands to reason that the defect in autophagy process in Arf-deficient CD4⁺ T cells causes accumulation of Bim protein. Alternatively, as has recently been reported, Arf deficiency may induce ER stress response, rendering the activated T cells susceptible to cell death (59). Given that Arf1/6-KO effector CD4⁺ T cells were resistant to apoptosis upon TCR stimulation, the difference between naive and effector T cells, like metabolic states, would provide a clue for mechanism in augmented apoptosis in Arf-deficient naive T cells. One must await detailed analysis to reveal the molecular linkage between Arf deficiency and enhanced apoptosis in activated T cells.

Despite the fact that inflammatory responses including colitis and EAE were nearly completely abrogated, Ab responses especially under Th2-polarizing conditions seemed intact in Arf1/6-KO mice (Fig. 2A). Essentially the same results were obtained during *Leishmania major* infection, which is prevented by Th1 immune response: Ab against *L. major* was produced to a level comparable to control mice, whereas Arf1/6-KO mice failed to completely eliminate the parasite presumably because of the inefficient activation of Th1 cells (data not shown, and the details will be described elsewhere). We speculate this puzzling phenotype reflects the difference in environmental cues. We found that, among the γ cytokine family, IL-21 and IL-4 efficiently suppressed apoptosis in activated Arf1/6-KO T cells (Fig. 4D). GCs found in secondary lymphoid tissues are important sites for Ab production. In GCs, Tfh cells support B cell differentiation into Ab-secreting plasma cell by producing a substantial amount of IL-21. Arf-deficient T cells could survive in GCs, where plenty amount of IL-21 exists compared with the nonlymphoid tissues like the colon. Actually, in the mixed bone marrow chimeric mice, we found that Arf-deficient T cells were maintained to a level comparable to control T cells in the MLN, although proportions of Arf-deficient

T cells were markedly decreased in the colonic LP (Supplemental Fig. 2A).

It is estimated that nearly 2.5 million people live with multiple sclerosis (MS) in the world, and 6.8 million patients are suffering from IBD primarily comprising of Crohn disease and ulcerative colitis globally in 2017 (60). Although most immune therapies for these patients are associated with immunosuppressive drugs, which typically target the adaptive immune system, these treatments may increase the risk of serious side effects like reduced Ab responses against bacteria and viruses. In marked contrast, loss of Arf function in T cells nearly completely suppressed the onset of naive CD4⁺ T cell-induced colitis as well as EAE without affecting OVA-specific Ab production, at least under Th2-polarizing conditions, demonstrating that the Arf pathway would be a good drug target for autoimmune disease like MS and/or IBD. Given that the ubiquitous role of the Arf pathways in vesicle trafficking, one can argue that the blockade of the Arf pathway would cause detrimental effects. To our surprise, however, the mice at 2 mo old were viable for 4 wk after Arf1 and Arf6 were systemically deleted by using the CreERT2 system (data not shown; the details will be described elsewhere), raising the possibility that the lack of Arf1 and Arf6 may have little or no fatal effect, at least within a short period of time. Interestingly, genome-wide association studies (<https://www.ebi.ac.uk/gwas/>) have linked common genetic variants at the locus of ASAP1, one of the ArfGAPs, to MS. In addition, another ArfGAP ASAP2 and an ArfGEF cytohesin 1 are suggested to associate with Crohn disease and ulcerative colitis, respectively. It should be noted that all of these molecules are known to regulate both Arf1 and Arf6 (2). Future studies will clarify the impact of therapeutic approach targeting upstream regulators of the Arf pathway on autoimmune diseases.

Acknowledgments

We thank Hans Joerg Fehling for *Rosa26*-tdRFP mice. We also thank Yoichi Maekawa, Yoshihiro Ueda, and Katsuhiko Yoshizawa for technical advice and Chikako Eguchi for technical assistance.

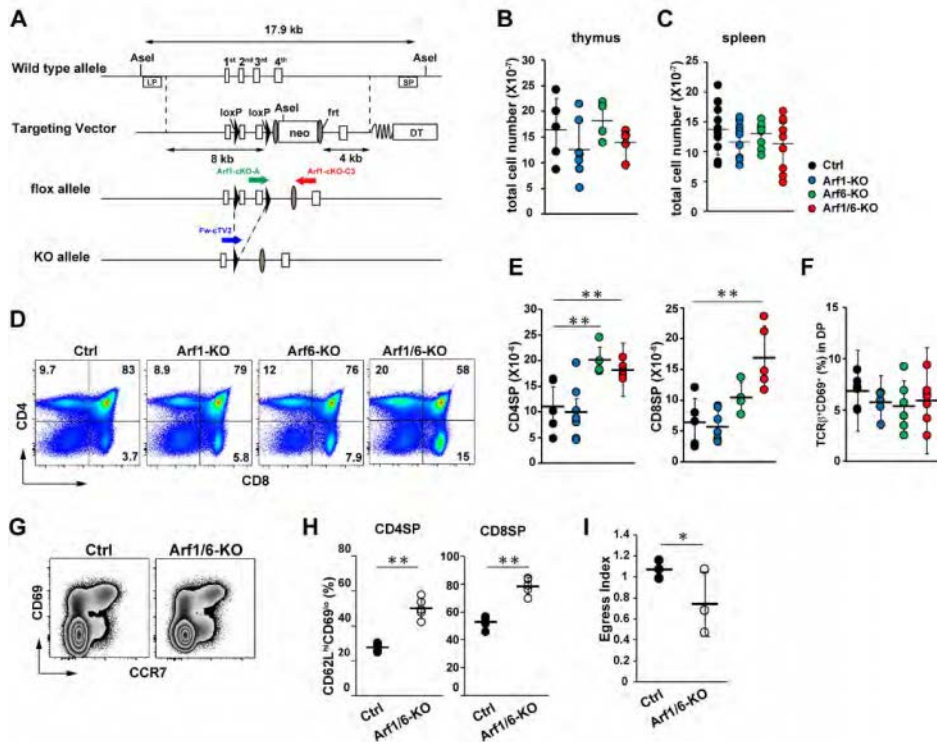
Disclosures

The authors have no financial conflicts of interest.

References

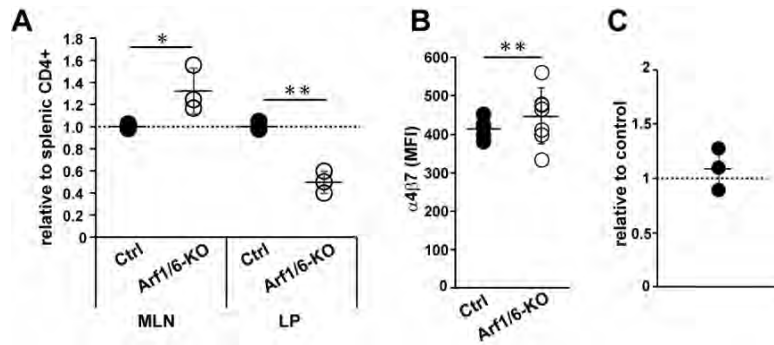
1. D'Souza-Schorey, C., and P. Chavrier. 2006. ARF proteins: roles in membrane traffic and beyond. *Nat. Rev. Mol. Cell Biol.* 7: 347–358.
2. Donaldson, J. G., and C. L. Jackson. 2011. ARF family G proteins and their regulators: roles in membrane transport, development and disease. [Published erratum appears in 2011 *Nat. Rev. Mol. Cell Biol.* 12: 533.] *Nat. Rev. Mol. Cell Biol.* 12: 362–375.
3. Gillingham, A. K., and S. Munro. 2007. The small G proteins of the Arf family and their regulators. *Annu. Rev. Cell Dev. Biol.* 23: 579–611.
4. Taylor, T. C., R. A. Kahn, and P. Melançon. 1992. Two distinct members of the ADP-ribosylation factor family of GTP-binding proteins regulate cell-free intra-Golgi transport. *Cell* 70: 69–79.
5. D'Souza-Schorey, C., G. Li, M. I. Colombo, and P. D. Stahl. 1995. A regulatory role for ARF6 in receptor-mediated endocytosis. *Science* 267: 1175–1178.
6. Radhakrishna, H., and J. G. Donaldson. 1997. ADP-ribosylation factor 6 regulates a novel plasma membrane recycling pathway. *J. Cell Biol.* 139: 49–61.
7. Honda, A., M. Nogami, T. Yokozeki, M. Yamazaki, H. Nakamura, H. Watanabe, K. Kawamoto, K. Nakayama, A. J. Morris, M. A. Frohman, and Y. Kanaho. 1999. Phosphatidylinositol 4-phosphate 5-kinase α is a downstream effector of the small G protein ARF6 in membrane ruffle formation. *Cell* 99: 521–532.
8. Geiger, C., W. Nagel, T. Boehm, Y. van Kooyk, C. G. Figdor, E. Kremmer, N. Hogg, L. Zeitlmann, H. Dierks, K. S. C. Weber, and W. Kolanus. 2000. Cytohesin-1 regulates β -2 integrin-mediated adhesion through both ARF-GEF function and interaction with LFA-1. *EMBO J.* 19: 2525–2536.
9. Powelka, A. M., J. Sun, J. Li, M. Gao, L. M. Shaw, A. Sonnenberg, and V. W. Hsu. 2004. Stimulation-dependent recycling of integrin β 1 regulated by ARF6 and Rab11. *Traffic* 5: 20–36.
10. Krdnja, D., C. Münzberg, U. Maass, M. Hafner, G. Adler, H. A. Kestler, T. Seufferlein, F. Oswald, and G. von Wichert. 2012. The phosphatase of regenerating liver 3 (PRL-3) promotes cell migration through Arf-activity-dependent stimulation of integrin α 5 recycling. *J. Cell Sci.* 125: 3883–3892.

11. Li, L., E. Kim, H. Yuan, K. Inoki, P. Goraksha-Hicks, R. L. Schiesher, T. P. Neufeld, and K. L. Guan. 2010. Regulation of mTORC1 by the Rab and Arf GTPases. *J. Biol. Chem.* 285: 19705–19709.
12. Knizhnik, A. V., O. V. Kovaleva, A. V. Komelkov, L. S. Trukhanova, V. A. Rybko, I. B. Zborovskaya, and E. M. Tchevkin. 2012. Arf6 promotes cell proliferation via the PLD-mTORC1 and p38MAPK pathways. *J. Cell. Biochem.* 113: 360–371.
13. Bernfeld, E., D. Menon, V. Vaghela, I. Zerlin, P. Faruque, M. A. Frias, and D. A. Foster. 2018. Phospholipase D-dependent mTOR complex 1 (mTORC1) activation by glutamine. *J. Biol. Chem.* 293: 16390–16401.
14. Akiyama, M., H. Hasegawa, T. Hongu, M. A. Frohman, A. Harada, H. Sakagami, and Y. Kanaho. 2014. Trans-regulation of oligodendrocyte myelination by neurons through small GTPase Arf6-regulated secretion of fibroblast growth factor-2. *Nat. Commun.* 5: 4744.
15. Miyamoto, Y., T. Torii, K. Tago, A. Tanoue, S. Takashima, and J. Yamauchi. 2018. BIG1/Arfge1 and Arf1 regulate the initiation of myelination by Schwann cells in mice. *Sci. Adv.* 4: eaar4471.
16. Sumiyoshi, M., N. Masuda, N. Tanuma, H. Ogoh, E. Imai, M. Otsuka, N. Hayakawa, K. Ohno, Y. Matsui, K. Hara, et al. 2015. Mice doubly-deficient in the Arf GAPs SMAP1 and SMAP2 exhibit embryonic lethality. *FEBS Lett.* 589(19 Pt B): 2754–2762.
17. Lou, J., J. Rossy, Q. Deng, S. V. Pagonis, and K. Gaus. 2016. New insights into how trafficking regulates T cell receptor signaling. *Front. Cell Dev. Biol.* 4: 77.
18. Bouchet, J., I. Del Río-Iñiguez, E. Vázquez-Chávez, R. Lasserre, S. Agüera-González, C. Cucho, M. W. McCaffrey, V. Di Bartolo, and A. Alcover. 2017. Rab11-FIP3 regulation of Lck endosomal traffic controls TCR signal transduction. *J. Immunol.* 198: 2967–2978.
19. Stinchcombe, J. C., D. C. Barral, E. H. Mules, S. Booth, A. N. Hume, L. M. Machesky, M. C. Seabra, and G. M. Griffiths. 2001. Rab27a is required for regulated secretion in cytotoxic T lymphocytes. *J. Cell Biol.* 152: 825–834.
20. Ménasché, G., E. Pastural, J. Feldmann, S. Certain, F. Ersoy, S. Dupuis, N. Wulfraat, D. Bianchi, A. Fischer, F. Le Deist, and G. de Saint Basile. 2000. Mutations in RAB27A cause Griscelli syndrome associated with haemophagocytic syndrome. *Nat. Genet.* 25: 173–176.
21. Srikanth, S., K. D. Kim, Y. Gao, J. S. Woo, S. Ghosh, G. Calmettes, A. Paz, J. Abramson, M. Jiang, and Y. Gwack. 2016. A large Rab GTPase encoded by CRACR2A is a component of subsynaptic vesicles that transmit T cell activation signals. *Sci. Signal.* 9: ra31.
22. Donaldson, J. G., D. Finazzi, and R. D. Klausner. 1992. Brefeldin A inhibits Golgi membrane-catalysed exchange of guanine nucleotide onto ARF protein. *Nature* 360: 350–352.
23. Nylander, S., and I. Kalies. 1999. Brefeldin A, but not monensin, completely blocks CD69 expression on mouse lymphocytes: efficacy of inhibitors of protein secretion in protocols for intracellular cytokine staining by flow cytometry. *J. Immunol. Methods* 224: 69–76.
24. Takahama, Y., K. Ohishi, Y. Tokoro, T. Sugawara, Y. Yoshimura, M. Okabe, T. Kinoshita, and J. Takeda. 1998. Functional competence of T cells in the absence of glycosylphosphatidylinositol-anchored proteins caused by T cell-specific disruption of the Pig-a gene. *Eur. J. Immunol.* 28: 2159–2166.
25. Luche, H., O. Weber, T. Nageswara Rao, C. Blum, and H. J. Fehling. 2007. Faithful activation of an extra-bright red fluorescent protein in “knock-in” Cre-reporter mice ideally suited for lineage tracing studies. *Eur. J. Immunol.* 37: 43–53.
26. Kanamori, M., H. Nakatsukasa, M. Ito, S. Chikuma, and A. Yoshimura. 2018. Reprogramming of Th1 cells into regulatory T cells through rewiring of the metabolic status. *Int. Immunol.* 30: 357–373.
27. Stromnes, I. M., and J. M. Goverman. 2006. Active induction of experimental allergic encephalomyelitis. *Nat. Protoc.* 1: 1810–1819.
28. Suzuki, T., Y. Kanai, T. Hara, J. Sasaki, T. Sasaki, M. Kohara, T. Maehama, C. Taya, H. Shitara, H. Yonekawa, et al. 2006. Crucial role of the small GTPase ARF6 in hepatic cord formation during liver development. *Mol. Cell. Biol.* 26: 6149–6156.
29. Hayakawa, N., H. Ogoh, M. Sumiyoshi, Y. Matsui, S. Nishikawa, K. Miyamoto, Y. Maeda, H. Kiyonari, M. Suzuki, and T. Watanabe. 2014. The ADP-ribosylation factor 1 gene is indispensable for mouse embryonic development after implantation. *Biochem. Biophys. Res. Commun.* 453: 748–753.
30. Weinreich, M. A., and K. A. Hogquist. 2008. Thymic emigration: when and how T cells leave home. *J. Immunol.* 181: 2265–2270.
31. Brewer, J. M. 2006. (How) do aluminium adjuvants work? *Immunol. Lett.* 102: 10–15.
32. Sastry, M., B. Zhang, M. Chen, M. G. Joyce, W. P. Kong, G. Y. Chuang, K. Ko, A. Kumar, C. Silacci, M. Thom, et al. 2017. Adjuvants and the vaccine response to the DS-Cav1-stabilized fusion glycoprotein of respiratory syncytial virus. *PLoS One* 12: e0186854.
33. Jewell, J. L., Y. C. Kim, R. C. Russell, F. X. Yu, H. W. Park, S. W. Plouffe, V. S. Tagliabracci, and K. L. Guan. 2015. Metabolism. Differential regulation of mTORC1 by leucine and glutamine. *Science* 347: 194–198.
34. Delgoffe, G. M., K. N. Pollizzi, A. T. Waickman, E. Heikamp, D. J. Meyers, M. R. Horton, B. Xiao, P. F. Worley, and J. D. Powell. 2011. The kinase mTOR regulates the differentiation of helper T cells through the selective activation of signaling by mTORC1 and mTORC2. *Nat. Immunol.* 12: 295–303.
35. Kurebayashi, Y., S. Nagai, A. Ikejiri, M. Ohtani, K. Ichiyama, Y. Baba, T. Yamada, S. Egami, T. Hoshii, A. Hirao, et al. 2012. PI3K-Akt-mTORC1-S6K1/2 axis controls Th17 differentiation by regulating Gfi1 expression and nuclear translocation of ROR γ . *Cell Rep.* 1: 360–373.
36. Kawabe, T., S. L. Sun, T. Fujita, S. Yamaki, A. Asao, T. Takahashi, T. So, and N. Ishii. 2013. Homeostatic proliferation of naive CD4⁺ T cells in mesenteric lymph nodes generates gut-tropic Th17 cells. *J. Immunol.* 190: 5788–5798.
37. Iwata, M., A. Hirakiyama, Y. Eshima, H. Kagechika, C. Kato, and S. Y. Song. 2004. Retinoic acid imprints gut-homing specificity on T cells. *Immunity* 21: 527–538.
38. Kurmaeva, E., J. D. Lord, S. Zhang, J. R. Bao, C. G. Kevil, M. B. Grisham, and D. V. Ostanin. 2014. T cell-associated α 4 β 7 but not α 4 β 1 integrin is required for the induction and perpetuation of chronic colitis. *Mucosal Immunol.* 7: 1354–1365.
39. Britschgi, M. R., A. Link, T. K. A. Lissandrini, and S. A. Luther. 2008. Dynamic modulation of CCR7 expression and function on naive T lymphocytes *in vivo*. *J. Immunol.* 181: 7681–7688.
40. Abram, C. L., and C. A. Lowell. 2009. The ins and outs of leukocyte integrin signaling. *Annu. Rev. Immunol.* 27: 339–362.
41. Verma, N. K., and D. Kelleher. 2017. Not Just an Adhesion Molecule: LFA-1 contact tunes the T lymphocyte program. *J. Immunol.* 199: 1213–1221.
42. Leonard, W. J., J. X. Lin, and J. J. O’Shea. 2019. The γ c family of cytokines: basic biology to therapeutic ramifications. *Immunity* 50: 832–850.
43. Boise, L. H., A. J. Minn, P. J. Noel, C. H. June, M. A. Accavitti, T. Lindsten, and C. B. Thompson. 1995. CD28 costimulation can promote T cell survival by enhancing the expression of Bcl-XL. *Immunity* 3: 87–98.
44. Hildeman, D. A., Y. Zhu, T. C. Mitchell, P. Bouillet, A. Strasser, J. Kappler, and P. Marrack. 2002. Activated T cell death *in vivo* mediated by proapoptotic bcl-2 family member bim. *Immunity* 16: 759–767.
45. Wensveen, F. M., K. P. J. M. van Gisbergen, I. A. M. Derks, C. Gerlach, T. N. Schumacher, R. A. W. van Lier, and E. Eldering. 2010. Apoptosis threshold set by Noxa and Mcl-1 after T cell activation regulates competitive selection of high-affinity clones. *Immunity* 32: 754–765.
46. Zhan, Y., E. M. Carrington, Y. Zhang, S. Heintel, and A. M. Lew. 2017. Life and death of activated T cells: how are they different from naive T cells? *Front. Immunol.* 8: 1809.
47. Hedrick, S. M., I. L. Ch’en, and B. N. Alves. 2010. Intertwined pathways of programmed cell death in immunity. *Immunol. Rev.* 236: 41–53.
48. Clybourn, C., D. Merino, T. Nebl, F. Masson, M. Robati, L. O’Reilly, A. Hübner, R. J. Davis, A. Strasser, and P. Bouillet. 2012. Alternative splicing of Bim and Erk-mediated Bim(EL) phosphorylation are dispensable for hematopoietic homeostasis *in vivo*. *Cell Death Differ.* 19: 1060–1068.
49. Hildeman, D. A., T. Mitchell, T. K. Teague, P. Henson, B. J. Day, J. Kappler, and P. C. Marrack. 1999. Reactive oxygen species regulate activation-induced T cell apoptosis. *Immunity* 10: 735–744.
50. Casanova, J. E. 2007. Regulation of Arf activation: the Sec7 family of guanine nucleotide exchange factors. *Traffic* 8: 1476–1485.
51. Volpicelli-Daley, L. A., Y. Li, C.-J. Zhang, and R. A. Kahn. 2005. Isoform-selective effects of the depletion of ADP-ribosylation factors 1-5 on membrane traffic. *Mol. Biol. Cell* 16: 4495–4508.
52. Zhang, N., and Y.-W. He. 2005. The antiapoptotic protein Bcl-xL is dispensable for the development of effector and memory T lymphocytes. *J. Immunol.* 174: 6967–6973.
53. Tripathi, P., B. Koss, J. T. Opferman, and D. A. Hildeman. 2013. Mcl-1 antagonizes Bax/Bak to promote effector CD4⁺ and CD8⁺ T-cell responses. *Cell Death Differ.* 20: 998–1007.
54. Zhu, S., S. Evans, B. Yan, T. J. Povsic, V. Tapson, P. J. Goldschmidt-Clermont, and C. Dong. 2008. Transcriptional regulation of Bim by FOXO3a and Akt mediates scleroderma serum-induced apoptosis in endothelial progenitor cells. *Circulation* 118: 2156–2165.
55. Sade, H., and A. Sarin. 2004. Reactive oxygen species regulate quiescent T-cell apoptosis via the BH3-only proapoptotic protein BIM. *Cell Death Differ.* 11: 416–423.
56. van der Vaart, A., J. Griffith, and F. Reggiori. 2010. Exit from the Golgi is required for the expansion of the autophagosomal phagophore in yeast *Saccharomyces cerevisiae*. *Mol. Biol. Cell* 21: 2270–2284.
57. Moreau, K., B. Ravikumar, C. Puri, and D. C. Rubinsztein. 2012. Arf6 promotes autophagosome formation via effects on phosphatidylinositol 4,5-bisphosphate and phospholipase D. *J. Cell Biol.* 196: 483–496.
58. Kovacs, J. R., C. Li, Q. Yang, G. Li, I. G. Garcia, S. Ju, D. G. Roodman, J. J. Windle, X. Zhang, and B. Lu. 2012. Autophagy promotes T-cell survival through degradation of proteins of the cell death machinery. *Cell Death Differ.* 19: 144–152.
59. Wang, G., J. Xu, J. Zhao, W. Yin, D. Liu, W. Chen, and S. X. Hou. 2020. Arf1-mediated lipid metabolism sustains cancer cells and its ablation induces anti-tumor immune responses in mice. *Nat. Commun.* 11: 220.
60. GBD 2017 Inflammatory Bowel Disease Collaborators. 2020. The global, regional, and national burden of inflammatory bowel disease in 195 countries and territories, 1990–2017: a systematic analysis for the Global Burden of Disease Study 2017. *Lancet Gastroenterol. Hepatol.* 5: 17–30.



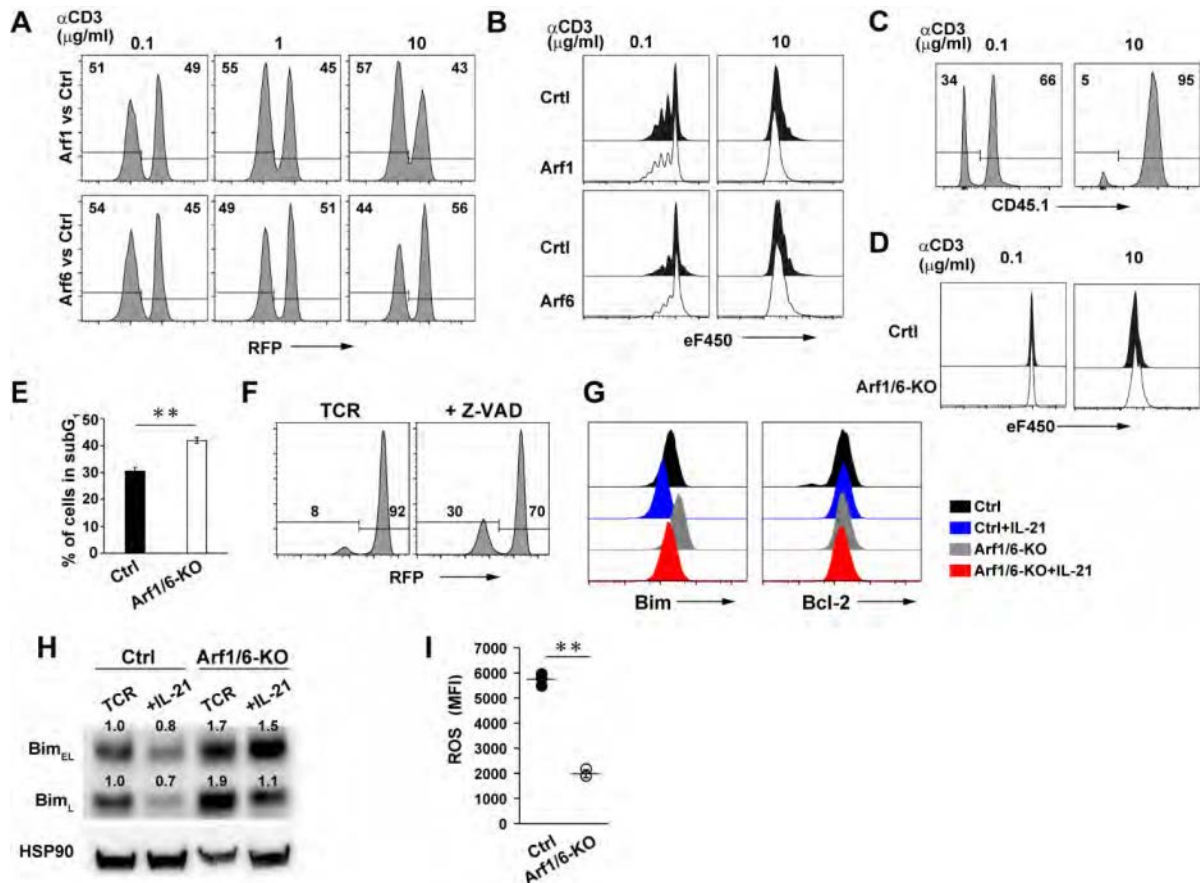
Supplemental Figure 1. Characterization of T-lineage specific Arf-deficient mice.

(A) *Arf1* conditional deficient mice were generated as described previously (<http://www2.clst.riken.jp/arg/methods.html>). Schematic representation of wild-type genomic locus of *Arf1* with 4 exons (boxes with 1st, 2nd, 3rd, 4th), introns (lines) and restriction enzyme sites of *AseI* are shown. LP and SP probes for Southern blot analysis of *AseI* digested genomic DNA are also shown (boxes with LP, SP). Targeting vector containing 2 loxP sites (black arrowheads) and 2 *frt* sites (shaded ellipses), a PGK-Neo-polyA cassette (box with neo) for positive selection, and a MC1-DT-A-polyA cassette (box with DT) for negative selection is represented. *AseI* site in the PGK-Neo-polyA cassette is also shown. The conditional allele after deleting the PGK-Neo-polyA cassette by using FLP deleter strain B6-Tg(CAG-FLPe)36, provided by RIKEN (RBRC01834), is shown as flox allele. The targeted allele following Cre recombination is shown as KO allele. Genotyping of offspring was performed by PCR with the following primers: Arf1-cKO-A (green), 5'-GCTTGATCTTCGTAGTGGACAGCAATGAC-3'; Arf1 cKO-C3 (red), 5'-TGAGGAAAAGGAAGAATTAGTGGCAGGGAC-3'; Fw-cTV2 (blue), 5'-CGTCTAAGAAACCATTATTATCATGAC-3'. Primer pair of Arf1-cKO-A and Arf1 cKO-C3 yields products of wild-type (249 bp) and floxed (377 bp) alleles, whereas primer pair of Fw-cTV2 and Arf1 cKO-C3 yields products of floxed (729 bp) and deleted (190 bp) alleles. (B) Number of total cells in the thymus from 5-7 weeks old control (n=5, black), Arf1-KO (n=7, blue), Arf6-KO (n=4, green), and Arf1/6-KO (n=5, red) mice. Each symbol represents an individual mouse (mean ± S.D.). (C) Number of total cells in the spleen from the indicated mice as in Fig. 1B. (D) FACS analysis for CD8 and CD4 in the thymocytes from the indicated mice. Data are representative of four independent experiments. (E) CD4SP (left) and CD8SP (right) thymocyte numbers in the indicated mice as in (B). Mean ± S.D. **p< 0.01. (F) Proportions of TCRβ⁺CD69⁺ cells in DP cells in the indicated mice as in (B) (mean ± S.D.). (G) Shown are CD69 and CCR7 expression in thymocytes of the indicated mice. Data are representative of three independent experiments. (H) Proportions of the most mature cells (CD62L^{hi}CD69^{lo}) in CD4SP and CD8SP in 5-7 weeks old control (n=5) and Arf1/6-KO (n=5) mice. Each symbol represents an individual mouse. Mean ± S.D. **p< 0.01. (I) Control (CD45.1⁺) and Arf1/6-KO (CD45.1⁻) bone marrow cells were mixed at an equal ratio and transferred into sub-lethally irradiated recipient (RFP⁺) mice (n=3). Two months after transfer, "Egress Index" was evaluated as the proportion of splenic CD4⁺ T cells relative to the proportion of thymic CD4SP cells. Mean ± S.D. *p< 0.05, Mann-Whitney U test.



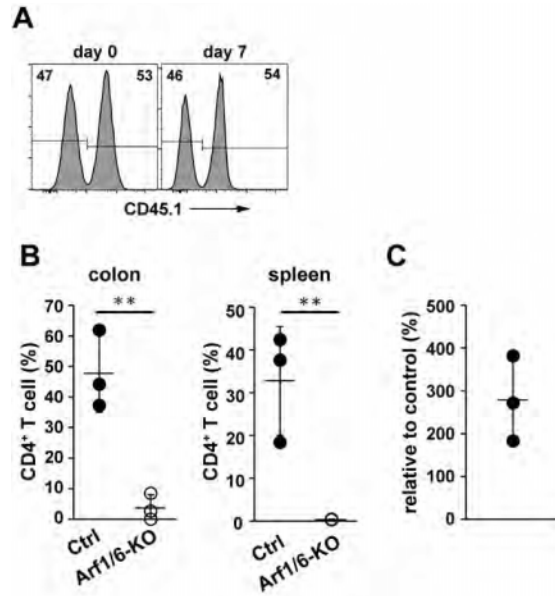
Supplemental Figure 2. Arf-deficient CD4⁺ T cells in the colonic LP are significantly decreased, but normally migrate into the colon.

(A) Control (CD45.1⁺) and Arf1/6-KO (CD45.1⁻) bone marrow cells were mixed at an equal ratio and transferred into sub-lethally irradiated recipient (RFP⁺) mice as in Supplemental Figure 1I. Two months after transfer, the ratios of MLN or colonic LP CD4⁺ T cells to splenic CD4⁺ T cells gated in RFP-CD45.1⁺ (control) or RFP-CD45.1⁻ (Arf1/6-KO) were evaluated by FACS analysis. Indicated are the values normalized to control. (B) Expression levels of α4β7 in the colonic LP CD4⁺ T cells from control (Ctrl, n=5) and Arf1/6-KO (n=7) mice. Each symbol represents an individual mouse. Mean ± S.D. **p < 0.01. (C) Mixture of CD4⁺ T cells from control (CD45.1⁺) and Arf1/6-KO mice (CD45.1⁻) at an equal ratio were transferred into *Rag2*^{-/-} mice (n=3). After 24 hours, the ratios of colonic LP CD4⁺ T cells between control and Arf-deficient cells were evaluated by FACS analysis.



Supplemental Figure 3. Survival and proliferation of Arf1- or Arf6-single deficient CD4⁺ T cells.

(A and B) Control (RFP⁺) CD4⁺ T cells were mixed with either Arf1-KO (RFP⁻) or Arf6-KO (RFP⁻) CD4⁺ T cells and labeled with eF450, followed by stimulation with 0.1-10 μ g/ml plate-bound anti-CD3 ϵ mAb along with 1 μ g/ml soluble anti-CD28 mAb for 4 days. Shown are representative FACS plots indicating proportions of control (Ctrl) and either Arf1-KO (*upper*) or Arf6-KO cells (*lower*) (A), or eF450 dilution plots of control (Ctrl) vs Arf1-KO (*upper*) and control (Ctrl) vs Arf6-KO (*lower*) (B). Data are representative of at least two independent experiments. (C and D) Control (CD45.1⁺) CD8⁺ T cells were mixed with Arf1/6-KO (CD45.1⁻) CD8⁺ T cells and labeled with eF450, followed by stimulation with 0.1 or 10 μ g/ml plate-bound anti-CD3 ϵ mAb along with 1 μ g/ml soluble anti-CD28 mAb for 3 days. Shown are representative FACS plots indicating proportions of control and Arf1/6-KO (C), or eF450 dilution plots of control (Ctrl) vs Arf1/6-KO (D). Data are representative of at least three independent experiments. (E) CD4⁺ T cells from the indicated mice (n=3, each) were activated with anti-CD3 ϵ mAb for 4 days, and proportions of subG1 cells were evaluated by FACS. Mean \pm S.D. **p < 0.01. (F) Mixture of CD4⁺ T cells from control (RFP⁺) and Arf1/6-TKO mice (RFP⁻) was stimulated with anti-CD3 ϵ /anti-CD28 mAbs (TCR) along with or without 50 μ M Z-VAD-FMK (+Z-VAD) for 4 days, followed by FACS analysis. Shown are representative of three. (G and H) Naïve CD4⁺ T cells from the indicated mice were stimulated with anti-CD3 ϵ /anti-CD28 mAbs along with or without IL-21, and analyzed at 48 h by FACS against Bcl-2 (G) or at 96 h by immunoblot against Bim and HSP90 as a loading control (H). The values indicated are relative density of the band normalized to HSP90. Data are representative of two independent experiments. (I) CD4⁺ T cells from the indicated mice (n=3, each) were activated with anti-CD3 ϵ /anti-CD28 mAbs for 3 days, followed by evaluation of ROS levels by FACS. Mean \pm S.D. **p < 0.01.



Supplemental Figure 4. Survival and differentiation of Arf-deficient CD4⁺ T cells *in vivo*.

(A) *In vitro*-differentiated control (CD45.1⁺) and Arf1/6-KO (CD45.1⁻) pathogenic Th17 cells were mixed at an equal ratio (day 0), and transferred into colitis-induced recipient mice. The ratios of control to Arf1/6-KO cells in the colonic LP of recipient mice were evaluated by FACS on day 7. Shown are representative of four independent experiments. (B) FACS analysis for CD4⁺ T cells found in the colon or spleen of recipient *Rag2*^{-/-} mice (n=3) three weeks after transfer with the indicated naïve CD4⁺ T cells. Mean ± S.D. **p< 0.01. (C) Proportions of IL-17A producing cells in the splenic CD4⁺ T cells of recipient *Rag2*^{-/-} mice (n=3) as in (B) were evaluated by FACS. Shown are proportions of IL-17A⁺ cells in *Rag2*^{-/-} mice transferred with Arf1/6-deficient naïve CD4⁺ T cells normalized to those found in *Rag2*^{-/-} mice with control. Mean ± S.D.

Appendiceal adenocarcinoma diagnosed by fine needle aspiration cytology

Dear Editor,

Appendiceal mucocele is a relatively rare macroscopic lesion that may be either benign or malignant,¹⁻³ often progressing to peritoneal pseudomyxoma. Preoperative diagnosis of primary appendiceal carcinoma is often difficult, and correct diagnoses are rarely made.¹⁻³ Cases of peritoneal pseudomyxoma have been reported in which peritoneal seeding is suspected by ascites cytology, suggesting the existence of cancer.¹⁻³ The present case is rare, as the critical diagnosis of primary adenocarcinoma in the appendix was made by fine needle aspiration (FNA) cytology of an appendiceal mucocele. In this report, the cytological features of primary appendiceal adenocarcinoma are described. Although reports of FNA cytology for low-grade mucinous neoplasms of the appendix have been published,⁴ the literature contains few reports of cytology for high grade appendiceal mucinous neoplasms.

An 83-year-old woman noticed right-sided flank pain while bending forward 1 month prior to visiting our hospital. Computed tomography showed a cystic lesion with an irregular wall on the dorsal side

of the cecum continuous from the appendix in contact with the iliopsoas muscle. A pale lamellar structure was observed inside the cystic lesion, suggestive of appendiceal mucocele. On abdominal ultrasonography, the lesion directly above the dorsal side of the caecum and right above the lumbar muscle was presumed to be localised in the appendix root and, although it was difficult to visualise the entire appendix, the blind end appeared to partly adhere to the terminal ileum. A jelly-like substance was collected by FNA of the cystic lesion, and atypical epithelial cells showing nuclear enlargement, increased chromatin, a distinct nucleolus, an unevenly distributed nucleus, an irregular nuclear shape, anisonucleosis, and irregular arrangement were observed cytologically (Figure 1); glandular-type carcinoma was strongly suspected. Lower endoscopy revealed a protruding lesion at the opening of the appendix in which mucin adhered to the centre and mild ulceration was present. Appendiceal cancer could not be ruled out, so three biopsy samples were taken. However, biopsy revealed only mild to moderate chronic inflammatory cell infiltration in the interstitium possibly because of no direct invasion to the cecum

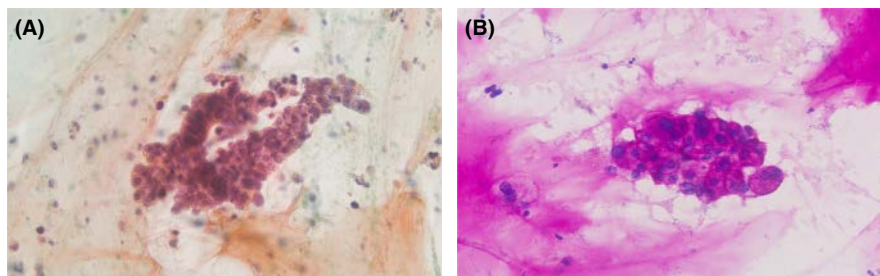


FIGURE 1 Cytological findings of aspirates from the appendiceal tumour. A cluster consisting of atypical cells with nuclear enlargement, increased chromatin, distinct nucleolus, unevenly distributed nucleus, irregular nuclear shape and anisonucleosis. Periodic acid Schiff reaction is positive suggestive of mucin production. (A: Papanicolaou stain, ×20; B: periodic acid Schiff, ×20)

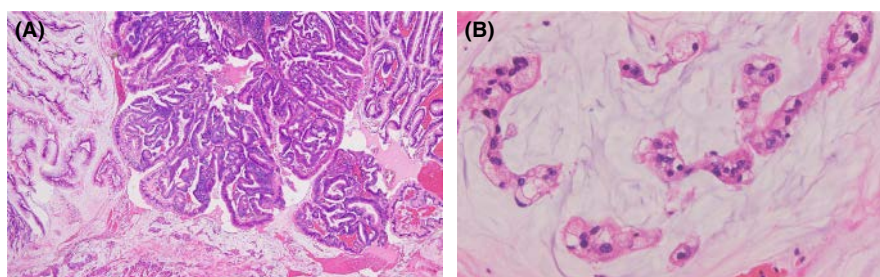


FIGURE 2 Histopathological findings of the appendiceal tumour. (A) Moderately differentiated tubular adenocarcinoma mainly in the mucosal to submucosal layers, massively forming various size of tubules. (B) In the muscular to subserosal layers, marked mucin production consistent with mucinous adenocarcinoma is seen continuously to tubular adenocarcinoma. (Haematoxylin-eosin stain, A:×4; B: ×20)

mucosa. As a result of performing surgical ileocecal resection based on a clinical diagnosis of appendiceal mucinous neoplasm, the lesion was diagnosed as mucinous adenocarcinoma (Figure 2), featuring a tumour 40 × 31 mm in size, TNM stage pT4a and ly0/ v1 vascular invasion. Neither invasion nor metastasis in lymph nodes and both ovaries was noticed at surgery, with histopathological confirmation in the right ovary and lymph nodes.

Peritoneal pseudomyxoma is a pathological condition in which gelatine-like mucin primarily derived from mucinous neoplasms originating in the ovaries and appendices accumulates in the peritoneal cavity. Histopathologically, both low- and high-grade cases have been reported.¹⁻³ Clinically, it develops as an ascites reservoir and can generally be diagnosed by collection of jelly-like contents from the peritoneal cavity or pouch of Douglas aspiration.¹⁻³ Although this condition represents intraperitoneal dissemination of tumour tissue, metastasis to distant organs is rare and the post-operative prognosis is moderately good, resulting in many patients surviving for 5 years or longer.^{1-3,5} Features of cells aspirated from appendiceal mucinous neoplasms are similar to ascites cytology, and the cells are usually small in number and scarce with atypia, so the probability of a definitive diagnosis is low.⁴ Onion skin sign is considered to be a characteristic finding of appendiceal mucocoele on ultrasonic examination⁶; however, this typical sign may not be present in high grade mucinous neoplasms, as in the present case. FNA cytology may have altered the surgical management plan in this appendiceal adenocarcinoma case. We report here a case of appendiceal adenocarcinoma that was difficult to diagnose by biopsy prior to pseudomyxoma peritonei, in which FNA cytology played a vital role in preoperative diagnosis. It is, of course, important to deliberate the risk and benefit values of FNA for either dissemination or early diagnosis.

AUTHOR CONTRIBUTIONS

A. Nishikawa wrote the manuscript. Cytological diagnosis was performed by T. Suemori, R. Aoki, S. Suzuki and A. Nishikawa; histological diagnosis was made by M. Shimoda, E. Miura and T. Yamada; and sonographic diagnosis was done by K. Uebayashi.

KEYWORDS

appendix cancer, fine needle aspiration cytology

Akiyoshi Nishikawa¹ 
Tomohiro Suemori¹

Rituko Aoki¹
Shinobu Suzuki¹
Kumiko Uebayashi²
Eisuke Miura³
Masayuki Shimoda³
Takeoto Yamada⁴

¹Division of Diagnostic Pathology, Saiseikai Utsunomiya Hospital, Utsunomiya, Japan

²Division of Ultrasonography, Saiseikai Utsunomiya Hospital, Utsunomiya, Japan

³Department of Pathology, School of Medicine, Keio University, Tokyo, Japan

⁴Division of Diagnostic Pathology, Saitama Medical University Hospital, Utsunomiya, Japan

Correspondence

Akiyoshi Nishikawa, Division of Diagnostic Pathology, Saiseikai Utsunomiya Hospital, Takebayashi-machi 911-1, Utsunomiya 321-0974, Japan.
Email: nishikaw@nihs.go.jp

ORCID

Akiyoshi Nishikawa  <https://orcid.org/0000-0003-1379-8640>

REFERENCES

1. Carr NJ, Cecil TD, Mohamed F, et al. A consensus for classification and pathologic reporting of pseudomyxoma peritonei and associated appendiceal neoplasia: the results of the Peritoneal Surface Oncology Group International (PSOGI) modified Delphi process. *Am J Surg Pathol*. 2016;40:14-26.
2. Smeenk RM, van Velthuysen ML, Verwaal VJ, Zoetmulder FA. Appendiceal neoplasms and pseudomyxoma peritonei: a population based study. *Eur J Surg Oncol*. 2008;34:196-201.
3. Morano WF, Gleeson EM, Sullivan SH, et al. Clinicopathological features and management of appendiceal mucocoeles: a systematic review. *Am Surg*. 2018;84:273-281.
4. Zuzarte JC, Liu YC, Cohen AM. Fine needle aspiration cytology of appendiceal mucinous cystadenoma: a case report. *Acta Cytol*. 1996;40:327-330.
5. Delhorme JB, Honoré C, Benhaim L, et al. Long-term survival after aggressive treatment of relapsed serosal or distant pseudomyxoma peritonei. *Eur J Surg Oncol*. 2017;43:159-167.
6. Nagata H, Kondo Y, Kawai K, et al. A giant mucinous cystadenocarcinoma of the appendix: a case report and review of the literature. *World J Surg Oncol*. 2016;14:64.



Associations of birthweight and history of childhood obesity with beta cell mass in Japanese adults

Hironobu Sasaki¹ · Yoshifumi Saisho¹ · Jun Inaishi¹ · Yuusuke Watanabe¹ · Tami Tsuchiya¹ · Masayoshi Makio¹ · Midori Sato¹ · Minoru Kitago² · Taketo Yamada^{3,4} · Hiroshi Itoh¹

Received: 4 January 2020 / Accepted: 20 February 2020
© The Author(s) 2020

Abstract

Aims/hypothesis Low birthweight is associated with a high risk of diabetes, but there are no reports discussing birthweight and pancreatic tissues in humans. The purpose of this study was to examine the correlation between birthweight and beta and alpha cell mass in humans.

Methods Sixty-four Japanese adults with and without diabetes who underwent pancreatectomy and were able to recall their weight history including birthweight were included. Pancreatic tissues were stained for insulin and glucagon, and fractional beta cell area (BCA) and alpha cell area (ACA) were quantified. Islet size and density and beta cell replication were also quantified and their associations with birthweight were evaluated.

Results In participants without diabetes, there was a weak positive correlation between birthweight and BCA ($R = 0.34, p = 0.03$). The group with a history of childhood obesity, but not the group with a history of obesity in adulthood only, showed higher BCA compared with those without a history of obesity ($1.78 \pm 0.74\%$ vs $0.99 \pm 0.53\%$, $p = 0.01$), and the correlation coefficient between birthweight and BCA increased after excluding those with a history of childhood obesity ($R = 0.51, p < 0.01$). In those with diabetes, there was no correlation between birthweight and BCA. No correlation was found between birthweight and ACA in either those with or without diabetes.

Conclusions/interpretation Birthweight and beta, but not alpha, cell mass are positively correlated in non-diabetic adults, and a history of childhood obesity may affect beta cell mass.

Keywords Alpha cell mass · Beta cell mass · Birthweight · Human pancreas · Islet size · Japanese cohort · Obesity

Electronic supplementary material The online version of this article (<https://doi.org/10.1007/s00125-020-05127-2>) contains peer-reviewed but unedited supplementary material, which is available to authorised users.

✉ Yoshifumi Saisho
ysaisho@keio.jp

¹ Department of Internal Medicine, Keio University School of Medicine, 35 Shinanomachi, Shinjuku-ku, Tokyo 160-8582, Japan

² Department of Surgery, Keio University School of Medicine, Tokyo, Japan

³ Department of Pathology, Keio University School of Medicine, Tokyo, Japan

⁴ Department of Pathology, Saitama Medical University, Saitama, Japan

Abbreviations

ACA	Alpha cell area
ACM	Alpha cell mass
BCA	Beta cell area
BCM	Beta cell mass
DM (group)	Participant group with diabetes
DOHaD	Developmental Origins of Health and Disease
NDM (group)	Participant group without diabetes
NDM-AO (group)	NDM group with history of obesity only in adulthood
NDM-CO (group)	NDM group with history of childhood obesity
NDM-LN (group)	NDM group with no history of obesity (lean)

Research in context

What is already known about this subject?

- Beta cell mass decreases not only in type 1 diabetes but also type 2 diabetes
- Beta cell regenerative capacity in response to obesity appears limited in adult humans, while there is wide inter-individual variation of beta cell mass even among non-diabetic individuals
- Infants with low birthweight are reported to be at increased risk of developing type 2 diabetes later in life, a process referred to as the Developmental Origins of Health and Disease (DOHaD) hypothesis

What is the key question?

- Is there any relationship between islet morphology and weight at birth or weight trajectory in childhood, when the capacity for beta cell replication is relatively high?

What are the new findings?

- Birthweight and fractional beta, but not alpha, cell area and mean islet size were positively correlated in Japanese non-diabetic adults
- These correlations were not observed in those with type 2 diabetes
- A history of childhood obesity may also affect beta cell area and mean islet size

How might this impact on clinical practice in the foreseeable future?

- Smaller beta cell mass in individuals born with low birthweight explains, at least in part, the relationship between low birthweight and high risk of future development of type 2 diabetes. This finding is an important basis for explaining the DOHaD hypothesis

Introduction

It has been reported that beta cell mass (BCM) decreases not only in type 1 diabetes but also type 2 diabetes [1–4]. Because the prevalence of type 2 diabetes is increasing worldwide, it is important to develop a strategy to preserve and restore BCM.

Normally, the decrease in insulin sensitivity induced by obesity is compensated for by increasing insulin secretion to maintain normal glucose tolerance [5]. However, it has been suggested that, in contrast to rodents, the increase in BCM in the presence of obesity is relatively small in humans. In the Europid population, it has been reported that BCM increases by approximately 20–50% in obese individuals without diabetes [6, 7], while we have previously reported that no significant increase in BCM occurs in obese non-diabetic Japanese adults [3, 8]. We have also shown that in non-diabetic Japanese individuals, corticosteroid administration, which induces insulin resistance, did not increase BCM [9], suggesting that beta cell regenerative capacity is very limited especially in this population. However, these studies have evaluated obesity and/or insulin resistance only in adulthood, when beta cell replication ability has decreased [6, 8, 10, 11]. In view of the wide inter-individual variation of BCM even in the non-diabetic population, exploring the factors that affect BCM

will have a significant impact on prevention and treatment strategies in diabetes.

In 1991, Hales et al. showed a negative correlation between birthweight and the onset of type 2 diabetes [12]. Subsequently, the Developmental Origins of Health and Disease (DOHaD) hypothesis has been proposed: that the risk of developing adult-onset non-communicable diseases, such as type 2 diabetes, hypertension, dyslipidaemia, ischaemic heart disease and kidney disease is affected by fetal development [13, 14]. Although the underlying mechanism of the DOHaD hypothesis has not been fully elucidated, it has been recently reported that birthweight correlates with glomerular number in the kidney [15], suggesting that birthweight affects organ development, which leads to susceptibility to the future development of diseases. However, there are no reports examining the relation between birthweight and pancreatic tissues in humans.

Therefore, in this study, to elucidate the mechanism of the association between low birthweight and future risk of type 2 diabetes, we sought to address the following questions by using pancreatic tissues resected by surgery: (1) Is there any correlation between birthweight and BCM? (2) Is there any correlation between birthweight and alpha cell mass (ACM)? (3) Does a history of childhood obesity affect them?

Methods

Participants This study was approved by the Ethics Committee of Keio University School of Medicine. From May 2012 to March 2019, 401 patients underwent pancreatectomy at Keio University Hospital. Of those, we included 64 Japanese patients with and without diabetes who could recall their weight history including birthweight (43 men and 21 women) in this study. The inclusion criteria were: (1) ability to recall their weight history in childhood and birthweight to at least 100 g; (2) gave written informed consent; and (3) the pancreatic tissue contained adequate amounts of normal pancreas for histological analysis. The exclusion criteria were: (1) type 1 diabetes; or (2) a functional neuroendocrine tumour such as insulinoma or glucagonoma. All of the patients with diabetes had been diagnosed with type 2 diabetes before the diagnosis of pancreatic disease (mean duration of diabetes 8.8 ± 5.9 years, Table 1). Some of the participants included in this study ($n = 11$) have also been included in our prior study [3].

Measurements and questionnaire We obtained information about the details of pancreatic diseases, surgical procedures, body height and weight at the time of the operation from medical records. HbA_{1c}, glycated albumin and plasma glucose levels were extracted from patients' blood test data. HbA_{1c} was measured by HPLC (HLC723G11, Tosoh, Tokyo, Japan) and expressed as National Glycohemoglobin Standardization Program value (%) and International Federation of Clinical Chemistry value (mmol/mol). Glycated albumin was measured by an enzymatic method (Lucica GA-L, Sekisui Medical, Tokyo, Japan).

The participants were asked to answer a questionnaire about their weight history and family history of diabetes. The detailed content of the questionnaire was as follows: (1) birthweight; (2) childhood and adolescent (i.e. early childhood, elementary school age, junior high school age and high school age) weight trajectories divided into five categories (i.e. very thin, thin, normal, fat, very fat); (3) body weight at the age of 20 and every decade thereafter; (4) maximum body weight in life; and (5) first- and second-degree family history of diabetes. We defined those who selected 'fat' or 'very fat' at least once in their childhood and adolescent weight trajectories as having a history of childhood obesity. All participants reached their maximum body weight after 20 years. Adulthood obesity was defined as current BMI of 25 kg/m^2 or greater [16], and patients whose maximum BMI was 25 kg/m^2 or greater were defined as having a history of adulthood obesity.

Pancreatic tissue processing Pancreatic tissue resected at operation was immediately fixed in formaldehyde and embedded in paraffin for subsequent analysis. Of every four patients who underwent total pancreatectomy, pancreatic head tissues were

sampled from two individuals and pancreatic body and tail tissues were sampled from the other two individuals, because of differences in surgical method. Then, $5 \mu\text{m}$ sections were cut from the tumour-free region and stained for light microscopy as follows: (1) with haematoxylin–eosin; (2) for insulin (peroxidase staining) with haematoxylin; (3) for glucagon with haematoxylin; and (4) for insulin and Ki67 for assessment of beta cell replication, as previously described [8, 9] (ESM Table 1). Antigen retrieval for Ki67 staining was carried out by heat treatment at 120°C in 0.01 mol/l citrate buffer pH 6.0 using an autoclave instrument for 20 min and cooled down to room temperature (RT) and moved into PBS. Quenching of endogenous peroxidase was performed in $0.3\% \text{ H}_2\text{O}_2$ in methanol, for 10 min at RT and rinsed with distilled water and then washed three times with PBS for 5 min. These slides were treated with primary antibodies for 3 h at RT and washed with PBS, then treated with peroxidase-conjugated secondary antibodies for 30 min at RT and rinsed with PBS. Color development was done using treatment with 3,3'-diaminobenzidine (DAB) or SG Peroxidase Substrate Kit SK4700 (Vector, Burlingame, CA, USA). Finally, haematoxylin or nuclear fast red counterstaining was performed.

Morphometric analysis To quantify fractional beta cell area (BCA), a single cross-sectional pancreatic section for each participant was used. The entire pancreatic section containing ~ 300 islets (total pancreas area $126 \pm 50 \text{ mm}^2$) was imaged at the original magnification of $\times 200$ ($\times 20$ objective) using a NanoZoomer-XR slide scanner and viewed with NDP.view2 software (Hamamatsu Photonics, Shizuoka, Japan), and the ratio of BCA to total pancreas area was digitally measured using Image Pro Premier software (Media Cybernetics, Silver Spring, MD, USA). Likewise, the ratio of alpha cell area (ACA) to total pancreas area was also digitally measured, and the ratio of ACA to BCA was determined in each case. All measurements were conducted by a single investigator (H. Sasaki); the inter-observer coefficient of variance was assessed between H. Sasaki and other colleagues in the laboratory and was approximately 11%; the intra-observer coefficient of variance was approximately 5%. All measurements were conducted twice, and the mean of the two measurements was used. At the time of the measurement, the investigator was blinded to birthweight, BMI and the glucose metabolism status for each specimen.

To conduct further morphometric analysis, mean islet size and islet density were quantified in randomly selected areas of the pancreas that contained at least 100 islets in each case (105 ± 5 islets, total 6741 islets, ESM Table 2) using NDP.view2 [8, 9]. Furthermore, as surrogate markers of beta cell turnover, scattered beta cells, insulin-positive duct cells and beta cell replication (i.e. by double staining with insulin and Ki67) were quantified. Since the frequency of beta cell

Table 1 Participant characteristics

Characteristic	NDM group	DM group	Total
<i>N</i> (male/female)	38 (20/18)	26 (23/3)	64 (43/21)
Age, years	61.7 ± 14.3	67.2 ± 11.2	63.9 ± 13.3
Current BMI, kg/m ²	22.3 ± 3.6	25.1 ± 3.5**	23.4 ± 3.8
Maximum BMI, kg/m ²	24.9 ± 4.0	28.5 ± 3.8**	26.3 ± 4.3
HbA _{1c} , mmol/mol	38 ± 4	51 ± 10**	43 ± 10
HbA _{1c} , %	5.7 ± 0.5	6.9 ± 1.0**	6.2 ± 0.9
Glycated albumin, % ^a	15.2 ± 2.3	18.9 ± 3.5*	17.6 ± 3.6
Plasma glucose, mmol/l ^b	6.0 ± 0.8	7.8 ± 2.3**	6.7 ± 1.8
Clinical diagnosis, <i>n</i> (%)			
Pancreatic cancer	13 (34)	14 (54)	27 (42)
IPMN	8 (21)	4 (15)	12 (19)
Non-functional neuroendocrine tumour	9 (24)	2 (8)	11 (17)
Bile duct cancer	3 (8)	2 (8)	5 (8)
Duodenal papilla cancer	1 (3)	1 (4)	2 (3)
Other ^c	4 (11)	3 (12)	7 (11)
Operative procedure, <i>n</i> (%)			
Pancreatoduodenectomy	24 (63)	16 (62)	40 (63)
Distal pancreatectomy	12 (32)	8 (31)	20 (31)
Total pancreatectomy	2 (5)	2 (8)	4 (6)
Birthweight, g	3023 ± 439	3030 ± 511	3026 ± 466
History of obesity, <i>n</i> (%)			
Up to adulthood	6 (16)	9 (35)	15 (23)
Early childhood	2 (5)	4 (15)	6 (9)
Elementary school age	4 (11)	4 (15)	8 (13)
Junior high school age	4 (11)	4 (15)	8 (13)
High school age	3 (8)	8 (31)	11 (17)
Adulthood	15 (39)	24 (92)	39 (61)
Obesity history throughout life	18 (47)	24 (92)	42 (66)
Duration of diabetes, years	–	8.8 ± 5.9	–
Family history of diabetes in second-degree relative, <i>n</i> (%)	11 (29)	13 (50)	24 (38)
Pancreas histology			
BCA, %	1.14 ± 0.58	0.75 ± 0.34**	0.98 ± 0.53
ACA, %	0.25 ± 0.17	0.22 ± 0.10	0.24 ± 0.15
ACA/BCA	0.24 ± 0.12	0.32 ± 0.14*	0.27 ± 0.14

Data are mean ± SD or *n* (%)

^a Glycated albumin data were obtained from 18 participants

^b Timing of blood sampling (i.e. fasting or postprandial) was not determined

^c Tumour-forming pancreatitis, disseminated sarcoma originating from small intestine, metastatic pancreatic tumour, solid pseudopapillary neoplasm, serous cystic neoplasm, gastrointestinal stromal tumour and gastric cancer; *n* = 1 for each

p* < 0.05, *p* < 0.01 vs NDM

IPMN, intraductal papillary mucinous neoplasm

apoptosis was very low, as observed in our prior reports [3, 8, 9], it was not evaluated in this study. Scattered beta cells were defined as a cluster of three or fewer beta cells in acinar tissue, and the density of scattered beta cells was determined as the number of scattered beta cells/pancreas area (/mm²). Insulin-

positive duct cells were also counted and expressed as the number of insulin-positive duct cells/pancreas area (/mm²). Frequency of beta cell replication was expressed as the percentage of islets. Mean beta cell diameter was measured as a surrogate of beta cell size, as previously described [8].

Statistical analysis Data are presented as mean \pm SD in the text and tables unless otherwise indicated. Mann–Whitney *U* test was used to analyse the difference between two groups, and Spearman correlation coefficient was used to assess the correlation between two variables. All analyses were performed using SPSS (version 25; SPSS, IBM, Chicago, IL, USA). A value of $p < 0.05$ was taken as statistically significant.

Results

Participant characteristics Characteristics of participants with (DM group, $n = 26$) and without diabetes (NDM group, $n = 38$) are shown in Table 1 and ESM Table 2. There was no significant difference in age between the two groups. In the DM group, HbA_{1c}, glycated albumin and plasma glucose levels, and current and maximum BMI, were significantly higher than in the NDM group. In both groups, pancreatic cancer was the most common pancreatic disease and pancreatoduodenectomy was the most frequent operative procedure. Mean birthweight was 3026 ± 466 g, and there was no significant difference between the groups. In the NDM and DM groups, 47% and 92% of patients, respectively, had a history of obesity during their life, and 16% and 35%, respectively, had a history of childhood obesity.

Effects of diabetes on islet morphology BCA was significantly smaller in the DM group compared with the NDM group ($0.75 \pm 0.34\%$ vs $1.14 \pm 0.58\%$, $p < 0.01$, Table 1, ESM Fig. 1). There was no difference in ACA between the two groups ($0.22 \pm 0.10\%$ vs $0.25 \pm 0.17\%$, $p = 0.98$). Thus, the ACA to BCA ratio in the DM group was higher than that in the NDM group (0.32 ± 0.14 vs 0.24 ± 0.12 , $p = 0.01$).

Islet density was significantly reduced in the DM group compared with the NDM group (2.69 ± 1.07 vs 3.90 ± 1.96 /mm², $p < 0.01$, ESM Fig. 1). Likewise, the DM group showed significantly smaller mean islet size than the NDM group (4505 ± 1459 vs 7052 ± 2663 μm^2 , $p < 0.01$).

Birthweight and beta and alpha cell mass In the NDM group, there was a weak positive correlation between birthweight and BCA ($R = 0.34$, $p = 0.03$, Fig. 1), but no correlation between birthweight and ACA ($R = -0.13$, $p = 0.43$). Thus, a negative correlation was observed between birthweight and ACA to BCA ratio in the NDM group ($R = -0.50$, $p < 0.01$). However, in the DM group, there was no correlation between birthweight and BCA, ACA, or ACA to BCA ratio (Fig. 1).

The NDM and DM groups were further classified according to the mean birthweight (Fig. 1, ESM Table 3). In the NDM group, those with birthweight ≥ 3000 g showed greater BCA than those with birthweight < 3000 g ($1.29 \pm 0.60\%$ vs $0.98 \pm 0.53\%$, $p = 0.04$), with no significant difference in individual beta cell size (ESM Fig. 2).

Birthweight and other islet morphology In the NDM group, birthweight and islet density were not correlated ($R = 0.13$, $p = 0.45$, Fig. 2), while there was a positive correlation between birthweight and mean islet size ($R = 0.46$, $p < 0.01$). Neither islet density nor mean islet size and birthweight were correlated in the DM group ($R = 0.13$, $p = 0.52$ and $R = 0.23$, $p = 0.25$, respectively). The NDM group with birthweight ≥ 3000 g showed greater mean islet size (8441 ± 2692 vs 5510 ± 1595 μm^2 , $p < 0.01$), but not islet density, than the NDM group with birthweight < 3000 g.

Regarding surrogate markers of beta cell turnover (ESM Fig. 2), a positive correlation was found between birthweight and density of insulin-positive duct cells in the NDM group ($R = 0.39$, $p = 0.02$, Fig. 3). The NDM group with birthweight ≥ 3000 g showed an increase in density of insulin-positive duct cells (0.11 ± 0.09 vs 0.07 ± 0.10 /mm², $p = 0.04$) and frequency of beta cell replication (0.82 ± 1.09 vs 0.22 ± 0.53 /100 islets, $p = 0.04$) compared with the NDM group with birthweight < 3000 g.

Effects of current and childhood obesity on islet morphology

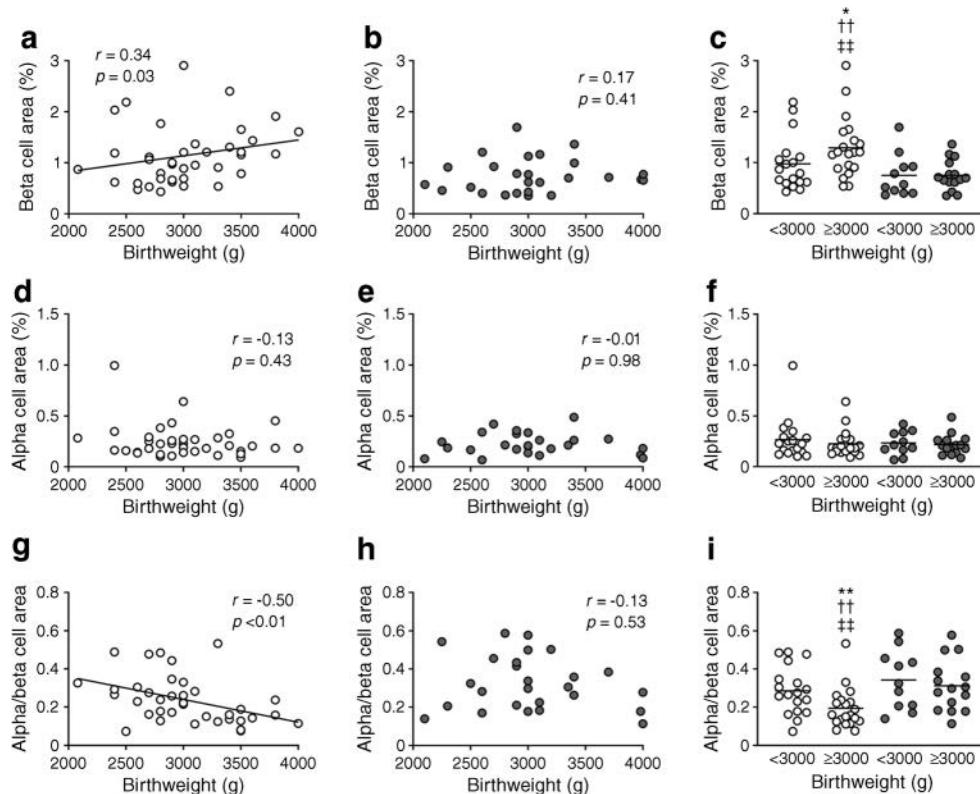
There was no correlation between current BMI and islet morphology including BCA, ACA, ACA to BCA ratio, islet density and mean islet size in either the NDM or DM group (ESM Fig. 3). Similarly, maximum BMI and islet morphology were not correlated in either group (ESM Fig. 4).

To explore the effects of childhood obesity, the NDM group was divided into three categories, i.e. participants with a history of childhood obesity (NDM-CO group, $n = 6$), those with a history of obesity only in adulthood (NDM-AO group, $n = 12$) and those with no history of obesity (lean; NDM-LN group, $n = 20$) (Fig. 4, ESM Table 4). The NDM-CO group, but not the NDM-AO group, showed greater BCA than the NDM-LN group ($1.78 \pm 0.74\%$ vs $0.99 \pm 0.53\%$, $p = 0.01$). The NDM-CO, but not NDM-AO, group also showed greater mean islet size compared with the NDM-LN group (9759 ± 1716 vs 6586 ± 2259 μm^2 , $p = 0.01$). In the NDM-CO group, no correlation was observed between birthweight and BCA ($R = -0.60$, $p = 0.21$, ESM Fig. 5), and there was no difference in BCA ($1.89 \pm 0.40\%$ vs $1.67 \pm 1.08\%$, $p = 0.51$) or mean islet size (8919 ± 585 vs $10,599 \pm 2215$ μm^2 , $p = 0.51$) between participants with and without adulthood obesity ($n = 3$, respectively). Of note, there was no difference in birthweight among the groups (ESM Table 4).

By contrast, in the DM group, when similarly classified by history of obesity, no difference in islet morphology was observed among the three groups (ESM Fig. 6, ESM Table 5), although there were only two participants in the DM-LN group.

Correlation coefficient between birthweight and BCA was increased in participants without a history of childhood obesity Finally, considering the possibility that a history of

Fig. 1 Correlation between birthweight and BCA (a–c), ACA (d–f), or ACA to BCA ratio (g–i) in participants with (DM group) and without (NDM group) diabetes. Grey and white circles show DM and NDM participants, respectively. Bars indicate mean. * $p < 0.05$, ** $p < 0.01$ vs NDM participants with birthweight < 3000 g; †† $p < 0.01$ vs DM participants with birthweight < 3000 g; ††† $p < 0.01$ vs DM participants with birthweight ≥ 3000 g



childhood obesity may affect BCA in the NDM group, we further analysed the association between birthweight and BCA after excluding the NDM-CO group ($n = 32$, Fig. 5). As a result, the positive correlation coefficient between birthweight and BCA was increased ($R = 0.51$, $p < 0.01$). The positive correlation coefficients between birthweight and mean islet size and the density of insulin-positive duct cells, and the negative correlation coefficient between birthweight and ACA to BCA ratio were also increased ($R = 0.50$, 0.45 and -0.53 , respectively, all $p < 0.01$). However, there remained no correlation between birthweight and ACA, islet density, density of scattered beta cells or frequency

of beta cell replication. The positive correlation between birthweight and BCA was observed in both sexes (ESM Fig. 7). These results were consistent when only the NDM-LN group was analysed ($n = 20$, ESM Fig. 8).

Discussion

In this study, we report that: (1) birthweight and BCA, but not ACA, were positively correlated in Japanese non-diabetic adults; (2) in these individuals, birthweight and mean islet size, but not islet density, were positively correlated; (3) these

Fig. 2 Correlation between birthweight and islet density (a–c) or mean islet size (d–f) in participants with (DM group) and without (NDM group) diabetes. Grey and white circles show DM and NDM participants, respectively. Bars indicate mean. ** $p < 0.01$ vs NDM participants with birthweight < 3000 g; †† $p < 0.01$ vs DM participants with birthweight < 3000 g; ††† $p < 0.01$ vs DM participants with birthweight ≥ 3000 g

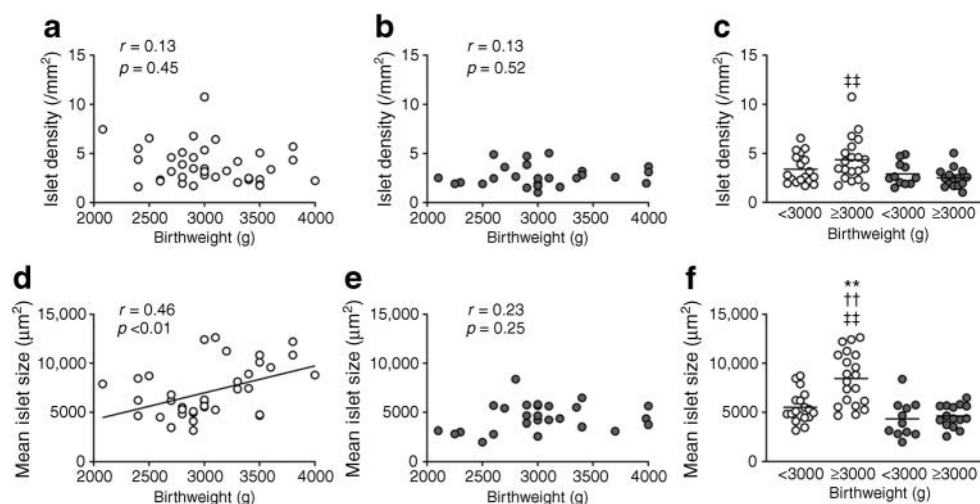
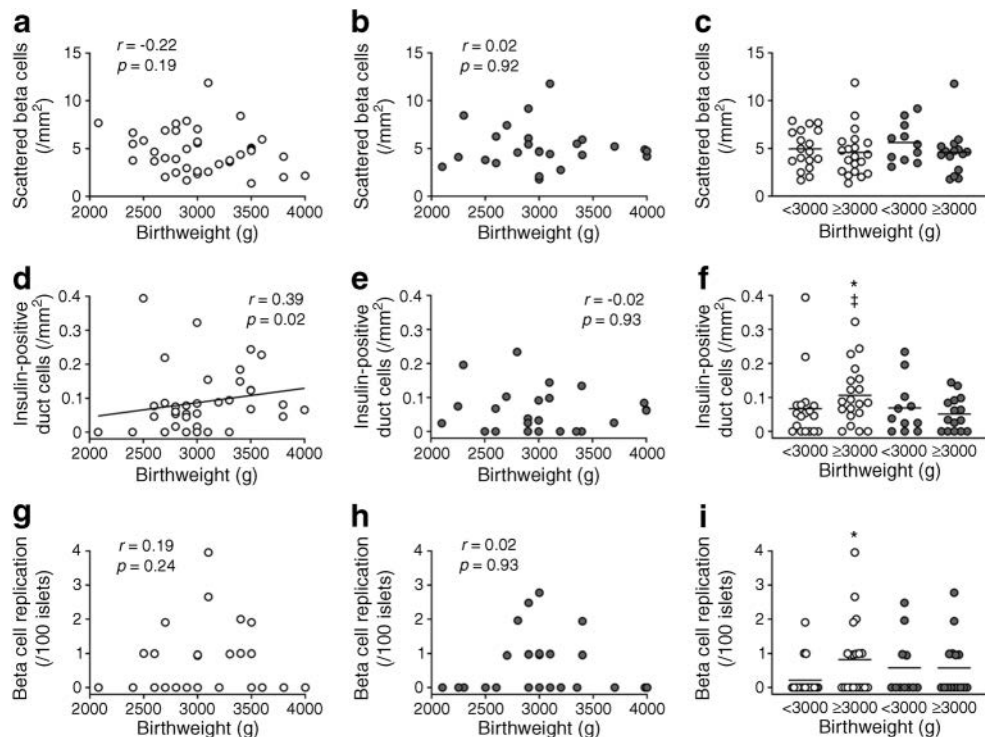


Fig. 3 Correlation between birthweight and number of scattered beta cells (a–c), number of insulin-positive duct cells (d–f) and beta cell replication (g–i) in participants with (DM group) and without (NDM group) diabetes. Grey and white circles show DM and NDM participants, respectively. Bars indicate mean. * $p < 0.05$ vs NDM participants with birthweight < 3000 g; † $p < 0.05$ vs DM participants with birthweight ≥ 3000 g



correlations were not observed in participants with type 2 diabetes; and (4) a history of childhood obesity, rather than adulthood obesity, may affect BCA and mean islet size.

Asians are thought to have a lower insulin secretion capacity compared with people of European or African descent [17]. In previous studies, including ours, neither current BMI nor maximum BMI in life were correlated with BCA in Japanese adults [3, 8, 18, 19]. The same results were also observed in this study, suggesting that Asians lack the capacity for beta cell proliferation to compensate for insulin resistance, compared with other ethnicities [1]. However, these previous studies only took into account obesity in adulthood.

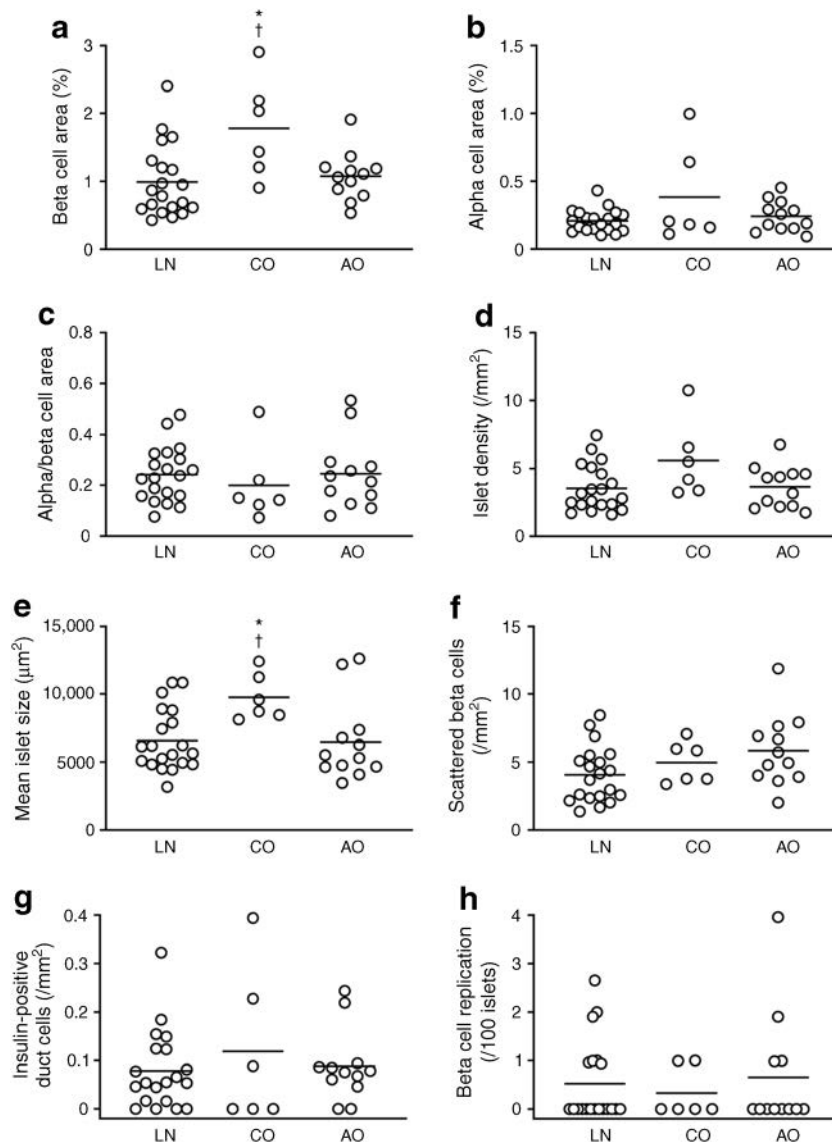
Although there are conflicting results regarding the association between high birthweight and incidence of type 2 diabetes [20–22], infants with low birthweight have been consistently reported to have increased incidence of type 2 diabetes [12, 23–31], which has been recently proposed as part of the DOHaD hypothesis [13, 14]. Although there is complex gene–environment interaction and the mechanisms of the association between low birthweight and future development of type 2 diabetes remain uncertain, an involvement of epigenetic modification has been recently proposed [32, 33]. Recent evidence has suggested that fetal undernutrition causes epigenetic modifications including DNA methylation, histone modifications and microRNA interaction, inducing beta cell dysfunction and insulin resistance in the offspring [32, 33]. It has been shown that mice with low birthweight are susceptible to impaired glucose tolerance due to epigenetic control, which suppresses beta cell proliferation [34]. In this study, we found

that birthweight and BCA were positively correlated in Japanese non-diabetic adults, indicating that birthweight is a major determinant of BCM not only in rodents but also in humans.

Obesity in adulthood is a well-known risk for the development of type 2 diabetes [35]. Although individuals with low birthweight are at risk of developing type 2 diabetes, it has been reported that those born with low birthweight and with obesity in adulthood showed the highest risk of type 2 diabetes compared with those with normal birthweight and without adulthood obesity [36, 37], suggesting a significant interaction between birthweight and adulthood obesity in the incidence of type 2 diabetes. Taken together, our findings suggest that smaller BCM in individuals born with low birthweight explains at least in part the relationship between low birthweight and high risk of future development of type 2 diabetes.

On the other hand, there was no correlation between birthweight and ACA in both non-diabetic and diabetic participants, suggesting that, unlike beta cells, alpha cells may be less susceptible to epigenetic effects of low birthweight. Nonetheless, a negative correlation was observed between birthweight and ACA to BCA ratio in non-diabetic participants, indicating that people born with low birthweight show a relative increase in ACM. Future studies will be needed to explore whether the likelihood of developing type 2 diabetes in infants with low birthweight is more attributable to a decrease in BCM or a relative increase in ACM.

Fig. 4 Effects of history of childhood obesity and adulthood obesity on BCA (a), ACA (b), ACA to BCA ratio (c), islet density (d), mean islet size (e) and beta cell turnover (f–h) in participants without diabetes (NDM group). LN, NDM-LN group; CO, NDM-CO group; AO, NDM-AO group. Bars indicate mean. * $p < 0.05$ vs NDM-LN; † $p < 0.05$ vs NDM-AO



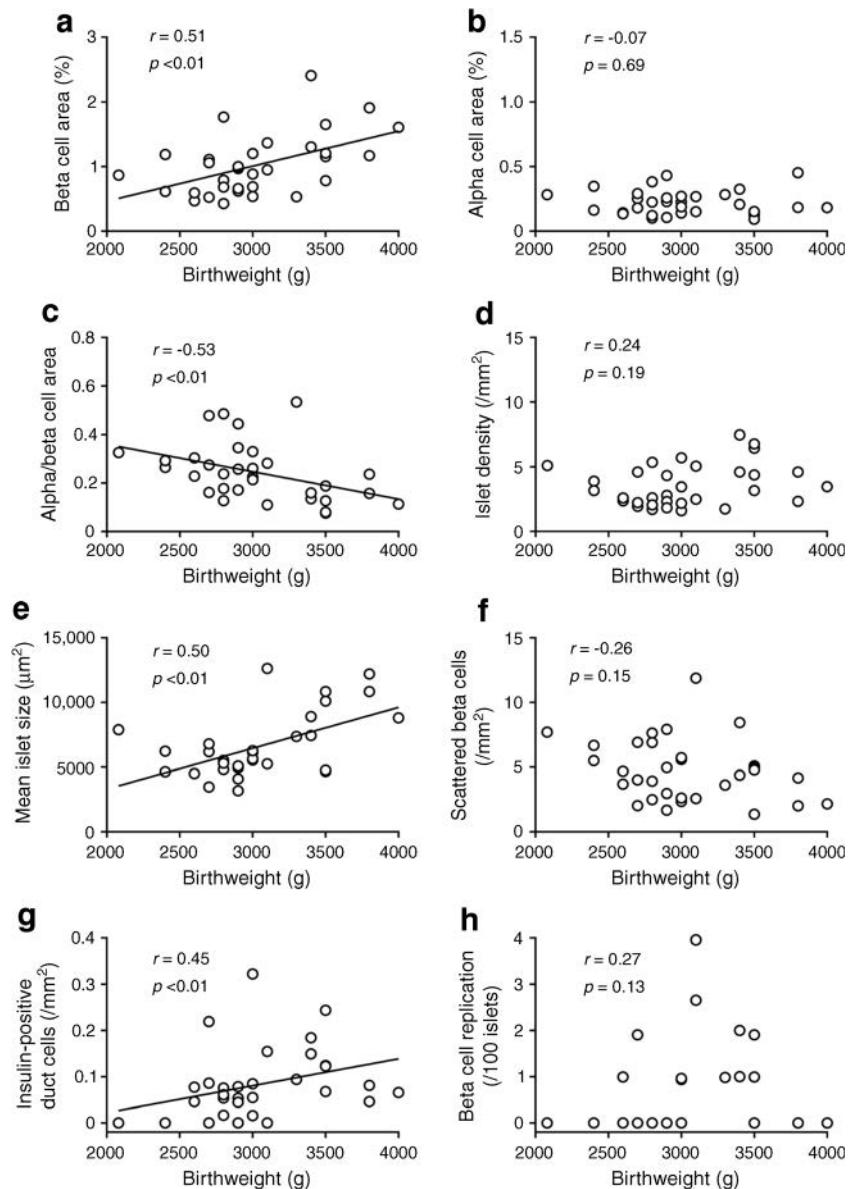
The second finding of this study was clarification of the associations of birthweight with islet density and mean islet size. Analysis of fetal pancreatic tissues has shown that lobular organisation of the pancreas as well as increase in islet size is observed from early prenatal stages [38]. A previous report has shown that BCM and islet size increase from birth to 20 years of age, but density of islets decreases with age [10], suggesting that new beta cell formation mainly occurs with increasing islet size. Here we found a significant correlation between birthweight and mean islet size, but not islet density, in non-diabetic individuals without a history of childhood obesity, suggesting that insufficient development of each islet rather than reduced number of islets is the mechanism of reduced BCM in people born with low birthweight.

Islet development involves beta cell replication, which is highest in neonates up to infancy and decreases with age [10, 11]. In this study, although beta cell replication was very rarely

observed in adult humans, the frequency of beta cell replication was significantly lower in those with birthweight < 3000 g than in those with birthweight ≥ 3000 g, suggesting the involvement of beta cell replication in greater islet size. Another source of beta cells may be insulin-positive duct cells, whose number was positively correlated with birthweight in this study. Although beta cell neogenesis and proliferation are active in the neonate, duct cells are assumed to have the capacity to convert to beta cells even in adulthood [39, 40]. Taken together, our findings suggest the possibility that the ability of beta cell production declines during the life course in people born with low birthweight, also highlighting the role of epigenetic modification, which is relatively stably transmitted until adulthood.

The third finding was that no correlation between birthweight and BCA or mean islet size was observed in participants with type 2 diabetes. Previous reports have shown

Fig. 5 Correlation between birthweight and BCA (a), ACA (b), ACA to BCA ratio (c), islet density (d), mean islet size (e) and beta cell turnover (f–h) in NDM participants without a history of childhood obesity (NDM-LN and NDM-AO groups; $n = 32$)



that BCM declines in type 2 diabetes [1–4]. However, it is not yet known whether the decline in BCM in individuals with type 2 diabetes is a cause or consequence of the disease in humans. Our findings indicate that the presence of type 2 diabetes modifies the relationship between birthweight and BCM, and therefore birthweight is no longer a major determinant of BCM in individuals with type 2 diabetes.

Finally, we confirmed the importance of childhood obesity as a factor affecting islet morphology. Intriguingly, compared with non-diabetic participants who did not have a history of childhood obesity, regardless of the presence or absence of adulthood obesity, those with a history of childhood obesity showed significantly larger BCA and mean islet size despite there being no significant difference in birthweight. Furthermore, the correlation coefficients between birthweight and BCA, mean islet size, and density of insulin-positive duct

cells in non-diabetic participants were further increased by excluding those with childhood obesity. Although the number of individuals with childhood obesity was small in this study, these results suggest that a history of childhood obesity is a modifier of BCM and islet size. It has been shown that elevated BMI only in adulthood rather than in adolescence was associated with development of diabetes [41]. Another study of Japanese female nurses has also reported an inverse relationship between BMI at age 18 and the incidence of diabetes [42]. Furthermore, adolescent low BMI is associated with an increase in the incidence of gestational diabetes [43, 44]. The inverse relationship between childhood obesity and diabetes may be in part explained by the capacity of beta cell expansion during this age, although it should be noted that an increase in body weight during childhood remains correlated with an increased risk of type 2 diabetes, especially in those with

low birthweight [45]. In addition, whether the poor response of BCM to obesity in Japanese is attributable to the lower incidence of childhood obesity in this population [46, 47] is an intriguing question that needs further clarification.

A limitation of this study is that birthweight and history of obesity were based on a questionnaire. The average age of participants in this study was over 60 years, and we were not able to obtain documented records in childhood. However, previous studies with respect to birthweight also used questionnaires to collect information [25–27, 36, 37, 42, 43]. Moreover, we sought to maintain the reliability of the data by including only those who were able to recall their birthweight on a scale of at least every 100 g. Second, different portions of the pancreas were sampled according to the operative procedure. However, the proportion of endocrine cells has been shown to be relatively consistent regardless of the pancreatic site, except for the ventral portion of the pancreatic head [4]. Furthermore, the results were not changed when we analysed the cases of pancreatic head and body/tail separately (ESM Fig. 9). Third, pancreatic diseases might affect islet morphology; however, the results did not change depending on whether or not the primary disease was pancreatic cancer in this study (ESM Fig. 10). In addition, in this study, because of the presence of pancreatic diseases we were not able to measure pancreas weight or volume, and therefore actual BCM, the product of BCA and pancreas weight, was undetermined, although BCA is widely used as a surrogate for BCM. Thus, difference in pancreas weight might affect our findings, as reduced pancreas weight has been reported in animal models of intrauterine growth retardation [48]. Nonetheless, these limitations and biases described above should make the correlations or differences between the groups tend towards zero. Fourth, since all participants of this study were Japanese, our findings may not be applicable to other ethnicities. Finally, in our participants, there were only seven participants with birthweight <2500 g, which is generally considered as low birthweight [21], furthermore, owing to the nature of the cross-sectional design of the study, it is unclear whether those with low BCM would develop type 2 diabetes in the future. Our findings should be confirmed by future studies including a larger sample size and multiple ethnicities.

In conclusion, there was a positive correlation between birthweight and BCM, and birthweight and mean islet size in Japanese non-diabetic adults. ACM and islet density were not related to birthweight. A history of childhood obesity and the presence of type 2 diabetes may be factors affecting BCM after birth. These findings will be important bases for explaining the DOHaD hypothesis.

Acknowledgements We thank Y. Madokoro, Department of Pathology, Keio University School of Medicine, for technical assistance, W. Gray (London, UK) for editing the manuscript and Y. Tsuda (Davinci Medical Illustration Office, Tokyo, Japan) for editing the graphical abstract.

Data availability The datasets generated during and/or analysed during the current study are available from the corresponding author on reasonable request.

Funding This study was supported by funding from the Japan Diabetes Foundation, Keio Gijuku Academic Development Funds, and a Grant-in-Aid for Scientific Research (18 K08488) from the Ministry of Education, Culture, Sports, Science and Technology (MEXT) (YS).

Authors' relationships and activities The authors declare that there are no relationships or activities that might bias, or be perceived to bias, their work.

Contribution statement All authors made substantial contributions to conception and design, acquisition of data, or analysis and interpretation of data. They were responsible for drafting the article and revising it critically for important intellectual content. They approved the version to be published. YS is responsible for the integrity of the work as a whole.

Open Access This article is licensed under a Creative Commons Attribution 4.0 International License, which permits use, sharing, adaptation, distribution and reproduction in any medium or format, as long as you give appropriate credit to the original author(s) and the source, provide a link to the Creative Commons licence, and indicate if changes were made. The images or other third party material in this article are included in the article's Creative Commons licence, unless indicated otherwise in a credit line to the material. If material is not included in the article's Creative Commons licence and your intended use is not permitted by statutory regulation or exceeds the permitted use, you will need to obtain permission directly from the copyright holder. To view a copy of this licence, visit <http://creativecommons.org/licenses/by/4.0/>.

References

1. Saisho Y (2015) Beta cell dysfunction: its critical role in prevention and management of type 2 diabetes. *World J Diabetes* 6(1):109–124. <https://doi.org/10.4239/wjd.v6.i1.109>
2. Butler AE, Janson J, Bonner-Weir S, Ritzel R, Rizza RA, Butler PC (2003) β -Cell deficit and increased β -cell apoptosis in humans with type 2 diabetes. *Diabetes* 52(1):102–110. <https://doi.org/10.2337/diabetes.52.1.102>
3. Inaishi J, Saisho Y, Sato S et al (2016) Effects of obesity and diabetes on α - and β -cell mass in surgically resected human pancreas. *J Clin Endocrinol Metab* 101(7):2874–2882. <https://doi.org/10.1210/jc.2016-1374>
4. Sakuraba H, Mizukami H, Yagihashi N, Wada R, Hanyu C, Yagihashi S (2002) Reduced beta-cell mass and expression of oxidative stress-related DNA damage in the islet of Japanese type II diabetic patients. *Diabetologia* 45(1):85–96. <https://doi.org/10.1007/s125-002-8248-z>
5. Polonsky KS, Given BD, Van Cauter E (1988) Twenty-four-hour profiles and pulsatile patterns of insulin secretion in normal and obese subjects. *J Clin Invest* 81(2):442–448. <https://doi.org/10.1172/jci113339>
6. Saisho Y, Butler AE, Manesso E, Elashoff D, Rizza RA, Butler PC (2013) β -Cell mass and turnover in humans: effects of obesity and aging. *Diabetes Care* 36(1):111–117. <https://doi.org/10.2337/dc12-0421>
7. Rahier J, Guiot Y, Goebbels RM, Sempoux C, Henquin JC (2008) Pancreatic β -cell mass in European subjects with type 2 diabetes. *Diabetes Obes Metab* 10(Suppl 4):32–42. <https://doi.org/10.1111/j.1463-1326.2008.00969.x>

8. Kou K, Saisho Y, Satoh S, Yamada T, Itoh H (2013) Change in β -cell mass in Japanese nondiabetic obese individuals. *J Clin Endocrinol Metab* 98(9):3724–3730. <https://doi.org/10.1210/jc.2013-1373>
9. Sato S, Saisho Y, Inaishi J et al (2015) Effects of glucocorticoid treatment on β - and α -cell mass in Japanese adults with and without diabetes. *Diabetes* 64(8):2915–2927. <https://doi.org/10.2337/db15-0151>
10. Meier JJ, Butler AE, Saisho Y et al (2008) Beta-cell replication is the primary mechanism subserving the postnatal expansion of β -cell mass in humans. *Diabetes* 57(6):1584–1594. <https://doi.org/10.2337/db07-1369>
11. Gregg BE, Moore PC, Demozay D et al (2012) Formation of a human β -cell population within pancreatic islets is set early in life. *J Clin Endocrinol Metab* 97(9):3197–3206. <https://doi.org/10.1210/jc.2012-1206>
12. Hales CN, Barker DJ, Clark PM et al (1991) Fetal and infant growth and impaired glucose tolerance at age 64. *BMJ* 303(6809):1019–1022. <https://doi.org/10.1136/bmj.303.6809.1019>
13. Gluckman PD, Hanson MA (2004) Living with the past: evolution, development, and patterns of disease. *Science* 305(5691):1733–1736. <https://doi.org/10.1126/science.1095292>
14. de Boo HA, Harding JE (2006) The developmental origins of adult disease (Barker) hypothesis. *Aust N Z J Obstet Gynaecol* 46(1):4–14. <https://doi.org/10.1111/j.1479-828X.2006.00506.x>
15. Manalich R, Reyes L, Herrera M, Melendi C, Fundora I (2000) Relationship between weight at birth and the number and size of renal glomeruli in humans: a histomorphometric study. *Kidney Int* 58(2):770–773. <https://doi.org/10.1046/j.1523-1755.2000.00225.x>
16. Kanazawa M, Yoshiike N, Osaka T, Numba Y, Zimmet P, Inoue S (2005) Criteria and classification of obesity in Japan and Asia-Oceania. *World Rev Nutr Diet* 94:1–12. <https://doi.org/10.1159/000088200>
17. Kodama K, Tojjar D, Yamada S, Toda K, Patel CJ, Butte AJ (2013) Ethnic differences in the relationship between insulin sensitivity and insulin response: a systematic review and meta-analysis. *Diabetes Care* 36(6):1789–1796. <https://doi.org/10.2337/dc12-1235>
18. Mizukami H, Takahashi K, Inaba W et al (2014) Age-associated changes of islet endocrine cells and the effects of body mass index in Japanese. *J Diabetes Investig* 5(1):38–47. <https://doi.org/10.1111/jdi.12118>
19. Fujita Y, Kozawa J, Iwahashi H et al (2015) Increment of serum C-peptide measured by glucagon test closely correlates with human relative beta-cell area. *Endocr J* 62(4):329–337. <https://doi.org/10.1507/endocrj.EJ14-0456>
20. Harder T, Rodekamp E, Schellong K, Dudenhausen JW, Plagemann A (2007) Birth weight and subsequent risk of type 2 diabetes: a meta-analysis. *Am J Epidemiol* 165(8):849–857. <https://doi.org/10.1093/aje/kwk071>
21. Zhao H, Song A, Zhang Y, Zhen Y, Song G, Ma H (2018) The association between birth weight and the risk of type 2 diabetes mellitus: a systematic review and meta-analysis. *Endocr J* 65(9):923–933. <https://doi.org/10.1507/endocrj.EJ18-0072>
22. Tian G, Guo C, Li Q et al (2019) Birth weight and risk of type 2 diabetes: a dose–response meta-analysis of cohort studies. *Diabetes Metab Res Rev* 35(5):e3144. <https://doi.org/10.1002/dmrr.3144>
23. Barker DJ, Hales CN, Fall CH, Osmond C, Phipps K, Clark PM (1993) Type 2 (non-insulin-dependent) diabetes mellitus, hypertension and hyperlipidaemia (syndrome X): relation to reduced fetal growth. *Diabetologia* 36(1):62–67. <https://doi.org/10.1007/bf00399095>
24. Lithell HO, McKeigue PM, Berglund L, Mohsen R, Lithell UB, Leon DA (1996) Relation of size at birth to non-insulin dependent diabetes and insulin concentrations in men aged 50–60 years. *BMJ* 312(7028):406–410. <https://doi.org/10.1136/bmj.312.7028.406>
25. Curhan GC, Willett WC, Rimm EB, Spiegelman D, Ascherio AL, Stampfer MJ (1996) Birth weight and adult hypertension, diabetes mellitus, and obesity in US men. *Circulation* 94(12):3246–3250. <https://doi.org/10.1161/01.cir.94.12.3246>
26. Yarbrough DE, Barrett-Connor E, Kritiz-Silverstein D, Wingard DL (1998) Birth weight, adult weight, and girth as predictors of the metabolic syndrome in postmenopausal women: the rancho Bernardo study. *Diabetes Care* 21(10):1652–1658. <https://doi.org/10.2337/diacare.21.10.1652>
27. Carlsson S, Persson PG, Alvarsson M et al (1999) Low birth weight, family history of diabetes, and glucose intolerance in Swedish middle-aged men. *Diabetes Care* 22(7):1043–1047. <https://doi.org/10.2337/diacare.22.7.1043>
28. Forsen T, Eriksson J, Tuomilehto J, Reunanen A, Osmond C, Barker D (2000) The fetal and childhood growth of persons who develop type 2 diabetes. *Ann Intern Med* 133(3):176–182. <https://doi.org/10.7326/0003-4819-133-3-200008010-00008>
29. Birgisdottir BE, Gunnarsdottir I, Thorsdottir I, Gudnason V, Benediktsson R (2002) Size at birth and glucose intolerance in a relatively genetically homogeneous, high-birth weight population. *Am J Clin Nutr* 76(2):399–403. <https://doi.org/10.1093/ajcn/76.2.399>
30. Eriksson JG, Forsen TJ, Osmond C, Barker DJ (2003) Pathways of infant and childhood growth that lead to type 2 diabetes. *Diabetes Care* 26(11):3006–3010. <https://doi.org/10.2337/diacare.26.11.3006>
31. Wadsworth M, Butterworth S, Marmot M, Ecob R, Hardy R (2005) Early growth and type 2 diabetes: evidence from the 1946 British birth cohort. *Diabetologia* 48(12):2505–2510. <https://doi.org/10.1007/s00125-005-0007-4>
32. Fernandez-Twinn DS, Hjort L, Novakovic B, Ozanne SE, Saffery R (2019) Intrauterine programming of obesity and type 2 diabetes. *Diabetologia* 62(10):1789–1801. <https://doi.org/10.1007/s00125-019-4951-9>
33. Zhu Z, Cao F, Li X (2019) Epigenetic programming and fetal metabolic programming. *Front Endocrinol* 10(764). <https://doi.org/10.3389/fendo.2019.00764>
34. Su Y, Jiang X, Li Y et al (2016) Maternal low protein isocaloric diet suppresses pancreatic β -cell proliferation in mouse offspring via miR-15b. *Endocrinology* 157(12):4782–4793. <https://doi.org/10.1210/en.2016-1167>
35. Guh DP, Zhang W, Bansback N, Amarsi Z, Birmingham CL, Anis AH (2009) The incidence of co-morbidities related to obesity and overweight: a systematic review and meta-analysis. *BMC Public Health* 9:88. <https://doi.org/10.1186/1471-2458-9-88>
36. Katanoda K, Noda M, Goto A, Mizunuma H, Lee JS, Hayashi K (2017) Impact of birth weight on adult-onset diabetes mellitus in relation to current body mass index: the Japan Nurses' Health Study. *J Epidemiol* 27(9):428–434. <https://doi.org/10.1016/j.je.2016.08.016>
37. Hu C, Mu Y, Wan Q et al (2020) Association between birth weight and diabetes: role of body mass index and lifestyle in later life. *J Diabetes* 12(1):10–20. <https://doi.org/10.1111/1753-0407.12960>
38. Meier JJ, Kohler CU, Alkhatib B et al (2010) Beta-cell development and turnover during prenatal life in humans. *Eur J Endocrinol* 162(3):559–568. <https://doi.org/10.1530/eje-09-1053>
39. Zare M, Rastegar S, Ebrahimi E, Roohipoor A, Shirali S (2017) Role of pancreatic duct cell in beta cell neogenesis: a mini review study. *Diabetes Metab Syndr* 11(Suppl 1):S1–S4. <https://doi.org/10.1016/j.dsx.2016.08.005>
40. Weir GC, Gaglia J, Bonner-Weir S (2020) Inadequate β -cell mass is essential for the pathogenesis of type 2 diabetes. *Lancet Diabetes Endocrinol*. [https://doi.org/10.1016/S2213-8587\(20\)30022-X](https://doi.org/10.1016/S2213-8587(20)30022-X)
41. Tirosh A, Shai I, Afek A et al (2011) Adolescent BMI trajectory and risk of diabetes versus coronary disease. *N Engl J Med* 364(14):1315–1325. <https://doi.org/10.1056/NEJMoa1006992>

42. Katanoda K, Noda M, Goto A, Mizunuma H, Lee JS, Hayashi K (2019) Being underweight in adolescence is independently associated with adult-onset diabetes among women: the Japan Nurses' health study. *J Diabetes Investig* 10(3):827–836. <https://doi.org/10.1111/jdi.12947>
43. Yeung EH, Hu FB, Solomon CG et al (2010) Life-course weight characteristics and the risk of gestational diabetes. *Diabetologia* 53(4):668–678. <https://doi.org/10.1007/s00125-009-1634-y>
44. Yachi Y, Tanaka Y, Nishibata I et al (2013) Low BMI at age 20 years predicts gestational diabetes independent of BMI in early pregnancy in Japan: Tanaka Women's clinic study. *Diabet Med* 30(1):70–73. <https://doi.org/10.1111/j.1464-5491.2012.03712.x>
45. Bhargava SK, Sachdev HS, Fall CH et al (2004) Relation of serial changes in childhood body-mass index to impaired glucose tolerance in young adulthood. *N Engl J Med* 350(9):865–875. <https://doi.org/10.1056/NEJMoa035698>
46. Wang Y, Lobstein T (2006) Worldwide trends in childhood overweight and obesity. *Int J Pediatr Obes* 1(1):11–25. <https://doi.org/10.1080/17477160600586747>
47. Anderson SE, Whitaker RC (2009) Prevalence of obesity among US preschool children in different racial and ethnic groups. *Arch Pediatr Adolesc Med* 163(4):344–348. <https://doi.org/10.1001/archpediatrics.2009.18>
48. Boehmer BH, Limesand SW, Rozance PJ (2017) The impact of IUGR on pancreatic islet development and β -cell function. *J Endocrinol* 235(2):R63–R76. <https://doi.org/10.1530/joe-17-0076>

Publisher's note Springer Nature remains neutral with regard to jurisdictional claims in published maps and institutional affiliations.

Current evidence and future perspectives of immune-checkpoint inhibitors in unresectable malignant pleural mesothelioma

Katsuyuki Hotta,¹ Nobukazu Fujimoto²

To cite: Hotta K, Fujimoto N. Current evidence and future perspectives of immune-checkpoint inhibitors in unresectable malignant pleural mesothelioma. *Journal for ImmunoTherapy of Cancer* 2020;**8**:e000461. doi:10.1136/jitc-2019-000461

Accepted 04 February 2020

ABSTRACT

Platinum-based chemotherapy is commonly used as the standard first-line treatment for unresectable malignant pleural mesothelioma (MPM). However, in recent times, immune-checkpoint inhibitors (ICIs) have led to a paradigm shift. Herein, we review relevant literature and ongoing trials of ICIs used as both first-line and salvage therapies. Specifically, in the Japanese single-arm, phase II trial, the MERIT trial, nivolumab, an antiprogrammed cell death 1 (PD-1) antibody showed favorable efficacy when used as a salvage therapy. Currently, multiple ICI monotherapy or combination therapy trials have been conducted, which could provide further evidence. Among available ICIs, the anti-PD-1 antibody is promising for unresectable MPM, despite the limited efficacy of anti-CTLA4 monotherapy. Ongoing studies will further confirm the potential efficacy of ICIs for MPM, as observed across other malignancies. It is also crucial to identify any clinically useful predictive biomarkers that could reveal ICIs with maximal effects in MPM.

INTRODUCTION

With increasing utilization of asbestos, the incidence of mesothelioma is considered to increase worldwide. Asbestos consumption in the USA has rapidly declined over the last 40 years, which has resulted in a considerable decline in mesothelioma incidence.¹ In Japan, the number of deaths had increased from 500 in 1995 to 1550 in 2016. Mesothelioma manifests mainly in the pleura, peritoneum and pericardium, although most commonly in the pleura.²

The major role of chronic inflammation and local tumor suppression in tumorigenesis observed in some experimental models led to the investigation of immunotherapy for malignant pleural mesothelioma (MPM).³ There have been intensive investigations on the efficacy and safety of immune-checkpoint inhibitors (ICIs) in the treatment of unresectable advanced diseases.^{4 5} Herein, we highlight relevant study results, as well as designs

and concepts of ongoing studies in both first-line and salvage settings.

Known biology

Among approximately 400 different mineral fibers present in nature, six fibers (amphiboles fibers (crocidolite, actinolite, tremolite, anthophyllite and amosite) and serpentine fiber (chrysotile)) are called as 'asbestos'.⁶ They are carcinogenic and have been associated with mesothelioma.^{6 7} Furthermore, exposure of the chest to therapeutic ionizing radiation, usually performed to treat lymphomas, has been causally linked to mesothelioma, especially in young patients.^{8–10}

The accumulation of genetic aberrations can induce malignancies. Recently, The Cancer Genome Atlas program investigated genetic alterations in mesotheliomas using next-generation sequencing (NGS).¹¹ The results revealed frequent mutations in BAP1, CDKN2A, NF2, TP53, LATS2 and SETD2.^{11 12} Recently, a considerably higher number of genetic alterations in mesotheliomas has been detected than that detected by NGS, including point mutations, minute deletions and copy number changes.^{13 14} Furthermore, the vast array of genetic alterations in mesothelioma may lead to producing neoantigens, which correlate with the clonal expansion of tumor-infiltrating T lymphocytes.^{13 15} These findings suggest that, in contrast to the hypotheses based on NGS studies, mesothelioma may be immunogenic.¹⁵

Rationale for the development of immunotherapy

A hallmark of cancer is immune evasion, in which the immune system does not mount an effective antitumor response.¹⁶ Programmed cell death 1 (PD-1) is a negative costimulatory receptor expressed primarily on the surface of activated T cells^{17 18} and is involved in maintaining peripheral tolerance. The binding of PD-1 to one of its ligands, PD-L1 or PD-L2,



© Author(s) (or their employer(s)) 2020. Re-use permitted under CC BY-NC. No commercial re-use. See rights and permissions. Published by BMJ.

¹Center for Innovative Clinical Medicine, Okayama University Hospital, Okayama, Japan

²Department of Medical Oncology and Medicine, Okayama Rosai Hospital/Okayama Rosai Hospital, Okayama, Japan

Correspondence to

Dr Katsuyuki Hotta;
khotta@okayama-u.ac.jp

can inhibit a cytotoxic T-cell response.^{19 20} Tumors can co-opt this pathway to escape T-cell-induced antitumor activity.^{21–23}

The biology of MPM shows significant heterogeneity in both tumor and the microenvironment. Several studies, on T-cell-inhibitory receptors and chemokines, have indicated the prognostic role of lymphocytes and the occurrence of immunosuppression in MPM.^{24 25} In a melanoma model, PD-1 blockade increased the proportion of antigen-specific CTLs that recognized melanoma targets by degranulation, suggesting increased recognition efficiency for cognate peptide.²⁶ The increased frequency and absolute number of antigen-specific CTLs by PD-1 blockade resulted from augmented proliferation, and not decreased apoptosis. These findings have led to the extensive development of agents blocking immun checkpoints and their clinical investigation in various malignancies including MPM.

Biomarker in the ICI treatment of MPM

Some sensitive and specific immunohistochemistry markers including calretinin and WT1 are used for diagnosing mesothelioma.⁴ However, markers for treatment efficiency have not been established. Generally, PD-L1 expression level is used as the representative maker for predicting the efficacy of ICIs. In the ICI monotherapy with the salvage setting in non-squamous cell non-small-cell lung cancer, the PD-L1 expression level affected the survival efficacy,²⁷ while its influence was weakened when combined with platinum-based chemotherapy in the first-line setting.²⁸

In MPM, 20%–70% of the specimens tested are usually PD-L1 positive.²⁹ Such a wide range can be attributed to several factors. It could be because tumors are heterogeneous in nature.⁴ It could be partially attributed to the antibodies used; SP-263 is the most commonly used antibody,^{30–32} and the others include clones E1L3N and 28–8.³³ Furthermore, the histological subtype influences its frequency; PD-L1 expression is higher in non-epithelial mesotheliomas.³⁴ The cut-off levels of PD-L1 positivity vary among trials.³⁵ Considering that the positive rates were reported from different small studies with a small number of accrued patients, the data may be limited and actual rates of expression have hardly been studied. In addition to this, whether the ICI efficacy is truly dependent on the PD-L1 expression level is still controversial.

ICIs in the first-line settings

The standard treatment for unresectable, advanced malignant mesothelioma is chemotherapy, although with a very poor prognosis.³⁶ Similar to its use in non-small-cell lung cancer,^{37–44} cisplatin (CDDP) and pemetrexed (PEM) combination therapy (CDDP/PEM) approved by the US Food and Drug Administration (FDA) in 2004, is strongly recommended as the first-line treatment for mesothelioma.⁴⁵ Moreover, molecularly targeted agents have been developed to augment cytotoxic chemotherapy. For instance, a randomized phase III MAPS study showed

that adding bevacizumab to platinum doublets improved survival (HR of overall survival (OS) and progression-free survival (PFS): 0.77 (95% CI: 0.62 to 0.95); $p=0.0167$ and 0.61 (0.50 to 0.75); $p<0.0001$, respectively).⁴⁶ However, this regimen is yet to be approved by the FDA. A double-blind, randomized, placebo-controlled phase III study, the LUME-Meso trial of CDDP and PEM with or without nintedanib, a multikinase inhibitor for unresectable epithelioid MPM, showed that the primary endpoint, PFS, was not met.⁴⁷ Even with such an aggressive chemotherapy, OS for unresectable mesothelioma remains ≤ 12 months.⁴⁸

Given the limitations in the efficacy of existing cytotoxic chemotherapy in MPM and recent advances in tumor immunology across various malignancies, ICIs have been investigated for the treatment of unresectable mesothelioma. A single-arm, Durvalumab with First-line Chemotherapy in Mesothelioma study examined treatment efficacy after adding durvalumab, a PD-L1 inhibitor, to CPPD/PEM, in 54 patients with untreated, unresectable MPM⁴⁹ (table 1). PFS (the primary endpoint) at 6 months was 57%, and the objective response rate (ORR) was 48%, with a median duration of response of 6.5 months. Immune-related adverse events of grade 3 and higher, occurred in eight patients (15%), including lipase elevation ($n=1$), pancreatitis ($n=1$) and renal impairment ($n=1$).

The Canadian Cancer Trials Group has launched a phase II/III study for unresectable MPM, to verify treatment efficacy following the addition of pembrolizumab, a PD-1 antibody, to the standard CPPD/PEM (NCT02784171) (table 2). The use of durvalumab as the first-line immunotherapy is also under evaluation, sponsored by PrECOG (NCT02899195). Japanese investigators are also conducting an exploratory phase II trial, using nivolumab combined with the standard CPPD/PEM, in patients with untreated, unresectable MPM.⁵⁰ Furthermore, a large-scale, randomized phase III study, the CheckMate 743 study is currently investigating the survival advantage of the nivolumab/ipilimumab combination immunotherapy, versus platinum/PEM, in 606 patients with untreated, unresectable MPM (NCT02899299).

Single-agent ICI therapy in the salvage setting

Although the salvage setting is discussed before advancements in the first-line setting, currently available agents in the salvage setting rarely work in MPM, with a median survival time (MST) of ≤ 6 months.⁵¹ Vorinostat, a histone deacetylase inhibitor, was proven not to have any survival advantage in a placebo-controlled randomized phase III trial, the VANTAGE-014 trial,⁵² without earlier trial result confirmation.

Thus far, four ICIs have been tested as an immunotherapy against relapsed tumors (table 1). A single-center, single-arm phase II study, the NivoMes trial, with single-agent nivolumab, an anti-PD-1 antibody showed that 16 (47%) of the 34 registered patients with recurrent MPM achieved disease control at 12 weeks (8 with

Table 1 Relevant trial results

Trial name	Year	Phase	RCT	Drug	Primary endpoint	No	PS 0-1	No of sarcomatoid histology	ORR	mPFS (mo)	MST (mo)	Pneumonitis*	Ref.
Frontline setting													
DREAM		No		Durvalumab	PFS, OR	54	100%	-	48%	6.9	-	NR	49
Salvage setting													
<Single agent>													
MERIT	2018	2	No	Nivolumab	OR	34	100%	3 (9%)	29%	6.1	17.3	6%	54
NivoMes	2018	2	No	Nivolumab	DCR	34	100%	2 (6%)	24%	2.6	11.8	12%	53
KN-028†,‡	2017	1b	No	Pembrolizumab	Safety	25	100%	2 (8%)	20%	5.4	18	NR	55
Chicago group	2018	2	No	Pembrolizumab	OR	65	100%	5 (8%)	19%	4.5	11.5	3%	56
JAVELIN	2019	1b	No	Avelumab	OR	53	100%	2 (4%)	9%	4.1	10.7	6%	57
Italian group	2013	2	No	Tremelimumab	OR	29	79%	3 (10%)	7%	6.2	10.7	NR	58
Italian group	2015	2	No	Tremelimumab	irOR	29	79%	1 (3%)	3%	-	-	NR	59
DETERMINE	2017	2b	Yes	Tremelimumab	OS	382	99%	22 (6%)	5%	2.8	7.7§	NR	60
<Combination>													
NIBIT-MESO-1¶	2018	2	No	Tremelimumab/durvalumab	irOR	40	100%	2 (5%)	28%	5.7	16.6	NR	30
MAPS2	2019	2	Yes	Nivolumab/ipilimumab	DCR	62	98%	9 (15%)**	28%	5.6	15.9	2%	31
INITIATE	2019	2	No	Nivolumab/ipilimumab	DCR	34	100%	3 (9%)	29%	6.2	NR	NR	32

*Any grade.

†Those with the following conditions were eligible: (1) failed standard therapy and (2) unable to receive standard therapy.

‡Those with PD-L1-positive tumors were registered.

§OS-HR of 0.92 with a 95% CI 0.76 to 1.12.

¶Subjects who refused the first line platinum-based chemotherapy, or those with disease progression after a maximum of one line of platinum-based therapy, were eligible. Including biphasic histology.

DCR, disease control rate; DREAM, Durvalumab with First-Line Chemotherapy in Mesothelioma; irOR, immune-related objective response; MST, median survival time; NR, not reported; ORR, objective response rate; OS, overall survival; PD-L1, programmed cell death ligand 1; PFS, progression-free survival; RCT, randomized controlled trial.

**Table 2** Ongoing relevant trials

Trial	Country	Phase	RCT	Regimen	Primary endpoint	No of planned pts	PS	Study start date	Registration no
Front-line setting									
Canadian group	Canada	2/3	Yes	Cis-pem±pembrolizumab	OS	126	0–1	07/10/16	NCT02784171
CM743	Global	3	Yes	Nivolumab/ipilimumab versus p-pem	OS	606	0–1	25/10/16	NCT02899299
PrE0505	USA	2	No	Cis-pem/durvalumab	OS	55	0–1	13/06/17	NCT02899195
JME-001	Japan	2	No	Cis-pem/nivolumab	OR	18	0–1	20/01/18	UMIN000030892
Salvage setting									
Confirm	UK	3	Yes	Nivolumab versus placebo	OS	336	0–1	28/03/17	NCT03063450

Cis-pem, cisplatin and pemetrexed; OS, overall survival; p-pem, platinum (cisplatin or carboplatin) and pemetrexed; PS, performance status; pts, patients; RCT, randomized controlled trial.

partial response (PR) and 8 with stable disease (SD)).⁵³ In this population, PD-L1 expression did not predict treatment responses. A Japanese single-arm phase II study, the MERIT study, also examined the efficacy and safety of nivolumab monotherapy in 34 patients with MPM with a history of prior chemotherapy.⁵⁴ The primary endpoint, ORR, was 29% (10/34), which was dependent on tumor PD-L1 expression, with an ORR of 40% and 8% when PD-L1 expression was $\geq 1\%$ and $< 1\%$, respectively. The median PFS and MST were 6.1 and 17.3 months, respectively. Twenty-six patients (76%) experienced treatment-related adverse events (TRAEs). In essence, these results led to the approval of nivolumab in Japan for unresectable recurrent pleural mesothelioma.

A single-agent pembrolizumab, anti-PD-1 antibody trial (KEYNOTE-028) demonstrated that 5/25 (20%) of previously treated patients with MPM achieved PR, while 13 (52%) had SD, with no treatment-related deaths or discontinuations.⁵⁵ The Chicago group also conducted a pembrolizumab monotherapy phase II trial in 65 patients with pretreated mesothelioma.⁵⁶ Nineteen per cent of the patients achieved PR, without unexpected AEs. The ORR was associated with PD-L1 expression; 7%, 26%, and 31% in patients harboring tumors with PD-L1-expression level of $< 1\%$, 1%–49% and $\geq 50\%$, respectively. The study also showed a median PFS and OS of 4.5 and 11.5 months, respectively.

With avelumab, a human anti-PD-L1 IgG₁ antibody, a phase Ib monotherapy trial (JAVELIN) was conducted in 53 patients with pretreated malignant mesothelioma.⁵⁷ Despite the 9% response in the whole cohort, ORR seemed different, stratified by the PD-L1 expression level in patients with PD-L1-positive (19% (3 of 16)) vs PD-L1-negative tumors (7% (2 of 27)), considering a $\geq 5\%$ PD-L1 cut-off. The median PFS was 4.1 months, whereas the MST extended to > 10 months. Five patients (9%) had grades 3–4 TRAEs, without treatment-related deaths.

Tremelimumab, an anti-CTLA4 antibody, was also evaluated in a salvage setting. In Europe, two single-arm, phase

II monotherapy trials showed preliminary efficacy, with an ORR of 3%–7%.^{58,59} Following these trials, a randomized phase IIb study, the DETERMINE study, revealed that tremelimumab failed to significantly prolong OS compared with that of placebo, in 571 patients with previously treated malignant mesothelioma. The MST showed no difference between treatment groups, with 7.7 and 7.3 months in the tremelimumab and placebo arms, respectively (HR 0.92, 95% CI 0.76 to 1.12).⁶⁰

ICI combination therapy in salvage settings

Given that enhanced immunogenicity can be achieved by combining PD1 or PDL1 and CTLA4 inhibitors,³ several studies evaluating the combination of anti-CTLA-4 and anti-PD-[L]1 antibodies have been reported. A phase II study, the NIBIT-MESO-1 trial, investigated an ICI combination of tremelimumab and durvalumab for unresectable mesothelioma.³⁰ Subjects who had refused first-line platinum-based chemotherapy, or subjects with disease progression after a maximum of one line of platinum-based therapy, were enrolled. Eleven (28%) of 40 patients had an immune-related objective response. The median PFS and MST were 5.7 and 16.6 months, respectively. Baseline tumor PD-L1 expression did not correlate with the immune-related objective response, and seven patients (18%) had grades 3–4 TRAEs.

A combination therapy of nivolumab and ipilimumab, over nivolumab monotherapy, was examined in a randomized phase II trial (IFCT MAPS2).³¹ A total of 125 patients with relapsed MPM were allocated to the combination therapy or monotherapy arm. Disease control rate (DCR), set as the primary endpoint, was 50% and 44%, whereas the ORR was 28% and 19%, respectively. As expected, the combination therapy had an increased risk of AE, with grades 3–4 of 26% and 14%, respectively. Three (5%) of 62 combination group patients had toxicities that led to death (hepatitis, encephalitis and acute kidney failure). When restricted to high PD-L1 tumors ($> 25\%$), either of

the regimens seemed effective, with ORRs of 63%–71% in the post hoc analyses.

Similar to this MAPS2 trial, a single-arm study, the INITIATE study,³² evaluated the efficacy of nivolumab and ipilimumab in mesothelioma refractory to at least one line of platinum-based chemotherapy. Of the 34 patients included in efficacy assessment, 10 (29%) attained PR and 13 (38%) attained SD, resulting in a DCR (primary endpoint) of 68%. Despite the smaller-scale, non-randomized design, this study could reproduce the tolerance and efficacy results obtained from the MAPS2 trial. It also showed a relationship between tumor PD-L1 expression and the efficacy of this combination therapy.

Based on the aforementioned completed trials, several MPM trials are either ongoing or being initiated. The most pivotal is the one initiated by Cancer Research UK: a randomized, double blind placebo controlled CONFIRM trial of nivolumab versus placebo in patients with relapsed mesothelioma (NCT03063450). A total of 336 patients will be recruited from 25 institutes in the UK over a 4-year period. All patients will be treated for 12 months, except in situations of progress or withdrawal. It will be intriguing if this reproduces the Japanese MERIT study results.⁵⁴

Overall, anti-PD-1 antibodies exhibited promising results when used alone as a salvage therapy after the first-line chemotherapy.^{53–56}

Unresolved, unmet needs for MPM ICI therapy

Compared with clinical trials targeting other malignancies, the majority of prior MPM trials employed ‘small-scale’ and ‘single-arm’ designs, and their primary endpoints were set at only ORR or DCR. No clear survival advantage of ICI has been demonstrated through randomized trials. This is mainly because of the extremely small patient population, and mostly exploratory-type trials.⁴ However, favorable responses and survival data could be observed across the studies, which are better than historical data. Considering the current limitations of treatment options in the salvage setting, ICI is now a potential rational and medically useful option for patients with unresectable, relapsed MPM, in the absence of any contraindications. Undoubtedly, well-designed randomized trials provide accurate and consistent data (ie, CONFIRM trial (NCT03063450); table 2). The accumulation of forthcoming relevant data through ongoing clinical trials is important for establishing better ICI use in daily practices.

Among toxicities induced by ICIs, pulmonary toxicity has to be properly managed, as it can be one of the most common causes of ICI-related death. The most common lung toxicity observed in patients receiving ICI treatment is pneumonitis.⁶¹ In our review, as shown in table 1, it occurred in 2%–12% of the patients (median; 6%) in all the trials evaluating ICIs. This seemed almost consistent with that observed in other cancers. The patterns of onset and severity may also vary, and MPM often has characteristics of limited reserve in pulmonary function at the

baseline. These findings suggest the importance of vigilance and rapid response. Thus, physicians still should recognize that the diagnosis of pneumonitis is particularly challenging and failure to detect and treat pneumonitis in a timely manner could lead to poor clinical outcomes.

Another unmet need is the identification of predictive biomarkers of ICI effects. Compared with other malignancies, progress in mesothelioma biomarker research is limited. Some of the single-arm ICI studies reveal the correlation between responses and higher PD-L1 expression. However, as insufficient survival data were generated, more established outcome data are needed to confirm the value of PD-L1 immunohistochemistry as a predictive biomarker for the OS effect. Recently, the tumor mutational burden (TMB) analysis using the whole exome sequence has garnered attention in nivolumab therapy.⁶² Moreover, in lung cancer, no association between TMB and PD-L1 expression was revealed.⁶² Rather, a combination of them would be of value as a predictive biomarker. Nevertheless, only a few precise biomarkers for ICI efficacy assessments seem to exist in MPM clinical trials, besides PD-L1 expression. Further development of new biomarkers is also required for unresectable mesothelioma.

A majority of patients diagnosed with untreated, unresectable mesothelioma exhibit all expected symptoms at the initial presentation, and thus, do not meet the eligibility criteria to participate in clinical trials. Therefore, study results have to be interpreted cautiously, taking into consideration how each of them can be applied per in-care patient, during daily clinical practices.

In the future, more novel immunotherapy results will be made available, which could possibly lead to further drastic changes in unresectable MPM treatment. Our goal is to carefully evaluate any relevant information and deliver better patient treatment.

CONCLUSIONS

MPM prognosis has been poor with the standard platinum chemotherapy. Recently, in the salvage setting, anti-PD-1 antibodies yielded favorable ORR. Nivolumab is approved for use in Japan. Ongoing studies will further confirm the potential efficacy of ICIs for MPM, as observed across other malignancies. It is also crucial to identify any clinically useful predictive biomarkers that could reveal the ICIs with maximal effects in MPM.

Contributors KH and NF carried out the search and assessment for relevant studies. KH drafted the manuscript. Both authors read and approved the final manuscript.

Funding This study was supported by grants-in-aid from the Ministry of Health, Labor and Welfare, Japan.

Competing interests KH has honoraria from AstraZeneca, Ono Pharmaceuticals, BMS, MSD, Eli Lilly Japan, Nihon Kayaku, Taiho Pharmaceuticals and Chugai Pharmaceuticals, as well as unrelated research funding from AstraZeneca, BMS, and Eli Lilly Japan. NF has received consultancy fees from Boehringer Ingelheim, Ono, Bristol-Myers Squibb, Kyorin, and Kissei, and honoraria or research funding from Ono, Boehringer Ingelheim, Bristol-Myers Squibb, Eli Lilly Japan, and MSD

related to this manuscript, as well as unrelated research funding from Hisamitsu, Chugai, Taiho, Novartis and GSK.

Patient consent for publication Not required.

Provenance and peer review Not commissioned; externally peer reviewed.

Open access This is an open access article distributed in accordance with the Creative Commons Attribution Non Commercial (CC BY-NC 4.0) license, which permits others to distribute, remix, adapt, build upon this work non-commercially, and license their derivative works on different terms, provided the original work is properly cited, appropriate credit is given, any changes made indicated, and the use is non-commercial. See <http://creativecommons.org/licenses/by-nc/4.0/>.

REFERENCES

- Henley SJ, Larson TC, Wu M, *et al.* Mesothelioma incidence in 50 states and the district of Columbia, United States, 2003-2008. *Int J Occup Environ Health* 2013;19:1-10.
- Ministry of the environment government of Japan. Available: <http://www.env.go.jp/air/asbestos/registration/> [Accessed 15 Aug 2019].
- Yap TA, Aerts JG, Popat S, *et al.* Novel insights into mesothelioma biology and implications for therapy. *Nat Rev Cancer* 2017;17:475-88.
- Carbone M, Adusumilli PS, Alexander HR, *et al.* Mesothelioma: scientific clues for prevention, diagnosis, and therapy. *CA Cancer J Clin* 2019;69:402-29.
- Forde PM, Scherpereel A, Tsao AS. Use of immune checkpoint inhibitors in mesothelioma. *Curr Treat Options Oncol* 2019;20:18.
- Baumann F, Ambrosi J-P, Carbone M. Asbestos is not just asbestos: an unrecognised health hazard. *Lancet Oncol* 2013;14:576-8.
- Carbone M, Kanodia S, Chao A, *et al.* Consensus report of the 2015 Weinman International Conference on mesothelioma. *J Thorac Oncol* 2016;11:1246-62.
- Goodman JE, Nascarella MA, Valberg PA. Ionizing radiation: a risk factor for mesothelioma. *Cancer Causes Control* 2009;20:1237-54.
- Vivero M, Bueno R, Chiriac LR. Clinicopathologic and genetic characteristics of young patients with pleural diffuse malignant mesothelioma. *Mod Pathol* 2018;31:122-31.
- Attanous RL, Churg A, Galateau-Salle F, *et al.* Malignant mesothelioma and its non-asbestos causes. *Arch Pathol Lab Med* 2018;142:753-60.
- Hmeljak J, Sanchez-Vega F, Hoadley KA, *et al.* Integrative molecular characterization of malignant pleural mesothelioma. *Cancer Discov* 2018;8:1548-65.
- Bueno R, Stawiski EW, Goldstein LD, *et al.* Comprehensive genomic analysis of malignant pleural mesothelioma identifies recurrent mutations, gene fusions and splicing alterations. *Nat Genet* 2016;48:407-16.
- Mansfield AS, Peikert T, Smadbeck JB, *et al.* Neoantigenic potential of complex chromosomal rearrangements in mesothelioma. *J Thorac Oncol* 2019;14:276-87.
- Yoshikawa Y, Emi M, Hashimoto-Tamaoki T, *et al.* High-Density array-CGH with targeted NGS unmask multiple noncontiguous minute deletions on chromosome 3p21 in mesothelioma. *Proc Natl Acad Sci U S A* 2016;113:13432-7.
- Carbone M, Yang H, Gaudino G. Does chromothripsis make mesothelioma an immunogenic cancer? *J Thorac Oncol* 2019;14:157-9.
- Hanahan D, Weinberg RA. Hallmarks of cancer: the next generation. *Cell* 2011;144:646-74.
- Sharpe AH, Freeman GJ. The B7-CD28 superfamily. *Nat Rev Immunol* 2002;2:116-26.
- Keir ME, Butte MJ, Freeman GJ, *et al.* PD-1 and its ligands in tolerance and immunity. *Annu Rev Immunol* 2008;26:677-704.
- Freeman GJ, Long AJ, Iwai Y, *et al.* Engagement of the PD-1 immunoinhibitory receptor by a novel B7 family member leads to negative regulation of lymphocyte activation. *J Exp Med* 2000;192:1027-34.
- Dong H, Strome SE, Salomao DR, *et al.* Tumor-Associated B7-H1 promotes T-cell apoptosis: a potential mechanism of immune evasion. *Nat Med* 2002;8:793-800.
- Schreiber RD, Old LJ, Smyth MJ. Cancer immunoeediting: integrating immunity's roles in cancer suppression and promotion. *Science* 2011;331:1565-70.
- Vesely MD, Kershaw MH, Schreiber RD, *et al.* Natural innate and adaptive immunity to cancer. *Annu Rev Immunol* 2011;29:235-71.
- Pardoll DM. The blockade of immune checkpoints in cancer immunotherapy. *Nat Rev Cancer* 2012;12:252-64.
- Ujiiie H, Kadota K, Nitadori J-I, *et al.* The tumoral and stromal immune microenvironment in malignant pleural mesothelioma: a comprehensive analysis reveals prognostic immune markers. *Oncoimmunology* 2015;4:e1009285.
- Chéné A-L, d'Almeida S, Blondy T, *et al.* Pleural effusions from patients with mesothelioma induce recruitment of monocytes and their differentiation into M2 macrophages. *J Thorac Oncol* 2016;11:1765-73.
- Wong RM, Scotland RR, Lau RL, *et al.* Programmed death-1 blockade enhances expansion and functional capacity of human melanoma antigen-specific CTLs. *Int Immunol* 2007;19:1223-34.
- Borghaei H, Paz-Ares L, Horn L, *et al.* Nivolumab versus docetaxel in advanced Nonsquamous non-small-cell lung cancer. *N Engl J Med* 2015;373:1627-39.
- Gandhi L, Rodríguez-Abreu D, Gadgeel S, *et al.* Pembrolizumab plus chemotherapy in metastatic non-small-cell lung cancer. *N Engl J Med* 2018;378:2078-92.
- Combaz-Lair C, Galateau-Sallé F, McLeer-Florin A, *et al.* Immune biomarkers PD-1/PD-L1 and TLR3 in malignant pleural mesotheliomas. *Hum Pathol* 2016;52:9-18.
- Calabrò L, Morra A, Giannarelli D, *et al.* Tremelimumab combined with durvalumab in patients with mesothelioma (NIBIT-MESO-1): an open-label, non-randomised, phase 2 study. *Lancet Respir Med* 2018;6:451-60.
- Scherpereel A, Mazieres J, Greillier L, *et al.* Nivolumab or nivolumab plus ipilimumab in patients with relapsed malignant pleural mesothelioma (IFCT-1501 MAPS2): a multicentre, open-label, randomised, non-comparative, phase 2 trial. *Lancet Oncol* 2019;20:239-53.
- Disselhorst MJ, Quispel-Janssen J, Lalezari F, *et al.* Ipilimumab and nivolumab in the treatment of recurrent malignant pleural mesothelioma (initiate): results of a prospective, single-arm, phase 2 trial. *Lancet Respir Med* 2019;7:260-70.
- Cedrès S, Ponce-Aix S, Zugazagoitia J, *et al.* Analysis of expression of programmed cell death 1 ligand 1 (PD-L1) in malignant pleural mesothelioma (MPM). *PLoS One* 2015;10:e0121071.
- Mansfield AS, Roden AC, Peikert T, *et al.* B7-H1 expression in malignant pleural mesothelioma is associated with sarcomatoid histology and poor prognosis. *J Thorac Oncol* 2014;9:1036-40.
- Nowak AK, McDonnell A, Cook A. Immune checkpoint inhibition for the treatment of mesothelioma. *Expert Opin Biol Ther* 2019;19:697-706.
- Mutti L, Peikert T, Robinson BWS, *et al.* Scientific advances and new frontiers in mesothelioma therapeutics. *J Thorac Oncol* 2018;13:1269-83.
- Hotta K, Matsuo K, Ueoka H, *et al.* Meta-Analysis of randomized clinical trials comparing cisplatin to carboplatin in patients with advanced non-small-cell lung cancer. *J Clin Oncol* 2004;22:3852-9.
- Hotta K, Matsuo K, Ueoka H, *et al.* Addition of platinum compounds to a new agent in patients with advanced non-small-cell lung cancer: a literature based meta-analysis of randomised trials. *Ann Oncol* 2004;15:1782-9.
- Hotta K, Matsuo K. Long-Standing debate on cisplatin- versus carboplatin-based chemotherapy in the treatment of advanced non-small cell lung cancer. *J Thorac Oncol* 2007;2:96.
- Hotta K, Fujiwara Y, Matsuo K, *et al.* Recent improvement in the survival of patients with advanced nonsmall cell lung cancer enrolled in phase III trials of first-line, systemic chemotherapy. *Cancer* 2007;109:939-48.
- Hotta K, Takigawa N, Hisamoto-Sato A, *et al.* Reappraisal of short-term low-volume hydration in cisplatin-based chemotherapy: results of a prospective feasibility study in advanced lung cancer in the Okayama lung cancer Study Group trial 1002. *Jpn J Clin Oncol* 2013;43:1115-23.
- Ninomiya K, Hotta K, Hisamoto-Sato A, *et al.* Short-Term low-volume hydration in cisplatin-based chemotherapy for patients with lung cancer: the second prospective feasibility study in the Okayama lung cancer Study Group trial 1201. *Int J Clin Oncol* 2016;21:81-7.
- Hotta K, Ninomiya K, Takigawa N, *et al.* Reappraisal of short-term low-volume hydration in cisplatin-based chemotherapy; hoping for it as a public domain. *Jpn J Clin Oncol* 2015;45:603-4.
- Nishii K, Hotta K, Ninomiya K, *et al.* Programmed cell death-ligand 1 expression and efficacy of cisplatin-based chemotherapy in lung cancer: a sub-analysis of data from the two Okayama lung cancer Study Group prospective feasibility studies. *Respir Investig* 2019;57:460-5.
- Vogelzang NJ, Rusthoven JJ, Symanowski J, *et al.* Phase III study of pemetrexed in combination with cisplatin versus cisplatin alone in patients with malignant pleural mesothelioma. *J Clin Oncol* 2003;21:2636-44.

- 46 Zalcman G, Mazieres J, Margery J, *et al.* Bevacizumab for newly diagnosed pleural mesothelioma in the mesothelioma Avastin cisplatin pemetrexed study (maps): a randomised, controlled, open-label, phase 3 trial. *Lancet* 2016;387:1405–14.
- 47 Scagliotti GV, Gaafar R, Nowak AK, *et al.* Nintedanib in combination with pemetrexed and cisplatin for chemotherapy-naïve patients with advanced malignant pleural mesothelioma (LUME-Meso): a double-blind, randomised, placebo-controlled phase 3 trial. *Lancet Respir Med* 2019;7:569–80.
- 48 Tsao AS, Lindwasser OW, Adjei AA, *et al.* Current and future management of malignant mesothelioma: a consensus report from the National Cancer Institute thoracic malignancy Steering Committee, International association for the study of lung cancer, and mesothelioma applied research Foundation. *J Thorac Oncol* 2018;13:1655–67.
- 49 Nowak A, Kok P, Lesterhuis W, *et al.* OA08.02 DREAM - A Phase 2 Trial of Durvalumab with First Line Chemotherapy in Mesothelioma: Final Result. *J Thorac Oncol* 2018;13:S338–9.
- 50 Fujimoto N, Aoe K, Kozuki T, *et al.* A phase II trial of first-line combination chemotherapy with cisplatin, pemetrexed, and nivolumab for unresectable malignant pleural mesothelioma: a study protocol. *Clin Lung Cancer* 2018;19:e705–7.
- 51 Kindler HL, Ismaila N, Armato SG, *et al.* Treatment of malignant pleural mesothelioma: American Society of clinical oncology clinical practice guideline. *J Clin Oncol* 2018;36:1343–73.
- 52 Krug LM, Kindler HL, Calvert H, *et al.* Vorinostat in patients with advanced malignant pleural mesothelioma who have progressed on previous chemotherapy (VANTAGE-014): a phase 3, double-blind, randomised, placebo-controlled trial. *Lancet Oncol* 2015;16:447–56.
- 53 Quispel-Janssen J, van der Noort V, de Vries JF, *et al.* Programmed death 1 blockade with nivolumab in patients with recurrent malignant pleural mesothelioma. *J Thorac Oncol* 2018;13:1569–76.
- 54 Okada M, Kijima T, Aoe K, *et al.* Clinical Efficacy and Safety of Nivolumab: Results of a Multicenter, Open-label, Single-arm, Japanese Phase II study in Malignant Pleural Mesothelioma (MERIT). *Clin Cancer Res* 2019;25:5485–92.
- 55 Alley EW, Lopez J, Santoro A, *et al.* Clinical safety and activity of pembrolizumab in patients with malignant pleural mesothelioma (KEYNOTE-028): preliminary results from a non-randomised, open-label, phase 1B trial. *Lancet Oncol* 2017;18:623–30.
- 56 Desai A, Karrison T, Rose B, *et al.* Phase II trial of pembrolizumab (NCT02399371) in previously treated malignant mesothelioma: final analysis, in IASLC (ED). 19th IASLC World Conference on Lung Cancer Toronto, Canada, 2018.
- 57 Hassan R, Thomas A, Nemunaitis JJ, *et al.* Efficacy and safety of avelumab treatment in patients with advanced unresectable mesothelioma: phase 1B results from the javelin solid tumor trial. *JAMA Oncol* 2019;5:351–7.
- 58 Calabrò L, Morra A, Fonsatti E, *et al.* Tremelimumab for patients with chemotherapy-resistant advanced malignant mesothelioma: an open-label, single-arm, phase 2 trial. *Lancet Oncol* 2013;14:1104–11.
- 59 Calabrò L, Morra A, Fonsatti E, *et al.* Efficacy and safety of an intensified schedule of tremelimumab for chemotherapy-resistant malignant mesothelioma: an open-label, single-arm, phase 2 study. *Lancet Respir Med* 2015;3:301–9.
- 60 Maio M, Scherpereel A, Calabrò L, *et al.* Tremelimumab as second-line or third-line treatment in relapsed malignant mesothelioma (determine): a multicentre, international, randomised, double-blind, placebo-controlled phase 2B trial. *Lancet Oncol* 2017;18:1261–73.
- 61 Puzanov I, Diab A, Abdallah K, *et al.* Managing toxicities associated with immune checkpoint inhibitors: consensus recommendations from the Society for immunotherapy of cancer (SITC) toxicity management Working group. *J Immunother Cancer* 2017;5:95.
- 62 Hellmann MD, Ciuleanu T-E, Pluzanski A, *et al.* Nivolumab plus ipilimumab in lung cancer with a high tumor mutational burden. *N Engl J Med* 2018;378:2093–104.



Nivolumab for the treatment of unresectable pleural mesothelioma

Katsuyuki Hotta, Nobukazu Fujimoto, Toshiyuki Kozuki, Keisuke Aoe & Katsuyuki Kiura

To cite this article: Katsuyuki Hotta, Nobukazu Fujimoto, Toshiyuki Kozuki, Keisuke Aoe & Katsuyuki Kiura (2020) Nivolumab for the treatment of unresectable pleural mesothelioma, Expert Opinion on Biological Therapy, 20:2, 109-114, DOI: [10.1080/14712598.2020.1703945](https://doi.org/10.1080/14712598.2020.1703945)

To link to this article: <https://doi.org/10.1080/14712598.2020.1703945>

 View supplementary material [↗](#)

 Accepted author version posted online: 11 Dec 2019.
Published online: 16 Dec 2019.

 Submit your article to this journal [↗](#)

 Article views: 46

 View related articles [↗](#)

 View Crossmark data [↗](#)

DRUG EVALUATION



Nivolumab for the treatment of unresectable pleural mesothelioma

Katsuyuki Hotta^{a,b}, Nobukazu Fujimoto^c, Toshiyuki Kozuki^d, Keisuke Aoe^e and Katsuyuki Kiura^b

^aCenter for Innovative Clinical Medicine, Okayama University Hospital, Okayama, Japan; ^bDepartment of Respiratory Medicine, Okayama University Hospital, Okayama, Japan; ^cDepartment of Medical Oncology and Medicine, Okayama Rosai Hospital, Okayama, Japan; ^dDepartment of Respiratory Medicine, National Hospital Organization Shikoku Cancer Center, Matsuyama, Japan; ^eDepartment of Medical Oncology, National Hospital Organization Yamaguchi-Ube Medical Center, Ube, Japan

ABSTRACT

Introduction: Platinum-based chemotherapy is the current first-line standard therapy for unresectable malignant pleural mesothelioma (MPM). Recently, immune-checkpoint inhibitors (ICI) have been intensively investigated as treatment options for this disease. Nivolumab, an anti-programmed cell death (PD)-1 agent, was one of the first drugs used and is representative of available ICIs.

Areas covered: This review discusses previous relevant reports and current ongoing trials of nivolumab. The efficacy and safety of nivolumab have been investigated mostly in second-line or later treatment settings as both monotherapy and in combination with other ICIs. Particularly, nivolumab monotherapy yielded promising efficacy with an objective response rate of 29% and median overall survival of 17.3 months in salvage settings in the single-arm, Japanese phase 2 trial (MERIT). Notably, the study led to Japanese approval of nivolumab for unresectable recurrent MPM. Several trials with monotherapy or cotherapy with nivolumab have commenced, including randomized trials of nivolumab monotherapy vs. placebo in the salvage setting, and cotherapy with nivolumab and ipilimumab vs. the platinum doublet in the frontline setting.

Expert opinion: Nivolumab seems like a reasonable option for unresectable, relapsed MPM despite the lack of randomized trial data. Ongoing pivotal trials will confirm its efficacy.

ARTICLE HISTORY

Received 19 August 2019
Accepted 9 December 2019

KEYWORDS

Mesothelioma; immune checkpoint inhibitor; PD-1; PD-L1; CTLA-4

1. Introduction

Malignant pleural mesothelioma (MPM) is a rare and aggressive malignancy that occurs in the mesothelial surface of the pleural and peritoneal cavities, and the pericardium [1]. The disease is closely associated with asbestos exposure and approximately 80% of MPM cases are caused by occupational or environmental exposure [2–6]. Despite policies banning asbestos use in Western countries, MPM has continued to increase in many countries where asbestos is still extensively used. It is expected that 500,000 new cases of MPM will be diagnosed in men with occupational exposure in Europe alone [7]. The prognosis of MPM is poor, with a median survival time (MST) of 18 months and a 5-year overall survival (OS) rate of < 5% [8]. In particular, those with unresectable, advanced disease at the initial presentation characteristically have a worse prognosis than patients in earlier stages. This disappointing outcome is principally due to the lack of efficient screening methods and effective systemic therapy [9,10]. Therefore, innovative agents are urgently anticipated and required.

The role of peripheral immune tolerance with the co-inhibitory immune-checkpoint molecules cytotoxic T-lymphocyte antigen 4 (CTLA-4) and programmed cell death 1 (PD-1) and its ligand (PD-L1) have been extensively investigated. PD-L1 is a transmembrane protein that binds to PD-1 and is expressed on cytotoxic T cells and other immune cells [11,12].

Various types of tumor cells have been shown to exhibit up-regulated PD-L1 expression levels, which enables them to escape the immune response and keep proliferating [11]. Based on this background knowledge, anti-CTLA4, PD-1, and PD-L1 antibodies have been widely developed against various advanced malignancies. In this review, among the available immune-checkpoint inhibitors (ICI), we specifically discuss nivolumab, which blocks the PD-1 receptor, focusing on relevant previous trial reports and ongoing trials of unresectable MPM both in the first-line and salvage settings.

2. Basic information on nivolumab

Nivolumab is a human monoclonal antibody (HuMAb; immunoglobulin G4 [IgG4]-S228P) that targets the PD-1 cluster of the CD279 cell surface membrane receptor [13,14] (See Box 1). Nivolumab is expressed in Chinese hamster ovary cells and is produced using standard mammalian cell culture and chromatographic purification technologies. The agent was approved for the treatment of several types of tumors in various countries including the United States of America and Japan in 2014 and the European Union in 2015.

The interaction of PD-1 with its ligands, PD-L1 and PD-L2, can be blocked by nivolumab, leading to enhanced T-cell proliferation and interferon (IFN- γ) release *in vitro* [15].

CONTACT Katsuyuki Hotta  khotta@okayama-u.ac.jp  Center for Clinical Innovative Medicine, Okayama University Hospital, 2-5-1, Shikata-cho, Okayama 700-8558, Japan

 The supplementary data for this article can be accessed [here](#).

© 2019 Informa UK Limited, trading as Taylor & Francis Group

Nivolumab binds with high affinity to activated human T-cells expressing cell surface PD-1 and cynomolgus monkey PD-1. Through a mixed lymphocyte reaction, nivolumab enhances reproducible IFN- γ release in a concentration-dependent manner [16].

In a population pharmacokinetic model, the overall distributions of nivolumab exposure are comparable after treatment with either 3 mg/kg or 240 mg nivolumab. The predicted range of nivolumab exposure following a 240 mg fixed dose across a 35 to 160 kg weight range is maintained well below corresponding exposure to the well-tolerated 10 mg/kg biweekly dosage of nivolumab. That is why a flat dose has been adopted in more recent nivolumab clinical trials.

The clinical activity and safety of nivolumab have been evaluated in patients with various malignancies including melanoma, non-small cell lung cancer (NSCLC), renal cell carcinoma, classical Hodgkin lymphoma, urothelial carcinoma, and head and neck carcinoma as a monotherapy or in combination with chemotherapy, targeted therapies, and other immunotherapies. In contrast, in mesothelioma, the clinical establishment of nivolumab has progressed slowly mainly because of the extremely small patient population and the difficulty associated with their accrual into relevant trials.

3. Nivolumab in the first-line setting

Patients with unresectable disease are often treated with systemic cytotoxic chemotherapy not as a cure but for disease management. Currently, the doublet chemotherapy of cisplatin and pemetrexed, antifolates, is the standard regimen for patients with frontline, unresectable MPM [17], followed by the regular approval in NSCLC [18–25]. However, the efficacy of this regimen is limited, with an objective response rate (ORR) of up to 30–40%, and some cancer-related symptoms can be relieved with the therapy, while the median OS is approximately 1 year in this disease setting [26].

Platinum agents can enhance the effector immune response through modulation of PD-L1 [27]. The observed encouraging results might extend ICI use to first-line treatment of MPM, particularly in combination with the standard

platinum-based chemotherapy. Based on this background knowledge, ICIs have been tested in untreated, unresectable mesothelioma. Unfortunately, to date, no nivolumab trials have been reported (Table 1), while the potential benefit of adding durvalumab, a PD-L1 inhibitor, to the cisplatin and pemetrexed standard regimen was tested in 54 patients with untreated, unresectable MPM [28]. The study showed promising results and the primary endpoint of progression-free survival (PFS) at 6 months was 57%, with an ORR of 48% and median duration of response of 6.5 months.

In parallel with this promising trial, in January 2018 we commenced a phase 2 trial of nivolumab as a third agent in combination with the standard chemotherapy of cisplatin and pemetrexed for untreated, unresectable MPM [29] (Table 2). The primary endpoint is centrally reviewed ORR, while the secondary endpoints are disease control rate (DCR), OS, PFS, and adverse events (AEs). This is an exploratory trial with a target enrollment of 18 Japanese patients with good performance status.

As a different approach, the survival advantage of frontline combination immunotherapy with nivolumab and ipilimumab over platinum and pemetrexed is currently under investigation in 606 patients with unresectable MPM. This is the industry-sponsored, large-scaled, randomized phase 3, CheckMate 743 study (NCT02899299), initiated in October, 2016, with an estimated completion date of 15 April 2022.

4. Single-agent nivolumab in the salvage setting

No systemic treatment has been proven effective for mesothelioma refractory to first-line platinum doublet therapy in randomized clinical trials. Although multiple systemic therapeutic options have been investigated, there has been little progress [30]. Cotherapy with vinorelbine or gemcitabine or rechallenge with platinum therapy is often chosen in clinical practice, but is rarely effective [31,32]. Therefore, this challenging situation has created the most reasonable clinical setting for developing new treatment strategies using ICIs.

Currently, four ICIs have been tested in the second-line or later setting, including nivolumab as a monotherapy or in combination with other ICIs. Single-agent nivolumab was evaluated

Table 1. Relevant nivolumab trial results in the salvage setting.

Trial	Year	Phase	RCT	Drug	Primary endpoint	No.	ORR	mPFS (mo)	MST (mo)	Ref.
MERIT	2018	2	No	Nivolumab	OR	34	29%	6.1	17.3	[34]
NivoMes	2018	2	No	Nivolumab	DCR	34	24%	2.6	11.8	[33]
MAPS2	2019	2	Yes	Nivolumab/ipilimumab	DCR	62	28%	5.6	15.9	[36]
				Nivolumab		63	19%	4.0	11.9	
INITIATE	2019	2	No	Nivolumab/ipilimumab	DCR	34	29%	6.2	NR	[37]

Abbreviations: RCT; randomized controlled trial, ORR; objective response rate, mPFS; median progression-free survival, MST; median survival time, DCR; disease control rate, OS; overall survival, NR; not reached.

Table 2. Ongoing relevant nivolumab trials.

Trial	Country	Phase	RCT	Setting	Regimen	Primary endpoint	No. of planned pts	Study start date	Registration No.
CM743	Global	3	Yes	Frontline	Nivolumab/ipilimumab vs. p-pem	OS	606	25/10/16	NCT02899299
JME-001	Japan	2	No	Frontline	cis-pem/nivolumab	OR	18	20/01/18	UMIN000030892
CONFIRM	UK	3	Yes	Salvage	Nivolumab vs. placebo	OS	336	28/03/17	NCT03063450

Abbreviations: RCT, randomized controlled trial; pts, patients; cis-pem, cisplatin and pemetrexed; p-pem, platinum (cisplatin or carboplatin) and pemetrexed; OS, overall survival; OR, objective response.

in a single-center, single-arm phase 2 trial (NivoMes) for patients with recurrent MPM [33]. The study revealed a DCR at 12 weeks, set as the primary endpoint, of 47% (16 of 34), including eight partial responders [33], while PD-L1 expression failed to predict responses in this population. The median PFS and MST were 2.6 and 11.8 months, respectively, and nine (26%) patients developed grade ≥ 3 treatment-related AEs, including gastrointestinal disorders and pneumonitis. The investigators documented that single-agent nivolumab had meaningful clinical efficacy and a manageable safety profile in previously treated patients with MPM.

Japanese investigators conducted the single-arm phase 2 MERIT study, assessing the efficacy of nivolumab monotherapy in 34 previously treated patients with pleural MPM [34]. The primary endpoint was centrally defined ORR while AEs, PFS, and OS were also evaluated. The ORR was 29% (10/34, 95% confidence interval [CI]: 16.846.2), which was clearly affected by PD-L1 expression level, with an ORR of 40 and 8% in PD-L1 $\geq 1\%$ and $<1\%$, respectively. The ORR also seemed to be differently stratified by histologic subtypes: 26%, 67%, and 25% for epithelioid, sarcomatoid, and biphasic histologies, respectively. The survival data were also favorable with median PFS and MST of 6.1 and 17.3 months, respectively while 26 patients (76%) experienced treatment-related AEs. The results of this study led the Japanese government to approve nivolumab monotherapy for unresectable recurrent MPM.

5. Combination nivolumab and anti-CTLA-4 antibody in the salvage setting

Assuming that combining ICIs can enhance their upregulation of tumor immunogenicity [35], the combination of an anti-CTLA-4 antibody with nivolumab was investigated in several clinical trials. A randomized phase 2 trial (IFCT MAPS2) evaluated the benefits of a combination of nivolumab and ipilimumab over nivolumab monotherapy in MPM progression after first-line or second-line pemetrexed and platinum-based treatments (Supplemental Figure 1) [36]. A total of 125 relapsed MPM patients were allocated to the cotherapy or monotherapy arm. The primary endpoint of disease control at 12 weeks in the first 108 patients was met in both groups: 27 (50%, 95% CI: 37–63) of 54 in the combination arm and 24 (44%, 95% CI: 31–58) of 54 patients in the monotherapy arm reached centrally assessed disease control at 12 weeks. The efficacy of both regimens was enhanced especially in high PD-L1-expressing tumors ($>25\%$), with an ORR of 63% to 71%. Sixteen (26%) of 61 patients in the combination arm and nine (14%) of 63 in the monotherapy arm had grade ≥ 3 toxicities, and the most frequent were hepatic injury, asthenia, and lipase increase. The authors concluded that nivolumab monotherapy or nivolumab plus ipilimumab cotherapy both showed promising activity in relapsed patients with malignant pleural mesothelioma, without unexpected toxicity.

In addition to the MAPS2 trial, the efficacy of nivolumab plus ipilimumab was also investigated in the single-arm, phase 2 INITIATE trial in patients with mesothelioma refractory to platinum-based chemotherapy [37]. The primary endpoint was also set as disease control at 12 weeks. Thirty-four patients were evaluable for the response assessment at 12 weeks, and

10 (29%) and 13 (38%) achieved partial response (PR) and stable disease (SD), respectively, resulting in a DCR of 68% (23/34, 95% CI: 50–83). Notably, this study showed similar safety and efficacy results to those of MAPS2 trial [36,37]. This study also showed the association of tumor PD-L1 expression with the efficacy of the cotherapy. The most common AEs were skin disorders, infusion-related reactions, and fatigue. Grade 3 treatment-related AEs were reported in 12 (34%) of the 35 patients.

Along with these reported trials, UK investigators have commenced a randomized, placebo controlled, double blind trial (CONFIRM) comparing nivolumab monotherapy with a placebo in the salvage setting (NCT03063450). The study will recruit 336 patients with mesothelioma who have a history of at least one prior line of treatment at 25 institutes in the UK over a 4-year period. All patients are to be treated for 1 year. The primary endpoint is set as OS while the secondary endpoints are ORR, safety, and patient-oriented outcome. The actual study start date was 28 March 2017, and the estimated study completion date will be July 2021.

6. Conclusion

We have reviewed clinical trial results and ongoing trials related to nivolumab therapy in unresectable MPM. In the frontline setting, the addition of nivolumab to standard cytotoxic chemotherapy is being investigated to overcome the current poor prognosis. With the expectation of enhancing tumor immunogenicity, the combination of anti-CTLA-4 antibody and nivolumab is also under investigation. In the salvage setting, the single-arm, phase 2 MERIT trial showed a favorable ORR of 29% [34], leading to the approval of nivolumab monotherapy in Japan. Other trials have also successfully demonstrated similar efficacy of this agent. Although, to date, no randomized trials have demonstrated a robust survival advantage of nivolumab over other therapies, ongoing pivotal trial may confirm its efficacy.

7. Expert opinion

Nivolumab has been extensively evaluated for efficacy and safety in treating unresectable MPM (Table 2) [33,34,36,37], similar to investigations conducted in other malignancies [38]. However, in contrast to trials of other tumors, MPM trials were often designed as single-arm studies with small sample sizes and OS or PFS was not set as the primary endpoint [33,34,36,37]. Thus, in terms of activity, it is still unknown whether nivolumab monotherapy possesses true survival advantage over other therapies because of the insufficient efficacy data.

However, the following critical points should be considered a focus: 1) single-agent pembrolizumab, another PD-1 antibody, also showed an ORR of approximately 20% with MST of 12 to 18 months; 2) no clearly effective agents are currently available in the salvage setting; and 3) the ORR in the MERIT study was better than that in studies of other malignancies (i.e. ORR of 19%–20% in the study of nivolumab monotherapy for recurrent NSCLC [39,40]). Thus, some, but not all patients could benefit substantially from anti-PD-1 antibodies in the

Box 1. Drug summary box.

Drug name	Nivolumab (OPDIVO)
Phase	Approved
Indication	OPTIVO is indicated for the second – or later-line treatment of mesothelioma by the Ministry of Health, Labor and Welfare of Japan.
Pharmacology description	See the previously published review article [35].
Route of administration	Intravenous infusion
Chemical structure	See the previously published review article [35].
Pivotal trial	The MERIT study [34], a single-arm, Japanese, phase II clinical trial of nivolumab in the treatment of patients with malignant pleural mesothelioma in the second- or third-line setting. The study showed nivolumab monotherapy showed activity. This directly led to the approval of nivolumab for mesothelioma treatment in Japan.

salvage setting. Moreover, based on the low incidence of mesothelioma, we assume that the approval based only on the results of single-arm phase II clinical trials is reasonable, making the agent available to more patients.

However, it is important to note that after approval, the activity of nivolumab should be cautiously reevaluated through post-market surveillance and relevant research with larger study populations. In addition, verification of the approval in large-scale randomized trials is essential, and it is worth paying special attention to the expected results of the CONFIRM trial (NCT03063450). Whether the Japanese MERIT study results would be reproduced by this trial is of great interest [34].

In addition, Mansfield and colleagues stressed the importance of using contemporaneous synthetic control groups to develop surrogate/predictive markers for efficacy [41]. Such an approach would herald the next potential trend of strategies for designing clinical trials of ICIs in the treatment of rare malignancies including mesothelioma.

Similarly, in other malignancies including melanoma, renal cell carcinoma, and NSCLC [42], cotherapy with nivolumab and ipilimumab may also have a potent survival advantage even in untreated, unresectable MPM. Consequently, the Checkmate 743 trial (NCT02899299) may directly change the existing treatment strategy in the frontline setting. Further accumulation of forthcoming relevant data is strongly needed to improve the use of ICIs in daily clinical practice. Ongoing relevant studies are currently strongly expected to further confirm the role of immunotherapy in several disease settings, in addition to MERIT study results, hopefully leading to changes in the current historical prognosis of mesothelioma.

Funding

This study was supported by grants-in-aid from the Ministry of Health, Labor, and Welfare, Japan.

Declaration of interest

K Hotta has received honoraria outside the current work from AstraZeneca, Ono Pharmaceutical,

BMS, MSD, Eli Lilly Japan, Nihon Kayaku, Taiho Pharmaceutical, and Chugai Pharmaceutical. K Hotta has received research funding outside of the current work from AstraZeneca, BMS, and Eli Lilly Japan. N Fujimoto

has received consultancy fees from Boehringer Ingelheim, Ono, Bristol-Myers Squibb, Kyorin, and Kissei, and honoraria or research funding from Ono, Boehringer Ingelheim, Bristol-Myers Squibb, Eli Lilly Japan, and MSD in the subject matter discussed in this manuscript.

N Fujimoto also has received research funding outside of the current work from Hisamitsu, Chugai,

Taiho, Novartis, and GlaxosmithKline. T Kozuki reports grants and personal fees from Chugai Pharmaceutical Co., grants and personal fees from AstraZeneca, grants and personal fees from Eli Lilly Japan, personal fees from Taiho, grants and personal fees from Bristol-Myers, personal fees from Ono, personal fees from MSD, personal fees from Pfizer Japan, personal fees from Kyowa Hakko Kirin, personal fees from Nippon Beohringer Ingelheim, grants from Merck Biophama, outside the submitted work. K Aoe has received consultancy fees from Boehringer Ingelheim, Ono, and

Bristol-Myers Squibb, and honoraria or research funding from Ono, Bristol-Myers Squibb, Eli Lilly Japan, Kissei and MSD in the subject matter discussed in this manuscript. K Aoe also has received research funding outside of the current work from Novartis. AstraZeneca, Ono, Bristol-Myers Squibb, and MSD. K Kiura reports grants from Daiichi-Sankyo, Taiho, Chugai, Teijin, Pfizer,

Boehringer Ingelheim, Nipponkayaku, Shionogi, Ono, Kyorin, MSD, and BMS, outside the submitted work. K Kiura also reports personal fees from AZ, Lilly, Novartis, BMS, Chugai, Pfizer, Taiho, Ono,

Boehringer Ingelheim, and MSD, outside the submitted work. The authors have no other relevant affiliations or financial involvement with any organization or entity with a financial interest in or financial conflict with the subject matter or materials discussed in the manuscript apart from those disclosed.

Reviewer disclosures

One of the reviewers on this manuscript has received consulting fees from Epizyme, Aldeyra, Novocure, and Atara; speaking honorarium from Medical Learning Institute; research funding to MSK: MedImmune, Epizyme, Polaris, Sellas Life Sciences, Bristol-Myers Squibb, Millenium, Roche, and Curis; and holds a leadership position in the Mesothelioma Applied Research Foundation (uncompensated). Peer reviewers on this manuscript have no other relevant financial relationships or otherwise to disclose.

References

Papers of special note have been highlighted as either of interest (*) or of considerable interest () to readers.**

1. Ministry of the Environment Government of Japan. [cited 2019 Aug 15]. Available from: www.env.go.jp/air/asbestos/registration/
2. Jasani B, Gibbs A. Mesothelioma not associated with asbestos exposure. *Arch Pathol Lab Med.* 2012;136:262–267.

3. Roe OD, Stella GM. Malignant pleural mesothelioma: history, controversy and future of a manmade epidemic. *Eur Respir Rev*. 2015;24:115–131.
4. Carbone M. Simian virus 40 and human tumors: it is time to study mechanisms. *J Cell Biochem*. 1999;76:189–193.
5. Gazdar AF, Carbone M. Molecular pathogenesis of malignant mesothelioma and its relationship to simian virus 40. *Clin Lung Cancer*. 2003;5:177–181.
6. Carbone M, Rizzo P, Pass H. Simian virus 40: the link with human malignant mesothelioma is well established. *Anticancer Res*. 2000;20:875–877.
7. Peto J, Decarli A, La Vecchia C, et al. The European mesothelioma epidemic. *Br J Cancer*. 1999;79:666–672.
8. Mutti L, Peikert T, Robinson BWS, et al. Scientific advances and new frontiers in mesothelioma therapeutics. *J Thorac Oncol*. 2018 Sep;13(9):1269–1283.
9. Carbone M, Adusumilli PS, Alexander HR Jr, et al. Mesothelioma: scientific clues for prevention, diagnosis, and therapy. *CA Cancer J Clin*. 2019;69:402–429. (in press).
10. Forde PM, Scherpereel A, Tsao AS. Use of immune checkpoint inhibitors in mesothelioma. *Curr Treat Options Oncol*. 2019;20:18.
11. Sweis RF, Luke JJ. Mechanistic and pharmacologic insights on immune checkpoint inhibitors. *Pharmacol Res*. 2017;120:1–9.
12. Ninomiya K, Hotta K. Pembrolizumab for the first-line treatment of non-small cell lung cancer. *Expert Opin Biol Ther*. 2018 Oct;18(10):1015–1021.
13. Sharma P, Allison JP. The future of immune checkpoint therapy. *Science*. 2015 Apr 3;348(6230):56–61.
14. Bedke J, Kruck S, Gakis G, et al. Checkpoint modulation—A new way to direct the immune system against renal cell carcinoma. *Hum Vaccin Immunother*. 2015;11(5):1201–1208.
15. Velu V, Titanji K, Zhu B, et al. Enhancing SIV-specific immunity in vivo by PD-1 blockade. *Nature*. 2009;458:206–210.
16. Wang C, Thudium KB, Han M, et al. In vitro characterization of the anti-PD-1 antibody nivolumab, BMS-936558, and in vivo toxicology in non-human primates. *Cancer Immunol Res*. 2014;2:846–856.
17. Vogelzang NJ, Rusthoven JJ, Symanowski J, et al. Phase III study of pemetrexed in combination with cisplatin versus cisplatin alone in patients with malignant pleural mesothelioma. *J Clin Oncol*. 2003;21:2636–2644.
 - **This is a traditional, pivotal study establishing the efficacy of cisplatin and pemetrexed combination chemotherapy.**
18. Hotta K, Matsuo K, Ueoka H, et al. Meta-analysis of randomized clinical trials comparing cisplatin to carboplatin in patients with advanced non-small-cell lung cancer. *J Clin Oncol*. 2004;22:3852–3859.
19. Hotta K, Matsuo K, Ueoka H, et al. Addition of platinum compounds to a new agent in patients with advanced non-small-cell lung cancer: a literature based meta-analysis of randomised trials. *Ann Oncol*. 2004;15:1782–1789.
20. Hotta K, Matsuo K. Long-standing debate on cisplatin- versus carboplatin-based chemotherapy in the treatment of advanced non-small-cell lung cancer. *J Thorac Oncol*. 2007;2:96.
21. Hotta K, Fujiwara Y, Matsuo K, et al. Recent improvement in the survival of patients with advanced non small cell lung cancer enrolled in phase III trials of first-line, systemic chemotherapy. *Cancer*. 2007;109:939–948.
22. Hotta K, Takigawa N, Hisamoto-Sato A, et al. Reappraisal of short-term low-volume hydration in cisplatin-based chemotherapy: results of a prospective feasibility study in advanced lung cancer in the Okayama lung cancer study group trial 1002. *Jpn J Clin Oncol*. 2013;43:1115–1123.
23. Ninomiya K, Hotta K, Hisamoto-Sato A, et al. Short-term low-volume hydration in cisplatin-based chemotherapy for patients with lung cancer: the second prospective feasibility study in the Okayama lung cancer study group trial 1201. *Int J Clin Oncol*. 2016;21:81–87.
24. Hotta K, Ninomiya K, Takigawa N, et al. Reappraisal of short-term low-volume hydration in cisplatin-based chemotherapy; hoping for it as a public domain. *Jpn J Clin Oncol*. 2015;45:603–604.
25. Nishii K, Hotta K, Ninomiya K, et al. Programmed cell death-ligand 1 expression and efficacy of cisplatin-based chemotherapy in lung cancer: a sub-analysis of data from the two Okayama lung cancer study group prospective feasibility studies. *Respir Investig*. 2019;57:460–465. (in press).
26. Tsao AS, Lindwasser OW, Adjei AA, et al. Current and future management of malignant mesothelioma: a consensus report from the national cancer institute thoracic malignancy steering committee, international association for the study of lung cancer, and mesothelioma applied research foundation. *J Thorac Oncol*. 2018 Nov;13(11):1655–1667.
27. Hato SV, Khong A, de Vries IJ, et al. Molecular pathways: the immunogenic effects of platinum-based chemotherapeutics. *Clin Cancer Res*. 2014;20:2831–2837.
28. Nowak A, Kok P, Lesterhuis W, et al. OA08.02 DREAM—a phase 2 trial of durvalumab with first line chemotherapy in mesothelioma: final result. *J Thorac Oncol*. 2018;13(10suppl):S338–S339.
29. Fujimoto N, Aoe K, Kozuki T, et al. A phase II trial of first-line combination chemotherapy with cisplatin, pemetrexed, and nivolumab for unresectable malignant pleural mesothelioma: a study protocol. *Clin Lung Cancer*. 2018 Sep;19(5):e705–e707.
 - **This is an ongoing, exploratory phase 2 trial of nivolumab as a third agent combined with the standard chemotherapy of cisplatin and pemetrexed for untreated, unresectable MPM.**
30. Krug LM, Kindler HL, Calvert H, et al. Vorinostat in patients with advanced malignant pleural mesothelioma who have progressed on previous chemotherapy (VANTAGE-014): a phase 3, double-blind, randomised, placebo-controlled trial. *Lancet Oncol*. 2015 Apr;16(4):447–456.
31. Kindler HL, Ismaila N, Armato SG 3rd, et al. Treatment of malignant pleural mesothelioma: American society of clinical oncology clinical practice guideline. *J Clin Oncol*. 2018;36:1343–1373.
32. Zauderer MG, Kass SL, Woo K, et al. Vinorelbine and gemcitabine as second- or third-line therapy for malignant pleural mesothelioma. *Lung Cancer*. 2014;84:271–274.
33. Quispel-Janssen J, van der Noort V, de Vries JF, et al. Programmed death 1 blockade with nivolumab in patients with recurrent malignant pleural mesothelioma. *J Thorac Oncol*. 2018;13:1569–1576.
 - **This study was a single-center, single-arm phase 2 trial to evaluate the efficacy and safety of single-agent nivolumab for patients with recurrent MPM.**
34. Okada M, Kijima T, Aoe K, et al. Clinical efficacy and safety of nivolumab: results of a multicenter, open-label, single-arm, Japanese phase 2 study in malignant pleural mesothelioma (MERIT). *Clin Cancer Res*. 2019;25:5485–5492. (in press).
 - **This was just a single-arm, nonrandomized study, but it led to the approval of nivolumab for MPM in Japan.**
35. Yap TA, Aerts JG, Papat S, et al. Novel insights into mesothelioma biology and implications for therapy. *Nat Rev Cancer*. 2017;17:475–488.
36. Scherpereel A, Mazieres J, Greillier L, et al. French cooperative thoracic intergroup. nivolumab or nivolumab plus ipilimumab in patients with relapsed malignant pleural mesothelioma (IFCT-1501 MAPS2): a multicentre, open-label, randomised, non-comparative, phase 2 trial. *Lancet Oncol*. 2019 Feb;20(2):239–253.
 - **This randomized phase 2 trial evaluated the advantage of combination nivolumab and ipilimumab over nivolumab monotherapy in MPM progressing after first-line or second-line pemetrexed and platinum-based treatments.**
37. Disselhorst MJ, Quispel-Janssen J, Lalezari F, et al. Ipilimumab and nivolumab in the treatment of recurrent malignant pleural mesothelioma (INITIATE): results of a prospective, single-arm, phase 2 trial. *Lancet Respir Med*. 2019 Mar;7(3):260–270.
 - **Independent of the MAPS2 trial, this single-arm, phase 2, INITIATE trial investigated the efficacy of nivolumab and ipilimumab in patients with mesothelioma refractory to platinum-based chemotherapy.**
38. Reck M, Rodríguez-Abreu D, Robinson AG, et al. KEYNOTE-024 investigators. Pembrolizumab versus chemotherapy for PD-L1-positive

- non-small-cell lung cancer. *N Engl J Med.* 2016 Nov 10;375(19):1823–1833.
39. Brahmer J, Reckamp KL, Baas P, et al. Nivolumab versus docetaxel in advanced squamous-cell non-small-cell lung cancer. *N Engl J Med.* 2015 Jul 9;373(2):123–135.
40. Borghaei H, Paz-Ares L, Horn L, et al. Nivolumab versus docetaxel in advanced nonsquamous non-small-cell lung cancer. *N Engl J Med.* 2015 Oct 22;373(17):1627–1639.
41. Mansfield AS, Zauderer MG. Nivo-lution in mesothelioma. *Clin Cancer Res.* 2019 Sep 15;25(18):5438–5440.
42. Motzer RJ, Tannir NM, McDermott DF, et al. CheckMate 214 investigators. Nivolumab plus ipilimumab versus sunitinib in advanced renal-cell carcinoma. *N Engl J Med.* 2018 Apr 5;378(14):1277–1290.
- **This pivotal randomized study clearly showed the survival advantage of combination therapy of nivolumab plus ipilimumab over the standard sunitinib monotherapy.**



Retrospective investigation on diagnostic process for benign asbestos pleural effusion (BAPE) using checklist

Takumi Kishimoto¹ | Nobukazu Fujimoto¹ | Keiichi Mizuhashi² | Satoko Kozawa³ | Motohiko Miura⁴

¹Research & Training Center for asbestos-related diseases, Okayama, Japan

²Toyama Rosai Hospital, Uozu, Japan

³Yokohama Rosai Hospital, Yokohama, Japan

⁴Tohoku Rosai Hospital, Sendai, Japan

Correspondence

Takumi Kishimoto, 1-10-25 Chikko Midorimachi, Minami-ku, Okayama 702-8055, Japan.

Email: nakisimt@okayamah.johas.go.jp

Funding information

This study is funded by The research and development, and the dissemination project on the occupational injuries and illnesses, the Japan Organization of Occupational Health and Safety.

Abstract

Objectives: In Japan, benign asbestos pleural effusion (BAPE) has been eligible for industrial accident compensation since 2003 as an asbestos-related disease despite the lack of good criteria. We compiled a criteria into a checklist of essential items and for excluding other diseases inducing pleural effusion as a diagnosis process.

Method: Thoracentesis was performed in order to confirm the presence of pleural effusion at the initial diagnosis, and 105 suspected BAPE patients were retrospectively examined. We compiled a checklist comprising the following diagnostic items: (a) occupational asbestos exposure; (b) confirmation of exudate of pleural effusion; (c) exclusion of pleural effusion with malignant tumors based on negative results of CEA and hyaluronic acid, and cytology of pleural effusion; (d) exclusion of rheumatic, bacterial, and tuberculous pleuritis; (d) radiological findings for exclusion of malignancies; and (e) histopathological findings based on thoracoscopy that exclude malignancies (when thoracoscopy was not performed, there was confirmation that no malignancies were present during 3-month follow-up observation). Cases that satisfied all items were defined as BAPE.

Results: Among the 105 suspected cases, there were five cases that had no occupational asbestos exposure; six cases in which transudate of on pleural effusion; one case each of rheumatoid pleuritis and tuberculous pleuritis; and five cases of pleural mesothelioma based on chest radiography and histopathological findings within 3 months after initial diagnosis. Therefore, we excluded 18 cases from the 105 candidates and determined 87 cases of BAPE.

Conclusion: We consider that six items described above are suitable for diagnosing BAPE.

KEYWORDS

benign asbestos pleural effusion, exudative, occupational asbestos exposure, pleural mesothelioma, pleural plaques

This is an open access article under the terms of the Creative Commons Attribution-NonCommercial-NoDerivs License, which permits use and distribution in any medium, provided the original work is properly cited, the use is non-commercial and no modifications or adaptations are made.

© 2020 Japan Organization of Occupational Health and Safety. *Journal of Occupational Health* published by John Wiley & Sons Australia, Ltd on behalf of The Japan Society for Occupational Health

1 | INTRODUCTION

Benign asbestos pleural effusion (BAPE) is a non-malignant pleural lesion induced by asbestos exposure, which is also known as asbestos pleuritis. Eisenstadt¹ reported BAPE as a new disease concept for the first time in 1964, and BAPE typically presents unilaterally and with a small volume of pleural effusion.

Epler et al² reported diagnostic criteria such as (a) asbestos exposure, (b) presence of pleural effusion by chest radiograph or thoracentesis, (c) no other causes except asbestos exposure, and (d) no appearance of malignancy during a period of 3 years from diagnosis. These criteria were generated for prospective epidemiological observation, and clinical follow-up for 3 years was set in order to exclude pleural mesothelioma. Hillerdal et al³ showed that clinical follow-up for only 1 year is sufficient if precise checking is followed by diagnostic imaging such as chest computed tomography (CT) scanning in 1989. However, other new criteria have not been proposed since. Therefore, we cannot compare with standard data described in the previous studies.

It is speculated that the pathogenic mechanism of BAPE is mechanical irritation of the visceral pleura by asbestos fibers, obstruction of the lymphatic drainage of the parietal pleura induced by pleural fibrosis,⁴ or autoimmunity due to the adjuvant effect of asbestos fibers.⁵ However, the true mechanism has not yet been established. It may be defined that the inflammation of visceral pleura induced by asbestos fibers induces BAPE.

In Japan, BAPE was approved in 2003 as an asbestos-related disease for industrial accident compensation. However, this compensation to BAPE patients was judged despite the lack of diagnosis criteria. It is suspected that some patients with BAPE have been overlooked because there are no diagnostic criteria for BAPE. Therefore, we examined retrospectively the diagnosis of BAPE based on occupational history, pleura, chest images, and laboratory data of pleural effusion together with data from reported BAPE patients.⁶⁻⁸ We then established a diagnosis manual for BAPE, and report the findings.

2 | MATERIALS AND METHODS

From 2012 to December in 2019, 105 patients who were diagnosed with BAPE at the initial diagnosis at the Okayama Rosai Hospital, Toyama Rosai Hospital, Yokohama Rosai Hospital, and Tohoku Rosai Hospital in Japan, were examined retrospectively, and the validity of the diagnosis was investigated. These cases were diagnosed as BAPE at the initial diagnosis based on data from laboratory and radiological findings. However, we reinvestigated these cases based on a checklist of proposed new criteria, and some cases were

deemed to be diagnosed incorrectly. Therefore, the remaining cases were diagnosed definitely as BAPE. It was made clear that BAPE should be diagnosed based on these procedures containing these exclusion items.

We compiled a checklist for diagnosing BAPE as given in Figure 1, and judged retrospectively the validity of the diagnosis depending on this checklist for the 105 cases who were diagnosed as BAPE at the initial diagnosis. The checklist was basically complied based on (a) the presence of occupational asbestos exposure for confirmation of asbestos exposure, (b) pleural effusion findings with thoracentesis and exclusion of other diseases in the criteria defined by Epler et al² in 1982.

1. In order to confirm asbestos exposure, we inquired concerning occupational asbestos exposure. In the cases with confirmed asbestos exposure, we inquired concerning the age at first exposure, exposure term, and job duty, and investigated the latent period from the first exposure to the onset of BAPE. We designated cases as questionable exposure to asbestos where pleural plaques appeared in radiographs without confirmation of occupational asbestos exposure. We, therefore, excluded these cases.
2. In order to exclude other diseases that might induce pleural effusion, we checked the past history and present illness. There were 15 cases with heart disease, two cases with kidney disease, and one case with prostate cancer. However, none of these cases were excluded because these diseases were assessed not to cause pleural effusion. In the next step, we examined the pleural fluid. Since pleural fluid results from inflammatory disease with asbestos fibers, the fluid was confirmed to be exudative based on Light's criteria.⁹
3. (a) For exclusion of cases with malignant pleural effusion, cytopathological examination of the pleural effusion as well as assay of carcinoembryonic antigen (CEA) and hyaluronic acid in the pleural effusion were performed. (b) To exclude rheumatoid pleuritis, rheumatoid factors (RFs) in the serum and effusion were examined. (c) For exclusion of bacterial pleuritis, a bacterial check of the pleural effusion was performed and we confirmed that lymphocytes were more than half in the leukocytes of the pleural effusion. (d) Furthermore, to exclude tuberculous pleuritis, adenosine deaminase (ADA) was checked, and a bacterial smear and culture for tuberculosis were performed in addition to polymerase chain reaction for *Mycobacterium tuberculosis* (Tbc-PCR).
4. At chest imaging, the absence of irregular pleural thickening and no tumorous mass were confirmed in order to exclude pleural mesothelioma.¹⁰
5. To exclude the early stages for pleural mesothelioma, macroscopic findings based on thoracoscopy and biopsy of the parietal pleura were checked. Histopathological examination had not been performed in some of the cases,

and no malignant tumor was confirmed in follow-up observation during a period of at least 3 months.

3 | RESULTS

All 105 cases suspected as BAPE at the initial diagnosis were male and aged 60 to 96 years with the median age of 79 years at diagnosis.

1. One hundred cases (95.2%) were confirmed to have occupational history of asbestos exposure and four cases were suspected to have asbestos exposure with pleural plaque imaging without definite occupational asbestos exposure. One case was not confirmed to have occupational asbestos exposure and pleural plaques as indicated in Figure 2.
2. Differential diagnosis of pleural effusion was performed according to the Diagnostic Approach to Pleural Effusion.¹¹ Thoracentesis was performed on all 105 cases and 79% proved to be bloody effusion.
3. Pleural fluids of 99 cases (94.3%) were proven to be exudative. Among these, 55% satisfied all three items of Light's criteria, 22% satisfied two items, and 17% satisfied

one item. Six cases (6%) that did not satisfy any item were determined as transudative, and were excluded at this stage.

4. (a) Only one case showed more than 5 ng/mL of CEA, and the malignant marker threshold was 6.5 ng/mL, but its malignancy was denied. Two point four percent of cases exhibited hyaluronic acid exceeding the 100 000 ng/mL threshold, but did not exceed 120 000 ng/mL, and pleural mesothelioma was denied. For cytology, with regard to Class III diagnosis, 4.9% of cases were Class III, but they were mild (Class IIIa) and malignant tumors such as mesothelioma were not observed during follow-up (Table 1). (b) One case with high levels of serum and effusion RFs was later proven to be rheumatoid arthritis. This case was diagnosed previously with rheumatoid pleuritis. (c) One case with an ADA level in the pleural effusion of 60.5 U/L was proven to be tuberculous pleuritis with detection of *Mycobacterium tuberculosis* (M. tb) after 2 weeks culture, despite negative results with Tbc-PCR and interferon-γ releasing assay (T-SPOT) as given in Figure 2. (d) In regard to bacterial pleuritis, all cases presented negative in the bacterial test. The majority of cases (97.5%) had more than 50% of lymphocytes among the leukocytes in pleural effusion, and 3.5% increased in eosinophils, but no case increased in neutrophils (Figure 2).
5. For radiological examination, 97.5% of cases presented with pleural plaques, but no pulmonary asbestosis. No tumorous thickening of the pleura was detected at the initial diagnosis; however, three cases exhibited irregular pleural thickening in 1-3 months of follow-up. Figure 3 shows one of these three cases without positive findings in all sites containing the left pleura except pleural effusion on the left side with PET-CT. After 3 months, the left pleura exhibited slight irregular thickening, and distinct narrowing of the left thorax was present as shown in Figure 4. We suspected left pleural mesothelioma and was diagnosed definitively based on thoracoscopy as given in Figure 2.

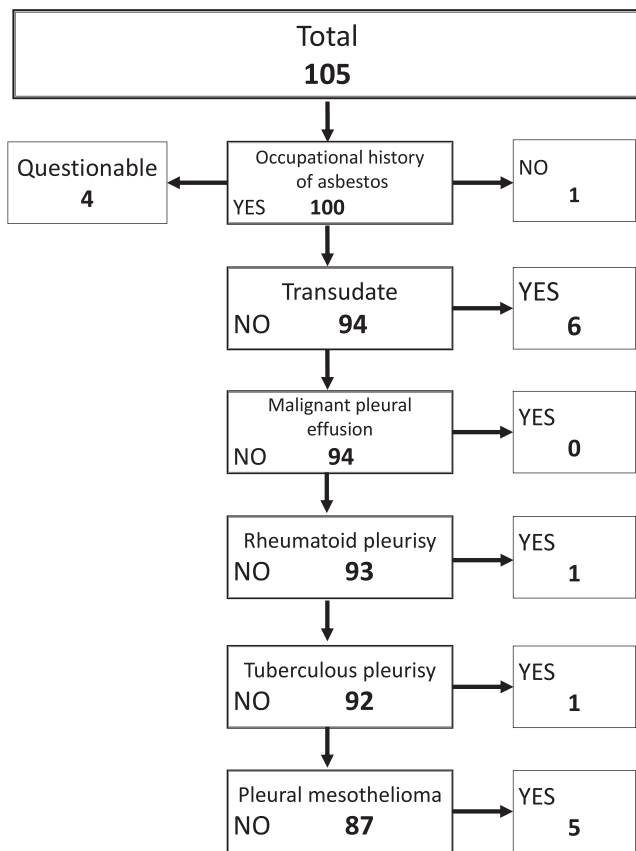


FIGURE 2 Differential diagnosis of BAPE from other diseases

TABLE 1 Laboratory findings in pleural effusion

CEA in PE less than 5.0 ng/mL	Lymphocytes dominant in PE
YES 98.8%	YES 96.5%
NO 1.2%	NO 3.5%
HA in PE less than 100,000 ng/mL	Exclusion of RA pleuritis
YES 97.6%	YES 96.4%
NO 2.4%	NO 3.6%
Cytology in PE	ADA in PE less than 40 IU/L
Class I 30.5%	YES 98.8%
Class II 64.6%	NO 1.2%
Class III 4.9%	

Abbreviations: HA, hyaluronic acid; PE, pleural effusion.



FIGURE 3 PET-CT shows no positive lesions in the left thorax with pleural effusion



FIGURE 4 Chest CT that was taken 6 mo after first visit shows irregular pleural thickening in the left pleura. The left thorax becomes smaller than the right thorax suggesting left pleural mesothelioma

6. Just after the initial diagnosis, thoracoscopy in three cases among these five cases was performed but biopsy results were negative. However, tumorous pleural thickening appeared during the 3-month follow-up period, and subsequent biopsy proved to be sarcomatoid pleural mesothelioma. The other two cases complained of persistent severe chest pain as a subjective symptom although there were negative radiological findings. Pleural biopsy with thoracoscopy was performed and these cases were

proved to be the epithelioid type of pleural mesothelioma. Therefore, we assessed the necessity of more than 3 months of follow-up after thoracentesis for the diagnosis of BAPE.

Based on the exclusion criteria, we determined BAPE induced by occupational asbestos exposure for 87 cases. All of the final defined 87 cases were male and aged 60 to 93 years with the median age of 79 years. In terms of the occupational history, the main occupation was shipbuilder followed by construction worker as indicated in Figure 5. The asbestos exposure term ranged from 2 to 55 years with the median of 38 years. The latency period ranged from 18 to 73 years with the median of 53.5 years.

4 | DISCUSSION

Pleural effusion comprises transudate occurring from impairment of the flow of body fluid such as heart failure or nephrotic syndrome, and exudate induced by local inflammation extending to the pleura or by malignancies. BAPE is visceral pleural pleuritis induced by asbestos fibers penetrating the pleural cavity, and has been considered to be an asbestos-related disease since the 1960s.¹ No new criteria for BAPE have been determined, since Epler et al² described criteria in 1982. In Japan in 2003, BAPE was added to the list of asbestos-related diseases for which patients were able to receive industrial accident compensation. Although no new criteria were identified, compensation for this disease was determined. Therefore, we present a new checklist to use as a reference in diagnosing BAPE based on a retrospective reinvestigation of the cases diagnosed as BAPE at the initial diagnosis that screens out the misdiagnosed cases.

Although asbestos exposure history is a criterion reported by Epler, we propose occupational history of asbestos exposure in order to ensure asbestos exposure. For this reason, there are no reports of BAPE induced by environmental asbestos exposure. Almost all cases were induced by occupational asbestos exposure. Based on the checklist, we excluded five cases including four cases whose occupational history of asbestos exposure was unclear from the 105 cases under investigation. Although almost all cases (97.5%) presented with pleural plaques, pleural plaques were considered as a reference item only and occupational asbestos exposure was considered more important.

By confirming the exudate as inflammatory pleural effusion using Light's criteria classification,⁹ six cases with transudate were excluded. Ninety-three percent to 96% of cases meeting this criterion were reported to have exudate. Furthermore, the cases that did not satisfy this criterion were determined to be transudative.

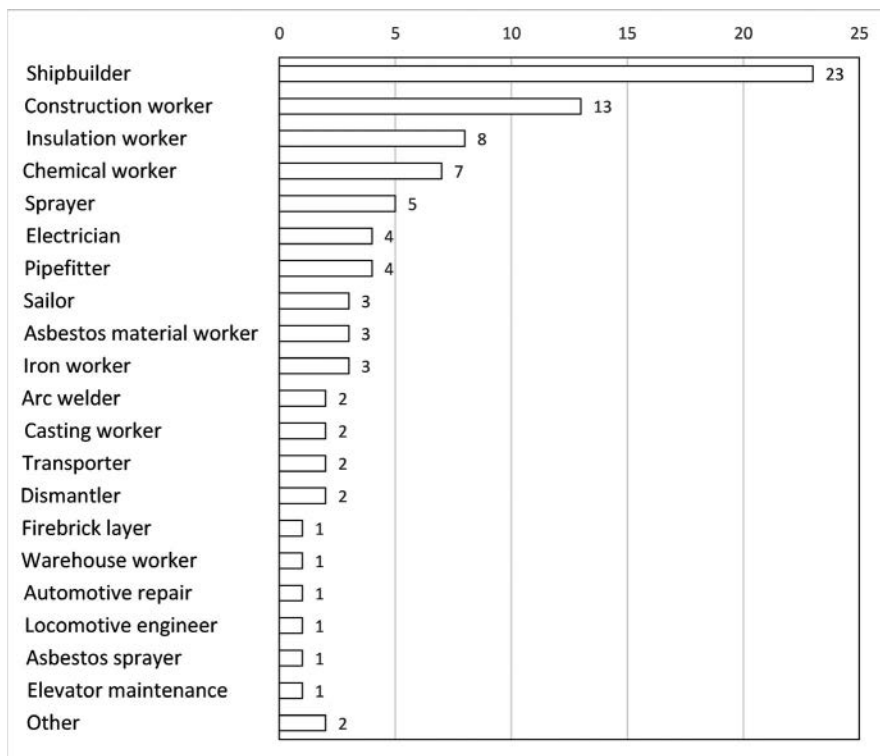


FIGURE 5 This figure shows the number of occupational histories for 87 confirmed BAPE cases. Shipbuilder and construction workers are main components for BAPE cases as reported for asbestos-related lung cancer or mesothelioma cases

For differential diagnosis to exclude malignant tumors, we considered CEA, hyaluronic acid, and cytology data. The CEA concentration in pleural effusion was reported to be less than 1.8 ng/mL for BAPE¹² and useful in identifying BAPE. However, for mesothelioma, CEA is not helpful in distinguishing from pleural mesothelioma because almost all pleural mesothelioma cases were within normal limits. The majority of pleural mesothelioma cases exhibited hyaluronic acid concentrations of greater than 100 000 ng/mL; however, almost all BAPE cases exhibited concentrations of less than 100 000 ng/mL.⁶ Fujimoto reported that three cases among 87 cases with BAPE exceeded the concentration of 100 000 ng/mL, but those were less than 120 000 ng/mL.⁷ Our results regarding hyaluronic acid in pleural effusion were consistent with this report and we assumed that there were no cases that suggested mesothelioma. It is relatively easy to differentiate malignant effusion using cytological examination. Five cases showed Class III, which was difficult to judge, and these were Class IIIa. We denied malignancies from clinical course. From these results, we judged that there were no cases with findings suggestive of a malignant tumor.

At the next step, differential diagnosis of collagen disease such as rheumatic pleuritis was performed. There was no case affected by these diseases based on past history and present illness. One case presented with high RFs in serum and pleural effusion, and was examined carefully at a later date. This was likely rheumatic pleuritis from diagnosis of rheumatoid arthritis,¹³ and was excluded. In addition, to exclude bacterial pleuritis, we performed bacterial examination and assayed the differential count of leukocytes in the pleural effusion.

There were no abnormal cases. Although the percentage of lymphocytes in leucocytes in the pleural effusion was greater than 50% in most cases, three cases presented with eosinophilia. BAPE cases with eosinophilia were reported,¹⁴ and these results did not affect this diagnosis.

To exclude tuberculous pleuritis, which presents with many lymphocytes in pleural effusion, we performed ADA assay and bacterial examination. Only one case showed a concentration of greater than 40 U/L (60.5 U/L) of ADA. It has been reported that cases with ADA of greater than 40 U/L are suspected to suffer from tuberculosis.¹⁵ This case presented negative for Tbc-PCR in effusion and serum T-SPOT tests, but culture of pleural effusion proved *M. tb* positive. We determined that this was tuberculous pleuritis. We excluded 13 cases due to the results so far.

Finally, it is difficult to differentiate diagnosis between BAPE and early stage pleural mesothelioma. Kato et al¹⁰ focused on the thickening of the mediastinal pleura for one of the features of pleural mesothelioma, but no positive cases presented with this indicator in 92 cases examined. Although clinical symptoms during 3 months of follow-up presented only as pleural effusion, two cases complained of severe chest pain and three cases exhibited irregular pleural thickening and narrowing of the affected thorax. In three cases among them pleural biopsy was performed under thoracoscopy. Visual change in the tumors was not observed in these cases, and they were diagnosed with fibrinous pleuritis based on biopsy. However, after manifestation of irregular pleural thickening, the second pleural biopsy indicated pleural mesothelioma. The reason for this discrepancy was that

the biopsied sites were thought not to be suitable for definite diagnosis. Two other cases had no positive radiological abnormality but indicated persistent chest pain. We again performed thoracoscopic biopsy and made a definite diagnosis of epithelioid mesothelioma. The diagnosis of these five cases changed during the 3 months of follow-up, and we assessed the necessity for a 3-month of follow-up observation period after administering a pleural effusion test.

From the report by Metintas et al.,¹⁶ in the 287 cases that underwent thoracoscopy, 101 cases diagnosed with fibrinous pleuritis by biopsy were examined more closely, and the rate of false negatives was 18%. All of these cases presented as malignant pleural diseases. Of the 142 cases exhibiting exudate as pleural effusion, 30% to 40% could not be diagnosed based on histopathological data using thoracoscopy. Of that group 8% to 12% were found to have malignant pleural lesions and almost all cases were diagnosed with pleural mesothelioma. The other 25% to 91% were classified as non-specific pleuritis and were treated as idiopathic pleuritis. If a definite diagnosis is reported to be determined, greater accuracy using invasive biopsy is required.¹⁷ For determining BAPE as a diagnosis by exclusion, we consider that a 3-month follow-up period is necessary. Nevertheless, a part of pleuritis in which definite diagnosis is not determined after thoracoscopic biopsy is thought to be grouped as BAPE. Using these criteria, we diagnosed 87 cases as BAPE.

Thus, when BAPE was diagnosed with (a) a history of occupational asbestos exposure and (b) the presence of exudate based on a pleural effusion test as the required main items; and (c) negative results of CEA and hyaluronic acid in pleural effusion, and cytology of pleural effusion for exclusion of malignancy; (d) exclusion of rheumatic, bacterial and tuberculous pleuritis; (e) exclusion of malignancy using radiological images; and (f) exclusion of histopathological malignancy using thoracoscopy (when thoracoscopy was not performed, no malignant tumor was confirmed in follow-up observation during at least 3 months) as required sub-items, BAPE could be determined with a more than 95% if cytology was class III. If some of these six sub-items are no, we should carefully make a differential diagnosis.

The age of BAPE onset induced by asbestos exposure has pointed out the relationship to the volume of asbestos to which the patient was exposed. The number of incidences increases and latency becomes short, if the exposure volume of asbestos increases.¹⁸ The median age of BAPE onset was 66 years at our previous report,⁸ but increased to 79 years at this report. Similar to previous reports, the history of occupational asbestos exposure is approximately the same such as No. 1 is shipbuilder and No. 2 is construction worker as shown in Figure 5, and asbestos exposure in these types of work was classified as moderate. The median exposure term was 38 years and the latency from the first exposure was 53.5 years, which was longer than that shown by previous data.^{6,8,12} As a reason for this, considered together

with many cases of advanced-age patients, it was suggested that the exposure dose was low when they worked with asbestos exposure. Workers were likely affected with BAPE after a long latency period with a low dose of past asbestos exposure.

On the other hand, five cases among those diagnosed as BAPE at the initial diagnosis were determined as pleural mesothelioma in their clinical course. The term of clinical observation was between 1 and 3 months. The reason why we did not confirm pleural mesothelioma was not that pleural mesothelioma changed from BAPE, but that we failed to make a definite diagnosis of pleural mesothelioma at the initial diagnosis due to the presence of only pleural effusion without malignant findings such as tumorous pleural thickening by chest CT and that definite diagnosis could be performed during the progression of the disease. Although we observed parietal pleura in three of the five cases using thoracoscopy and performed a pleural biopsy under thoracoscopy at the initial diagnosis, we failed to reach a definite diagnosis.

If we do not detect malignant findings that suggest mesothelioma based on chest CT, we should pursue more precise observation through thoracoscopy and perform a biopsy at the proper site. In particular, in cases presenting with persistent chest pain, we need to consider early stage pleural mesothelioma based on Positron Emission Tomography-Computed Tomography (PET-CT) scanning and perform biopsy at suitable sites for final diagnosis.

As mentioned above, we are convinced that the presented criteria such as occupational asbestos exposure, exudative pleural effusion, tumor marker in pleural effusion, bacterial test results, radiological findings and histopathological findings are suitable for diagnosing BAPE, and it is valid that cases that satisfied these criteria during the 3 months of follow-up be diagnosed as BAPE.

DISCLOSURE

Approval of the research protocol: N/A. *Informed consent:* All participants provided written informed consent before inclusion in the study. *Registry and the registration no. of the study/trial:* N/A. *Animal studies:* N/A. *Conflict of interest:* N/A.

AUTHOR CONTRIBUTIONS

Takumi Kishimoto was involved in data analysis and writing manuscript. Nobukazu Fujimoto, Keiichi Mizuhashi, Satoko Kozawa, and Motohiko Miura were involved in accumulation of patients for BAPE.

ETHICAL APPROVAL

This study was approved by the 11th research ethics committee of the Japan Organization of Occupational Health and Safety on June 18, 2018 (No. 9).

ORCID

Takumi Kishimoto  <https://orcid.org/0000-0003-2718-1713>
Nobukazu Fujimoto  <https://orcid.org/0000-0002-4516-0433>

REFERENCES

1. Eisenstadt HB. Asbestos pleurisy. *Dis Chest*. 1964;46:78-81.
2. Epler GR, McLoud TC, Gaensler EA. Prevalence and incidence of benign asbestos pleural effusions in a working population. *J Am Med Assoc*. 1982;247(5):617-622.
3. Hillerdal G, Ozesmi M. Benign asbestos pleural effusion. 73 exudates in 60 patients. *Eur J Respir Dis*. 1987;71(2):113-121.
4. Lees PSJ, Breyse PN, McArthur BB, et al. End user exposure to man-made vitreous fibers: I Installation of residual insulation products. *Appl Occup Environ Hyg*. 1993;8:1022-1030.
5. Warheit DB, Chang LY, Hill LH, et al. Pulmonary macrophage accumulation and asbestos induced lesions at sites of fiber deposition. *Am Rev Respir Dis*. 1984;129(2):301-310.
6. Kishimoto T, Gemba K, Aoe K, et al. Asbestos pleural effusion. *Res Physician*. 2010;17:374-379.
7. Fujimoto N, Gemba K, Asano M, et al. Hyaluronic acid in the pleural fluid of patients with malignant pleural mesothelioma. *Respir Investig*. 2013;51(2):92-97.
8. Kishimoto T, Okahara M, Chikamori K, et al. Clinical evaluation of benign asbestos pleural effusion. *Jap J Thorac Dis*. 1998;36(1):18-22.
9. Light RW, Macgregor MI, Luchsinger PC, et al. Pleural effusions: the diagnostic separation of transudates and exudates. *Ann Intern Med*. 1972;77(4):507-513.
10. Kato K, Gemba K, Fujimoto N, et al. Pleural irregularities and mediastinal pleural involvement in early stages of malignant pleural mesothelioma and benign asbestos pleural effusion. *Eur J Radiol*. 2016;85(9):1594-1600.
11. Saguil A, Wyrick K, Hallgren J. Diagnostic approach to pleural effusion. *Am Fam Physician*. 2014;15:90(2):99-104.
12. Fujimoto N, Gemba K, Aoe K, et al. Clinical investigation of benign asbestos pleural effusion. *Pul Med*. 2015;2015:1-6.
13. Walker WC, Wright V. Rheumatoid pleuritis. *Ann Rheum Dis*. 1967;26(6):467-474.
14. Robinson BW, Musk AW. Benign asbestos pleural effusion: diagnosis and course. *Thorax*. 1981;36(12):896-900.
15. Porcel JM. Tuberculous pleural effusion. *Lung*. 2009;187(5):263-270.
16. Metintas M, Ak G, Cadirci O, et al. Outcome of patients diagnosed with fibrinous pleuritis after medical thoracoscopy. *Respir Med*. 2012;106(8):1177-1183.
17. Wrightson JM, Davies HE. Outcome of patients with non-specific pleuritis at thoracoscopy. *Curr Opin Pulm Med*. 2011;17(4):242-246.
18. Peacock C, Copley SJ, Hansell DM. Asbestos-related benign pleural disease. *Clin Radiol*. 2000;55(6):422-432.

How to cite this article: Kishimoto T, Fujimoto N, Mizuhashi K, Kozawa S, Miura M. Retrospective investigation on diagnostic process for benign asbestos pleural effusion (BAPE) using checklist. *J Occup Health*. 2020;62:e12182. <https://doi.org/10.1002/1348-9585.12182>



First-line nivolumab plus ipilimumab in unresectable malignant pleural mesothelioma (CheckMate 743): a multicentre, randomised, open-label, phase 3 trial

Paul Baas, Arnaud Scherpereel, Anna K Nowak, Nobukazu Fujimoto, Solange Peters, Anne S Tsao, Aaron S Mansfield, Sanjay Popat, Thierry Jahan, Scott Antonia, Youssef Oulkhair, Yolanda Bautista, Robin Cornelissen, Laurent Greillier, Francesco Grossi, Dariusz Kowalski, Jerónimo Rodríguez-Cid, Praveen Aanur, Abderrahim Oukessou, Christine Baudelet, Gérard Zalcman

Summary

Background Approved systemic treatments for malignant pleural mesothelioma (MPM) have been limited to chemotherapy regimens that have moderate survival benefit with poor outcomes. Nivolumab plus ipilimumab has shown clinical benefit in other tumour types, including first-line non-small-cell lung cancer. We hypothesised that this regimen would improve overall survival in MPM.

Methods This open-label, randomised, phase 3 study (CheckMate 743) was run at 103 hospitals across 21 countries. Eligible individuals were aged 18 years and older, with previously untreated, histologically confirmed unresectable MPM, and an Eastern Cooperative Oncology Group performance status of 0 or 1. Eligible participants were randomly assigned (1:1) to nivolumab (3 mg/kg intravenously once every 2 weeks) plus ipilimumab (1 mg/kg intravenously once every 6 weeks) for up to 2 years, or platinum plus pemetrexed chemotherapy (pemetrexed [500 mg/m² intravenously] plus cisplatin [75 mg/m² intravenously] or carboplatin [area under the concentration-time curve 5 mg/mL per min intravenously]) once every 3 weeks for up to six cycles. The primary endpoint was overall survival among all participants randomly assigned to treatment, and safety was assessed in all participants who received at least one dose of study treatment. This study is registered with ClinicalTrials.gov, NCT02899299, and is closed to accrual.

Findings Between Nov 29, 2016, and April 28, 2018, 713 patients were enrolled, of whom 605 were randomly assigned to either nivolumab plus ipilimumab (n=303) or chemotherapy (n=302). 467 (77%) of 605 participants were male and median age was 69 years (IQR 64–75). At the prespecified interim analysis (database lock April 3, 2020; median follow-up of 29.7 months [IQR 26.7–32.9]), nivolumab plus ipilimumab significantly extended overall survival versus chemotherapy (median overall survival 18.1 months [95% CI 16.8–21.4] vs 14.1 months [12.4–16.2]; hazard ratio 0.74 [95% CI 0.60–0.91]; p=0.0020). 2-year overall survival rates were 41% (95% CI 35.1–46.5) in the nivolumab plus ipilimumab group and 27% (21.9–32.4) in the chemotherapy group. Grade 3–4 treatment-related adverse events were reported in 91 (30%) of 300 patients treated with nivolumab plus ipilimumab and 91 (32%) of 284 treated with chemotherapy. Three (1%) treatment-related deaths occurred in the nivolumab plus ipilimumab group (pneumonitis, encephalitis, and heart failure) and one (<1%) in the chemotherapy group (myelosuppression).

Interpretation Nivolumab plus ipilimumab provided significant and clinically meaningful improvements in overall survival versus standard-of-care chemotherapy, supporting the use of this first-in-class regimen that has been approved in the USA as of October, 2020, for previously untreated unresectable MPM.

Funding Bristol Myers Squibb.

Copyright © 2021 Elsevier Ltd. All rights reserved.

Introduction

Malignant pleural mesothelioma (MPM) is a highly aggressive cancer and typically unresectable at diagnosis, with less than 10% of patients surviving 5 years or beyond.^{1,2} Historically, age, sex, tumour grade and stage, and histology have been shown to be independent prognostic factors. Notably, worse prognosis has been reported for non-epithelioid histology versus the epithelioid subtype.^{1,3} Until October, 2020, platinum agents plus folate antimetabolites, such as pemetrexed,

have been the only approved first-line treatment regimens for MPM since 2004.^{4,5} However, long-term survival outcomes remain poor with chemotherapy;^{6–9} bevacizumab has been added to these regimens¹⁰ but its use varies across regions. As such, there is an urgent need for new and effective therapeutic options.

Nivolumab, a fully human anti-programmed cell death 1 (PD-1) antibody, and ipilimumab, a fully human anti-cytotoxic T-lymphocyte 4 (CTLA-4) antibody are immune checkpoint inhibitors with distinct but

Published Online
January 21, 2021
[https://doi.org/10.1016/S0140-6736\(20\)32714-8](https://doi.org/10.1016/S0140-6736(20)32714-8)

See Online/Comment
[https://doi.org/10.1016/S0140-6736\(21\)00147-1](https://doi.org/10.1016/S0140-6736(21)00147-1)

The Netherlands Cancer Institute and Leiden University Medical Center, Amsterdam, Netherlands (Prof P Baas MD); Pulmonary and Thoracic Oncology, University of Lille, CHU Lille, INSERM U1189, OncoThAI, Lille, France (Prof A Scherpereel MD); Medical School, University of Western Australia Perth, WA, Australia (Prof A K Nowak PhD); Department of Medical Oncology, Sir Charles Gairdner Hospital, Perth, WA, Australia (Prof A K Nowak); Okayama Rosai Hospital, Okayama, Japan (Prof N Fujimoto MD); Lausanne University Hospital, Lausanne, Switzerland (Prof S Peters MD); MD Anderson Cancer Center, Houston, TX, USA (Prof A S Tsao MD); Mayo Clinic, Rochester, MN, USA (A S Mansfield MD); Royal Marsden Hospital, London, UK (Prof S Popat FRCP); Institute of Cancer Research, London, UK (Prof S Popat); UCSF Helen Diller Family Comprehensive Cancer Center, San Francisco, CA, USA (Prof T Jahan MD); H Lee Moffitt Cancer Center & Research Institute, Tampa, FL, USA (Prof S Antonia MD); Hôpital Côte de Nacre CHU de Caen, Caen, France (Y Oulkhair MD); Centro Médico Nacional Siglo XXI, Mexico City, Mexico (Prof Y Bautista MD); Erasmus MC Cancer Institute, Rotterdam, Netherlands (R Cornelissen MD);

Aix Marseille University, APHM, INSERM, CNRS, CRCM, Hôpital Nord, Multidisciplinary Oncology and Therapeutic Innovations Department, Marseille, France (Prof L Greillier MD); Fondazione IRCCS Ca' Granda Ospedale Maggiore Policlinico, Milan, Italy (F Grossi MD); Department of Lung Cancer and Chest Tumours, Maria Skłodowska-Curie National Research Institute of Oncology, Warsaw, Poland (Prof D Kowalski MD); Centro Oncológico, Médica Sur-Instituto Nacional de Enfermedades Respiratorias, Mexico City, Mexico (Prof J Rodríguez-Cid MD); Bristol Myers Squibb, Princeton, NJ, USA (P Aanur MD, A Oukessou MD, C Baudalet PhD); Bichat-Claude Bernard University Hospital, AP-HP, Université de Paris, Paris, France (Prof G Zalcman MD)

Correspondence to: Prof Paul Baas, The Netherlands Cancer Institute, Amsterdam, 1066CX, Netherlands p.baas@nki.nl

For the most recent and complete version of the NCCN guidelines see NCCN.org
See Online for appendix

Research in context

Evidence before this study

We searched PubMed and abstracts from major oncology congresses for studies published from database inception until Oct 2, 2020, relevant to unresectable malignant pleural mesothelioma (MPM) and cancer immunotherapy regimens, with a focus primarily on first-line phase 3 trials, using search terms that included, but were not limited to ("mesothelioma" AND "nivolumab") OR "chemotherapy" OR "pembrolizumab" OR "atezolizumab" OR "avelumab" OR "durvalumab" OR "ipilimumab" OR "tremelimumab" OR "PD-1" OR "PD-L1" OR "CTLA-4" (full names and abbreviations). Although we identified several studies assessing immunotherapy in MPM, we found no published randomised phase 3 studies investigating the efficacy or safety of immunotherapy regimens in the first-line setting. Various phase 1 and 2 studies in previously treated patients with MPM have suggested that immunotherapy regimens might provide clinical benefit. Notably, the multicentre, open-label, single-arm, phase 2 MERIT study led to the approval of nivolumab monotherapy for unresectable recurrent MPM in Japan. However, with recommended first-line systemic treatments limited to chemotherapy since 2004, with or without bevacizumab, there remains a need for new and effective therapeutic options. In the single-arm phase 2 DREAM study, first-line durvalumab plus chemotherapy exhibited promising activity in 54 patients with MPM, but the combination requires evaluation in a larger, randomised, phase 3 study. CheckMate 743 was designed to investigate the efficacy and safety of nivolumab plus ipilimumab versus chemotherapy. A previous non-comparative phase 2 trial (MAPS2) and single-arm

complementary mechanisms of action. Ipilimumab induces T-cell proliferation and de-novo anti-tumour T-cell responses, including in memory T cells, whereas nivolumab restores the function of existing anti-tumour T cells.¹¹ Nivolumab plus ipilimumab is approved in various tumours¹² and has shown durable overall survival benefit in melanoma,¹³ renal cell carcinoma,¹⁴ and in non-small-cell lung cancer (NSCLC).¹⁵ Furthermore, National Comprehensive Cancer Network (NCCN) Clinical Practice Guidelines in Oncology (NCCN guidelines) recommend nivolumab with or without ipilimumab as a preferred treatment option (category 2A) in second-line or later MPM settings based on results from three phase 2 trials,^{16–18} including the multicentre, open-label, randomised, non-comparative IFCT-1501 MAPS2 trial that showed encouraging clinical activity of the combination therapy.¹⁶

CheckMate 743 is a phase 3 study designed to assess efficacy and safety of first-line nivolumab plus ipilimumab versus platinum plus pemetrexed chemotherapy in unresectable MPM. Here we present results from the prespecified interim analysis, which has led to nivolumab plus ipilimumab gaining approval in the USA.¹²

phase 2 study (INITIATE) assessing nivolumab plus ipilimumab in MPM showed that this regimen was tolerable and exhibited encouraging clinical activity.

Added value of this study

Here we provide results from the randomised CheckMate 743 study, which is the first phase 3 study to show significant and clinically meaningful improvements in overall survival with immunotherapy versus standard-of-care platinum plus pemetrexed chemotherapy for first-line treatment of unresectable MPM. This regimen was found to show clinical benefit and tolerability, thus providing patients with a new first-line chemotherapy-free treatment option. Notably, survival with nivolumab plus ipilimumab was similar in patients with both non-epithelioid and epithelioid histologies, suggesting that the regimen could be considered for all patients with unresectable MPM. Responses were durable, with a 2-year duration of response rate of 32% of immunotherapy-treated patients. The safety profile of nivolumab plus ipilimumab was consistent with that observed in first-line non-small-cell lung cancer at this dose and schedule and no new safety signals were reported.

Implications of all the available evidence

Nivolumab plus ipilimumab can provide notable and clinically meaningful improvements in overall survival versus the current standard of care. Data from CheckMate 743 support a favourable clinical benefit-risk profile for nivolumab plus ipilimumab. Nivolumab plus ipilimumab is now indicated in the USA and Brazil as a first-line treatment for unresectable MPM.

Additionally, NCCN guidelines recommend nivolumab plus ipilimumab as a preferred first-line option (category 2A) for patients with biphasic or sarcomatoid histology and is also an option for those with epithelioid histology.

Methods

Study design and participants

CheckMate 743 is a global, open-label, randomised, controlled, phase 3 study run at 103 hospitals across 21 countries (appendix pp 2–4, 22). Eligible patients were aged 18 years or older with histologically confirmed unresectable MPM that was not amenable to curative therapy (surgery with or without chemotherapy), and an Eastern Cooperative Oncology Group performance status of 0 or 1.¹⁹ Unresectability of the disease was determined by the investigator at individual sites using local standards. Patients must have completed any previous palliative radiotherapy 2 weeks or longer before initiating study treatment, with no residual signs of toxicity, and have measurable disease according to the modified Response Evaluation Criteria in Solid Tumors (mRECIST)²⁰ for pleural mesothelioma. Patients without measurable pleural lesions but with metastatic non-pleural lesions

measurable per RECIST version 1.1 could be considered for inclusion after consultation with the study's medical monitor. Patients were required to have tumour samples available for programmed cell death ligand 1 (PD-L1) testing. Baseline laboratory tests required to assess eligibility included white blood cell counts, neutrophils, platelets, haemoglobin, serum creatinine, alanine aminotransferase, aspartate aminotransferase, and total bilirubin (appendix p 6).

Exclusion criteria included brain metastases (unless resected or treated with stereotactic radiotherapy and asymptomatic with no evolution within 3 months before study inclusion), autoimmune disease, and previous treatment with drugs targeting T-cell costimulation or checkpoint pathways. Patients were excluded if they presented with primitive peritoneal, pericardial, tunica vaginalis, or testis mesotheliomas. Other exclusion criteria included inadequate haematological, renal, or hepatic function; known HIV infection; or interstitial lung disease that was either symptomatic or might affect the detection or management of suspected drug-related pulmonary toxicity. Patients with current or previous malignancy with less than 3 years of complete remission (except for non-melanoma skin cancers and in-situ cancers) requiring or likely to require concurrent intervention during the study period were ineligible, as were patients requiring systemic corticosteroids (>10 mg daily prednisone or equivalent) or immunosuppressive medication within 14 days of the first dose of study drug. More detail on eligibility criteria are in the appendix (p 5) and study protocol (appendix pp 27–410).

An institutional review board or independent ethics committee at each study centre approved all versions of the protocol. An independent Data Monitoring Committee provided general oversight of efficacy and safety for the trial. The trial was done in accordance with the Declaration of Helsinki and the International Conference on Harmonisation Good Clinical Practice guidelines. All patients provided written informed consent.

Randomisation and masking

Patients were enrolled and randomly assigned (1:1) using an interactive web response system, stratified by sex and histology (epithelioid vs non-epithelioid [including sarcomatoid and mixed subtypes]) to nivolumab plus ipilimumab or platinum plus pemetrexed chemotherapy. The trial was open label and so patients and investigators were not masked to treatment assignment.

Procedures

Participants in both treatment groups were pretreated with folic acid (350–1000 µg orally daily) and vitamin B12 (1000 µg intramuscularly) 1 week before administration of the first dose of study drug (appendix p 5). Participants in the experimental group were given nivolumab (3 mg/kg intravenous infusion once every 2 weeks) plus

ipilimumab (1 mg/kg intravenous infusion once every 6 weeks). Nivolumab was administered first, followed by ipilimumab. Participants in the chemotherapy group were given an intravenous infusion of cisplatin (75 mg/m²) or carboplatin (area under the concentration-time curve 5 mg/mL per min) plus pemetrexed (500 mg/m²) every 3 weeks for a maximum of six cycles. Treatment was continued until disease progression, unacceptable toxicity, or for 2 years for immunotherapy. Treatment with nivolumab plus ipilimumab was permitted beyond disease progression if prespecified requirements were met (appendix p 7). Dose reductions were permitted for chemotherapy, but not for nivolumab or ipilimumab; concomitant use of corticosteroids was permitted. Patients could receive subsequent therapy upon the discontinuation of study treatment in either group at the discretion of the investigator.

Tumour assessments were done 6 weeks after the date of the first dose of study drug and then every 6 weeks for the first 12 months. After 12 months, tumours were assessed every 12 weeks until blinded independent central review (BICR) confirmed disease progression per mRECIST or RECIST version 1.1 criteria, or both. At the time of investigator-assessed initial radiographic progression, the site had to request the blinded independent central review of progression from a third-party radiology vendor (E-research Technologies in St Louis, MO, USA); if progression was not confirmed, treatment could continue.

Adverse events were assessed at baseline and continuously throughout the study and during follow-up. Adverse events were graded according to the National Cancer Institute Common Terminology Criteria for Adverse Events (version 4.0). Select adverse events consisted of a list of preferred terms with potential immune aetiology grouped by specific category (gastrointestinal adverse events, pulmonary adverse events, renal adverse events, hepatic adverse events, skin adverse events, infusion reactions, and endocrinopathies). The definition for serious adverse events is in the appendix (p 6). Treatment-related adverse events were defined as those reported between the first dose of study drug and 30 days after the last dose of study drug. According to study sponsor practice, only events that led to death within 24 h were documented as grade 5 events and reported as deaths here. Events leading to death more than 24 h after onset are reported with the worst grade before death.

Tumour histology was determined by individual sites using local protocols. Archival or fresh formalin-fixed paraffin-embedded tumour samples were collected before randomisation. Optional on-treatment fresh tumour samples were collected at weeks 6–8 and at disease progression, at the discretion of the investigator. Samples were sent to a central laboratory (Cancer Genetics, Rutherford, NJ, USA, and for patients in China, PD-L1 testing was done at Covance, Shanghai) to

determine the proportion of tumour cells showing plasma membrane PD-L1 staining of any intensity using the validated immunohistochemical 28-8 pharmDx assay (Dako, Carpinteria, CA, USA).

Laboratory tests were done within 14 days before randomisation and within 3 days before each dose. Full details of all assessments done are in the appendix (p 6). Hepatitis C RNA and HIV (where locally mandated) tests were done at screening only. All tests had to be done at follow-up visits 1 and 2.

Outcomes

The primary endpoint was overall survival in all patients randomly assigned to treatment after the US Food and Drug Administration provided guidance to change progression-free survival from a coprimary endpoint to a secondary endpoint (protocol amendment April 25, 2019;

appendix p 7).²¹ Overall survival was defined as the time from randomisation to the date of death due to any cause. Secondary endpoints were progression-free survival, objective response rate, time to response, duration of response, and disease control rate (radiographic tumour assessments per adapted mRECIST for pleural lesions and RECIST [version 1.1] for the other lesions by BICR) in all patients randomly assigned to treatment, as well as overall survival, progression-free survival, and objective response rate by PD-L1 expression.

Progression-free survival was defined as the time from randomisation to the date of the first documented tumour progression or death due to any cause. Participants who died were considered to have progressed on the date of death. Participants who received subsequent therapy without previous reported progression were considered to have progressed on the date of death or were censored at the date of last evaluable tumour assessment before or on initiation of subsequent therapy. Objective response rate was defined as the proportion of patients with a best overall response of complete response, partial response, or stable disease. Duration of response was defined as the time between the date of first response to the date of the first documented tumour progression, or death due to any cause, whichever occurred first.

Exploratory endpoints included safety and tolerability in all treated patients. Analysis of other exploratory endpoints that are ongoing but not reported here include pharmacokinetics, biomarkers, patient-reported outcomes, and immunogenicity; a full list is in the appendix (pp 119–122).

Statistical analysis

For the primary endpoint of overall survival, a sample of approximately 600 patients randomly assigned to treatment with 473 deaths would provide 90% power to detect a target hazard ratio (HR) of 0.72 with a two-sided type 1 error of 0.05, by means of a log-rank test. One prespecified interim analysis of overall survival was planned for superiority at approximately 403 deaths (85% of total anticipated events). At the time of database lock for the interim analysis, 419 patients had died (89% of total anticipated events); the boundary for declaring superiority for overall survival was a p value of less than 0.0345, based on the Lan-DeMets alpha spending function with O'Brien-Fleming boundaries. None of the secondary endpoints were included in the testing procedure; therefore, we did no formal statistical testing or allocation of alpha values for progression-free survival, objective response rate, and disease control rate.

We included all patients randomly assigned to treatment in demographic and efficacy analyses. We stratified analyses for overall survival and progression-free survival by sex and histology. We estimated HRs

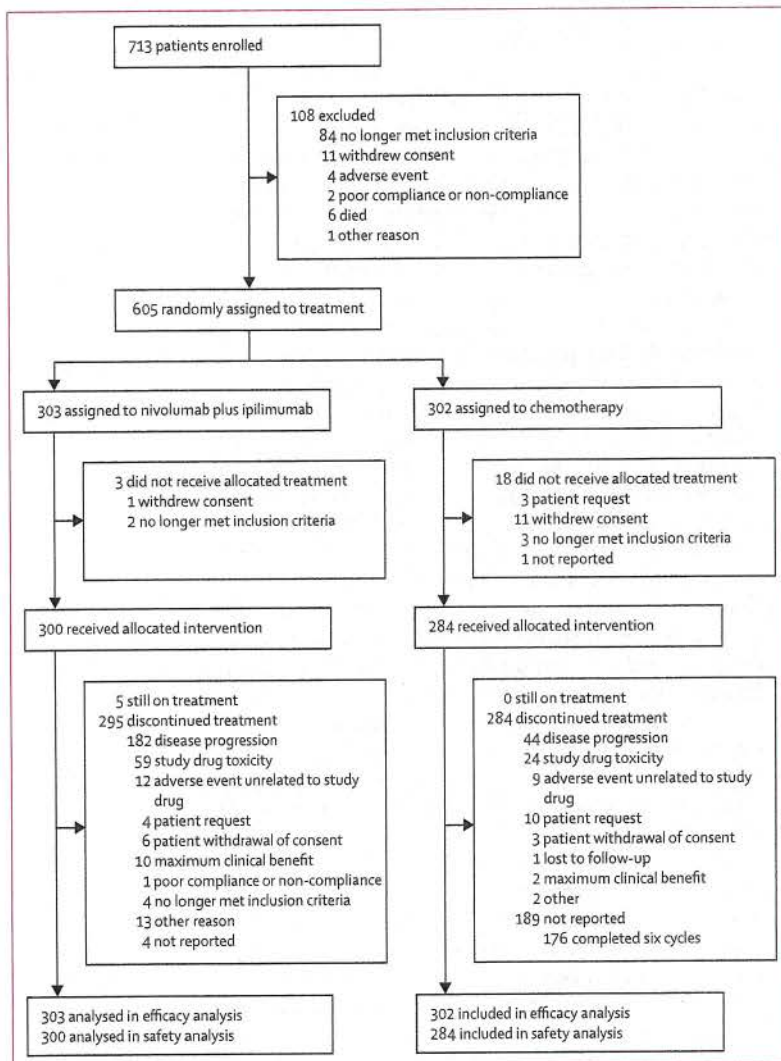


Figure 1: Trial profile

and CIs (96·6% CIs for the overall survival primary analysis [alpha adjusted for interim analysis], and 95% CI elsewhere) using a stratified Cox proportional hazards model with treatment group as a single covariate. We checked the proportional hazards assumption only for the primary endpoint of overall survival by adding a time-dependent covariate, defined by treatment-by-time interaction, into the stratified Cox regression model of overall survival. We estimated survival curves and rates using the Kaplan-Meier method. We calculated exact two-sided 95% CIs for objective response and disease control rates using the Clopper-Pearson method. We did prespecified descriptive subgroup analyses for overall survival, summarised using HRs (with 95% CIs) calculated using an unstratified Cox proportional hazards model. Safety analyses included all patients who received at least one dose of study drug. We also did exposure adjusted safety analyses, taking into account all on-treatment events on the basis of the total exposure time. We calculated the person-year exposure as the sum over the participants' exposure expressed in years. More details on all analyses are in the appendix (pp 7–8).

We did all statistical analyses using SAS software (version 9.2). An independent Data Monitoring Committee reviewed efficacy and safety data on a periodic basis and at the time of the preplanned interim analysis. This trial is registered with ClinicalTrials.gov, NCT02899299.

Role of the funding source

The study was designed by the funder (Bristol Myers Squibb) and study steering committee. The funder had a role in data collection with the investigators, data analysis and interpretation in collaboration with the authors, and the writing of the report by funding professional medical writing assistance. All authors had full access to all the data in the study and had final responsibility for the decision to submit for publication.

Results

Between Nov, 29, 2016, and April 28, 2018, we enrolled 713 patients, of whom 605 were eligible and randomly assigned to nivolumab plus ipilimumab (n=303) or chemotherapy (n=302). 300 participants in the nivolumab plus ipilimumab group and 284 in the chemotherapy group received at least one dose of study drug (figure 1). At the prespecified interim analysis (database lock April 3, 2020), the median follow-up for overall survival was 29·7 months (IQR 26·7–32·9), with a minimum of 22·1 months. Baseline characteristics were well balanced between treatment groups (table 1). 467 (77%) of 605 participants were male and median age was 69 years (IQR 64–75). Overall, 456 (75%) of 605 patients had epithelioid tumour histology.

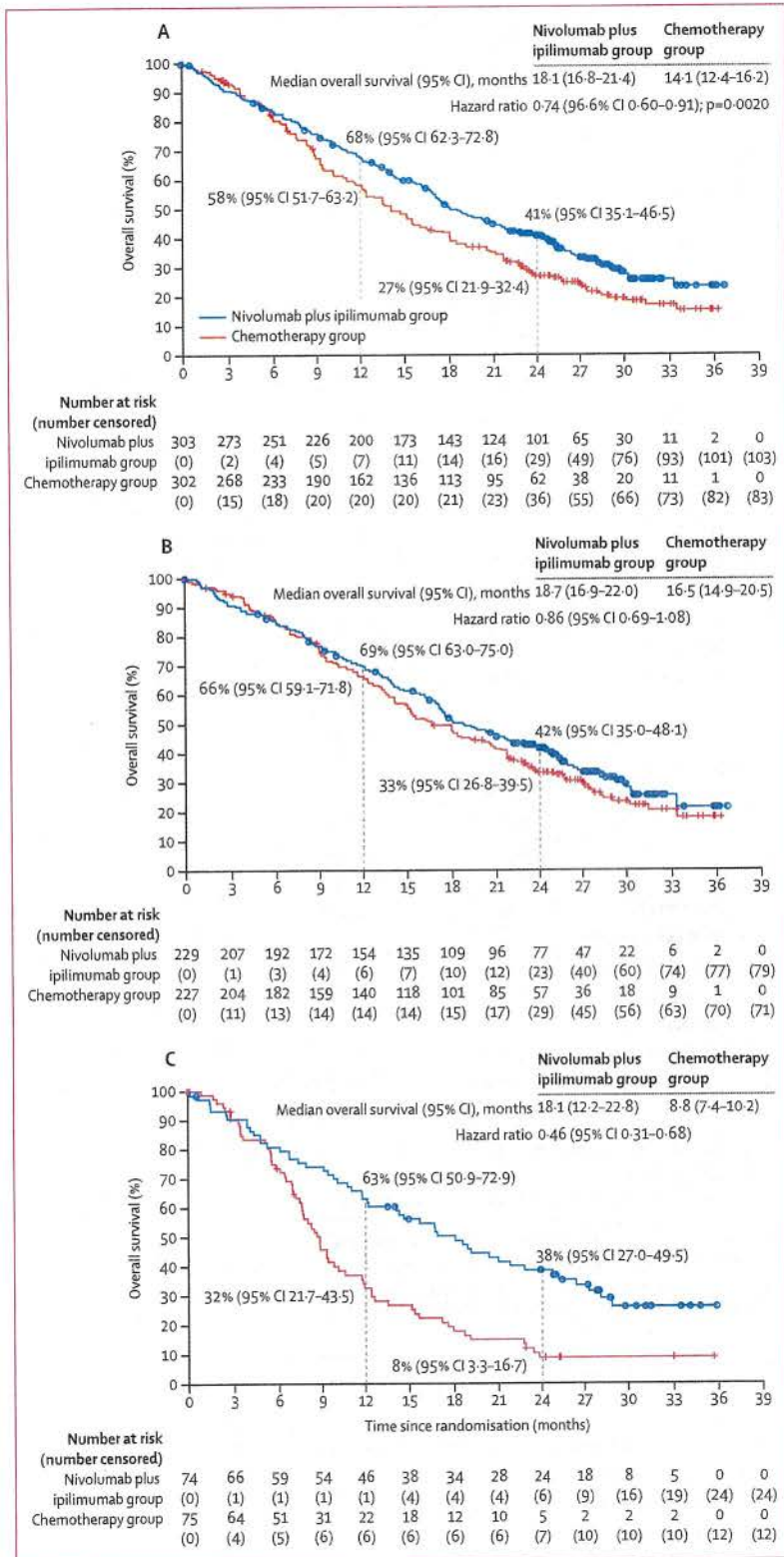
As of database lock, five (2%) of 300 patients in the nivolumab plus ipilimumab group who received

	Nivolumab plus ipilimumab group (n=303)	Chemotherapy group (n=302)
Age, years	69 (65–75)	69 (62–75)
<65	71 (23%)	96 (32%)
≥65 to <75	154 (51%)	127 (42%)
≥75	78 (26%)	79 (26%)
Sex		
Male	234 (77%)	233 (77%)
Female	69 (23%)	69 (23%)
Region		
North America	32 (11%)	27 (9%)
Europe	177 (58%)	175 (58%)
Asia	26 (9%)	39 (13%)
Rest of the world*	68 (22%)	61 (20%)
Eastern Cooperative Oncology Group performance status†		
0	114 (38%)	128 (42%)
1	189 (62%)	173 (57%)
Smoking status		
Current or former	173 (57%)	171 (57%)
Never	127 (42%)	122 (40%)
Unknown	3 (1%)	9 (3%)
Histology		
Epithelioid	229 (76%)	227 (75%)
Non-epithelioid	74 (24%)	75 (25%)
Sarcomatoid	35 (12%)	36 (12%)
Mixed or other	39 (13%)	39 (13%)
Stage		
1	12 (4%)	20 (7%)
2	23 (8%)	22 (7%)
3	103 (34%)	106 (35%)
4	160 (53%)	149 (49%)
Not reported	5 (2%)	5 (2%)
Previous cancer therapy		
Radiotherapy‡	29 (10%)	28 (9%)
Systemic therapy§	1 (<1%)	0
PD-L1 status		
Quantifiable	289 (95%)	297 (98%)
<1%¶	57/289 (20%)	78/297 (26%)
≥1%¶	232/289 (80%)	219/297 (74%)

Data are median (IQR) or n (%). PD-L1=programmed cell death ligand 1. *Includes Australia, Brazil, Chile, and South Africa. †On a score of 0 to 5, with higher scores indicating greater disability. One patient in the chemotherapy group had a baseline Eastern Cooperative Oncology Group performance status of 2 (protocol deviation). ‡Previous radiotherapy was provided for palliative support, pain management, or prophylactic track irradiation for tumour biopsy. §Due to incorrect data entry, one patient was reported as having previous systemic cancer therapy in the nivolumab plus ipilimumab group. ¶Calculated as a proportion of quantifiable patients.

Table 1: Baseline characteristics

treatment remained on treatment and no patients in the chemotherapy group remained on treatment (figure 1). The main reasons for treatment discontinuation in the nivolumab plus ipilimumab group were disease progression (182 [61%] of 300) and study drug toxicity



(59 [20%]); 25 (8%) of 300 patients completed 2 years of immunotherapy. During the study, one patient in the nivolumab plus ipilimumab group discontinued study drug but received subsequent therapy from the investigator before BICR confirmation of disease progression. In the chemotherapy group, 176 (62%) of 284 patients completed all six cycles; 44 (16%) discontinued due to disease progression and 24 (8%) due to study drug toxicity. Median duration of treatment was 5.6 months (IQR 2.0–11.4) in the nivolumab plus ipilimumab group and 3.5 months (IQR 2.7–3.7) in the chemotherapy group (appendix p 9). The median number of nivolumab doses received was 12.0 (IQR 5.0–23.5) and of ipilimumab was 4.0 (2.0–7.0). After randomisation, 104 (34%) of 302 patients in the chemotherapy group were given cisplatin and 180 (60%) were given carboplatin; 29 (28%) of 104 patients given cisplatin switched to carboplatin after the first dose due to investigator decision. The median number of doses of cisplatin was 5.0 (IQR 3.0–6.0), of carboplatin was 6.0 (4.0–6.0), and of pemetrexed was 6.0 (4.0–6.0). Further information on treatment exposure is in the appendix (pp 9–10).

In the nivolumab plus ipilimumab group, 134 (44%) of 303 patients were given subsequent systemic therapy, ten (3%) were given subsequent immunotherapy, and 131 (43%) were given subsequent chemotherapy. In the chemotherapy group, 123 (41%) of 302 patients were given subsequent systemic therapy, 61 (20%) were given subsequent immunotherapy, and 95 (31%) were given subsequent chemotherapy (appendix p 11).

The study met its primary endpoint at the prespecified interim analysis according to the recommendation of the independent Data Monitoring Committee. Given that the study was able to reject the null hypothesis at the interim analysis, this analysis is considered final. Median overall survival was 18.1 months (95% CI 16.8–21.4) with nivolumab plus ipilimumab versus 14.1 months (12.4–16.2) with chemotherapy, with a stratified HR of 0.74 (95% CI 0.60–0.91; p=0.0020; figure 2). The p value for the time-dependent covariate was 0.9646, indicating that there was no evidence of a non-constant treatment effect over time. Overall survival rates at 1 year were 68% (95% CI 62.3–72.8) versus 58% (51.7–63.2) and at 2 years were 41% (35.1–46.5) versus 27% (21.9–32.4). Overall survival was similar between chemotherapy regimens: median overall survival was 13.7 months (95% CI 11.8–17.9) with pemetrexed plus cisplatin, and 15.0 months (12.2–17.9) with pemetrexed plus carboplatin (appendix p 25). Overall survival favoured nivolumab plus ipilimumab across most

Figure 2: Overall survival in all randomised patients (A) and in patients with epithelioid tumour histology (B) and non-epithelioid tumour histology (C). The hazard ratio in part A is stratified by sex and histology. The hazard ratios in parts B and C are from unstratified Cox proportional hazard models.

subgroups, although survival in patients aged 75 years and older ($n=157$) was similar between treatment groups (figure 3). Notably, overall survival was improved with nivolumab plus ipilimumab versus chemotherapy regardless of histology (study stratification factor; figure 2). We found some evidence of higher treatment effect in patients with non-epithelioid histology (HR 0.46 [95% CI 0.31–0.68]) than in those with the epithelioid subtype (0.86 [0.69–1.08]). Median overall survival with nivolumab plus ipilimumab was similar between non-epithelioid and epithelioid subtypes (18.1 months [95% CI 12.2–22.8] vs 18.7 months [16.9–22.0]), as were 2-year overall survival rates (38% [95% CI 27.0–49.5] vs 42% [35.0–48.1]). By contrast, median overall survival with chemotherapy differed substantially between non-epithelioid and epithelioid subtypes (8.8 months [95% CI 7.4–10.2] vs 16.5 months [14.9–20.5]), as did 2-year overall survival rates (8% [95% CI 3.3–16.7] vs 33% [26.8–39.5]). Overall survival benefit by tumour PD-L1 expression level for nivolumab plus ipilimumab versus chemotherapy was greater in patients with tumour expression of PD-L1 of 1% or higher (HR 0.69 [95% CI 0.55–0.87]) than in patients with expression of less than 1% (0.94 [0.62–1.40];

figure 3; appendix pp 23–24). Nonetheless, median overall survival with nivolumab plus ipilimumab was similar in patients with tumours with PD-L1 expression of 1% or higher (18.0 months [95% CI 16.8–21.5]) and of less than 1% (17.3 months [95% CI 10.1–24.3]); 1-year survival rates were 70% (95% CI 63.4–75.3) and 59% (45.5–70.9); and 2-year survival rates were 41% (34.3–47.2) and 39% (25.9–51.3; appendix pp 23–24). Conversely, median overall survival with chemotherapy differed between patients with PD-L1 expression of 1% or higher (13.3 months [95% CI 11.6–15.4]) and less than 1% (16.5 months [13.4–20.5]); 1-year survival rates were 55% (95% CI 48.2–61.8) and 64% (52.3–73.9); and 2-year survival rates were 28% (22.1–34.7) and 25% (15.5–35.0; appendix pp 23–24).

The minimum follow-up for progression-free survival was 19.8 months. Median progression-free survival was similar between treatment groups: 6.8 months (95% CI 5.6–7.4) with nivolumab plus ipilimumab and 7.2 months (95% CI 6.9–8.0) with chemotherapy (HR 1.00 [95% CI 0.82–1.21]). However, progression-free survival rates at 2 years were numerically greater with nivolumab plus ipilimumab (16% [95% CI 11.7–21.5]) versus chemotherapy (7% [4.0–11.7]; figure 4).

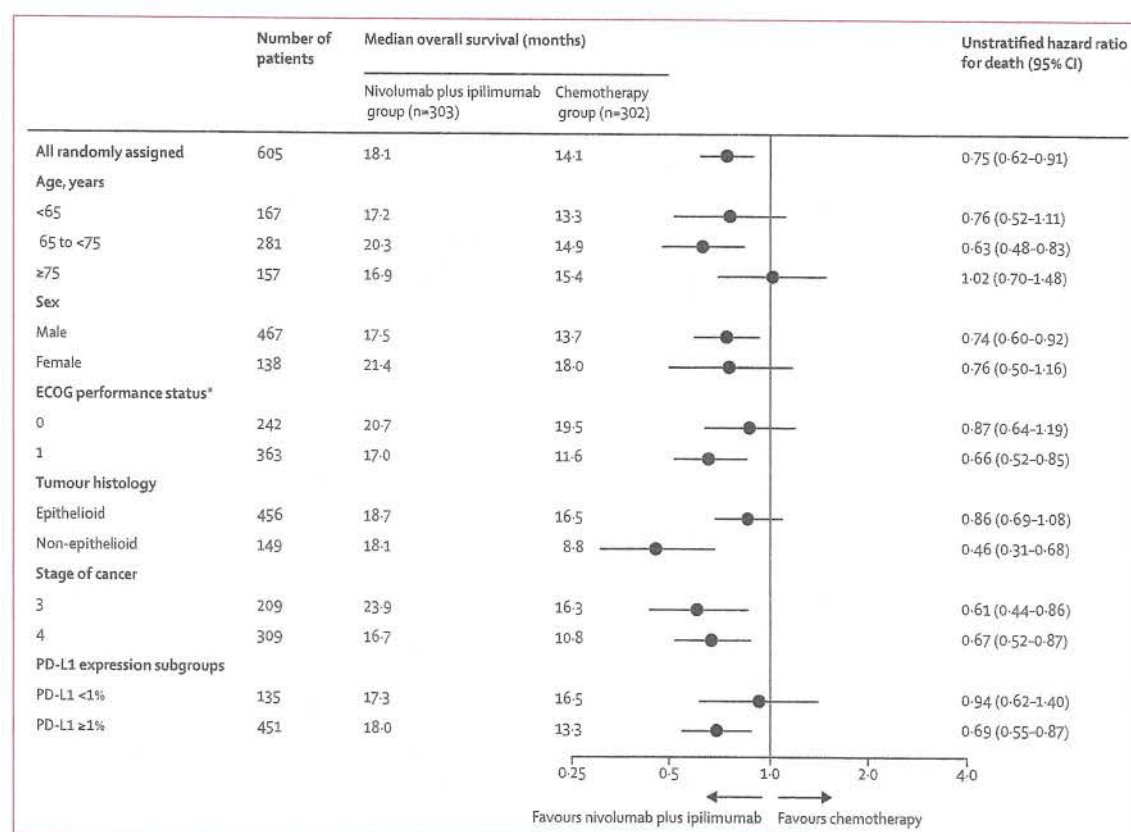


Figure 3: Overall survival in predefined patient subgroups

ECOG=Eastern Cooperative Oncology Group. PD-L1=programmed cell death ligand 1. *One patient in the chemotherapy group had a baseline performance status of 2 (protocol deviation).

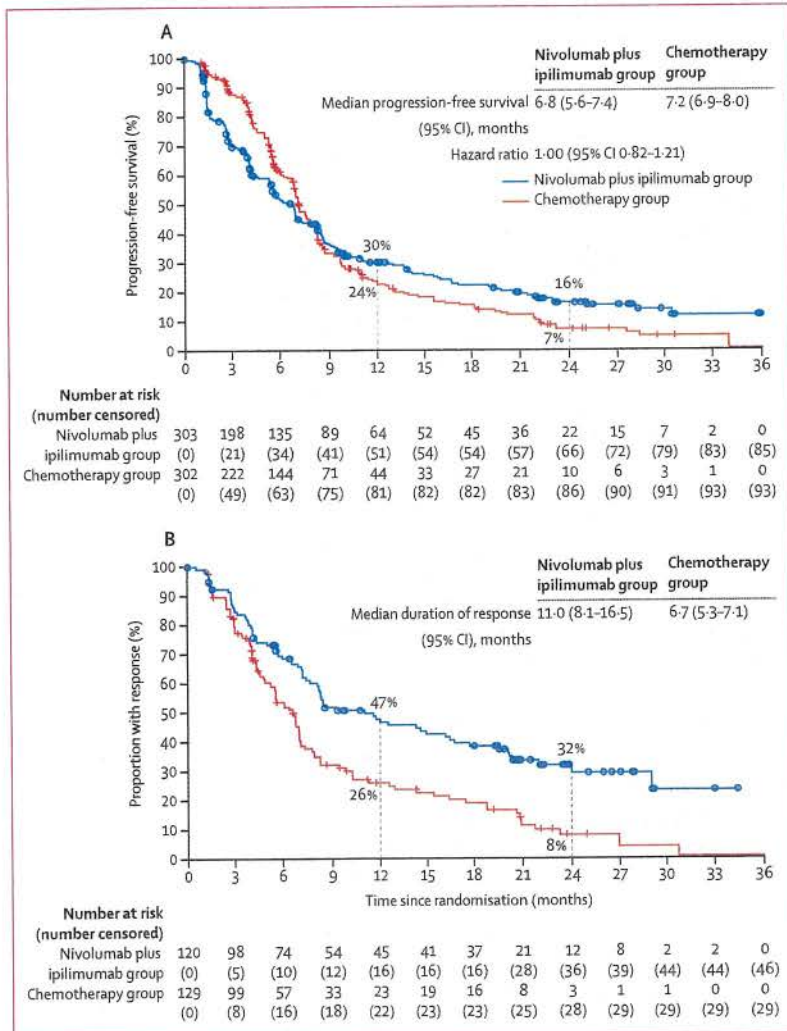


Figure 4: Progression-free survival in all patients randomly assigned to treatment (A) and duration of response in confirmed responders (B). Progression-free survival and duration of response are both per blinded independent central review. The hazard ratio in part A is stratified by sex and histology.

An objective response was reported in 120 of 303 patients (40%; 95% CI 34.1-45.4) in the nivolumab plus ipilimumab group versus 129 of 302 patients (43%; 95% CI 37.1-48.5) in the chemotherapy group (table 2). Complete responses were only observed in the nivolumab plus ipilimumab group (five [2%] of 303 patients). Disease control was seen in 232 of 303 patients (77%; 95% CI 71.4-81.2) with a median time to response of 2.7 months (IQR 1.45-3.27) for the nivolumab plus ipilimumab group versus 257 of 302 (85%; 95% CI 80.6-88.9) with a median time to response of 2.5 months (IQR 1.41-3.02) for the chemotherapy group. Median duration of response in all confirmed responders was 11.0 months (95% CI 8.1-16.5) in the nivolumab plus ipilimumab group versus 6.7 months (95% CI 5.3-7.1) in the chemotherapy group (figure 4). The 2-year duration of response rate was 32%

	Nivolumab plus ipilimumab group (n=303)	Chemotherapy group (n=302)
Objective response rate		
n (%)	120 (40%)	129 (43%)
95% CI	34.1-45.4	37.1-48.5
Best overall response		
Complete response	5 (2%)	0
Partial response	115 (38%)	129 (43%)
Stable disease	112 (37%)	125 (41%)
Non-complete response and non-progressive disease	0	3 (1%)
Progressive disease	55 (18%)	14 (5%)
Unable to determine	4 (1%)	5 (2%)
Not reported	12 (4%)	26 (9%)
Disease control rate		
n (%)	232 (77%)	257 (85%)
95% CI	71.4-81.2	80.6-88.9
Time to response, months		
Median	2.7	2.5
IQR	1.45-3.27	1.41-3.02
Duration of response, months		
Median	11.0	6.7
95% CI	8.1-16.5	5.3-7.1
Proportion of patients with a response of at least 1 year or 2 years*		
At 1 year	47%	26%
95% CI	37-56	18-34
At 2 years	32%	8%
95% CI	23-41	3-15

Data are n (%), unless indicated otherwise. Minimum follow-up for objective response rate was 19.8 months. *Estimates are based on Kaplan-Meier estimates of duration of response.

Table 2: Tumour response, as per blinded independent central review, in all patients randomly assigned to treatment

(95% CI 23-41) in the nivolumab plus ipilimumab group versus 8% (95% CI 3-15) in the chemotherapy group.

Safety is summarised in table 3, and all reported grade 3 and 4 treatment-related adverse events are listed in the appendix (pp 13-16). Of 300 patients treated with nivolumab plus ipilimumab, 28 (9%) discontinued ipilimumab early. In the chemotherapy group, dose reductions occurred in 89 (31%) of 284 participants who were given pemetrexed, 18 (17%) of 104 patients who were given cisplatin, and 85 (41%) of 209 participants who were given carboplatin, whereas dose reductions were not permitted for the nivolumab plus ipilimumab group. Grade 3-4 treatment-related adverse events were reported in 91 (30%) of 300 participants treated with nivolumab plus ipilimumab and 91 (32%) of 284 participants treated with chemotherapy. Any-grade serious treatment-related adverse events were reported in 64 (21%) patients treated with nivolumab plus ipilimumab versus 22 (8%) patients treated with chemotherapy; grade 3-4 treatment-related serious

	Nivolumab plus ipilimumab group (n=300)			Chemotherapy group (n=284)		
	Grade 1-2	Grade 3	Grade 4	Grade 1-2	Grade 3	Grade 4
Any	148 (49%)	79 (26%)	12 (4%)	141 (50%)	73 (26%)	18 (6%)
Diarrhoea	52 (17%)	10 (3%)	0	19 (7%)	2 (1%)	0
Pruritus	46 (15%)	3 (1%)	0	1 (<1%)	0	0
Rash	40 (13%)	3 (1%)	0	15 (5%)	0	0
Fatigue	38 (13%)	3 (1%)	0	50 (18%)	5 (2%)	0
Hypothyroidism	32 (11%)	0	0	0	0	0
Nausea	29 (10%)	1 (<1%)	0	97 (34%)	7 (2%)	0
Anaemia	5 (2%)	1 (<1%)	0	70 (25%)	32 (11%)	0
Decreased appetite	27 (9%)	2 (1%)	0	48 (17%)	2 (1%)	0
Constipation	12 (4%)	0	0	41 (14%)	1 (<1%)	0
Vomiting	8 (3%)	0	0	35 (12%)	6 (2%)	0
Asthenia	25 (8%)	0	0	32 (11%)	12 (4%)	0
Increased lipase	7 (2%)	11 (4%)	2 (1%)	0	1 (<1%)	0
Colitis	3 (1%)	7 (2%)	0	1 (<1%)	1 (<1%)	0
Increased amylase	10 (3%)	6 (2%)	1 (<1%)	1 (<1%)	0	0
Thrombocytopenia	0	2 (1%)	0	16 (6%)	4 (1%)	6 (2%)
Neutropenia	0	1 (<1%)	1 (<1%)	28 (10%)	31 (11%)	12 (4%)

Data are n (%). Safety was assessed in all patients who received at least one dose of study drug. Treatment-related adverse events with an incidence of $\geq 10\%$ in any group or grade 3 or 4 severity with an incidence of $\geq 2\%$ in any group are shown. All grade 3 and 4 events are listed in the appendix (pp 13-16). Treatment-related adverse events included those reported between the first dose of study drug and 30 days after the last dose of study drug. *Only events that led to death within 24 h were documented as grade 5 and reported as deaths. Events leading to death >24 h after onset are reported with the worst grade before death.

Table 3: Summary of treatment-related adverse events in all treated patients*

events were reported in 46 (15%) patients treated with nivolumab plus ipilimumab versus 17 (6%) treated with chemotherapy (appendix pp 17-19). Any-grade treatment-related adverse events that led to discontinuation (due to either component of the regimen) were reported in 69 (23%) of 300 patients treated with nivolumab plus ipilimumab and 45 (16%) of 284 patients treated with chemotherapy, and 45 (15%) patients treated with nivolumab plus ipilimumab and 21 (7%) patients treated with chemotherapy had grade 3-4 events that led to discontinuation (appendix p 20).

The most frequent any-grade treatment-related adverse events were diarrhoea in the nivolumab plus ipilimumab group (62 [21%] of 300 patients) and nausea in the chemotherapy group (104 [37%] of 284 patients). The most frequently reported any-grade serious treatment-related adverse events were colitis in the nivolumab plus ipilimumab group (nine [3%]) and anaemia in the chemotherapy group (six [2%]; appendix pp 17-19). The median exposure time was 6.5 months (IQR 2.99-12.22) for nivolumab plus ipilimumab and 4.5 months (3.65-4.68) for chemotherapy. Treatment exposure was 220.3 person-years with nivolumab plus ipilimumab and 94.5 person-years with chemotherapy. The overall exposure-adjusted incidence of treatment-related adverse events was 502.1 per 100 person-years with nivolumab plus ipilimumab versus 1355.3 per 100 person-years with chemotherapy.

A summary of treatment-related select adverse events (those with a potential immunological cause), time to

onset and resolution of treatment-related select adverse events, the proportion of patients requiring immune-modulating concomitant medication (mostly corticosteroids), and the duration of use of immune-modulating concomitant medication are shown in the appendix (p 21). The most commonly reported any-grade treatment-related select adverse events with nivolumab plus ipilimumab were skin (108 [36%] of 300 patients) and gastrointestinal (66 [22%]) events. Overall, 198 (66%) of 300 patients who were given nivolumab plus ipilimumab died, with 183 (61%) deaths due to disease progression. 212 (75%) of 284 patients given chemotherapy died, with 199 (70%) deaths due to disease progression. Three (1%) treatment-related deaths occurred in the nivolumab plus ipilimumab group, due to pneumonitis, encephalitis, and heart failure. One (<1%) treatment-related death occurred in the chemotherapy group due to myelosuppression.

Discussion

To our knowledge, CheckMate 743 is the first large, randomised, phase 3 study to show significant and clinically meaningful improvement in overall survival with immunotherapy versus standard-of-care platinum plus pemetrexed chemotherapy for first-line treatment of unresectable MPM. Based on these results, in October, 2020, the US Food and Drug Administration approved nivolumab plus ipilimumab for this patient population.¹² With a median follow-up of 29.7 months, nivolumab plus ipilimumab provided durable survival benefit versus chemotherapy, with a 50% improvement

in the 2-year overall survival rate (41% vs 27%). Furthermore, estimated rates of patients who still had a response at 2 years was 8% with chemotherapy versus 32% with nivolumab plus ipilimumab. The safety profile of nivolumab plus ipilimumab in this study was consistent with that seen previously in NSCLC at this dose and schedule¹⁵ and no new safety signals were reported.

The frequencies of grade 3 or 4 serious treatment-related adverse events and those leading to discontinuation were higher with nivolumab plus ipilimumab than with chemotherapy; however, most were manageable and resolved with steroids or supportive treatment. Moreover, when treatment-related adverse events were adjusted for exposure, the overall incidence of treatment-related adverse events was lower with nivolumab plus ipilimumab than with chemotherapy.

Benefit with nivolumab plus ipilimumab was observed in most subgroups assessed, with the exception of patients aged 75 years or older. However, these subgroups were small and did not have statistical power. As such, results from these subgroup analyses should be interpreted with caution. Importantly, benefits were observed across histological groups, albeit at different magnitudes. For example, median overall survival with nivolumab plus ipilimumab was consistent between patients with epithelioid histology (18.7 months; HR 0.86 [95% CI 0.69–1.08]) and non-epithelioid histology (18.1 months; HR 0.46 [0.31–0.68]), showing clinically meaningful survival improvements across both groups; 1-year and 2-year overall survival rates were also similar between the two histological subgroups. Notably, in the epithelioid subgroup, nivolumab plus ipilimumab showed an improvement of 2 months in median overall survival compared with chemotherapy, with an HR favouring nivolumab plus ipilimumab despite the 95% CI overlapping 1. Furthermore, the 2-year overall survival rate in the epithelioid subgroup showed a long-term benefit of nivolumab plus ipilimumab with a 9% absolute difference versus chemotherapy. The larger magnitude of benefit observed in the non-epithelioid subgroup was primarily driven by the inferior effect of chemotherapy in the non-epithelioid subtype, as previously reported.³ This difference in outcomes between the subgroups treated with chemotherapy could not be attributed to the type of chemotherapy received because exploratory data from CheckMate 743 suggest that patients derive a similar overall survival benefit regardless of platinum backbone; median overall survival was similar between pemetrexed plus cisplatin and pemetrexed plus carboplatin.

Median progression-free survival and objective response rates were each numerically similar for nivolumab plus ipilimumab and chemotherapy. Median progression-free survival was similar to results from previously reported clinical trials in recurrent MPM.^{16,18} The progression-free survival Kaplan-Meier curves crossed at approximately 8 months, reflecting more rapid, although not durable,

disease control with chemotherapy. However, radiographic assessments in MPM can be challenging because of the absence of distinguishable tumour margins over time and successive CT evaluations.²² Thus, overall survival is considered to be a more objective and reliable endpoint in this tumour type. Notably, nivolumab plus ipilimumab provided long-term overall survival benefit, although the slight early survival benefit observed with chemotherapy was not durable.

The duration of response and durable survival benefit observed with nivolumab plus ipilimumab in patients with MPM in CheckMate 743 builds on the existing body of evidence that shows extended survival benefit with this dual immunotherapy regimen across a number of other tumour types, including NSCLC.^{13–15,23} Ipilimumab is hypothesised to drive memory T-cell production leading to durable responses when combined with nivolumab.¹¹ Results of the current study also corroborate the promising activity seen with anti-PD-1 or anti-PD-L1, and anti-CTLA-4 combination therapies in phase 2 studies in second-line or later settings of MPM,^{16,18,24} and support the use of dual immunotherapy over single-agent anti-PD-1 or anti-CTLA-4 inhibitors, which have shown little benefit over chemotherapy.^{25,26}

Some treatment guidelines (eg, NCCN guidelines) include the optional addition of the anti-angiogenic agent bevacizumab to platinum plus pemetrexed chemotherapy for first-line treatment of MPM in select patients, based on the survival benefit seen in a phase 3 trial;^{5,10} however, this regimen is not approved by regulators. Nonetheless, given the durable survival benefit seen in CheckMate 743, combining nivolumab plus ipilimumab with other therapies, including anti-angiogenic agents or, as approved for NSCLC in May, 2020, a short course of chemotherapy,¹² merits investigation to determine whether survival outcomes can be further enhanced. Similarly, future trials assessing the benefit of second-line targeted therapies (eg, bevacizumab and ramucirumab) after nivolumab plus ipilimumab treatment are warranted.

Reliable biomarkers to predict the benefit of dual-agent immunotherapy in the treatment of MPM have not yet been identified. Although PD-L1 expression is an established biomarker for single-agent immunotherapy in NSCLC,²⁷ its role in predicting treatment outcomes with dual immunotherapy regimens has not been established. More specifically, in MPM trials investigating immunotherapies, the association between PD-L1 expression and efficacy is inconsistent.^{17,18,24} In CheckMate 743, overall survival outcomes with nivolumab plus ipilimumab were similar in the subgroups with less than 1% and with 1% or higher PD-L1 expressions and better outcomes were seen with nivolumab plus ipilimumab than with chemotherapy at 2 years in both subgroups. However, survival with chemotherapy was better in patients with tumour PD-L1 expression of less than 1% than those with expression of 1% or higher. These observations suggest that absence of PD-L1 expression might be indicative of better prognosis

with chemotherapy. However, these descriptive and exploratory data should be interpreted with caution given their potential limitations—ie, PD-L1 expression was not a stratification factor in the study and the sample size of the PD-L1 expression less than 1% group was small. As such, the potential for imbalances in known or unknown prognostic factors does not allow us to draw definitive conclusions. Better characterisation of this heterogeneous disease using transcriptomic and epigenetic profiling should guide future patient selection and therapeutic strategies, and aid in the identification of novel biomarkers.^{28,29}

In summary, first-line nivolumab plus ipilimumab provided a significant and clinically meaningful improvement in overall survival versus platinum plus pemetrexed chemotherapy. Nivolumab plus ipilimumab has a favourable clinical benefit–risk profile that has led to approval in the USA and should be considered as a new standard of care for previously untreated patients with unresectable MPM, regardless of histological subtype.

Contributors

PB, AS, AKN, NF, SPe, AST, ASM, SPo, TJ, PA, AO, CB, and GZ provided substantial contributions to the conception and design of the study. PB, AS, AKN, NF, SPe, AST, ASM, SA, YO, YB, RC, LG, FG, DK, JR-C, and GZ enrolled and treated patients. CB wrote the study statistical analysis plan, did all statistical analyses, and generated data. PB, AKN, NF, SPe, AST, ASM, SPo, TJ, PA, AO, CB, and GZ analysed and interpreted the data. PA and CB verified the underlying data from the study. All authors reviewed the data, contributed to the development of the manuscript, and approved the final version for publication.

Declaration of interests

PB has received institutional grant funding from Bristol Myers Squibb and MSD and has a consultancy or advisory role for Bristol Myers Squibb, MSD, Roche, Beigene, Epizyme, Takeda, Trizell, and Daiichi-Sankyo (all honoraria are paid to his institute). AS has received grant funding and personal fees from Bristol Myers Squibb (for provided work on advisory boards, consultancy, service on the speaker's bureau, provision of expert testimony, and for travel or accommodation expenses) and their institution has also received support from Bristol Myers Squibb (payment for work as a principal investigator or coprincipal investigator in clinical trials); has received personal fees from AstraZeneca and MSD (for provided work on advisory boards, consultancy, service on the speaker's bureau, provision of expert testimony, and for travel or accommodation expenses) and their institution also received support from AstraZeneca and MSD (payment for work as a principal investigator or coprincipal investigator in clinical trials); and has received personal fees from Roche (for provided work on advisory boards, consultancy, service on the speaker's bureau, provision of expert testimony, and for travel or accommodation expenses) and their institution also received support from Roche (payment for work as a principal investigator or coprincipal investigator in clinical trials). AKN has received grant funding from Atara Biotherapeutics and Douglas Pharmaceuticals; received non-financial, travel support, and grant funding from AstraZeneca; received personal fees from Bayer Pharmaceuticals, Pharmabinc, and Trizell (honoraria and provided consulting); received personal fees, non-financial, and travel support from Boehringer Ingelheim (honoraria, served on the advisory board and travel funding); received personal fees from Douglas Pharmaceuticals, Merck Sharp Dohme, and Roche Pharmaceuticals (served on the advisory board and honoraria); and received personal fees from Atara Biotherapeutics (served on the advisory board). NF has received personal fees from Bristol Myers Squibb and Daiichi Sankyo (honoraria) and received grant funding and personal fees from ONO pharmaceutical (honoraria, and provided advice and consulting). SPe has received personal fees and non-financial support from AstraZeneca,

Boehringer Ingelheim, Bristol Myers Squibb, F Hoffmann-La Roche, MSD, Novartis, and Pfizer (served on the advisory board, gave talks, honoraria, and investigation in trials); received personal fees from Amgen, Clovis, Illumina, and Merck Serono (served on the advisory board, honoraria, and investigation in trials); received personal fees from Takeda (gave talks, and honorarium); received personal fees from Eli Lilly and Sanofi (served on the advisory board, honoraria, and gave talks); received personal fees from AbbVie, Bayer, Biocartis, Biovent, Daiichi Sankyo, Debiopharm, Foundation Medicine, Janssen, Merrimack, Pharma Mar, Regeneron, Seattle Genetics, and Takeda (served on the advisory board and honoraria). AST has received personal fees from Bristol Myers Squibb, Eli Lilly, Genentech, Roche, Novartis, Ariad, EMD Serono, Merck, Seattle Genetics, AstraZeneca, Boehringer Ingelheim, Sellas Life Science, and Takeda (for advisory boards); and has received grant support from Millenium, Polaris, Epizyme, EMD Serono, and Seattle Genetics (for research grants). ASM's institution received support from AbbVie, AstraZeneca, Bristol Myers Squibb, and Genentech/Roche (paid honoraria to the institution); received grant funding from Novartis and Verily (paid to institution); and ASM has received travel expenses from Roche; and ASM has acted as a non-remunerated director for the Mesothelioma Applied Research Foundation. SPo received personal fees from AbbVie, AstraZeneca, Bayer, Beigene, Blueprint, Boehringer Ingelheim, Bristol Myers Squibb, Chugai, Daiichi Sankyo, EMD Serono, Eli Lilly, GlaxoSmithKline, Guardant Health, Incyte, Janssen, Merck Sharp & Dohme, Novartis, Pfizer, Roche, Seattle Genetics, Takeda, and Tesaro (served on the advisory board and provided consulting); received personal fees from Elsevier (employment); and received personal fees from Paradox (provided consulting). TJ has received personal fees from Atara Pharmaceuticals; grant funding from AstraZeneca, Eli Lilly, Epizyme, Polaris, Springworks, and Trizell; and retired during manuscript development. SA has received personal fees from Bristol Myers Squibb (consulting or advisory role); personal fees from Achilles Biotech, Celcius Therapeutics, Memgen, Rapt Therapeutics, Venn Therapeutics, Glympse, and Samyang (for advisory boards); personal fees from AstraZeneca, Caris Life Science, G1 Therapeutics, GlaxoSmithKline, Merck, and Nektar (as an advisor); personal fees and non-financial support from Amgen (as an advisor and for travel fees); grant support from Cellular Biomedicine Group (for clinical trial support); and personal fees from EMD Serono (for a data review committee). YO has received personal fees from AstraZeneca, Bristol Myers Squibb, and MSD (served on the advisory board). RC has received personal fees from MSD and Roche (served on the advisory board), and personal fees from Bristol Myers Squibb, Pfizer, and Roche (served on the speaker's bureau). LG has received personal fees from AbbVie, AstraZeneca, Boehringer Ingelheim, Bristol Myers Squibb, MSD, Novartis, Pfizer, Roche, and Takeda (advisory board). FG has received grant funding from Bristol Myers Squibb; personal fees from AstraZeneca, Bristol Myers Squibb, Eli Lilly, MSD, and Roche (served on the advisory board and served on the speaker's bureau); personal fees from Amgen, Boehringer Ingelheim, Pierre Fabre, and Pfizer (served on the speaker's bureau); and personal fees from Takeda and Bayer (served on the advisory board). DK has received personal fees from Amgen, AstraZeneca, Boehringer Ingelheim, Bristol Myers Squibb, Merck, Merck Sharp & Dome, Pfizer, Roche, and Takeda (served on the advisory board and provided consulting). JR-C has received other funding (sponsored research) from Bristol Myers Squibb; grant support, personal fees, and non-financial support (for advisory boards, as a speaker and in a research role) from Bristol Myers Squibb, MSD, and Roche; grant support and personal fees (for advisory boards, as a speaker and in a research role) from Takeda, Novartis, Pfizer, and AstraZeneca; personal fees (for advisory boards, as a speaker and in a research role) for Beigene; personal fees (for a research role) from Celltrion and Janssen; grant support and personal fees (for advisory boards and as a speaker) from Merck and Bayer; and grant support, personal fees, and non-financial support (for advisory boards and as a speaker) from Boehringer Ingelheim. PA was an employee of Bristol Myers Squibb. AO and CB are employees of and hold stocks in Bristol Myers Squibb. GZ has received grant funding from Inventiva and Roche; personal fees and reimbursement for attendance of international meetings from AbbVie, AstraZeneca, Bristol Myers Squibb, Boehringer Ingelheim, Pfizer, and Roche (travel or

accommodation expenses); personal fees from AstraZeneca, Bristol Myers Squibb, and Roche (served on the advisory board and honoraria); personal fees from Bristol Myers Squibb and Inventiva (provided consulting); and personal fees from MSD and Da Volterra (served on the advisory board). YB declares no competing interests.

Data sharing

The Bristol Myers Squibb policy on data sharing is available online.

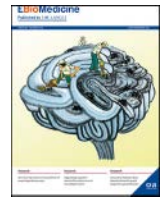
Acknowledgments

This study was funded by Bristol Myers Squibb. We thank the patients and families who participated for making this trial possible, and the investigators (appendix p 2) and clinical study teams who participated in the trial. We also thank Ama Day for contributions as protocol manager of this trial; Dako for collaborative development of the PD-L1 IHC 28-8 pharmDx assay; and Mhairi Laird, of Caudex (Oxford, UK), for her assistance in the preparation of the manuscript. The NCCN guidelines were cited with the permission of NCCN. NCCN makes no warranties of any kind whatsoever regarding their content, use, or application, and disclaims any responsibility for their application or use in any way.

References

- 1 Van Gerwen M, Alpert N, Wolf A, et al. Prognostic factors of survival in patients with malignant pleural mesothelioma: an analysis of the National Cancer Database. *Carcinogenesis* 2019; 40: 529–36.
- 2 Milano MT, Zhang H. Malignant pleural mesothelioma: a population-based study of survival. *J Thorac Oncol* 2010; 5: 1841–48.
- 3 Billé A, Krug LM, Woo KM, Rusch VW, Zauderer MG. Contemporary analysis of prognostic factors in patients with unresectable malignant pleural mesothelioma. *J Thorac Oncol* 2016; 11: 249–55.
- 4 Baas P, Fennell D, Kerr KM, Van Schil PE, Haas RL, Peters S. Malignant pleural mesothelioma: ESMO Clinical Practice Guidelines for diagnosis, treatment and follow-up. *Ann Oncol* 2015; 26 (suppl 5): v31–39.
- 5 Scherpereel A, Opitz I, Berghmans T, et al. ERS/ESTS/EACTS/ESTRO guidelines for the management of malignant pleural mesothelioma. *Eur Respir J* 2020; 55: 1900953
- 6 Santoro A, O'Brien ME, Stahel RA, et al. Pemetrexed plus cisplatin or pemetrexed plus carboplatin for chemo-naïve patients with malignant pleural mesothelioma: results of the International Expanded Access Program. *J Thorac Oncol* 2008; 3: 756–63.
- 7 Taylor P, Castagneto B, Dark G, et al. Single-agent pemetrexed for chemo-naïve and pretreated patients with malignant pleural mesothelioma: results of an International Expanded Access Program. *J Thorac Oncol* 2008; 3: 764–71.
- 8 Vogelzang NJ, Rusthoven JJ, Symanowski J, et al. Phase III study of pemetrexed in combination with cisplatin versus cisplatin alone in patients with malignant pleural mesothelioma. *J Clin Oncol* 2003; 21: 2636–44.
- 9 van Meerbeeck JP, Gaafar R, Manegold C, et al. Randomized phase III study of cisplatin with or without raltitrexed in patients with malignant pleural mesothelioma: an intergroup study of the European Organisation for Research and Treatment of Cancer Lung Cancer Group and the National Cancer Institute of Canada. *J Clin Oncol* 2005; 23: 6881–89.
- 10 Zalcman G, Mazieres J, Margery J, et al. Bevacizumab for newly diagnosed pleural mesothelioma in the Mesothelioma Avastin Cisplatin Pemetrexed Study (MAPS): a randomised, controlled, open-label, phase 3 trial. *Lancet* 2016; 387: 1405–14.
- 11 Wei SC, Duffy CR, Allison JP. Fundamental mechanisms of immune checkpoint blockade therapy. *Cancer Discov* 2018; 8: 1069–86.
- 12 Bristol Myers Squibb. OPDIVO (nivolumab) prescribing information. US Food and Drug Administration, December, 2020. https://packageinserts.bms.com/pi/pi_opdivo.pdf (accessed Jan 14, 2021).
- 13 Larkin J, Chiarion-Sileni V, Gonzalez R, et al. Five-year survival with combined nivolumab and ipilimumab in advanced melanoma. *N Engl J Med* 2019; 381: 1535–46.
- 14 Motzer RJ, Rini BI, McDermott DF, et al. Nivolumab plus ipilimumab versus sunitinib in first-line treatment for advanced renal cell carcinoma: extended follow-up of efficacy and safety results from a randomised, controlled, phase 3 trial. *Lancet Oncol* 2019; 20: 1370–85.
- 15 Hellmann MD, Paz-Ares L, Bernabe Caro R, et al. Nivolumab plus ipilimumab in advanced non-small-cell lung cancer. *N Engl J Med* 2019; 381: 2020–31.
- 16 Scherpereel A, Mazieres J, Greillier L, et al. Nivolumab or nivolumab plus ipilimumab in patients with relapsed malignant pleural mesothelioma (IFCT-1501 MAPS2): a multicentre, open-label, randomised, non-comparative, phase 2 trial. *Lancet Oncol* 2019; 20: 239–53.
- 17 Quispel-Janssen J, van der Noort V, de Vries JF, et al. Programmed death 1 blockade with nivolumab in patients with recurrent malignant pleural mesothelioma. *J Thorac Oncol* 2018; 13: 1569–76.
- 18 Disselhorst MJ, Quispel-Janssen J, Lalezari F, et al. Ipilimumab and nivolumab in the treatment of recurrent malignant pleural mesothelioma (INITIATE): results of a prospective, single-arm, phase 2 trial. *Lancet Respir Med* 2019; 7: 260–70.
- 19 Oken MM, Creech RH, Tormey DC, et al. Toxicity and response criteria of the Eastern Cooperative Oncology Group. *Am J Clin Oncol* 1982; 5: 649–55.
- 20 Byrne MJ, Nowak AK. Modified RECIST criteria for assessment of response in malignant pleural mesothelioma. *Ann Oncol* 2004; 15: 257–60.
- 21 US Department of Health and Human Services, Food and Drugs Administration, Oncology Center of Excellence, Center for Drug Evaluation and Research (CDER), Center for Biologics Evaluation and Research (CBER). Clinical trial endpoints for the approval of cancer drugs and biologics. December, 2018. <https://www.fda.gov/media/71195/download> (accessed Jan 14, 2021).
- 22 US Department of Health and Human Services, Food and Drug Administration, Oncology Center of Excellence, Center for Drug Evaluation and Research (CDER), Center for Biologics Evaluation and Research (CBER). Clinical trial endpoints for the approval of cancer drugs and biologics: guidance for industry. December, 2018. <https://www.fda.gov/media/71195/download> (accessed July 24, 2020).
- 23 Ramalingam SS, Ciuleanu TE, Pluzanski A, et al. Nivolumab + ipilimumab versus platinum-doublet chemotherapy as first-line treatment for advanced non-small cell lung cancer: three-year update from CheckMate 227 part 1. *J Clin Oncol* 2020; 38 (suppl 15): 9500 (abstr).
- 24 Calabrò L, Morra A, Giannarelli D, et al. Tremelimumab combined with durvalumab in patients with mesothelioma (NIBIT-MESO-1): an open-label, non-randomised, phase 2 study. *Lancet Respir Med* 2018; 6: 451–60.
- 25 Popat S, Curioni-Fontecedro A, Dafni U, et al. A multicentre randomised phase III trial comparing pembrolizumab versus single-agent chemotherapy for advanced pre-treated malignant pleural mesothelioma: the European Thoracic Oncology Platform (ETOP 9-15) PROMISE-meso trial. *Ann Oncol* 2020; 31: 1734–45.
- 26 Maio M, Scherpereel A, Calabrò L, et al. Tremelimumab as second-line or third-line treatment in relapsed malignant mesothelioma (DETERMINE): a multicentre, international, randomised, double-blind, placebo-controlled phase 2b trial. *Lancet Oncol* 2017; 18: 1261–73.
- 27 Reck M, Rodríguez-Abreu D, Robinson AG, et al. Pembrolizumab versus chemotherapy for PD-L1-positive non-small-cell lung cancer. *N Engl J Med* 2016; 375: 1823–33.
- 28 Blum Y, Meiller C, Quétel L, et al. Dissecting heterogeneity in malignant pleural mesothelioma through histo-molecular gradients for clinical applications. *Nat Commun* 2019; 10: 1333.
- 29 Mansfield AS, Peikert T, Smadbeck JB, et al. Neoantigenic potential of complex chromosomal rearrangements in mesothelioma. *J Thorac Oncol* 2019; 14: 276–87.

For the Bristol Myers Squibb policy on data sharing see <https://www.bms.com/researchers-and-partners/clinical-trials-and-research/disclosure-commitment.html>



Commentary

An appropriate choice for immunotherapy in malignant pleural mesothelioma

Nobukazu Fujimoto

Department of Medical Oncology, Okayama Rosai Hospital, 1-10-25 Chikkomidorimachi, Okayama 7028055, Japan



ARTICLE INFO

Article History:

Received 23 September 2020

Accepted 23 September 2020

In this article of *EBioMedicine*, Mankor and colleagues [1] report the results of immune monitoring of peripheral blood immune cell subsets in patients with malignant pleural mesothelioma (MPM) treated with so-called immune checkpoint inhibitors (ICIs). Combination treatment with anti-PD-1/anti-CTLA-4 antibodies induced an increase in the proliferation and activation of T cells. In addition, patients who responded to the combination treatment had low frequencies of naïve CD8 T cells and high frequencies of effector memory CD8 T cells expressing cytokines, such as granzyme-B and interferon- γ . These findings suggest that immune monitoring of peripheral blood immune cell subsets may provide information for predicting clinical benefit from ICI-ICI combination therapy.

MPM is strongly associated with asbestos exposure and has continued to increase in many developing countries. The combination of platinum and pemetrexed is considered a standard regimen, but median survival is approximately 1 year [2]. There is no established treatment option once cases are refractory or intolerable to the regimen. The immunosuppressive tumor microenvironment in MPM suggests that patients may benefit from this kind of immunotherapy. In recent years, some encouraging results of ICIs have been reported for MPM. In a Japanese single-arm phase II study examining the efficacy and safety of nivolumab monotherapy, the primary endpoint, objective response rate, was 29%, and the median progression-free and overall survival were 6.1 and 17.3 months, respectively [3]. These results led to the approval of nivolumab in Japan for unresectable recurrent MPM. However, the efficacy of anti-PD-1 antibody has not been established in randomised clinical studies.

Recently, the combination of nivolumab and ipilimumab was demonstrated to significantly improve overall survival compared to standard chemotherapy in the Checkmate-743 study [4]. An important clinical issue is to determine which patients can expect a response or unacceptable toxicity, as not all patients could benefit

from the treatment, and some specific adverse events have been reported for the ICI-ICI combination. Some studies have revealed the correlation between responses and higher PD-L1 expression. In MPM, however, more established outcome data are needed to confirm the value of PD-L1 expression as a predictive biomarker. The tumor mutation burden and tumor microenvironment are associated with the response to ICIs in some neoplasms, but their roles as biomarkers have not been shown in MPM.

In this study, Mankor and colleagues show that patients who respond to combination treatment with nivolumab and ipilimumab have low frequencies of naïve CD8 T cells and high frequencies of cytokine-expressing effector memory CD8 T cells. A strength of this monitoring is that it can be performed before treatment induction. Notably, there are some limitations in this study, including a limited number of responding patients. However, the findings suggest that immune monitoring of peripheral blood immune cell subsets may act as a biomarker predicting a clinical benefit from ICI combination therapy. A prospective study with more subjects should be planned to validate these findings. In addition, basic or translational research to identify the mechanisms of action of T cells and cytokines against mesothelioma cells is warranted.

As a future perspective, the combination of an anti-PD-1 or anti-PD-L1 antibody and conventional chemotherapy is also under investigation. Nowak et al. recently presented favorable results from a phase II trial testing durvalumab, an anti-PD-L1 antibody, combined with cisplatin/pemetrexed in MPM [5]. A large-scale randomised study for testing the combination of pembrolizumab, another anti-PD-1 antibody, and cisplatin/pemetrexed is also ongoing. Platinum agents can enhance the effector immune response through modulation of PD-L1 [6]. Further development of new biomarkers to determine patients who would benefit from ICI-ICI combinations, ICI plus chemotherapy, or conventional chemotherapy is also needed.

A new era in systemic chemotherapy for MPM has just begun. Immune monitoring would be the key to choosing appropriate treatments.

Contributors

Dr Fujimoto wrote the commentary.

Declaration of Competing Interests

The author reports grants from MSD, grants and personal fees from ONO, grants and personal fees from Bristol-Meyers Squib,

E-mail address: nfujji@okayamah.johas.go.jp

<https://doi.org/10.1016/j.ebiom.2020.103057>

2352-3964/© 2020 The Author. Published by Elsevier B.V. This is an open access article under the CC BY-NC-ND license (<http://creativecommons.org/licenses/by-nc-nd/4.0/>)

during the conduct of the work; grants from Kissei, grants and personal fees from Kyorin, personal fees from Chugai, personal fees from Daiichi-Sankyo, outside the submitted work

Acknowledgments

The author is supported by grants-in-aid from the Ministry of Health, Labor, and Welfare, Japan. The funding source had no role in the current work.

References

- [1] Mankor J, Disslhorst M, Poncin M, Baas P, Aerts J, Vroman H. Efficacy of nivolumab and ipilimumab in patients with malignant pleural mesothelioma is related to a subtype of effector memory T cells: translational evidence from two clinical trials. *EBioMedicine* 2020. doi: [10.1016/j.ebiom.2020.103040](https://doi.org/10.1016/j.ebiom.2020.103040).
- [2] Vogelzang NJ, Rusthoven JJ, Symanowski J, et al. Phase III study of pemetrexed in combination with cisplatin versus cisplatin alone in patients with malignant pleural mesothelioma. *J Clin Oncol* 2003;21:2636–44.
- [3] Okada M, Kijima T, Aoe K, et al. Clinical efficacy and safety of nivolumab: results of a multicenter, open-label, single-arm, Japanese phase II study in malignant pleural mesothelioma (MERIT). *Clin Cancer Res* 2019;25:5485–92.
- [4] Baas P, Scherpereel A, Nowak AN, et al. First-line nivolumab + ipilimumab vs chemotherapy in unresectable malignant pleural mesothelioma: CheckMate 743. *J Thorac Oncol* 2020;15(10, Supplement):e41–2. doi: [10.1016/j.jtho.2020.08.004](https://doi.org/10.1016/j.jtho.2020.08.004).
- [5] Nowak AK, Lesterhuis WJ, Kok PS, et al. Durvalumab with first-line chemotherapy in previously untreated malignant pleural mesothelioma (DREAM): a multicentre, single-arm, phase 2 trial with a safety run-in. *Lancet Oncol* 2020;21:1213–23.
- [6] Hato SV, Khong A, de Vries IJ, Lesterhuis WJ. Molecular pathways: the immunogenic effects of platinum-based chemotherapeutics. *Clin Cancer Res* 2014;20:2831–7.

第2部 免疫組織化学技術の発展

1. 免疫染色の基礎：抗原賦活法，増感法，ラビット抗体

山田健人

病理と臨床【臨時増刊号】・別刷

2020 vol. 38

東京／文光堂／本郷

1. 免疫染色の基礎：抗原賦活法，増感法，ラビット抗体

山田健人

はじめに

ホルマリン固定された病理検体における免疫染色はルーチン検査となっているが、近年増加しつつある分子標的療法においては、益々その重要性が増している。ここでは病理検体の免疫染色において、結果を大きく左右する抗原賦活法、増感法および近年飛躍的に利用が広まってきたラビット抗体について概説する。

I 抗原賦活法

病理検体の一般的固定法であるホルマリン（ホルムアルデヒド溶液）は、ホルムアルデヒドが蛋白質と結合するが、その条件は構成アミノ酸により異なり、結合力も様々である。ホルマリンの固定作用の一つは、ホルムアルデヒド分子内で発生する電気的陰性度の差に基づく電子の偏りによるアミノ酸残基末端との結合であり、非解離の残基末端との結合が可能とする求核反応である。いま一つはホルムアルデヒドとアミノ酸末端残基とが脱水縮合した形で共有結合するもので、特にリジン、アルギニン等の末端アミノ基との反応により生成されるメチレンアミン（シッフ塩基）やトリプトファン、チロキシンなど芳香族活性炭素に対する反応は不可逆的で非常に安定した共有結合を示す。もう一つは、ホルムアルデヒドが単一アミノ酸残基末端との結合、さらにヒドロメチル基により別のアミノ酸末端残基と連結してメチレン架橋を形成することにより、ループ形成や2本のポリペプチド鎖を架橋し蛋白質の安定化をさせるものであり、一級アミノ基やフェニル基等を介して形成されるメチレン架橋は非常に安定した強固な固定作用を誘導する。このような強力に安定した固定作用を有するホルマリンであるが、共有結合を主体としたホルムアルデヒドは蛋白質の高次構造を変形させるため、抗原決定基の立体障害や抗原分

子が覆いかくされた状態（マスキング）となり、抗体が抗原に接近できない、あるいは認識できないことがある。このような抗原のマスキングや抗体の抗原へのアクセスを開通させるために賦活化を行う。固定された抗原分子が、ホルマリンによってどのように変性しているかで賦活化が必要かどうか、どのような賦活化が適しているか、抗原および抗体ごとに至適条件を決めていく綿密な作業が必須である。

賦活化は、大きく分けると、①蛋白質分解酵素、②熱処理、の2種類に分類される。この賦活化がうまくいくかどうかを左右する因子としては、①方法（酵素か熱か）、②緩衝液の種類、濃度、pH、③時間、④温度、が挙げられる。これらの処理方法と条件や特徴について表1に示す。

このように抗原賦活化は、抗原と一次抗体の種類と特徴によるために、市販の抗体を用いる場合は、まずはデータシートで推奨されている条件と方法で行うことが推奨される。賦活化条件が不明な場合には、まずは無処理と熱処理〔クエン酸緩衝液（pH 6.0）、Tris-EDTA緩衝液（pH 9.0）〕と酵素処理（プロテアーゼ K、トリプシン）を試してみて、染色性を確認しながら至適条件を探っていくことになる。抗原によっては、熱処理と酵素処理の両方を用いると良い結果が得られるものもある（免疫グロブリン軽鎖など）。

II 増感法

抗原が組織・細胞に多量に存在していて、抗体の特異性と抗体価が高い場合には、シグナル検出は容易であるが、抗原が微量しかない場合や特異性あるいは抗体価が低い場合には、シグナル増幅法が有効である。このシグナルを増幅する方法として、これまでに、①ABC (avidin biotin complex) 法、②標識ポリマー法が用いられてきた。

ABC法は、ビオチンがアビジンと特異的に強い結合を示す性質を利用した方法であり、ビオチン結合二次抗体を用いて、ビオチンとアビジンを結合させて、

表1 抗原賦活法の比較

	蛋白質分解酵素	熱処理
特徴	<ul style="list-style-type: none"> 特定のアミノ酸残基のペプチド結合を加水分解により切断し，メチレン架橋を解離する 抗原決定基を構成するアミノ酸が切断されると抗原が消失するため酵素種類，濃度，反応時間と温度の設定が重要 熱処理が無効な場合にも効果が期待できる 	<ul style="list-style-type: none"> 固定による蛋白質の立体構造やメチレン架橋が加熱で解離される 固定の際に金属イオンと蛋白質が共有結合した複合体を形成している場合には，EDTAやクエン酸溶液による金属イオンの除去が期待できる 組織へのダメージが少ない
方法	pepsin：酸性アミノ残基，芳香族アミノ残基に続くC末側，pH2~4 trypsin：塩基性アミノ酸のカルボキシル基側，pH8~9 proteinase K：アミノ酸C末端隣のエステルペプチド結合，広汎，pH7.5~10 pronase：グルタミン酸，アスパラギン酸C末端，広汎，pH5~9	恒温槽 圧力鍋 オートクレーブ 電子レンジ
pH	中性緩衝液 (pH 7.4)	クエン酸緩衝液 (pH 6.0~7.0) Tris-EDTA (pH 9.0~11)
温度	37℃	90~95℃
時間	5~30分	10~40分
注意する点	酵素処理のやりすぎは組織の形態にダメージを与えるので，酵素濃度や反応時間に厳密な設定が必要	加熱に電子レンジを用いる場合，突沸による組織形態へのダメージや剝離の危険性がある。またホット・スポットやコールド・スポットの形成による不均一な抗原賦活化が起こる場合がある
実例	ケラチン，ビメンチン	白血球表面マーカー，p53，ER，MIB-1

さらにペルオキシダーゼ標識ビオチンを反応させることで，結果として多数の標識ペルオキシダーゼが標識されることで増幅効果を発揮して検出感度が上がる¹⁾。ただし，ビオチンは，細胞内に内在性のものがあり，さらに抗原賦活化過程でこの内在性ビオチンが露出することで，非特異的な反応が生じることがある。またアビジンは塩基性分子であり，それによる非特異的な反応も起こることから，アビジンの代わりに中性のストレプトアビジンを用いることが多い。

標識ポリマー法は，デキストランポリマー骨格に二次抗体を多数結合させることで，最終的に抗原，一次抗体，二次抗体とともに多数の標識ペルオキシダーゼの複合体が生じて，増幅効果が得られる方法である。この方法の利点として，多くの未標識一次抗体が使用できること，工程を減らすことができること，バックグラウンドを上げずに感度が上がることが挙げられる。また内在性ビオチンのように，抗原賦活化による非特異的な反応の増強もない。この標識ポリマー法の欠点としては，ポリマーの分子量が大きいため，組織・細胞への浸透性が悪く，時に感度が低下することがある。

1. TSA (tyramide signal amplification) 増感法

上記の二つの方法を超越する高感度な検出を可能にしたのがTSA法である(図1a)。このTSA法は，Perkin-Elmer社が開発したCARD (catalyzed reporter deposition) 法の原理に基づくシグナル増幅法である²⁾。CARD法は，酵素等を利用して，その基質をラジカル化したり，発色させたりする方法である。この原理を免疫染色に応用することで，ビオチン化タイラマイドがラジカル化タイラマイドになって，抗原抗体反応部位に沈着し，ペルオキシダーゼ標識ストレプトアビジンが反応することで，多数のペルオキシダーゼが集積して，反応が増幅されるものである。タイラマイドは，アミノ基を有するp-フェノール誘導体であり，過酸化水素存在下において，ペルオキシダーゼの触媒作用によりラジカル化される。このラジカルが，芳香族化合物(チロシンやトリプトファンなどのアミノ酸)と非特異的な共有結合を形成して，ペルオキシダーゼ分子の近傍に結合・局在して分布する。このTSA法を免疫染色に応用することで，免疫染色において，簡便にその感度を向上させることが可能となっており，これまで検出できなかった微量な抗原が検出可能となってきた³⁾。前述したとおり，ビオチンは，細胞内に内在性

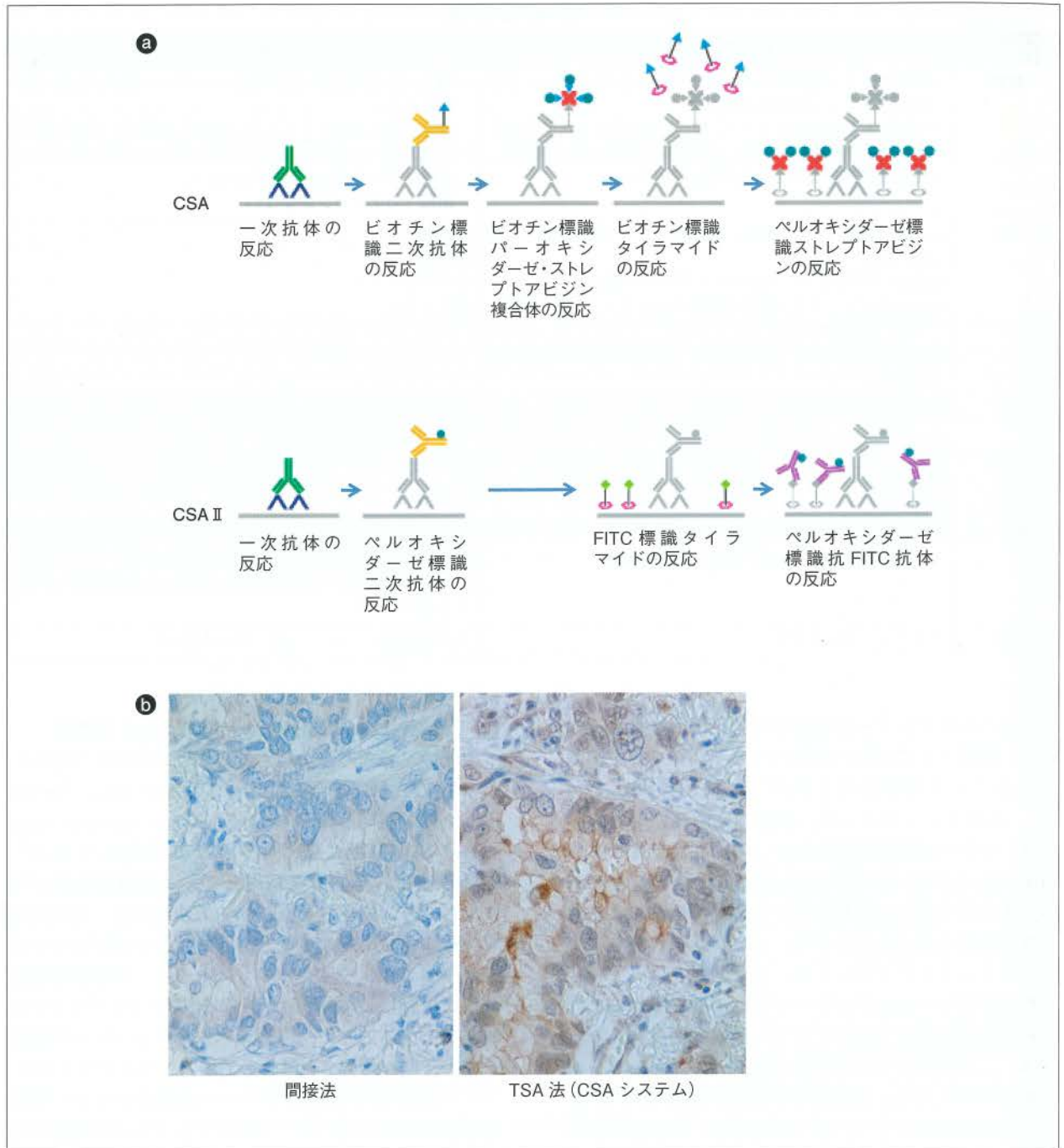
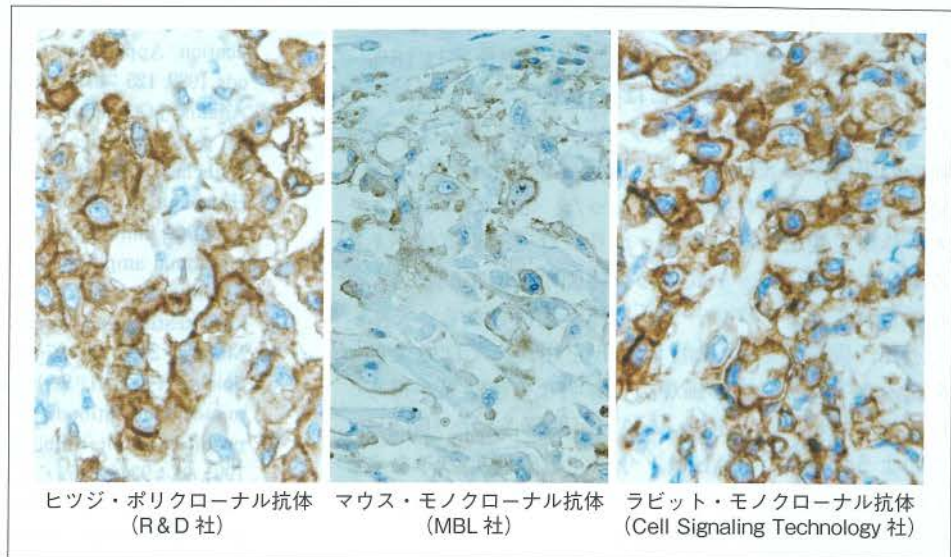


図1 TSA増幅法(a)とヒト肺腺癌におけるリン酸化HER2の検出(TSA法)(b) b:リン酸化HER2分子は、主に細胞膜に存在するが、従来の間接法(左)ではほとんど検出できないが、TSA法(右)を用いることで可視化が可能となる。FITC:フルオレセインイソチオシアネート。

のものがあ、抗原賦活化によりこの内在性ビオチンがさらに露出して、非特異的な反応(背景の偽シグナル)が生じることがあるため、ビオチンの代わりにフル

オレセインイソチオシアネート標識タイラミドを用いたCSAII法も開発され、内在性ビオチンによる非特異的な反応を回避することが可能となっている(図1a)。

図2 ラビット・モノクローナル抗体の有効性(ヒト悪性中皮腫におけるCD26染色) ヒッジ・ポリクローナル抗体は抗体価が高く、良い染色性が得られるが、臨床試験に使用するにはロット間での相違が問題となる。マウス・モノクローナル抗体は、抗体価が低く染色性が悪いが、ラビット・モノクローナル抗体は抗体価が高く鮮明な染色結果が得られる。



またリン酸化などで修飾された分子を特異的に認識する抗体を用いて、これまで検出できなかった分子形態が免疫染色により同定されてきている⁴⁾。例えば、これまでに生化学的あるいは分子生物学的手法により、肺癌や乳癌症例において、リン酸化 epidermal growth factor receptor (EGFR) やリン酸化 epidermal growth factor receptor 2 (HER2) 分子が発現していることが証明されていたが、TSA法を用いることで組織切片でのリン酸化EGFRやリン酸化HER2の発現・局在を同定することが可能となっている(図1b)。

III ラビット抗体

従来、モノクローナル抗体の多くはマウス由来であったが、マウスと比べて多様性、親和性、特異性などの利点があるウサギ(ラビット)・モノクローナル抗体(Rab MoAb)が開発されてきた^{5,6)}。ウサギの免疫系はユニークで、そのBリンパ球のレパートリーは極めて多彩であり、短いペプチドや低分子化合物などマウスでは作りにくい免疫原性が低い抗原でも抗体を作り出すことができる。特にリン酸化、メチル化、アセチル化、SUMO化といった蛋白質分子上の微小な相違を認識し、これらを厳密に識別し、反応する抗体も作成可能となった。またウサギ抗体は、マウスやラットと比較してその親和性が高く、Rab MoAbにおいても、マウス・モノクローナル抗体よりも10倍～1,000倍高い親和性を有するため、パラフィン包埋ホ

ルマリン固定切片において一次抗体の濃度を下げることが可能となってきた。実際、抗原抗体親和性を平衡解離定数Kdで表すと、マウス・モノクローナル抗体では、 $10^{-7\sim-9}$ Kd(M)であるのに対して、Rab MoAbでは、 $10^{-10\sim-12}$ Kd(M)と10～1,000倍親和性が高いものが多い。またウサギではBリンパ球レパートリーが多彩であることによって、修飾、点突然変異、立体構造変化などの抗原決定基のわずかな違いを識別することができるような抗体を作製できるのが利点である。さらにウサギに免疫して得られる抗体は、マウスやラット組織・細胞とも交叉反応があり、マウスやラットを用いた基礎研究と前臨床研究の両者で同一の抗体が使用できることも利点である。またマウスやラットのモノクローナル抗体とRab MoAbを組み合わせることで、二重染色も容易になっている。一方、ウサギのハイブリドーマは、細胞当たりの抗体産生能が低くマウスの1/10～1/100であったが、その後、抗体産生細胞をハイブリドーマではなくリコンビナント抗体遺伝子を組み込んだ細胞による産生経路としたことで抗体の収量も同等以上となってきた。

Rab MoAbの応用例を図2に示す。CD26は広汎なヒトがんにおいて発現している細胞膜貫通型糖蛋白質であり、ヒト化抗CD26モノクローナル抗体による分子標的療法の臨床試験が行われた⁷⁾。この抗体療法の適応症例の選別において、病理検体によるCD26免疫染色が行われた。その際、入手可能なすべての一次抗体(モノクローナル抗体)23種類を試験したところ、唯一、MBL社のマウス・モノクローナル抗体のみが

ホルマリン固定パラフィン切片での染色が可能であったが、その抗体価は低く、中皮腫での陽性率は15%でありコンパニオン診断には採用できなかった。一方、R & D社ヒツジ・ポリクローナル抗体では中皮腫での陽性率は85%となり、臨床試験におけるCD26発現評価に使用されることとなった。しかしコンパニオン診断に使用する抗体が、ポリクローナル抗体である場合には常にロット間での抗体価の相違が問題となることから、モノクローナル抗体が期待される。そこで近年、開発されたRab MoAbを用いたCD26染色を試みたところ、抗体価が高く鮮明な染色結果が得られるリコンビナントRab MoAbが確認された(図2)。このようにRab MoAbは、今後、基礎研究のみならず病理補助診断やコンパニオン診断試薬としても広く活用されていくものと思われる。

文 献

- 1) Hsu, S.M., Raine, L., Fanger, H. : Use of avidin-biotin-peroxidase complex (ABC) in immunoperoxidase techniques : a comparison between ABC and unlabeled antibody (PAP) procedures. J Histochem Cytochem 1981, 29 : 577-580
- 2) Bobrow, M.N., Harris, T.D., Shaughnessy, K.J. et al. : Catalyzed reporter deposition, a novel method of signal amplification. Application to immunoassays. J Immunol Methods 1989, 125 : 279-285
- 3) Adams, J.C. : Biotin amplification of biotin and horserish peroxidase signals in histochemical stains. J Histochem Cytochem 1992, 40 : 1457-1463
- 4) Hatanaka, Y., Imaoka, Y., Torisu, K. et al. : A simplified sensitive immunohistochemical detection system employing signal amplification based on fluorescein-tyramide/tetrafluorescein antibody reaction : its application to pathologic testing and research. Appl Immunohistochem Morphol 2008, 16 : 87-93
- 5) Spieker-Polet, H., Sethupathi, P., Yam, P.C. et al. : Rabbit monoclonal antibodies : generating a fusion partner to produce rabbit-rabbit hybridomas. Proc Natl Acad Sci 1995, 92 : 9348-9352
- 6) Rossi, S., Laurino, L., Furlanetto, A. et al. : Rabbit monoclonal antibodies : a comparative study between a novel category of immunoreagents and the corresponding mouse monoclonal antibodies. Am J Clin Pathol 2001, 124 : 295-302
- 7) Angevin, E., Isambert, N., Yamada, T. et al. : First-in-human phase 1 of YS110, a monoclonal antibody directed against CD26 in advanced CD26-expressing cancers. Br J Cancer 116 : 1126-1134



皮膚科サブスペシャリティシリーズ

1冊でわかる皮膚病理

ゲスト編集●木村鉄宣

◆「皮膚病理は苦手」という医師が楽しく学べるような工夫を満載し、豊富な写真とポイントを押さえた解説で、すらすらと読める構成になっている。ごく基本から学び、臨床像と病理を結びつけて理解し、この1冊で皮膚疾患全体を総括できる、まさに皮膚病理テキストの決定版。

●B5変型判・548頁・4色刷/定価(本体 19,000円+税) ISBN978-4-8306-3454-3



<https://www.bunkodo.co.jp> 〒113-0033 東京都文京区本郷7-2-7 tel.03-3813-5478/fax.03-3813-7241